

**EFFECTS OF VIBRATION ONTO THE FLOW
STRUCTURES AND DYNAMICS OF GAS-LIQUID
TWO-PHASE FLOW**

MOHD ZAMRI ZAINON

**FACULTY OF ENGINEERING,
UNIVERSITY OF MALAYA,
KUALA LUMPUR
2013**

Abstract

The investigations on the effects of heavy class disaster shakes and vibration have been conducted for the bubble column and vertical upward gas-liquid two-phase flow channel via experimental studies. The effects of four modes of vibrations with ground accelerations in the range of 0~12 m/s^2 were examined using a specially constructed vibration platform that move vertically. The facility was equipped with high speed video camera and sensors for various parameters measurement.

The first part of the work focused on the behavior of the rising bubble in a 2-D column of air-water with further analyses on the rising velocity of the gas bubbles at various sizes. The results revealed that the behavior of rising bubble has a totally different characteristic when compared to the situation with the absent of vibration. The coalescences of bubbles with clustering and breakup were seen and for the most critical case, the bubble distorted very badly under the effect of vibration with higher modes. On the other hand, the rising velocity of gas bubbles shows some range fluctuation compared to normal rise without vibration. The bubbles move very quickly during the positive acceleration and show slower movement during the negative acceleration.

The second part of this work concentrated on the flow patterns, flow patterns mapping, measurement of void fraction and instantaneous bubble velocity under the same range of ground acceleration with various flow condition. Under the vibration effects, the flow pattern change very easily for example from bubbly to slug flow during the low liquid superficial velocities and they show very obvious patterns transition as the gas superficial velocities increased. At higher liquid superficial velocities, as a result of higher dynamic force from the liquid flow, the change of flow patterns was not so critical but at some level the transition of patterns can be observed particularly for higher gas superficial velocities. From the flow pattern analysis, the data were then

interpreted into the flow mapping where completely different maps were constructed based on the sizes of vibrations and flow conditions.

On the other hand, the measurements of void fraction were performed using the Constant Electric Current Method sensor that is capable to measure both the void fraction and the liquid film thickness, and therefore the effect of annular flow on the measurement can be avoided. The results show that as the liquid superficial velocity increases the fluctuation of void fraction receives very small effect from the vibration. In addition the effects of axial location were also conducted in order to investigate the variation of void fraction along the flow channel. The numerical data from void fraction measurement were then used to calculate the instantaneous bubble velocity.

Using the peaks of voids from the graph and the relation of distance and time travels of the bubbles and slugs contribute to calculations of their velocities. During these calculations, the void peaks were compared with the sinuous motions during the vibration and as a result the effects of negative and positive acceleration on the bubbles velocities were analyzed. In this case, the bubble velocities were strongly affected by the scale of vibrations but they differ in term of speed during the positive and negative acceleration. However, for the case of high velocity liquid flow regime, the influences of vibration were seen to be very low.

In general, throughout this thesis work, the effects of vibration onto the flow structures and dynamics of gas-liquid two-phase flow are very obvious. The results can be a good reference for the safety design and analysis on the two-phase flow, particularly on the problems regarding heavy disaster shakes as discussed in this thesis.

Abstrak

Penyelidikan telah dijalankan terhadap kesan getaran bersekala gegaran musnah ke atas ruangan gelembung dua dimensi dan aliran gas-cecair dua fasa yang bergerak menegak ke atas di dalam paip melalui kaedah ujikaji. Kesan empat mod getaran dengan pecutan bumi dalam lingkungan $0\sim 12\text{ m/s}^2$ telah diperiksa dengan menggunakan sebuah platform getaran yang diciptakan khas dengan keupayaan gerakan menegak pada skala pecutan tersebut. Kemudahan ujikaji juga dilengkapi dengan kamera video berkelajuan tinggi untuk pemeriksaan foto keatas kelakuan gelembung gas yang dinyatakan.

Bahagian pertama penyelidikan ini ditumpukan kepada kelakuan gelembung semasa ia menaik di dalam ruangan gas-cecair dua dimensi dengan analisis lanjutan ke atas halaju gelembung berbagai saiz. Keputusan telah menunjukkan bahawa kelakuan gelembung semasa menaik ke atas ini sangat berbeza daripada ciri-cirinya semasa keadaan mantap yang tidak dikenakan gegaran. Tautan gelembung membentuk kluster dan perpecahan semula adalah antara fenomena yang dilihat dan pada keadaan kritikal, rupa bentuk gelembung ini telah terganggu dengan teruk sekali di bawah pengaruh getaran berpecutan tinggi. Manakala halaju menaik gelembung pula menunjukkan pelbagaian turun-naik bila dibandingkan dengan keadaan menaik secara normal semasa tiada getaran. Antara fenomena lain yang dapat dilihat ialah peningkatan halaju menaik pada kadar yang sangat tinggi dan penurunan kadar gerakan disebabkan oleh pecutan negatif.

Bahagian kedua kajian ini ditumpukan kepada corak aliran, pemetaan corak aliran, pengukuran pecahan lompang dan pengukuran halaju seketika di bawah pelbagaian pecutan bumi dan keadaan aliran. Di bawah pengaruh getaran, corak aliran berubah dengan mudah pada keadaan halaju permukaan cecair yang rendah dan menunjukkan alihan corak yang sangat ketara apabila halaju permukaan gas semakin

meninggi. Pada keadaan halaju permukaan cecair yang tinggi, perubahan corak aliran adalah kurang kritikal disebabkan oleh daya dinamik tinggi oleh aliran cecair tetapi kadangkala alihan bentuk aliran dapat dilihat pada aras tertentu terutamanya di dalam keadaan halaju permukaan gas yang tinggi. Daripada analisa corak aliran, data ini diterjemahkan ke dalam pemetaan corak aliran di mana peta aliran yang amat berbeza sekali telah dapat dibina berdasarkan saiz getaran dan keadaan aliran yang diberikan.

Pengukuran pecahan lompang pula telah dilakukan melalui penderia khas yang dibina menggunakan kaedah aliran elektrik malar. Penderia ini mampu mengukur dua jenis parameter berbeza iaitu pecahan lompang dan ketebalan filem cecair. Keputusan ujikaji menunjukkan kesan getaran kepada turun-naik pecahan lompang adalah padakadar minima apabila halaju permukaan cecair makin meninggi. Sebagai tambahan, ujikaji terhadap kesan lokasi kepaksian juga dijalankan untuk menyiasat variasi pecahan lompang di sepanjang saluran aliran. Data berangka daripada ukuran pecahan lompang kemudiannya digunakan untuk mengira halaju seketika gelembung dengan menganalisa puncak-puncak lompang di dalam carta. Dengan menggunakan hubungan jarak dan masa perjalanan gelembung dari satu lokasi kepaksian ke lokasi lain yang menempatkan penderia, halaju seketika dapat ditentukan. Semasa pengiraan ini, puncak-puncak lompang dibezakan dengan gerakan sinus semasa getaran dan dengan itu analisa kesan pecutan negatif dan positif ke atas halaju gelembung dapat dilakukan.

Melalui hasil kerja tesis ini, secara amnya dapat didapati kesan getaran ke atas struktur aliran dan dinamik aliran dua fasa adalah amat ketara. Hasil kerja ini adalah akan menjadi bahan rujukan penting kepada rekabentuk dan analisis keselamatan untuk aliran dua fasa terutamanya dalam kes-kes yang melibatkan gegaran musnah seperti dibincang di dalam tesis ini.

Acknowledgement

Alhamdulillah, after such a long time, this study has been completed. I thank ALLAH the Almighty for giving me the strength and excellent health along the way of this work. There were many challenges through the whole process of this work; during experimentation, data analyses and thesis writing.

Without my family, I never thought this work could ever be accomplished. Therefore, I would like to dedicate this work to them and thank them for all the loves and supports, especially to my wife, Maizatul Safinaz for sharing the life with me.

This thesis is also dedicated to Emeritus Professor Dr. Akimi Serizawa, my former supervisor at Department of Nuclear Engineering, Kyoto University. He is the person who thought me about the beauty of two-phase flow and inspired me to study this subject, something that had never been conducted up to this date concerning many earthquake events in Japan from the past 20 years. Dear Sir, I am truly indebted to your guidance, kindness and understanding, thank you very much.

My appreciation is extended to the thesis supervisor and my good friend, Dr. Rahizar Ramli. I deeply appreciate your guidance and continuous support. Thank you for being a good teacher and friend. God bless you.

I also would like to convey my appreciation to all academicians at University of Malaya, particularly at the Faculty of Engineering whom are my best buddies ever that continuously provide very strong support toward this study. The appreciations are also extended to everybody at Department of Mechanical Engineering, University of Malaya for their help directly or indirectly toward this study.

Lastly, I also would like to convey my gratitude to University of Malaya, Ministry of Higher Education and Ministry of Science, Technology and Innovation, Malaysia that provided the grants for this work.

TABLE OF CONTENT

CHAPTER 1 : INTRODUCTION

1.1	Background of the Study	1
1.2	General Power Plant Safety Regulations	2
1.3	History of Heavy Disaster Shakes and Consequences on Power Plants	4
1.4	Current Situation on the Vibration Problems	6
1.5	Objective	7
1.6	Scopes of Works	7
1.7	Development and Analyses	10

Part I : Fundamental Studies of Vibration and Two-Phase Flow

CHAPTER 2 : LITERATURE REVIEW – FUNDAMENTAL ANALYSIS

2.1	Fundamental of Two Phase Flow	12
2.2	Two-Phase flow in Two-Dimensional Column	14
2.3	Basic Analysis on Seismic Vibrations	16

CHAPTER 3 : DEVELOPMENT OF VIBRATION PLATFORM

3.1	Introduction	21
3.2	Basic Analysis on the Damped Free Vibration	23
3.3	Construction of Vibration Platform	25
3.4	Results and Measurement	28

CHAPTER 4 : BEHAVIOR OF RISING BUBBLE IN A TWO-DIMENSIONAL COLUMN UNDER VIBRATION

4.1	Introduction	32
4.2	Experimental Setup and Methodology	33
4.3	Results and Discussions	35
4.3.1	Typical Trajectories of a Single Bubble	35
4.3.2	Vibration Effects on the Rising Bubble	36
(a)	Vibration Modes	36
(b)	Bubble Sizes	39
4.3.3	Rising Velocity	41
4.3.4	Bubble Interactions	44

Part II : The Effects of Vibration on the Vertical Upward Two-phase Flow

CHAPTER 5 : LITERATURE REVIEW 2 - TWO-PHASE FLOW IN ANNULAR CHANNEL

5.1	Introduction to Two-phase Flow in Annular Channel	46
5.2	Flow Patterns	48
5.2.1	Types of Flow Patterns in Vertical Pipes	49
5.2.2	Identification Techniques of Flow Patterns	52
5.2.3	Effects of Flow Patterns in Two-phase Flow	55
5.2.4	Transition of Flow Pattern	56
5.3	Flow Patterns Mapping	58
5.4	Void Fraction	63
5.4.1	Definition and Models	63
5.4.2	Measurement Techniques of Void Fraction	67

5.4.3	Relation of Void Fraction, Measurement Techniques and Other Parameters	70
5.5	Two-Phase Flow Boiling	72
5.6	Bubble velocity in a Vertical Annulus Channel	74
5.7	Vertical Upward Two-phase Flow and Vibration	77

CHAPTER 6 : RESEARCH METHODOLOGY

6.1	Introduction	81
6.2	Development of Two-phase Flow Loop	82
6.2.1	Basic Principle of the Facilities	83
6.2.2	Experimental Apparatus	84
6.2.3	Analytical Flow Chart	85
6.3	Development of Sensor for Measurement in Two-phase Flow	88
6.3.1	<u>C</u> onstant <u>E</u> lectric <u>C</u> urrent <u>M</u> ethod (CECM)	88
6.3.2	Basic Equations	90
6.3.3	Construction of the Sensor	91
6.3.4	Calibrations	92
	(a) Static Calibration	92
	(b) Dynamic Calibration	97
6.3.5	Reliability Test	98
	(a) Comparison of Void Fraction	99
	(b) Comparison of Liquid Film Thickness	102

CHAPTER 7 : RESULTS AND DISCUSSIONS

7.1	Outline of the Analyses	106
7.2	Flow Patterns	108
7.2.1	Liquid Superficial Velocity, $j_L=0.25\text{ m/s}$	109
7.2.2	Liquid Superficial Velocity, $j_L=0.50\text{m/s}$	113
7.2.3	Liquid Superficial Velocity, $j_L=0.75\text{m/s}$	118
7.2.4	Liquid Superficial Velocity, $j_L=1.0\text{ m/s}$	122
7.2.5	Liquid Superficial Velocity, $j_L=2.0\text{m/s}$	127
7.2.6	Effects of Vertical Motion Effects	132
7.3	Flow Patterns Mapping	135
7.3.1	Flow Mapping based on Vibration Modes	137
7.3.2	Discrete Bubbles Distribution	146
7.4	Void Fraction	147
7.4.1	Measurement and Analysis Procedures	147
7.4.2	Basic Measurements	149
	(a) Effects of Vibration	149
	(b) Effects of Superficial Velocities	152
7.4.3	Vibration Effects on Total Average Void Fraction	154
7.4.4	Effects of Vibration and Axial Position On Void Fractions	162
	(a) Local Average Void Fraction	163
	(b) Local Maximum Void Fraction	174
7.4.6	Drift Flux Analyses on Void Fraction due to the Effect of Vibration	184

	(a) Relationship of Void Fraction, Slip Ratio and Vibration	184
	(b) Local Average Void Fraction	186
	(c) Local Maximum Void Fraction	187
7.5	Bubble Instantaneous Velocities	189
7.5.1	Analysis of Bubble Velocities	189
7.5.2	Evaluation of Bubble Velocities Due to the Scales of Vibration	192
7.5.3	Effects of Liquid Flux on the Bubble Velocities	201

Part III : Summary and Conclusions

CHAPTER 8 : CONCLUSIONS AND RECOMMENDATIONS

8.1	Conclusion	207
8.1.1	Chapter 1	207
8.1.2	Chapter 2	208
8.1.3	Chapter 3	211
8.1.4	Chapter 4	212
8.1.5	Chapter 5	213
8.1.6	Chapter 6	213
8.1.7	Chapter 7	215
8.1.8	General Conclusions	230
8.2	Recommendations	231

REFERENCES	234
-------------------	-----

APPENDICES	254
-------------------	-----

APPENDICES

Appendix 1.1 Statistics of World Energy Sources and Number of Nuclear Reactor

- (a) Electricity production and supply statistics
- (b) Number of reactors in operation worldwide

Appendix 1.2 PWR and BWR Emergency Core Cooling System

Appendix 1.3 Thermal-hydraulics and Power Plant Laboratory, University of Malaya

Appendix 2.1 Rising of Single Bubble in Liquid

- (a) Sinuous motion of gas bubble by Leonardo da Vinci
- (b) Two-dimensional VOF simulation on bubble rising

Appendix 2.2 Bubble column for processing industries

Appendix 3.1 Sophisticated shaker for vibration test

Appendix 3.2 Calculation code for harmonic motion of damped free vibration

Appendix 4.1 Example of datasheet for coordinate of rising trajectories of a bubble

Appendix 5.1 Core Meltdown of Nuclear Reactor

- (a) Core meltdown in fuel pool of Fukushima Nuclear Power Plant
- (b) Depiction of core meltdown consequences at Fukushima NPP

Appendix 5.2 Void Fraction Measurement and Flow Patterns in Vertical Upward
Two-phase Flow

- (a) Void fraction measurement for BWR
- (b) Flow pattern mapping with reference of flow patterns

Appendix 6.1 Close-up of test section and measurement facilities

Appendix 6.2 Example of datasheet for calibration of CECM sensor

Appendix 6.3 DNB Model

- (a) Wiesman-Pei Model
- (b) Katto Model

Appendix 7.1 Example of Datasheet for Flow Pattern Mapping

Appendix 7.2 Example of Datasheet for Total Average Void Fraction

Appendix 7.3 Example of Datasheet for Drift Flux Model

Appendix 7.4 Example of Datasheet for Calculation of Instantaneous Bubble Velocities

LIST OF FIGURES

- Figure 3.1 : Seismic spectrum of El Centro earthquake in 1940 (Park et al., 2008)
- Figure 3.2 : Seismic spectrum of Kobe earthquake in 1995 (Park et al., 2009)
- Figure 3.3 : A simple system of damped free vibration
- Figure 3.4 : Depiction of harmonic motion in a damped free vibration
- Figure 3.5 : Configuration of the vibration platform
- Figure 3.6 : Actual photo of the vibration platform
- Figure 3.7 : Comparison of vibration spectra : Experimental versus theoretical
- Figure 3.8: Acceleration spectra for four modes of vibration by four different amplitudes (tested based on $f=2.5Hz$)
- Figure 3.9 : Acceleration spectra for continuous vibration approximately with amplitude $20\text{-}mm$
- Figure 4.1 : Experimental apparatus for vibration effects on bubble behavior in a 2-D column
- Figure 4.2 : A 3-D Configuration of the apparatus for vibration effects on bubble behavior in a 2-D column
- Figure 4.3 : Meandering trajectories of three single bubbles
- Figure 4.4 : Bubble trajectories under four modes of vibration
- Figure 4.5 : Shape oscillations during the rising under vibration with mode M2
- Figure 4.6 : Shape oscillations and damage under vibration with mode M4
- Figure 4.7 : Trajectories of bubbles with different diameters under vibration with mode M3
- Figure 4.8 : Rising velocities of single bubbles with different diameters

- Figure 4.9 : Rising velocities of single bubble with different diameter under the effect of vibration with mode M3
- Figure 4.10 : Rising velocities of single bubble with 4-mm diameter under the effect of various scales of vibration
- Figure 4.11 : Snapshots of interaction of the two bubbles with different sizes
- Figure 4.12 : Trajectories of interaction of two bubbles released at close gap
- Figure 5.1: Gas-liquid two-phase flow pattern in vertical upward flow
- Figure 5.2 : Flow boiling in vertically heated annular tube (Collier, 1981)
- Figure 5.3: Two-phase flow pattern map for vertical flow (Hewitt and Robertson 1969)
- Figure 5.4: Two-phase flow pattern map for vertical flow (Fair, 1960)
- Figure 5.5: Two-phase flow pattern map for vertical flow (Taitel and Duckler, 1976)
- Figure 5.6: Fundamental depiction of void fraction
- Figure 5.7: Comparison of the measurement results for tomography method
- Figure 6.1 : Experimental apparatus for vertical upward two-phase flow
- Figure 6.2 : Detail configuration of the test section for vertical upward two-phase flow
- Figure 6.3: Flow chart for vertical upward two-phase flow experimental procedures
- Figure 6.4 : Actual photo of experimental facility for vibration effects on vertical upward two-phase flow
- Figure 6.5. Configuration of CECM sensors
- Figure 6.6 : Electric current effect on holdup
- Figure 6.7 : Voltage drop by radial location
- Figure 6.8 : Radial location effect on holdup
- Figure 6.9 : Static calibration for CECM sensors
- Figure 6.10 : Dynamic calibration for CECM sensors

- Figure 6.11 : Example of voltage fluctuation for holdup to measure void fraction
- Figure 6.12 : Comparison of measured void fraction with other scholars' for $j_L=0.1m/s$
- Figure 6.13 : Comparison of measured void fraction with other scholars' for
 $j_L=0.75m/s$
- Figure 6.14 : Comparison of measured void fraction with other scholars' for $j_L=1.0m/s$
- Figure 6.15 : Comparison of measured void fraction with other scholars' for $j_L= 2.0m/s$
- Figure 6.16 : Comparison of measured void fraction with other scholars' for $j_L= 2.5m/s$
- Figure 6.17 : Comparison of liquid film thickness (low liquid superficial velocities)
- Figure 6.18 : Comparison of liquid film thickness (high liquid superficial velocities)
- Figure 7.1 : Changes of flow patterns due to vibration sizes, for $j_L=0.25 m/s$, $j_G=0.025 m/s$
- Figure 7.2 : Changes of plow patterns due to vibration sizes, for $j_L=0.25 m/s$, $j_G=0.05 m/s$
- Figure 7.3 : Changes of flow patterns due to vibration sizes, for $j_L=0.25 m/s$, $j_G=0.075 m/s$
- Figure 7.4 : Changes of flow patterns due to vibration sizes, for $j_L=0.25 m/s$, $j_G=0.1 m/s$
- Figure 7.5 : Changes of flow patterns due to vibration sizes, for $j_L=0.25 m/s$, $j_G=0.15 m/s$
- Figure 7.6 : Changes of flow patterns due to vibration sizes, for $j_L=0.25 m/s$, $j_G=0.25 m/s$
- Figure 7.7 : Changes of flow patterns due to vibration sizes, for $j_L=0.5 m/s$, $j_G=0.025 m/s$
- Figure 7.8 : Changes of plow patterns due to vibration sizes, for $j_L=0.5 m/s$, $j_G=0.05 m/s$
- Figure 7.9 : Changes of flow patterns due to vibration sizes, for $j_L=0.5 m/s$, $j_G=0.075 m/s$
- Figure 7.10 : Changes of plow patterns due to vibration sizes, for $j_L=0.5 m/s$, $j_G=0.1 m/s$
- Figure 7.11 : Changes of flow patterns due to vibration sizes, for $j_L=0.5 m/s$,
 $j_G=0.15m/s$ and $j_G=0.25 m/s$
- Figure 7.12 : Changes of flow patterns due to vibration sizes, for $j_L=0.75 m/s$,
 $j_G=0.025 m/s$ and $j_G=0.050 m/s$
- Figure 7.13 : Changes of flow patterns due to vibration sizes, for $j_L=0.75 m/s$,
 $j_G=0.075 m/s$ and $j_G=0.1 m/s$
- Figure 7.14 : Changes of flow patterns due to vibration sizes, for $j_L=0.75 m/s$, $j_G=0.150 m/s$

- Figure 7.15 : Changes of flow patterns due to vibration sizes, for $j_L=0.75 \text{ m/s}$, $j_G=0.250 \text{ m/s}$
- Figure 7.16 : Changes of flow patterns due to vibration sizes, for $j_L=0.75 \text{ m/s}$, $j_G=0.500 \text{ m/s}$
- Figure 7.17 : Changes of flow patterns due to vibration sizes, for $j_L=1.0 \text{ m/s}$, $j_G=0.025 \text{ m/s}$
- Figure 7.18 : Changes of flow patterns due to vibration sizes, for $j_L=1.0 \text{ m/s}$, $j_G=0.05 \text{ m/s}$
- Figure 7.19 : Changes of flow patterns due to vibration sizes, for $j_L=1.0 \text{ m/s}$, $j_G=0.075 \text{ m/s}$
- Figure 7.20 : Changes of flow patterns due to vibration sizes, for $j_L=1.0 \text{ m/s}$, $j_G=0.1 \text{ m/s}$
- Figure 7.21 : Changes of flow patterns due to vibration sizes, for $j_L=1.0 \text{ m/s}$, $j_G=0.15 \text{ m/s}$
- Figure 7.22 : Changes of flow patterns due to vibration sizes, for $j_L=1.0 \text{ m/s}$, $j_G=0.25 \text{ m/s}$
- Figure 7.23 : Changes of flow patterns due to vibration sizes, for $j_L=1.0 \text{ m/s}$, $j_G=0.5 \text{ m/s}$
- Figure 7.24 : Changes of flow patterns due to vibration sizes, for $j_L=1.0 \text{ m/s}$,
 $j_G=0.75 \text{ m/s}$ and $j_G=1.0 \text{ m/s}$
- Figure 7.25 : Changes of flow patterns due to vibration sizes, for $j_L=2.0 \text{ m/s}$, $j_G=0.025 \text{ m/s}$
- Figure 7.26 : Changes of flow patterns due to vibration sizes, for $j_L=2.0 \text{ m/s}$, $j_G=0.05 \text{ m/s}$
- Figure 7.27 : Changes of flow patterns due to vibration sizes, for $j_L=2.0 \text{ m/s}$, $j_G=0.075 \text{ m/s}$
- Figure 7.28 : Changes of flow patterns due to vibration sizes, for $j_L=2.0 \text{ m/s}$, $j_G=0.1 \text{ m/s}$
- Figure 7.29 : Changes of flow patterns due to vibration sizes, for $j_L=2.0 \text{ m/s}$, $j_G=0.15 \text{ m/s}$
- Figure 7.30 : Changes of flow patterns due to vibration sizes, for $j_L=2.0 \text{ m/s}$, $j_G=0.25 \text{ m/s}$
- Figure 7.31 : Changes of flow patterns due to vibration sizes, for $j_L=2.0 \text{ m/s}$,
 $j_G=0.5 \text{ m/s}$ and $j_G=0.75 \text{ m/s}$
- Figure 7.32 : Changes of flow patterns due to vibration sizes, for $j_L=2.5 \text{ m/s}$, $j_G=0.75 \text{ m/s}$
- Figure 7.33 : Flow structures for $j_L=0.5 \text{ m/s}$, $j_G=0.05 \text{ m/s}$ during vibration with mode M3
- Figure 7.34 : Flow structures for $j_L=0.5 \text{ m/s}$, $j_G=0.1 \text{ m/s}$ during vibration with mode M3
- Figure 7.35 : Comparison of flow patterns maps with other scholars
- Figure 7.36 : Flow pattern map during steady state condition (mode M0)
- Figure 7.37 : Flow patterns map for damped vibration with mode M1
- Figure 7.38 : Flow patterns map for damped vibration with mode M2

- Figure 7.39 : Flow pattern map for damped vibration with mode M3
- Figure 7.40 : Flow patterns map for damped vibration with mode M4
- Figure 7.41 : Flow patterns map with continuous vibration with amplitude 20-*mm*
- Figure 7.42 : Flow chart of void fraction analyses
- Figure 7.43: Fluctuation of void fraction due to scales of vibration
- Figure 7.44 : Fluctuation and damping of void fraction due to vibration
- Figure 7.45 : Void peaks show the frequency similar to vibration frequency
- Figure 7.46: Low vibration effect during high liquid superficial velocity
- Figure 7.47: Low vibration effects during high gas superficial velocities
- Figure 7.48 : Effects of vibration on average void fraction for $j_L=0.25$ *m/s*
- Figure 7.49 : Effects of vibration on average void fraction for $j_L=0.5$ *m/s*
- Figure 7.50 : Effects of vibration on average void fraction for $j_L=0.75$ *m/s*
- Figure 7.51 : Effects of vibration on average void fraction for $j_L=1.0$ *m/s*
- Figure 7.52 : Effects of vibration on average void fraction for $j_L=1.5$ *m/s*
- Figure 7.53 : Effects of vibration on average void fraction for $j_L=2.0$ *m/s*
- Figure 7.54 : Effects of vibration on average void fraction for $j_L=2.5$ *m/s*
- Figure 7.55: Effects of vibration and axial position on the fluctuation of average void fraction, for $j_L=0.25$ *m/s*
- Figure 7.56 : Effects of vibration and axial position on the fluctuation of average void fraction, for $j_L=0.50$ *m/s*
- Figure 7.57 : Effects of vibration and axial position on the fluctuation of average void fraction, for $j_L=0.75$ *m/s*
- Figure 7.58: Effects of vibration and axial position on the fluctuation of average void fraction, for $j_L=1.0$ *m/s*
- Figure 7.59 : Effects of vibration and axial position on the fluctuation of average void fraction, for $j_L=2.0$ *m/s*

- Figure 7.60 : Effects of vibration and axial position on the fluctuation of average void fraction, for $j_L=2.5$ m/s
- Figure 7.61 : Effects of vibration on maximum void fraction for two different axial position, for $j_L=0.25$ m/s
- Figure 7.62 : Effects of vibration on maximum void fraction for two different axial position, for $j_L=0.50$ m/s
- Figure 7.63 : Effects of vibration on maximum void fraction for two different axial position, for $j_L=0.75$ m/s
- Figure 7.64 : Effects of vibration on maximum void fraction for two different axial position, for $j_L=1.0$ m/s
- Figure 7.65 : Effects of vibration on maximum void fraction for two different axial position, for $j_L=1.5$ m/s
- Figure 7.66 : Effects of vibration on maximum void fraction for two different axial position, for $j_L=2.0$ m/s
- Figure 7.67 : Effects of vibration on maximum void fraction for two different axial position, for $j_L=2.5$ m/s
- Figure 7.68: Drift flux analysis - effects of slip ratio and size of vibration on the total average (mean) void fraction, α_{avg}
- Figure 7.69: Drift flux analysis - effects of slip ratio and size of vibration on the local average void fraction, $\alpha_{avg(L)}$
- Figure 7.70 : Drift flux analysis - effects of slip ratio and size of vibration on the local maximum void fraction, $\alpha_{max(L)}$
- Figure 7.71 : Unit cell for bubble and slug flow analysis
- Figure 7.72 : Evaluation of bubble velocities using the void peaks for steady state condition (M0) with flow condition of $j_L=0.50$ m/s and $j_G=0.05$ m/s

- Figure 7.73 : Evaluation of bubble velocities using the void peaks for vibration with mode(M1) under flow condition of $j_L=0.50\text{ m/s}$ and $j_G=0.05\text{ m/s}$
- Figure 7.74 : Evaluation of bubble velocities using the void peaks for vibration with mode (M2) under flow condition of $j_L=0.50\text{ m/s}$ and $j_G=0.05\text{ m/s}$
- Figure 7.75 : Evaluation of bubble velocities using the void peaks for vibration with mode(M3) under flow condition of $j_L=0.50\text{ m/s}$ and $j_G=0.05\text{ m/s}$
- Figure 7.76 : Evaluation of bubble velocities using the void peaks for steady state condition (M4) with flow condition of $j_L=0.50\text{ m/s}$ and $j_G=0.05\text{ m/s}$
- Figure 7.77 : Evaluation of bubble velocities with comparison to theoretical calculation under flow condition of $j_L=0.5\text{m/s}$ and $j_G=0.05\text{ m/s}$ with all vibration modes
- Figure 7.78 : Evaluation of bubble velocities using the void peaks on the effects of gas superficial velocities under vibration with mode(M3) with flow condition of $j_L=0.25\text{m/s}$ and $j_G=0.05\text{ m/s}$.
- Figure 7.79 : Evaluation of bubble velocities using the void peaks on the effects of gas superficial velocities under vibration with mode M3 with flow condition of $j_L=0.75\text{m/s}$ and $j_G=0.05\text{ m/s}$
- Figure 7.80 : Evaluation of bubble velocities using the void peaks on the effects of gas superficial velocities under vibration with mode(M3) with flow condition of $j_L=1.0\text{m/s}$ and $j_G=0.05\text{ m/s}$
- Figure 7.81 : Evaluation of bubble velocities with comparison to theoretical calculation under flow condition of $j_G=0.05\text{ m/s}$ and various j_L with vibration modes M3

LIST OF TABLES

- Table 3.1 : Range of frequency based on the applied mass with spring constant of 0.6632kgf/mm
- Table 3.2 : Modes of Vibration
- Table 5.1 : Drift flux suggested values
- Table 6.1 : Area ratio based on calibration diameter
- Table 7.1 : List of gas and liquid superficial velocities
- Table 7.2: Drift velocities estimated by various correlations

University of Malaya

NOMENCLATURES

Roman Letters

a	Ground acceleration [m/s^2]
A	Area [m^2]
A_C	Cross sectional area of calibration rod [m^2]
A_E	Cross sectional area of experimental flow channel [m^2]
A_G	Cross sectional area of bubble [m^2]
c	Damping coefficient [-]
c_0	Constant for drift flux model [-]
d	Diameter of a bubble [mm]
D_C	Diameter of calibration rod [mm]
D_E	Diameter of flow or experimental channel ($=D$ or ID) [mm]
f	Frequency [Hz]
F	Force [N]
g	Gravitational acceleration [m/s^2]
I_0	Electric current [mA]
ID	Internal diameter [mm]
j	Volumetric flux ($=j_G+j_L$) [m/s]
j_G	Superficial velocity of gas phase [m/s]
j_L	Superficial velocity of liquid phase [m/s]
k	Spring constant [kg/mm]
L_B	Length of a bubble [mm]
L/D	Axial position (for sensor) [-]
m	Mass [kg]
\dot{m}	Mass flow rate [kg/s]

p	Pressure [MPa]
Q_b	Volumetric gas flow rate [m^3/min]
r_0	Radius of flow channel [mm]
Re	Reynolds number [-]
R_G	Electric resistance in the gas phase [Ω]
R_L	Electric resistance in the liquid phase [Ω]
R_{TP}	Electric resistance in the gas-liquid two-phase flow [Ω]
s	Thickness of bubble layer [mm]
S	Slip ratio [-]
t	Time [sec]
T	Temperature [$^{\circ}C$]
T_0	Period of circle [sec]
v	Velocity [m/s]
v_b	Velocity of a rising bubble [m/s]
v_G	Gas mean velocity [m/s]
v_L	Liquid mean velocity [m/s]
v_{Gj}	Drift velocity of gas phase [m/s]
v_{∞}	Terminal velocity of rising bubble [m/s]
V_L	Voltage fluctuation for single phase flow [V]
V_{TP}	Voltage fluctuation for two-phase flow [V]
x	Quality of vapor [-]
z	Displacement [m]
z_0	Initial amplitude or Eigen value amplitude [m]
\dot{z}	Velocity in z -direction [m/s]
\ddot{z}	Acceleration in z -direction ($=a$) [m/s^2]

Greek Letters

α	Void fraction [-]
α_{avg}	Average of void fraction between two axial position [-]
$\alpha_{avg(l)}$	Average of void fraction at local position [-]
$\alpha_{avg(L)}$	Lowest value of average void fraction [-]
$\alpha_{avg(H)}$	Highest value of average void fraction [-]
α_{limit}	Limit of void fraction [-]
$\alpha_{max(l)}$	Maximum value of local void fraction[-]
$\alpha_{max(L)}$	Lowest value of maximum local void fraction[-]
$\alpha_{max(H)}$	Highest value of maximum local void fraction [-]
β	Volumetric quality [-]
δ	Thickness of liquid film [mm]
Δ	Gap (for time and position of sensor)
Δt	Time lag [sec]
Δz	Gap of sensor position [mm]
ξ	Damping ratio [-]
η	Holdup [-]
ρ	Density [kg/m ³]
μ	Viscosity [Pa·s], [kg/m·s]
ν	Kinematic viscosity [m ² /s]
σ	Electrical conductivity [S/m]
ψ	Phase angle [rad]
ω	Angular velocity [rad/s]
ω_d	Natural circular frequency [rad/s]

Abbreviation

BWR	Boiling Water Reactor
CECM	Constant Electric Current Method
CHF	Critical Heat Flux
DNB	Departure from Nucleate Boiling
LDV	Laser Doppler Velocimetry
LOCA	Loss of Coolant Accident
PIV	Particle Image Velocimetry
PWR	Pressurized Water Reactor
UVP	Ultrasonic Velocity Profile

Modes of Vibrations

M0	Steady State Condition (no vibration)
M1	Mode 1 ($a = \pm 3m/s^2$)
M2	Mode 2 ($a = \pm 6m/s^2$)
M3	Mode 3 ($a = \pm 9m/s^2$)
M4	Mode 4 ($a = \pm 12m/s^2$)
C	Continuous (approximately at, $a = \pm 6m/s^2$)

Properties (at room temperature and atmospheric pressure)

Density of Water	$\rho_{water} = 998 \text{ kg/m}^3$
Density of Air	$\rho_{air} = 1.2 \text{ kg/m}^3$
Viscosity of Water	$\mu_{water} = 8.9 \times 10^{-4} \text{ Pa}\cdot\text{s}$
Viscosity of Air	$\mu_{air} = 18.6 \times 10^{-5} \text{ Pa}\cdot\text{s}$
Conductivity of Copper	$\sigma = 5.96 \times 10^7 \text{ S/m}$

1.1 Background of the study

Statistically from the point of sources of electric power in the world, there are a total of 67% generation by fossil power plants and 13% by nuclear power plant, (IEA, 2011). This figure concludes that 80% of the electric power generations depending on the thermal power plants with the rest of sources are from renewable energy such as hydro, solar, wind etc. With the increase number in the world populations, developments of many areas such as industrial and housing sectors will increase that as a result increase the demand of electricity. Therefore, the number of thermal power plants also will increase. For example, the World Resources Institute identifies 1,200 coal plants in planning across 59 countries, with about three-quarters in China and India (The Guardian, 2012). Furthermore, as of January 18, 2013 there are about 500 new Nuclear Power Plants (NPP) of capacity range in 65 ~ 372 GW are under construction in 46 countries around the world (ENS, 2013). This statistic is supplied in Appendix 1.1.

With this number of thermal power plants there are also many accidents that occur during their operations that ultimately resulted in loss of power generation that directly affect the users. Examples of recent accidents in thermal power plant are such as, Vasilikos in Cyprus (2011) due to munitions explosions, Tilbury in UK (2012) due to fire, and also small incidents such as water hammer problems in many plants around the world including Janamanjung in Malaysia (2006). These accidents mostly due to bad maintenance, failures of equipment, lack of awareness, poor managing systems and from human error as well. Since these plants are not releasing the radioactive into the atmosphere, the catastrophic consequences are minimal.

From the experiences of Three Miles Island, Pennsylvania, USA in 1979 (Kemeny, 1979) and Chernobyl of former Soviet Union (now Ukraine) in 1986 (Gray 2002 and WNA, 2013) drove all the governments, international authorities, and down to researchers and engineers to have continuous charge into increasing the safety of the

nuclear power plant. Regulations, training, new sophisticated equipment were introduced in order to maintain the trust of the public in the applications of nuclear technology for power generations. And in fact, there should be no denial of this action since the demand for energy is escalating very fast.

The impacts of the above two events promote more serious efforts for the authority to channel more funds into safety analyses, design and high end research in the field of nuclear engineering. Even though the accidents in nuclear power plants becoming the scariest incidents to the world, it does not give any room to ignore the safety in the conventional thermal power plant. There are continuous efforts among researchers and engineers at all the time to increase the safety level in the thermal power plant and for most of the cases; the same technologies and procedures also can be applied for any chemicals processing plants, oil recovery and refinery plants and other industries as well.

However, there is another factor that should be considered in the initiatives to secure the safety of the plants regardless of their applications, which is the natural disaster that strike without warning of which at most of time less attention being paid on. With recent technologies from research and development, there are equipment that have been created to sense the occurrence of the natural disaster prior to the strike. Such gadgets are like the typhoon sensor that uses that concept of wind velocities and patterns detector and the seismic sensor that detect the underground vibration.

1.2 General Power Plant Safety Regulations

In order to ensure the safety of the plants as discussed above, or in particular for the power plant, which is the main concern of the current work, it is very important to consider the hazardous possibility that will come when the external forces such as vibrations with a scale of heavy disaster shakes strike. The scariest natural disaster

would be the earthquakes, which so far in the history have resulted massive destructions to buildings, human lives and even changed the geographical landscapes. The safety level of power plant therefore should be revised in order to protect the inhabitants in the surrounding area and the life of the people that work in that facility or at least to minimize the casualties (WNA, 2013).

In term of durable construction, nuclear facilities are designed so that earthquakes and other external events will not jeopardise the safety of the plant. In France for instance, nuclear plants are designed to withstand an earthquake twice as strong as the 1000-year event calculated for each site. It is estimated that, worldwide, 20% of nuclear reactors are operating in areas of significant seismic activity. The International Atomic Energy Agency (IAEA) has a Safety Guide on Seismic Risks for Nuclear Power Plants. Various systems are used in planning, including Probabilistic Seismic Hazard Assessment (PSHA), which is recommended by IAEA and widely accepted.

Because of the frequency and magnitude of earthquakes in Japan, particular attention is paid to seismic issues in the siting, design and construction of nuclear power plants. The seismic design of such plants is based on criteria far more stringent than those applying to non-nuclear facilities. Power reactors are also built on hard rock foundations (not sediments) to minimise seismic shaking.

Japanese nuclear power plants are designed to withstand specified earthquake intensities evident in ground motion. These used to be specified as S1 and S2, but now simply Ss, in Gal units. The plants are fitted with seismic detectors. If these register ground motions of a set level, systems will be activated to automatically bring the plant to an immediate safe shutdown. The logarithmic Richter magnitude scale (or more precisely the Moment Magnitude Scale more generally used today) measures the overall energy released in an earthquake, and there is not always a good correlation between

that and intensity (ground motion) in a particular place. Japan has a seismic intensity scale in shindo (quake level) units 0 to 7, with weak or strong divisions at levels 5 and 6, hence ten levels. This describes the surface intensity at particular places, rather than the magnitude of the earthquake itself.

1.3 History of Heavy Disaster Shakes Consequences on Power Plants

The tragedy such as happened at Fukushima Power Plant in Japan during a major earthquake and tsunami, of which the event took place on March 11, 2011, is a great example. This tragedy causes eleven operating nuclear power plants shut down automatically and the three of these subsequently caused an INES Level 7 Accident, due to loss of power leading to loss of cooling and subsequent radioactive releases (IRSN, 2012).

In addition, Fukushima-Daiichi Nuclear Power Plant accident was the first occurrence showing that an extreme natural event, that generated stress levels far beyond nuclear power plant design-basis values, could lead to a core meltdown accident. It also showed how massive destruction of a site and the surrounding infrastructures could delay and complicate all accident management operations. However, the world's nuclear reactors were built without making allowance for risk associated with such events, because of their extremely improbable character.

Beside this event, there are also many tragedies that have affected the power plant in Japan, and all over the world. They are such as :

- In 1995, the closest nuclear power plants, some 110 km north of Kobe, were unaffected by the severe Kobe-Osaka earthquake, (Shibata, 1998) but in 2004, 2005, 2007, 2009 and 2011 Japanese reactors shut down automatically due to ground acceleration exceeding their trip settings (WNA, 2012).

- In 1999, three nuclear reactors shut down automatically during the devastating Taiwan earthquake, and were restarted two days later, (You and Wu, 2002).
- Reactors of both western and Soviet design have been subjected to major seismic activity in North America and Europe without damage. California's power reactors, San Onofre 2 and 3 (1,070 and 1,080 *MWe*, PWRs) and Diablo Canyon 1 and 2 (1,073 *MWe* and 1,087 *MWe*, PWRs) continued to operate normally during the 6.6 magnitude earthquake in January 1994. San Onofre, the closer station, was about 112 *km* from the epicentre (WNA, 2012).
- In December 1988 a magnitude of 6.9 earthquakes, resulting in the deaths of at least 25,000 people, occurred in north-western Armenia. It was felt at the two-unit Armenian nuclear power station located approximately 75 *km* south of the epicentre, but both Soviet-designed PWRs operated normally and no damage was reported, (Hadjian, 1993).
- Sumatra tsunami in 2004 claimed the life of more than 200,000 people, but there was no accident of nuclear power plant recorded. This is actually because there was no nuclear plant operated in the region but the damage on the 5.25 *MW* Kalpong hydroelectric power plant near Diglipur, North Andaman Islands was reported (Jain et al., 2005)
- In May 2008 a magnitude of 7.9 earthquakes affected south-western Sichuan province in central China. The main nuclear facilities affected were military ones, apparently without any radioactive releases. About 250 *km* from the epicentre the Yibin fuel fabrication plant which produces both power reactor and research reactor fuel assemblies was undamaged. China's power reactors were all at least 900 *km* from the epicentre, (WNA, 2012).

1.4 Current Situation on the Vibration Problems

There are numerous studies on structural analysis that are capable to predict the effect of vibration for the safety of buildings, and lead to the endurance design which the buildings are believed to stand tough even during a class of heavy shakes such as an earthquake. However, in the Kobe and Fukushima cases for example, these design capabilities have been denied and proved that the natural disasters are too strong for human to resist.

In contrary, there were very minimal attentions being paid on the effect of heavy disaster shakes to the fluid in containers particularly for a working fluid in power plant or heavy machineries. It would be more complicated, if they are in engineering application that involves the two-phase flow. For a safety treatment of the nuclear reactor, there is a safety shutdown system (SSS) that is believed to enable the reduction of hazardous accident during a class of heavy shakes like the earthquake (She et al., 2011). An example of SSS can be referred to Appendix 1.2. However, considering on the natural phenomena such as boiling in the reactor that could not be stopped instantly, there should be an analysis that can predict the behavior of the two-phase flow in such system that experience a situation of those serious impacts. Similarly, in various systems that has a multi-phase flow as a working or containing fluid should also consider this safety analysis.

Most of the studies that associate vibrations and the two-phase flow are concentrating on the flow induced vibration (Khushnood et al., 2004). This is a phenomenon where vibration occurred due to the instability of the flow inside the two-phase flow channel of which the similar consequences might occur (Huda, 1999). However, due to their very small vibration scale, damages that might occur from heavy shakes such as the earthquake may not be predicted. A direct impact of such mentioned heavy disaster shakes therefore must be studied in the field of two-phase flow.

1.5 Objective

With the above discussions, it is therefore very important to conduct some physical experimentations to study the changes on flow structures and dynamics effects that resulted by vibration on the two-phase flow in pipe as replication to the real plants. Hence, the current study with concerns on a scale of heavy disaster shakes has objectives as the following :

- (i) To study the vibration effects on bubble behaviors and rising trajectories in a 2-dimensional column
- (ii) To investigate the changes of flow patterns in a vertical gas-liquid two-phase flow due to vibrations.
- (iii) To conduct a remapping on the flow pattern in a vertical gas-liquid two-phase flow due to vibrations.
- (iv) To conduct direct measurement on the void fraction as it might change due to the vibration effects with a full scale analyses.
- (v) To predict the instantaneous bubble velocity in a vertical gas-liquid two-phase flow due to vibrations.

1.6 Scopes of Works

In order to conduct the above experimentation, a proper shaker that can replicate the vibration produced by a scale of heavy disaster shakes is needed. A shaker or better explained as the vibration platform was designed, developed and constructed for this purpose. It met some criteria of ground acceleration and frequency during the earthquake but very limited to vertical movement only due to the limitation of the current situation in term of financial, expertise and time. Besides, the purpose of the current experimentations were put more concentration on the development of two-phase flow facility.

In many power and processing plants, there are a lot of configurations of systems that hold the working fluid, which could be the single- or two-phase flow. The current study tried to tackle as many aspects as possible in the problems of two-phase flow under the influence of a class of heavy disaster shakes such as earthquake as discussed above. The first step was to see the behavior of rising bubble in a two-dimensional column where the investigation concentrated on bubble shapes, change of sizes, rising trajectories, velocities and interaction among bubbles. This is a very important approach since the result can be applied as prediction of the pool boiling in a container where this kind of situation can be found in many fire tube boilers in conventional thermal power plant and boiling water reactors (BWR) in nuclear power plant.

Beside the analyses on the safety factor for the power plant, the application of the vibration on the bubble column can contribute to better understanding on the mechanism of processing with applying the concept of mass transfer. Vibration can increase the gas-liquid mass transfer coefficient which is often a beneficial effect on the reactor performance.

For most of the very important case, the piping systems in processing and power plant is the aspect that should be concentrated on. In these piping, the working fluids are transported into the various parts of the plant for many kind of applications. The behavior and dynamics of these fluids determine the efficiency of the systems and therefore they must be managed, controlled and treated well. In the event of the earthquake, the vibration will hit the plant and thus will agitate the whole flow system and therefore, it is predicted to cause serious damage to the plants such as piping systems and fluid containers. As mentioned above, it is very critical when the system deals with high temperature fluid such as boiling and condensation, as many equipment in the industrial scale utilize the heat for processing purposes and energy transportation.

For example, the heating elements in the water tube boilers in conventional thermal power plant and the control rods in the pressurized water reactors (PWR) that has high temperature fluid working on their surfaces, in the form of single- or two-phase flow. For two-phase flow, particularly for boiling application, the liquid film thickness on the heating wall is one of the critical parameter that must be taken care since the depletion of this liquid film will result in the loss of coolant accident and thus will cause the core meltdown and lead to major explosion. The vibration in this case, can be predicted to change the normal condition of the flow and will contribute to change of flow pattern that promote to quicker dryout on the heating surfaces and lead to the accident as discussed. With latest technology that can sense the seismic motion, knowing the behavior of the fluid in the flow channel can help the arrangement of better prediction to avoid such tragedy to happen and very much important if casualties can be avoided.

In order to achieve this part of familiarity, a proper investigation must be carried out and thorough analyses are in very high demand. The current study made an approach to investigate many aspects of air-water two-phase flow as widely encountered in many processing and power plant applications. The analyses on the behavior of two-phase flow under the influence of vibration are such as the flow patterns, the patterns transition and the re-mapping of these patterns as they change due to vibration impact as additional force. For this investigation, the methods of flow patterns identifications are discussed. They were analyzed for a considerable range of flow condition as to meet certain criteria in the industrial application of two-phase flow and details discussion are carried out in this thesis.

The dynamic aspects of the two-phase flow regarding the influence from vibration were investigated based on the fluctuation of volumetric gas rate in the flow channel or simply termed as void fraction. The terminology and definition of void

fraction are described in detail to provide a clear objective of the current work. The investigations are including the examination on how the vibration will contribute to the fluctuation of the void fraction value from original as recorded during the steady state condition (without vibration) and details analyses were carried on the spread between the maximum and the average value. This analysis is very important in order to present that the average value of void fraction as normally used for analyses during the steady state can be totally useless since vibration drastically change the whole situation of the maximum value. In this dissertation also, these data were examined using the Drift Flux Model (Zuber and Findlay, 1965), a famous void fraction analyses model.

1.7 Development and Analyses

In order to conduct the above measurements, a systematic sensor has been developed and installed in the flow channel. This sensor is therefore becoming one of the important facilities for two-phase flow experimentation at the Thermal-hydraulics and Power Plant Laboratory, Department of Mechanical Engineering, University of Malaya, Malaysia (Appendix 1.3). The performance of this sensor has been validated by the calibration conducted both for the static and dynamics methods with tested reliability on many parameters including the void fraction and liquid film thickness on the wall of flow channel.

In view of the practical importance of the drift-flux model for two-phase-flow analysis in general and in the analysis of nuclear-reactor transients and accidents in particular, the distribution parameter and the drift velocity also being extended as part of the investigations in the current study. The bubble instantaneous velocity due to vibration has been investigated since this parameter determines the capacity of the flow system to change the flow patterns where as a result will contribute to major problems and accidents as discussed.

It has been mentioned and discussed for so many time as the above that the vast applications of the two-phase flow for processing and power plant involve with heat transfer and high temperature fluid. However, throughout the current work, the heat application was not possible due to many aspects of limitations. Therefore all the experimentations were carried out based on the two-phase flow at the atmospheric pressure and room temperature conditions as replication for the real condition. This condition however, very well met many criteria of the heat application which is very importantly in terms of ratios of void fraction that determine the condition during heat addition into the flow in pipes.

In addition, the flow conditions that applied here are the combination of wide range of gas and liquid superficial velocities and very much suited the conditions of industrial applications with working fluid of air and water. The experimental rig also has been designed with very sophisticated and reliable instrumentations and very well calibrated. The outcome of this work is actually a first move to provide the database for two-phase flow under the influence of vibration in wide range of flow conditions. Therefore, it would be a new chapter in this subject and sketch a new history in the field of two-phase flow.

2.1 Fundamental of Two Phase Flow

Two-phase flow can theoretically be described as the simultaneous flow of two of any of the three discrete phases; the gas, liquid and solid, of any substance or combination of substances. It is therefore can be defined as the interacting flow between two phases either gas-liquid, gas-solid or liquid-solid flow. The motion of the flow, whether it is slow, fast or at high speed will influence the interface between those phases (Butterworth, 1975 and Hewit 1996). Two-phase flow is also separated or classified into various kinds of model, where they are referred to the way of examining the existing behavior and pattern in a particular condition.

In general, there are three ways of exploration of the two-phase flow models. The first or the most classical would be the experimental approach through laboratory scales referring to industrial scales that is equipped with appropriate instrumentation, where it is practiced as far as 1950s such as, works by Sterman (1956), Hughmark (1962), Serizawa (1972), Gardner (1980) and many more to be listed. The second is via the theoretical studies based on the calculation and correlation with the support from the previously obtained experimental data and they can be referred in early works by Barcozy (1962), Gregory et al. (1978), Mukherjee et al. (1983), and a lot more until as recent as, Vallejo and Reiriz (2011). The third and most increasingly grow of works is via the modeling and analyses using the Computational Fluid Dynamics (CFD) which has been speed up parallel with the development in computer technologies. Some of the analytical and CFD works in two-phase flow are such as by Kataoka et al. (1987), Huq et al. (1992) and Okawa et al. (2002).

As the two phases flow together in the same dimensional area it become a very complicated mixture of flow, and therefore the analysis of this flow system also becomes very challenging. In some analyses, in order to simplify the work and to be able understand easily, certain assumptions are needed and it is particularly very

important to define the boundary conditions of the two-phase flow (Lenzinger and Schweizer, 2010). For most convenient cases, the two-phase flow can be treated as one-dimensional flow and it becomes easy to study the continuity relationship to obtain the single- and two-phase energy and momentum (Wallis, 1969). The respective distributions of each phase in the two-phase flow are really important in order to identify the characteristics of the flow. The fundamental information in two-phase flow such as heat transfer, flow pattern, void fraction, phase distribution and pressure loss are all related parameters in the two-phase flow study. There are abundant of information that will guide the analyses using these parameters, such as excellent works performed by, Scott (1962), Zuber and Findlay (1965), Taitel and Duklear (1976), Revankar and Ishii (1992), and a lot more.

In this work, the two-phase flow system is concentrated on the mixture of gas-liquid, and in particular the discussions are mostly focus for the cases of air-water flow in pipes and containers. In general, gas-liquid two-phase flows are widely encountered in many engineering applications such as the cooling systems, household equipment, thermal power plants, oil recovery/refinery plants, chemical processes, etc.

A very good knowledge in two-phase flow is the requirement for engineers and designers working in many of engineering and manufacturing sectors. This knowledge will enable the economic designs, optimization of operating conditions and assessment of safety factors for the system. For the economic designs, related information is needed by designers to optimize the system or equipment to be manufactured in the competitive market (Boccardi et al. 2008). Optimum operating conditions is the second contribution of the quantitative information from the study where the operators of the plant must decide, and the requirements on related knowledge are needed to diagnose faults and to operate at maximum capacity.

The solution to this type of problem may involve an experimental investigation of a particular geometry or two-phase flow regime which has not previously been studied, for example, the failure of boiler tubes due to flow stratification which might be able to be prevented by the changes of flow condition, and those flow condition must be based on the history of works recorded previously (Rahmani et al., 2009). Moreover, the study of two-phase flow is necessary in the safety aspect, particularly in design and analysis. Knowing the maximum safe operating limits in plant operation is really important in order to balance the optimum operation condition and safety limit of the system. For example, in some critical conditions such as nuclear reactors, the maximum heat absorbed from the fuel bundle must be carefully calculated and knowledge of the full range of operating conditions are required in order to ensure that the safety margins can be allowed (Chun and Ryu, 2000).

2.2 Two-Phase Flow in Two-Dimensional Column

In many engineering applications, liquids are usually stored in a large containers of various shapes; cylinders, spheres and rectangular. In this section, discussion on the large cylinder and rectangular containers will be focused with fluid stored inside having interchangeable of phases, or containing both the liquid and gas at the same time. An example of this kind of system is the steam generators where it produces steam from water and the phase might alternately changes as the condensation occurs. For the simplicity of analysis many workers start with examining the behavior of rising bubbles in a container such as works done by Krishna and van Baten(1999), Tomiyama et al. (2001) and, Zainon and Serizawa (2002). They performed experimentation on rising bubbles with different diameters in a two-dimensional column with a static liquid. All these studies found out that in a gas-liquid system, detail descriptions of rising characteristics of gas bubbles are quite important. As a fact, the gas bubble will move

upward in a system that has a gas bubble generation from the bottom of the vessel and in any observation, it can be seen the motion is not in a straight line. This phenomenon happens because the gas is traveling below a substance that has a higher density, then the motion will not be smooth but it is rather as a sinuous curve, depending on their sizes. This phenomenon has also been obtained around 500 years ago by Leonardo da Vinci as in the original drawing shown in Appendix 2.1 (a).

Krishna and van Baten (1999) simulated the trajectories of rising bubbles of 4, 5, 7, 8, 9, 12 and 20-*mm* in diameter and also performed experimentations in a two-dimensional rectangular column which was filled with water. They applied the volume-of-fluid (VOF) technique as the CFD tool which was also implemented by Hirt and Nichols (1981). From the simulation-experimental comparison, small bubbles at 4 and 5-*mm* diameter show large side-to-side motions similar to observations by Da Vinci. Medium size bubbles at 7, 8 and 9-*mm* diameter bubbles move like jellyfish, and another bigger size in this work, bubble at 12-*mm* diameter behave like flutter wings. They concluded that the swing of motion of the bubbles will become lower by the increasing bubble diameter. At larger diameter, around 20*mm* and above, the bubble will form a spherical cap where both the experiment and simulation agreed well. This simulation can be referred to Appendix 2.1 (b).

Another work on this issue focuses on the effects of drag forces and buoyancy on the bubble velocity while rising in a liquid column (Talaia, 2007) where it is naturally depends on the gravitational force, property of fluids and the bubble diameter as well. They investigated the terminal velocity of the bubble and concluded that the viscosity played an important role.

Many engineering processes also involve with more bubbles generation in a container such as mixing of different substances in the chemical stirrer, paint industries etc. This type of processes requires bubbles generation in huge amount or in group of

bubbles called swarms. Acuna et al. (2010) also used the two-dimensional column with spargers and high-speed camera to track the velocity of swarm bubbles of diameters 0.2 to 5-mm.

For more heavy duty processes, large volume of gas will be injected into the column for better mass transfer rate and hence the gas concentration and density will affect the process. Ellenberger and Krishna (2002), in other work, focused on the effect of gas density on two-phase flow in a two-dimensional column. They performed experimentation with pressures at 0.1 – 2.0 MPa using different types of gases and sum up that the higher densities tends to form better homogeneous flow and delay the transition of flow pattern during churn-turbulent regime. Application of bubble column in processing industries can be referred to Appendix 2.2.

A direct impact of vibrations were tested on many structures and they were reported mostly in the absent of the two-phase flow channels or equipment involved with two-phase flow. For the preparation of this thesis some literatures were selected to obtain more knowledge on the real seismic effect on the structure and therefore can provide a clear picture for the design of vibration facilities to be incorporated in the experiments.

2.3 Basic analysis on Seismic Vibrations

Seismic behavior is one the most difficult phenomena to be studied. The lack of significant activity in the 1990s on development of new power plants has faded variation of studies on the ability those facilities to stand in the event of earthquakes and other types of disaster shakes. This problem has been raised by Roesset (1998) and expressed his anxiety about only basic nature studies have been conducted without any proper experimental research concerning this problem. Roesset also brought up some issues on progress that has been made in this area such as continuation of works on

seismic studies on nuclear power plant, dam and major power generation facilities. Highlights on some issue that must be look into as future studies such as ground acceleration as a major factor to be focused with detail experimental investigation is needed.

However, until today there is no general conclusion being suggested by any scholar on the spectral response during the earthquake since it never shown the exact pattern. As the one of the most important parameters in vibration studies, the frequency of the vibration is the first to be identified. Despite of these difficulties, Smith (1972) summarized that the evaluation of vibration frequency during the earthquake is very low and is fair to be ranged as $0.06 \sim 26 \text{ Hz}$. Many of investigations on the seismic analysis however, applied a wider range of frequency as well.

Amongst all of the recorded seismic data in the history, there are two cases that always being applied in many analyses both via computational and experimental work. The seismic spectrum from El Centro earthquake which happened in 1940 and Kobe in 1995 are the most classic where they are in nearly in the form of harmonic motion of damn free vibration as reported by Park et al. (2008) and Park et al. (2009). Due to the simple form of spectral responses in these two cases, the reproduction of a similar wave could be easy and therefore has been applied in this work as well.

For the safety analysis of nuclear plant, accurate measurement of velocity and acceleration of sites were normally studied before and after the construction (Arif et al., 2012). After many tragedies involving major earthquakes around the world such as Sumatra 2004 and Japan 2011, many precautions studies have been conducted as well. Therefore the prediction of time and location for the earthquake to take place is one of the major concerns. In Arif et al. (2012) studies, they analyzed the frequency during the earthquake as $0 \sim 10 \text{ Hz}$ with large variation of magnitudes and therefore resulted in variation of velocity and ground acceleration as well.

Many structural designs also, focus on the method to minimize the vibration effects, and many devices were designed for this particular purpose. One of them is the X-plate damper (XPD) that capable to sustain many cycle of yielding deformation in high impact of vibration and damping (Bakrea, 2006). In order to design this equipment, many preliminary works were also conducted theoretically (Frano, 2009 ~ 2011), (Bommer, 2011), experimentally (Chen, 2009), (Fukuyama, 2000) or numerically (Farrar, 1995), (Ebisawa, 2000), Dimova (2002). Using numerical methods, with the avoidance of structural damages, many arrangement of complicated system including the piping system can also be conducted. In their study, Bakrea (2006) concluded that it is very difficult to implement the XPD system on the piping systems after examining the vibration characteristics and XPD properties for piping system. Therefore, again, the piping systems, particularly in high energy flow, which already a complicated and hazardous facilities having no solution when facing the seismic vibration.

With the concern of seismic vibration, studies on seismic hazard analysis on nuclear plant are studied extensively. There are many methodologies on predicting this possibility including the soil analysis, location, property of structures and many more (Bazurro et al., 1996). However, due to complication of direct analysis to be conducted on a full scale of nuclear plant, many attempts have been conducted as well on the smaller parts such as the small structures and water tanks. The seismic fragility of structures particularly the one involves with fluid is also one of the concerns in the present work. For a water retaining structure, as one of the parts that can be found in any processing and power plant, a rigid and sustainable structure for this equipment is very important. Bhargava et al. (2002) evaluated the seismic fragility on water tank and analyzed for both cases; the empty and occupied condition. They summarized that the effective pre-stress, strength of concrete and reinforce steel are some factors that may affect the structural response to seismic vibration. Seismic fragility studies on the power

plant are also studied by Dimovaa et al. (2002) on the energy dissipating devices, Cho et al. (2005) with focus on ground acceleration effects and Nakamura et al. (2010) also on the high ground motions using the 3-D Finite Element Method.

Lo Frano and Forasassi (2009) conducted an exclusive study on the effect of seismic event on the fluid structure interaction and their influence on other components associated in the systems. They focused on the sloshing effects during the event of safety shutdown system and the dynamic buckling involved in the structure to analyze the seismic induced hydrodynamics responses. The result highlighted that the structures are mostly receiving the influence from the seismic responses and particularly very strong for those containing liquid where the fluid-structure interaction are found to be more complicated in any reactor analysis against the seismic responses. This is due to generation of significant seismic load from ground acceleration during the earthquake and heavy class disaster shakes (Zhengming, et al., 2007).

As discussed above, the analyses on seismic responses on structures and structure–fluid coupling problem, many simplified theoretical methods were studied and suggested. This effort however, cannot satisfy the requirements of engineering design since there is no evident to support the analyses.

In most of the cases of analyses on the seismic effects, the shaker table is always applied and it is always a down scale model of seismic base to study the case through experiments. At the advanced research institutes with good financial background, a big scale of shaker is also available such as work by Kim et al. (2012) that used a motor driven shaker table with range of acceleration of 0.2 – 3.0 g which enable them to reproduce the real seismic capacity. In their study they focused on the seismic effects on the behavior of electrical cabinets in the nuclear power plant. Koo et al. (2010) on the other hand, used the impact hammer test for the same purpose but also imposed the impact on the shaker table. The seismic motions were reproduced using the spectral

recorded from the El Centro, Kobe and Northridge earthquakes. Using these facilities they have an agreement of 65% -75% compared to prediction results.

An immersed cylindrical shell in fluid that representing the fast breeding reactor thermal baffles has been a subject to Fukuyama et al., (2001) in their analyses on seismic sustainability design. They performed the experiments using the lateral acceleration shaker table with acceleration at the range of $\pm 15 \text{ m/s}^2$ and with motor driven shaker the frequencies are in wide range of $0 \sim 100 \text{ Hz}$.

It is therefore, very important to realize that in any analysis concerning the seismic vibration, the ground acceleration effect must be taken into account and should be the base parameter beside the seismic frequency. In more detail study, Sato et al., (2000) propose a method to evaluate underground seismic coefficients, taking into account dynamic response along the depth in horizontally multi-layered ground.

Lastly, the very least vibration effect on the power plant that must not be forgotten is the large airplane crash that from 9/11 experience has changed people perspective regarding this issue through the entire world. This subject has been studied by Petrangeli (2010) and suggested an external thick wall, capable to withstand the aircraft impact throughout their study most of the arguments are circulated around the reinforcement of the wall.

With this basic knowledge, the current study endeavored into new experimentation to investigate the effects of vibration onto the flow structures and the dynamics of gas-liquid two-phase flow. The following chapters will discuss all the experimentations works and analyses on the problems that has been discussed.

3.1 Introduction

For a real analysis on the vibration effects on any structure, the application shaker table is a very good solution. This method has been applied widely such as by Koo et al. (2010) and Kim et al. (2012). In the current study, the objective is to investigate the ground acceleration effects at a class of heavy disaster shakes such as the earthquake on the dynamics of two-phase flow in a bubble column and the vertical upward channel. Therefore, a careful analysis on the characteristic of vibrations during the mentioned event is very important. However to reproduce the same vibration spectral would be near to impossible, and hence, a close approach would be satisfactory.

In the previous chapter, a detail literature survey has been conducted and from Smith (1988), the vibration frequency during the earthquake would be fair in the range of $0.06 - 26 \text{ Hz}$ and the ground accelerations as recorded in the history are in the range of $-10 \text{ m/s}^2 - 10\text{m/s}^2$. This argument has been supported by Fukuyama et al. (2000), Bieloret al. (2000) and as recent as Ariefet al. (2012). The reproduction of vibration spectral during the earthquake can also be carried out using the recorded data as such the El Centro or Kobe as shown in figure 3.1 and 3.2, but require very high technology and expensive instrumentation.

As shown in these figure, the both spectral responses having high fluctuation and damped harmonically in the time domain. Furthermore, the designs and constructions of shaker tables that replicate this type of resonance are mostly based on the lateral motions; where else the real occurrence of earthquake is actually in vertical direction impact. An example of sophisticated shaker table can be referred to Appendix 3.1. Since the current study has a bigger objective which is to observe the effects on the gas-liquid two-phase flow, and in general as an approach to examine the effect of vibration onto the working fluid in power plant, a basic facility such as a shaker table that can generate a scale of vibrations as discussed above is satisfactory.

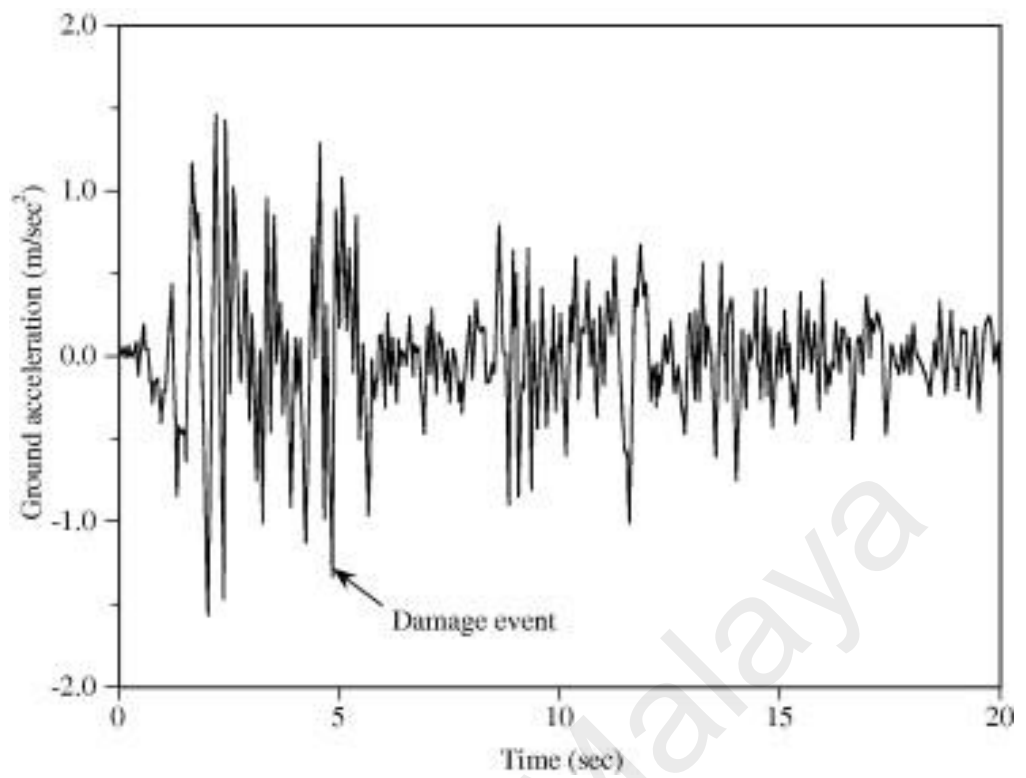


Figure 3.1 : Seismic spectrum of El Centro earthquake in 1940, (Park et al., 2008).

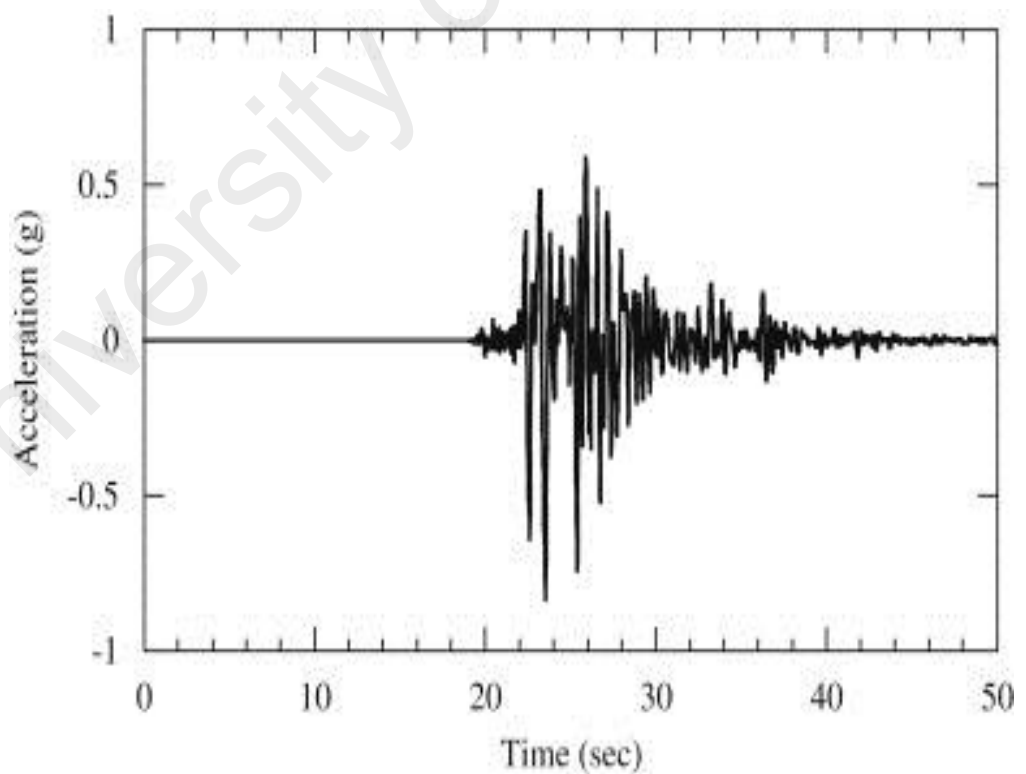


Figure 3.2 : Seismic spectrum of Kobe earthquake in 1995 (Park et al., 2009)

The major concern with this shaker table is to fix a certain parameter in order to obtain an accurate and a steady measurement and also to avoid the complication of data analysis. With the recommended vibration frequency as in the mentioned range, and particularly, the ground accelerations as the most important parameter during a class of heavy disaster shakes, focus should be paid on the variation of this parameter. In view of this, a fix frequency for the entire analysis and throughout this work can be applied for the development of a shaker table.

3.2 Basic Analysis on the Damped Free Vibration

In order to recount the motion of the vibration platform, a basic study on the harmonic damped free vibration has been conducted. Figure gives the whole idea on how the vibration platform has been designed to replicate some characteristics during a heavy disaster shakes such as the earthquake as applied in this work.

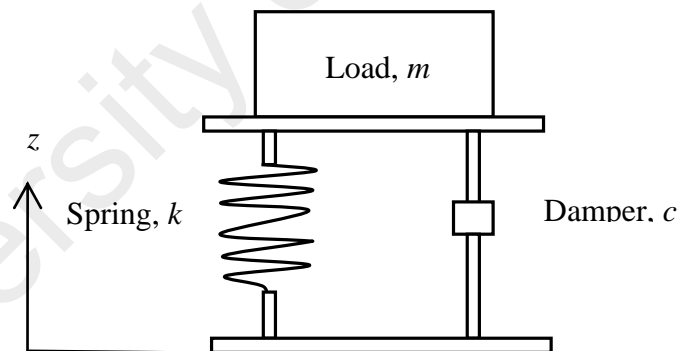


Figure 3.3 :A simple system of damped free vibration

Let us consider a load with mass, m rest on a system with a spring constant, k and damping coefficient c . From the energy balance, the equation of motion can be written as,

$$m\ddot{z} + kz - c\dot{z} = 0 \quad (3.1)$$

dividing equation 3.1 with m , gives,

$$\ddot{z} + \frac{k}{m}z - \frac{c}{m}\dot{z} = 0 \quad (3.2)$$

and can be rewrite as,

$$\ddot{z} + \omega^2 z - 2\xi\rho\dot{z} = 0 \quad (3.3)$$

where,

$$\omega^2 = \frac{k}{m}, \quad 2\xi\rho = \frac{c}{m} \quad \text{and} \quad \xi = \frac{c}{2\sqrt{mk}} \quad (3.4)$$

and hence, the frequency for the system can be written as,

$$f = \frac{\omega}{2\pi} = \frac{1}{2\pi} \sqrt{\frac{k}{m}} \quad (3.5)$$

Here, ω is the angular velocity, ξ is the damping ratio and ρ is the spring material density. Solving equation 3.1 to find the final solution for displacement and can be rearrange as,

$$\begin{aligned} z &= e^{-\xi\omega t} \left\{ z_0 \cos\omega_d t + \frac{z_0 + \xi\omega z_0}{\omega_d} \sin\omega_d t \right\} \\ &= a e^{-\xi\omega t} \cos(\omega_d t - \psi) \end{aligned} \quad (3.6)$$

Here, $a = \sqrt{z_0^2 + \left(\frac{z_0 + \xi\omega z_0}{\omega_d}\right)^2}$ is the eigen-value amplitude and

$\psi = \tan^{-1}\left(\frac{z_0 + \xi\omega z_0}{\omega_d z_0}\right)$ is the phase angle.

Figure 3.4 shows the behaviour of harmonic motion in a damped free vibration as discussed in equations 3.1 ~ 3.6. This figure suggests that the motion of a system under this condition would have decreasing amplitudes as it damp in time. The same phenomenon would also happen to the acceleration, where the smaller amplitudes would have weaker accelerations and therefore would exhibit the same spectral as in this figure and open the possibility for the reproduction of acceleration spectrum similar as in figure 3.1 and 3.2.

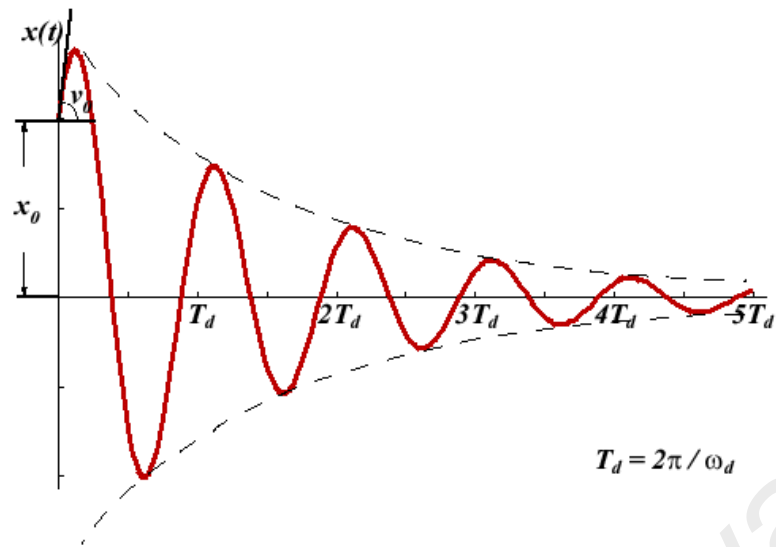


Figure 3.4 : Depiction of harmonic motion in a damped free vibration

3.3 Construction of Vibration Platform

Based on the theoretical studies as discussed above, a small shaker table or will be addressed as **Vibration Platform** throughout this thesis was constructed. It was made with design configuration as shown in figure 3.5 and the real platform is as shown in figure 3.6. All the three plates were made using the aluminium plate with thickness of 10 mm. The static plate that hold the two-phase flow experimental apparatus is connected to the active plate by four stainless steel pillars or called legs. The active plate is then connected with four piston rods where each of them is supported by four iron springs with constant of 0.1658 kgf/mm each that made a total of, $k=0.6632 \text{ kgf/mm}$ for the whole composition. This plate will move up and down vertically where the piston rod will be pulled and released for the purpose of damped vibration and continuously shook by pedal. From the relation in equation 3.5, the vibration frequency of this platform is determined and varied by the total mass of load placed on it. With test load of 50 kg in mass, the frequency was obtained at 2.5 Hz and this is in the range of target from the design phase and in more detail, the range of frequency that can be applied using the current vibration platform is listed in Table 3.1.

Table 3.1 : Range of frequency based on the applied mass with
spring constant of 0.6632kgf/mm

Mass, kg	Frequency, Hz
50	2.5
75	2.0
100	1.8
150	1.5

For the current work, since there were two different of experimental apparatus have been applied, there were some adjustment of the total mass on the vibration platform that has been carried out in order to maintain the frequency at 2.5 Hz . For the two-dimensional column rig, the mass would easily meet 50 kg , but the vertical upward two-phase flow rig would be lighter, and therefore, extra load has been put together.

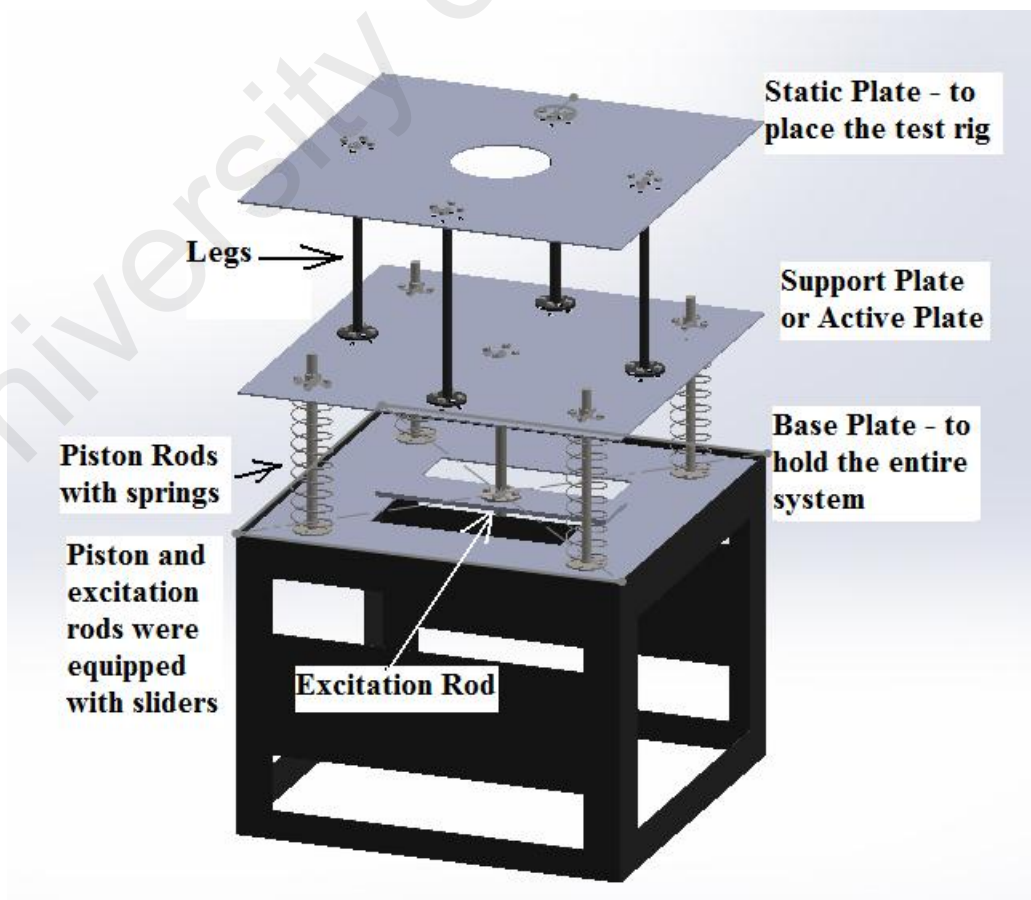


Figure 3.5 : Configuration of the vibration platform

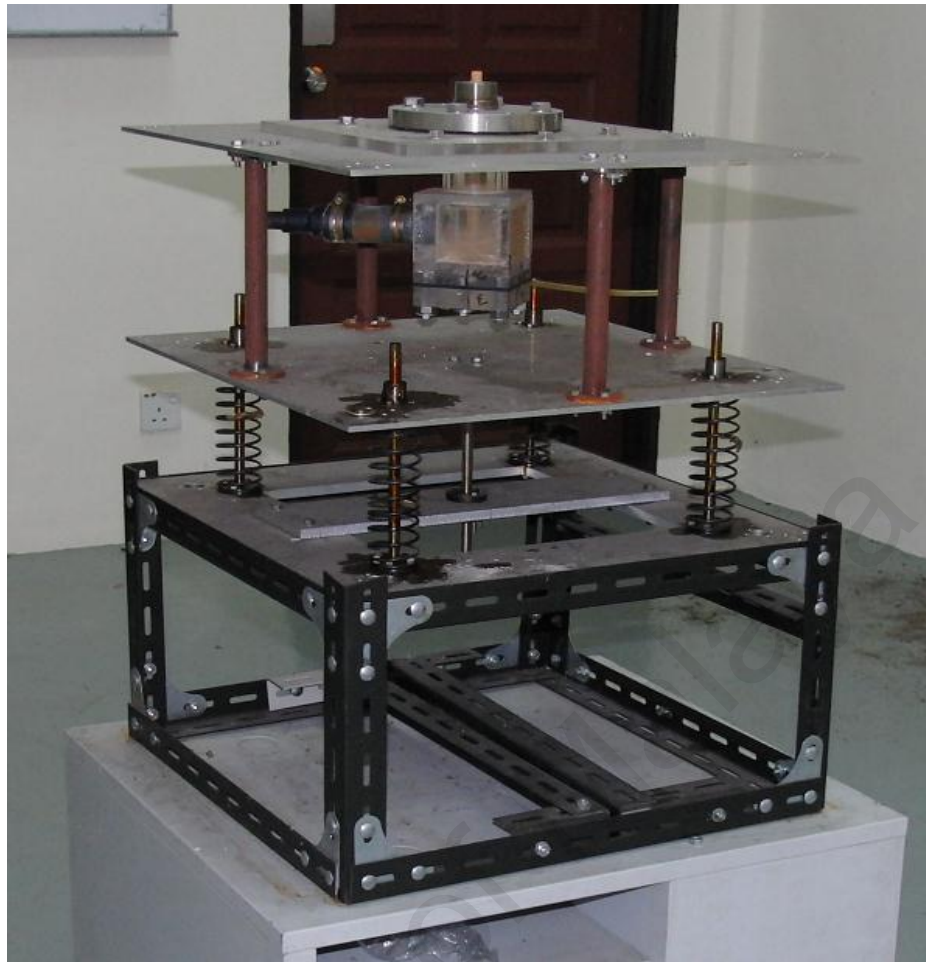


Figure 3.6 : Actual photo of the vibration platform

As in figures 3.5 and 3.6, this platform is constructed to move vertically with the direction of acceleration is as good as the real ground acceleration and can be represented on the z -axis, giving a clear expression of positive and negative values. This vibration platform has an ability to produce a simple harmonic damped free vibration spectrum in the expected range of acceleration. As discussed above, the basic principal of this platform is by pulling the excitation rod, up to certain amplitude for the required ground acceleration and release to let it move in a harmonic vibration and damped naturally by the spring damping coefficient. Therefore the sizes of accelerations are determined by the selected vibration amplitude, and the frequency which is subjected to the total load on the platform as shown in equation 3.5 and 3.6. In the current study, these vibration accelerations were classified into four modes as in Table 3.2.

3.4 Measurement of Ground Accelerations

By fixing the vibration frequency at 2.5Hz , Mode M1 of the vibration is classified based on the 10-mm amplitude which gives a fluctuation of vertical acceleration in the range of $\pm 3\text{ m/s}^2$. Similarly, Mode M2 was set as a bigger shakes based on 20-mm amplitude that produces acceleration at $\pm 6\text{ m/s}^2$ as well as Mode M3 that based on 30-mm amplitude with acceleration at $\pm 10\text{ m/s}^2$. The largest shake obtained in this experiment is Mode M4 at amplitude 40-mm which is the highest limit allowed by the current spring, produced the ground acceleration at $\pm 12\text{ m/s}^2$. A result of spectral wave by damped free vibration obtained from theoretical calculation of which the calculation code is shown in Appendix 3.2 is plotted against the experimental result for vibration with mode M2 in figure 3.7. For a clear figure of these modes of vibration, the details are listed in Table 3.2, which shows that the scale of vibration applied in this work are varied by changing the initial amplitude.

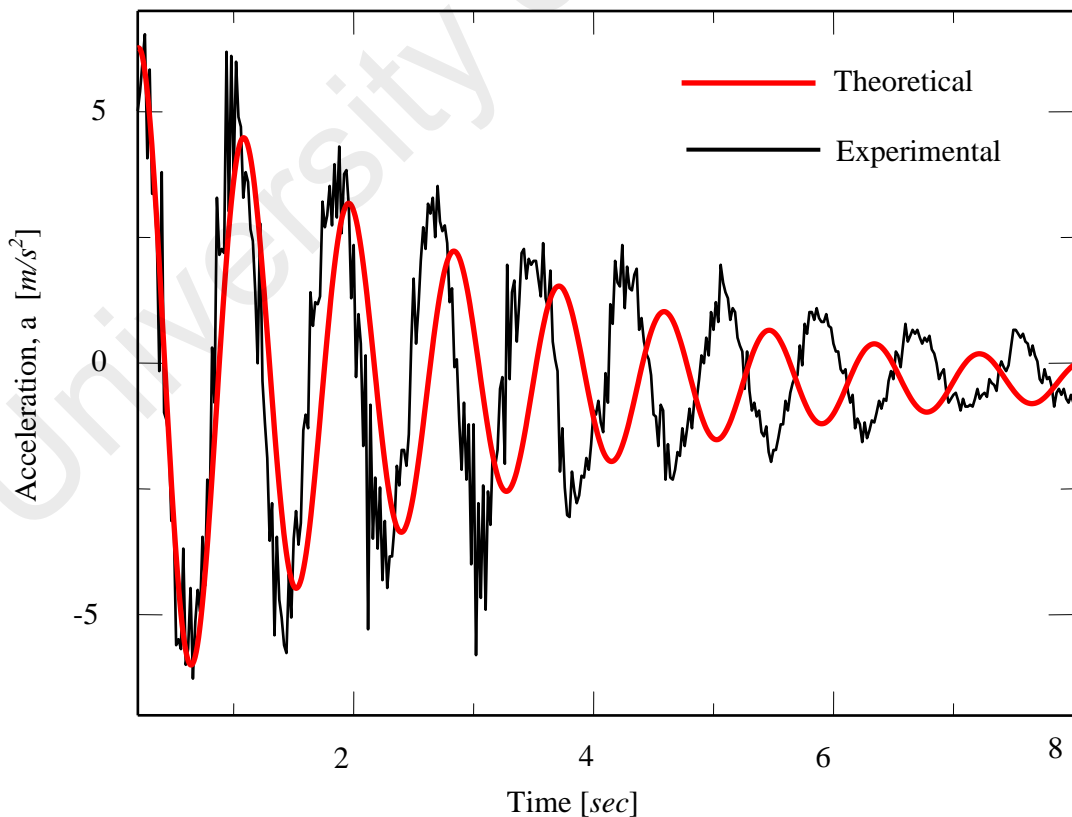


Figure 3.7 : Comparison of vibration spectra : experimental versus theoretical

Measurements of the ground accelerations produced by this platform were recorded by the Kyowa Electric Co.'s PDC-300 and transferred the numerical data into the personal computer. This device has capability to detect the acceleration in 3-dimensional with range of ± 2 g. Even though the current study only concentrates on the vertical acceleration, in the real application however, there also exist small lateral vibrations on the x - and y -axis, due to imperfect reciprocating motion on the z -axis. This effect is very small and can be neglected and hence, only the vibration on z -axis was considered for the entire analyses in this work. Figure 3.8 shows all the four modes of vibration applied in this entire works with the range of ground accelerations as listed in Table 3.2.

Table 3.2 : Modes of Vibration

Modes	Amplitude, <i>mm</i>	Approximate Acceleration,	
		<i>m/s²</i>	(<i>gal, g</i>)
M1	10	± 3	(0.3)
M2	20	± 6	(0.6)
M3	30	± 9	(0.9)
M4	40	± 12	(1.2)

Referring to the El Centro and Kobe earthquakes spectral, respectively in figures 3.1 and 3.2, the ground accelerations produced in both of the cases are about the same as listed in Table 3.2 and figure 3.8, even though the El Centro's data seem a little higher. In term of the spectral wave, it also has some similarities, which suggest that this vibration platform has been designed in order with the requirement of the scale of vibration from the earthquake. In fact, for more details investigation, it has been found that there is no fix pattern spectrum produced by different occurrence of earthquakes and therefore, the resonance produced this vibration platform can also be accepted.

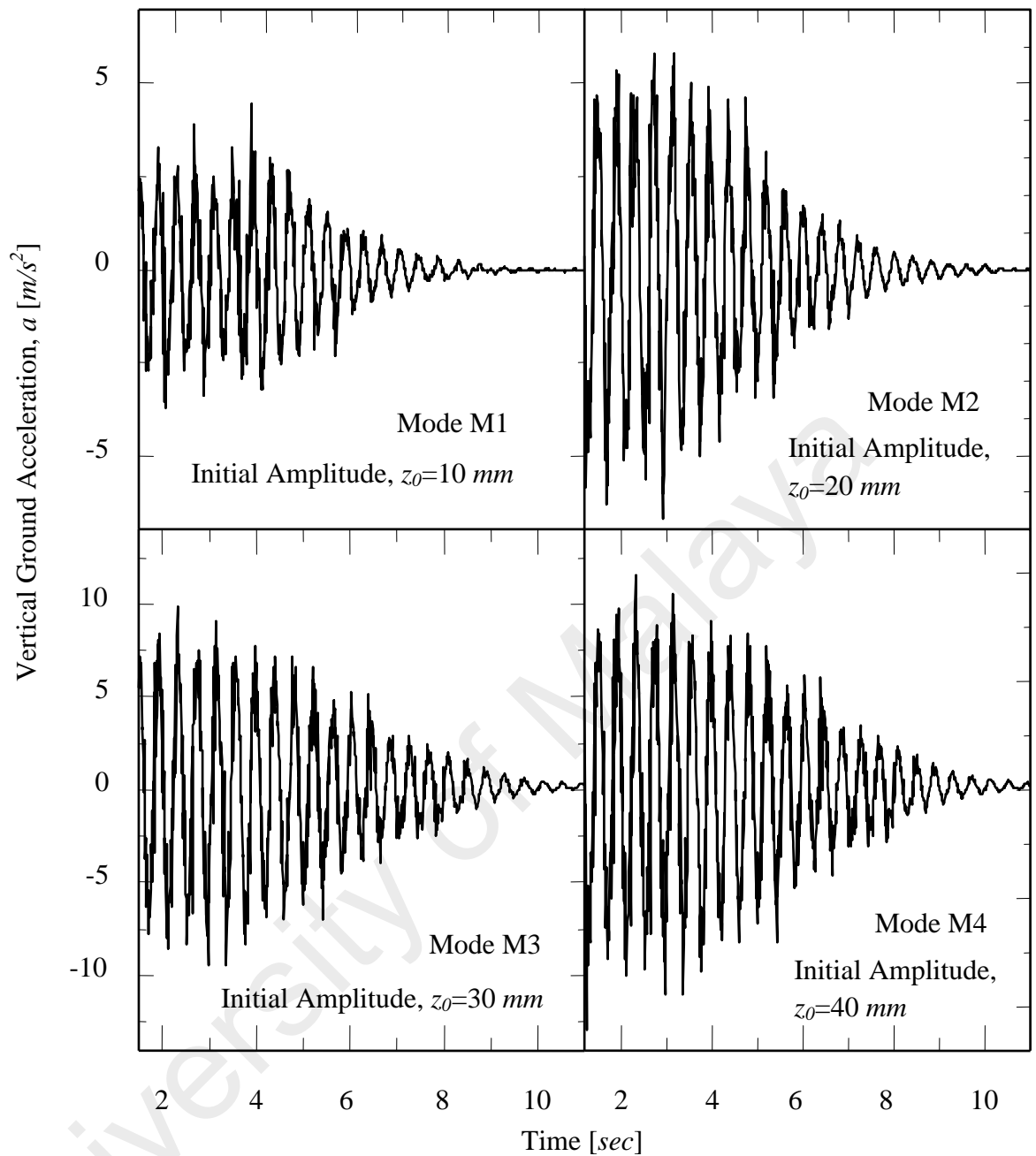


Figure 3.8 : Acceleration spectra for four modes of vibration by four different amplitudes (tested based on $f=2.5Hz$)

In addition, there is another mode of vibration that also has been considered in this work, which is a continuous harmonic vibration as shown in figure 3.9. The application of this mode is due to some practical importance such as in processing industries where the requirement of longer time for mixing of substance is essential (Ellenberger and Krishna, 2003). This mode is based on the amplitude of 20-mm, and it

is particularly applied in analyses of flow patterns and void fractions, as described in detail in sections 7.1 ~ 7.3.

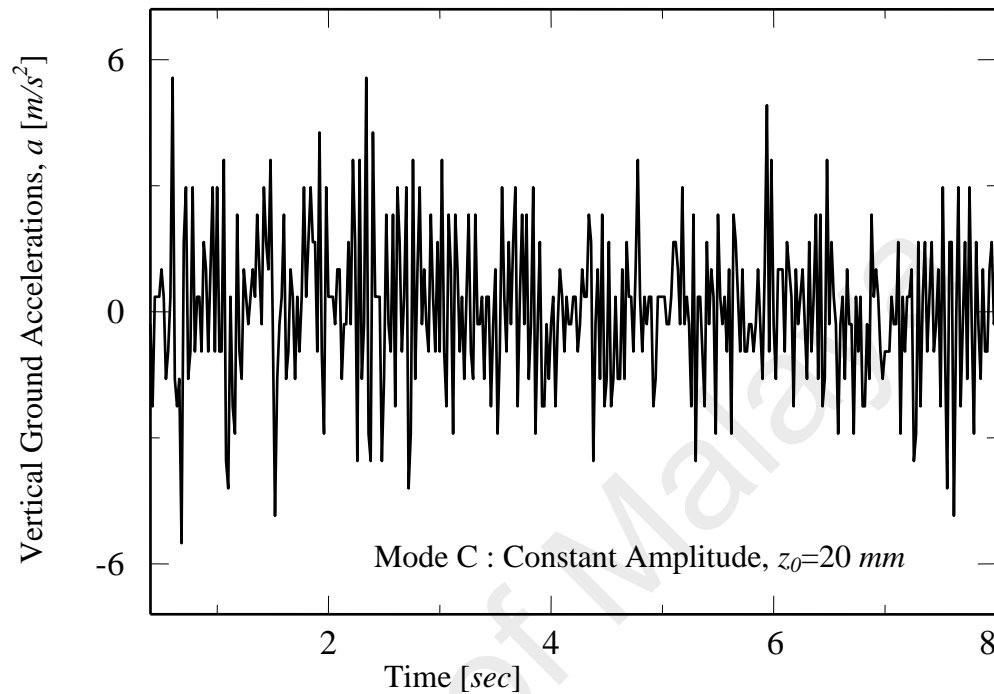


Figure 3.9 : Acceleration spectra for continuous vibration with amplitude 20-mm

With successful measurement as the above results, this vibration platform is applied in all of the experimentations to study the effects of vibration onto the flow structures and the dynamics of gas-liquid two-phase flow in this work. As mentioned in the previous section, this platform is very simple where it only uses the concept of pull and release, and it takes around 5 ~ 7 seconds to damp and fade, producing the spectra as in figure 3.8. For continuous vibration, it is pulled and shook using the pedal installed at the bottom of the experimental table. Throughout all of the experimentations, the vibration data were measured along with other required data such as voltage fluctuation during the void fraction and the photographic data for flow patterns investigations.

4.1 Introduction

The first chapter has discussed about very few effort that has been paid on the studies on the behavior of fluid in containers that affected by the vibration, particularly for a working fluid in power plant or heavy machineries. It would be more complicated, if they were in engineering application that involves the two-phase flow. For example, in a gas-liquid system, detail descriptions of rising characteristics of gas bubbles are found to be quite important. In short, the gas bubble will move upward in a system that has a gas bubble generation from the bottom of the vessel and since it is traveling below a substance that has a higher density, the motion is however will not be smooth as a straight-line but it is rather as a sinuous curve, depending on their sizes. In nuclear reactor safety steps and precautions, safety shutdown system (She et al., 2012) was introduced.

However, considering on the natural phenomena such as boiling in the reactor that could not be stopped instantly, there should be an analysis that can predict the behavior of the two-phase flow in such system that experience a situation of those serious impacts. Similarly, in various systems that has a multi-phase flow as a working or containing fluid should also consider this safety analysis. In this study, as a first move, the focus has been paid on the behavior of the rising bubble in a two-dimensional column of liquid that experience a vertical vibration and the motions were compared with the situation without the vibration. Vibrations with a wide range of vertical accelerations were reproduced to achieve a class of heavy disaster shakes such as an earthquake and they are with similar characteristics in numbers of categories as in the previous chapter and their influences onto the rising bubbles were then investigated in various parameters. This investigation however, was conducted mainly to serve as an observation on the phenomena of vibration effects and therefore has been performed with minimum measurements.

4.2 Experimental Setup and Methodology

The apparatus for this particular investigation is as shown in figure 4.1. The test vessel was constructed from a rectangular acrylic channel of dimension $0.2m \times 0.2m \times 0.4m$ and installed on a vibration platform as described in the previous chapter. Experiments were conducted for air-water two-phase flow systems in the case of stagnant water. In this case, air was fed up from the compressible air tank or air bomb and channeled via various diameter of nozzle submerged at the bottom of the vessel to generate bubbles. Nozzles with different inner diameters of 0.5, 0.8, 1.5 and 5.0- mm were replaced in every set of experiment in order to produce different sizes of bubble.

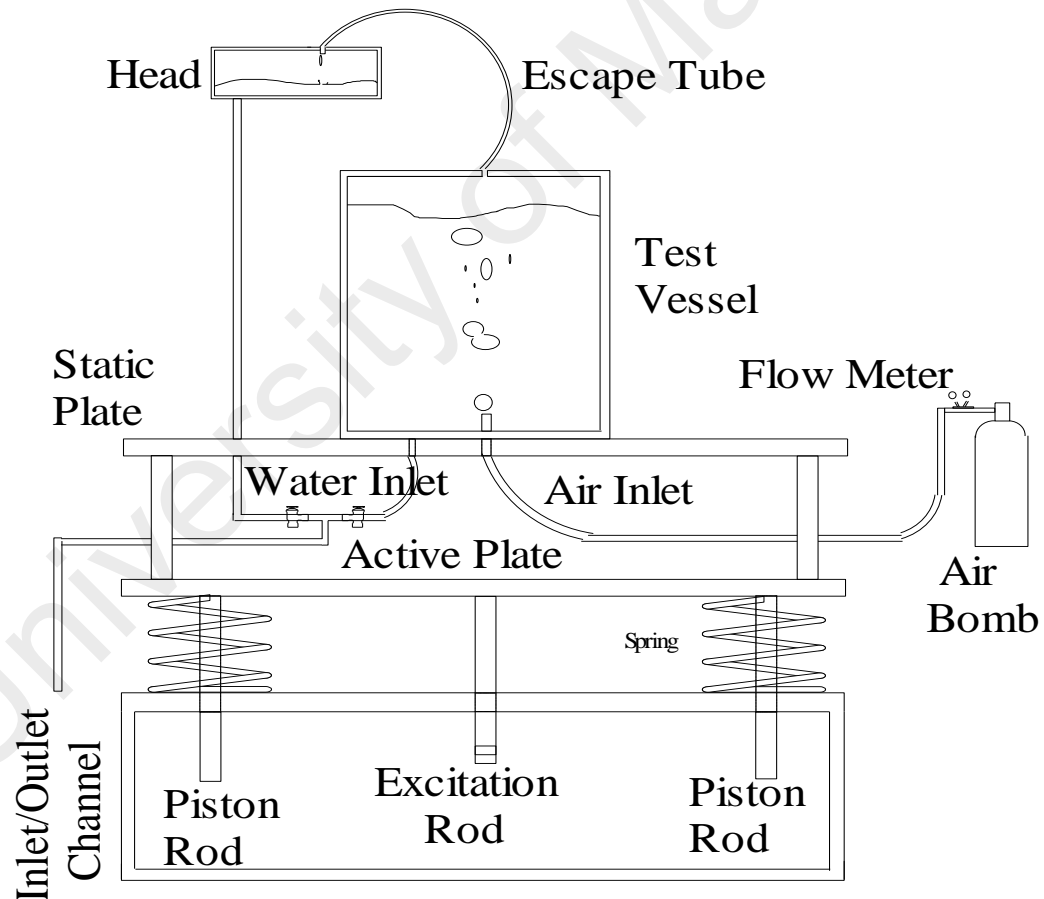


Figure 4.1 : Experimental apparatus for vibration effects on bubble behavior in a 2-D column

In order to reduce the effects of surface sloshing, that can influence the motion of the bubbles, water is maintained at fix level. In this case, the head at the above of the test section re-circulate the water into the test vessel to fulfill the vessel up to ceiling. Hence, the effect of water surface fluctuation to the rising bubble could be reduced and can be neglected. Air flow rate were measured from a low flow rate at 10 mL/min to obtain a solid single bubble to 1000 mL/min to obtain the swarm bubbles at every single nozzle in every set of the experiments. The acceleration data from vibration is recorded into a PC with a real time observation of resonance spectra. Rising gas bubbles were recorded by a Canon Fastcam-Rabbit high-speed video camera at 400 frames per second with shuttering speed of $1/1000$ seconds.

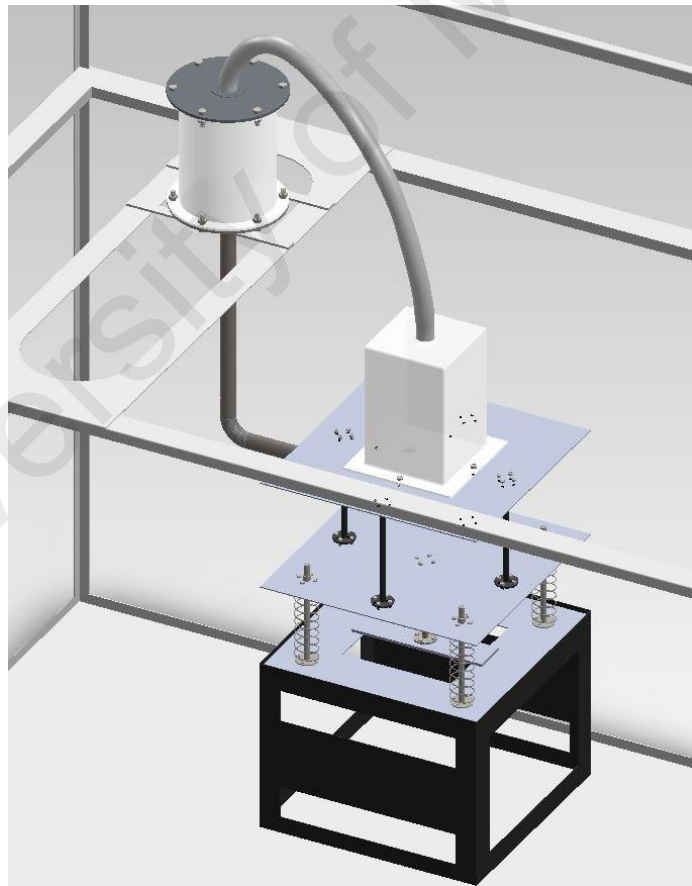


Figure 4.2 : A 3-D Configuration of the apparatus for vibration effects on bubble behavior in a 2-D column

4.3 Results and Discussions

4.3.1 Typical Trajectories of a Single Bubble

In most of the literatures, such as discussed in chapter 2, many researchers such as Tomiyama et al. (2001) and Vandu et al. (2004) reported that the rise characteristics of a bubble are strongly dependent on the bubble sizes. In this investigations, bubbles with diameter sizes at $2 \sim 7 \text{ mm}$ were generated by a constant air injection at a very low flow rate ($10 \sim 25 \text{ mL/min}$) accordingly to the inner diameter of the nozzles. Photographic results of the rising air bubbles, which obtained from the high-speed video camera, were analyzed to determine every single coordinate of the bubbles at time interval of 0.005 sec . The typical trajectories of the rising bubbles as a sinuous motion in a non-vibrated channel is shown in figure 4.3. Example of numerical coordinate for this purpose can be referred to Appendix 4.1.

These meandering trajectories show that the excursion amplitudes in the z -direction decrease with the increases of the bubble sizes. This results agreed well with the summarized work by Krishna and van Baten (1999), which demonstrated meandering trajectories for bubbles with diameters $3 \sim 7 \text{ mm}$. Since these bubbles were forcedly released, they show high interface oscillations. However, the sinuous curved drawn by their motion are also with two modes, the zigzag and helical as stressed by Tomiyama et al.(2001) that bubbles with small diameter (3-mm and below) also rises with helical motion. In this experiment, this motion is observed by naked eyes and could not be proved by any single evident since the motion of these rising bubbles were photographed two-dimensionally.

For longer travel such as presented by Hayashi and Tomiyama(2012) where bubbles rising in a 4-m column, the meandering trajectories were much obvious in both of the two modes of spiral and helical, which unfortunately unable to be presented in this work due to limitation of column instruction that has other objective on vibration effects.

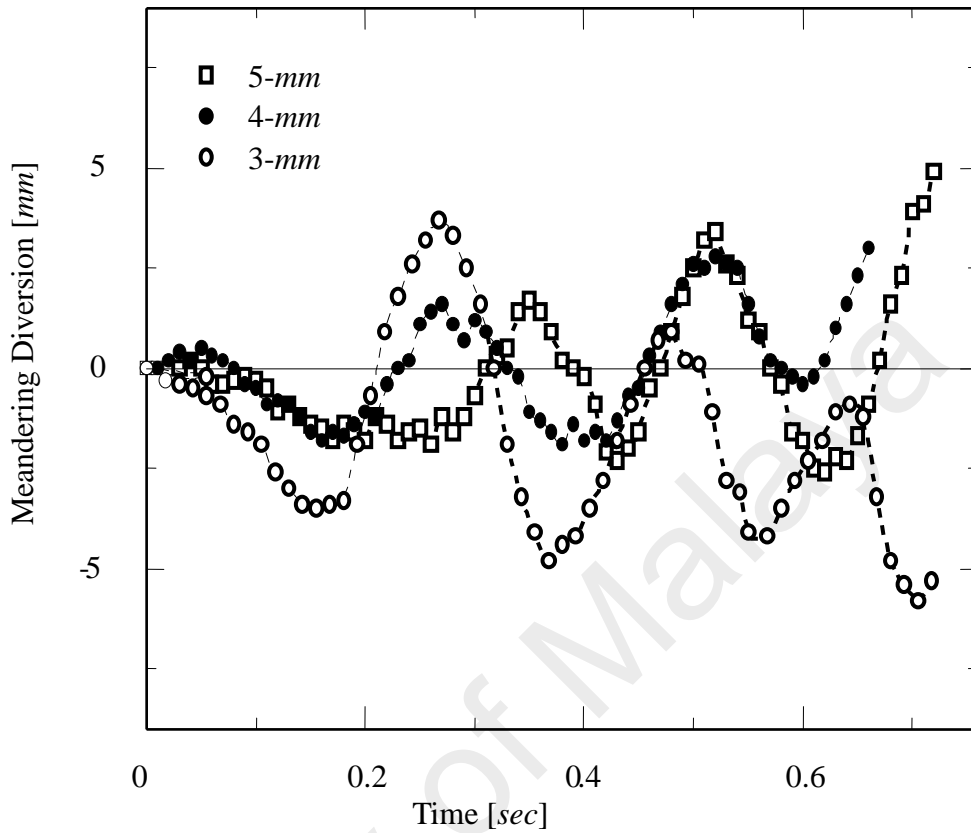


Figure 4.3 : Meandering trajectories of three single bubbles

4.3.2 Vibration Effects on the Rising Bubble

(a) Vibration Modes

With an objective to investigate the effect of the heavy shakes on the rising bubbles, their motions were recorded when the shaker as shown in figure 3.6 was vibrated vertically. It would be a satisfaction if various parameters involved here can be related in many ways so that it could be convenient for the prediction in various applications. In short, the relation of bubbles sizes and mode of vibrations to describe the effect of vibration onto the behavior of the rising bubbles can be presented for this purpose which therefore offers quite beneficial information for future analyses.

Figure 4.4 shows the trajectories of bubbles with 4-*mm* diameter under four modes of vibrations as described. Obviously as compared to the non-vibrated channel as shown in figure 4.3, they are diverted far from the meandering line. For comparatively low acceleration, for example with modes M1 and M2, diversions were seen with maintaining of the sinuous motion but some notable diversion from the meandering line can be seen. The increases of vertical acceleration, where in this situation explained by higher modes, resulted in bigger diversions of the gas bubble trajectories, very far from their meandering line. The excursions amplitude is no more as meandering trajectories and sometimes they break the order of the sinuous curve motion as discussed, as clearly observed for the trajectories under vibration in Mode 3 and 4. Hence, in short it can be summarized that the rising bubbles were strongly affected by the sizes of vibration.

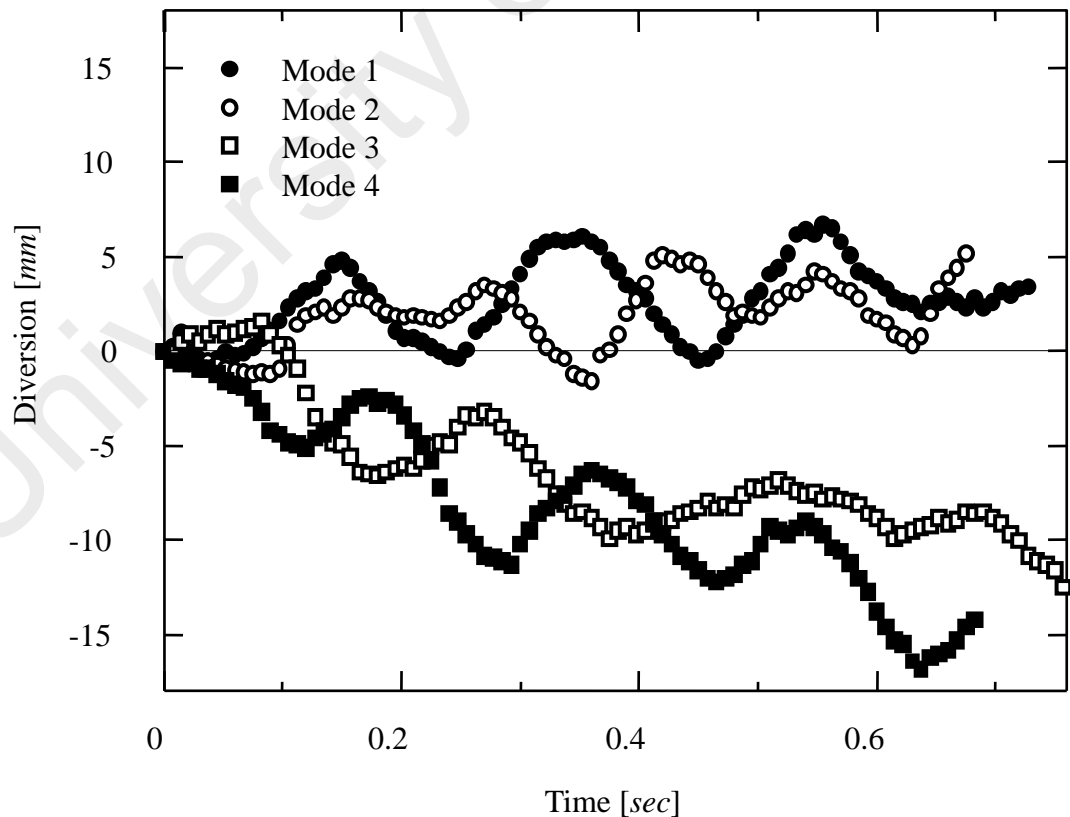


Figure 4.4 : Bubble trajectories under the influence of four modes of vibration

By receiving the vertical acceleration as extra forces, the shapes of these bubbles were distorted from the beginning when they were released from the nozzle and these interface oscillations are continuous as they traveling up the column with large lateral movement. The example of these phenomena is shown in figure 4.4. There is no big distinction on these shapes oscillations however as to compare with the non-vibrated channel but in this case, the oscillations are quicker and they show less continuous helical motion.

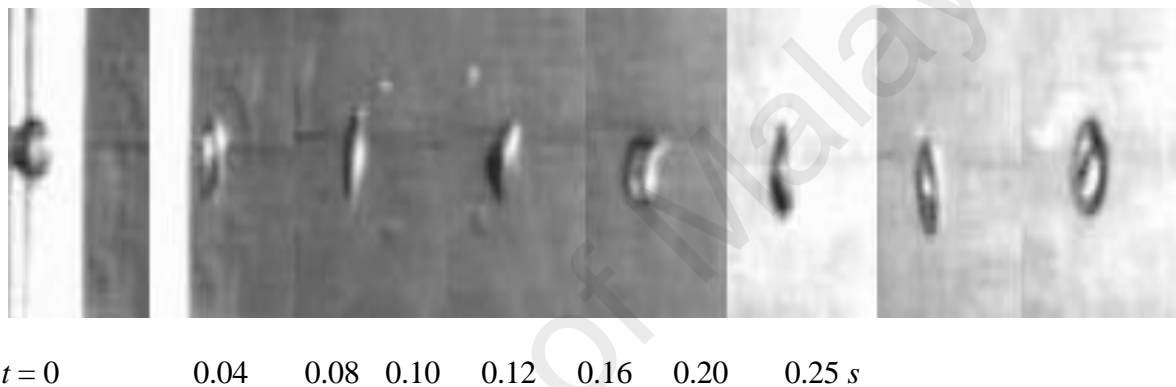


Figure 4.5 : Shape oscillations during the rising under vibration with mode M2

In this case, the vibration not only disturbs the trajectories of the rising bubbles, but it also affects the shapes of the bubble when they travel upward. It is obviously observed that they made a self-rotation while rising upwards and sometimes moves backward and continues traveling upward as in figure 4.5. This phenomenon happened due to the up-down oscillations of the external vibration which somehow also move the liquid together even though the surface level was fixed. With bigger accelerations, the sizes of the released bubbles were disordered. Sometimes there was a big bubble formatted at the nozzle and as they move upwards, their shapes were badly damaged and up to certain stage they dispersed forming small sized of bubbles as shown in figure 4.6.

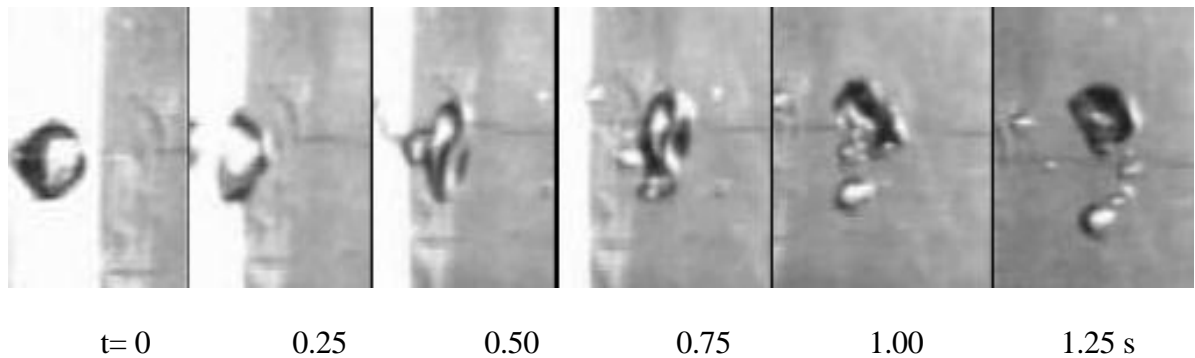


Figure 4.6 : Shape oscillations and damage under vibration with mode M4

The initial stage from results in figure 4.6, with formation of a big bubble whether it was affected by the additional acceleration or not, give an image for the theoretical equation introduced in literatures by Wallis (1979) as well as Davidson (1963), as follows.

$$v_b = 1.138 \frac{Q_G^{6/5}}{g^{3/5}} \quad (4.1)$$

where v_b is the volume of formation bubble, Q_G is volumetric gas flow rate through the nozzle and g is the gravitational acceleration. In the future, it is desirable to confirm the validity of this equation based on the current experimental results by examining the additional ground accelerations, which are widely considered so far.

(b) Bubble Sizes

Bubble sizes that play an important role in the two-phase flow systems differ with various kinds of engineering applications and this parameter would strongly influence the behavior of the rising bubbles. As observed in figure 4.3 that the excursion amplitude increases with decreases of the bubble sizes; hence difference sizes of solid single bubble were produced in this experiment by installing different diameter of nozzles to study how the vibration would affects them. Figure 4.7 shows trajectories of five different diameters, 3, 4, 5, 6 and 7-*mm* of single bubbles traveling in a vibrated channel with vibration in mode M3. For

comparatively small bubbles, which are with diameters 3, 4 and 5-*mm*, they were strongly receiving the influence of the ground acceleration that diverted them far away from the original path.

In this case, there were no more meandering trajectories of the excursion curve as the tradition of sinuous motion is disturbed by the external forces and they behave as a disordered curve. The rising motion of bubbles with diameters 6 and 7-*mm*, were also disturbed by the vertical acceleration, but they still exist near the meandering line but meander on different axis. Similar to the previous section, the shapes of these bubbles were badly distorted with interface oscillations were seen as well. Another observation in this investigation was the dispersed bubbles forming smaller diameter bubbles that follow the same trajectories with other smaller bubbles.

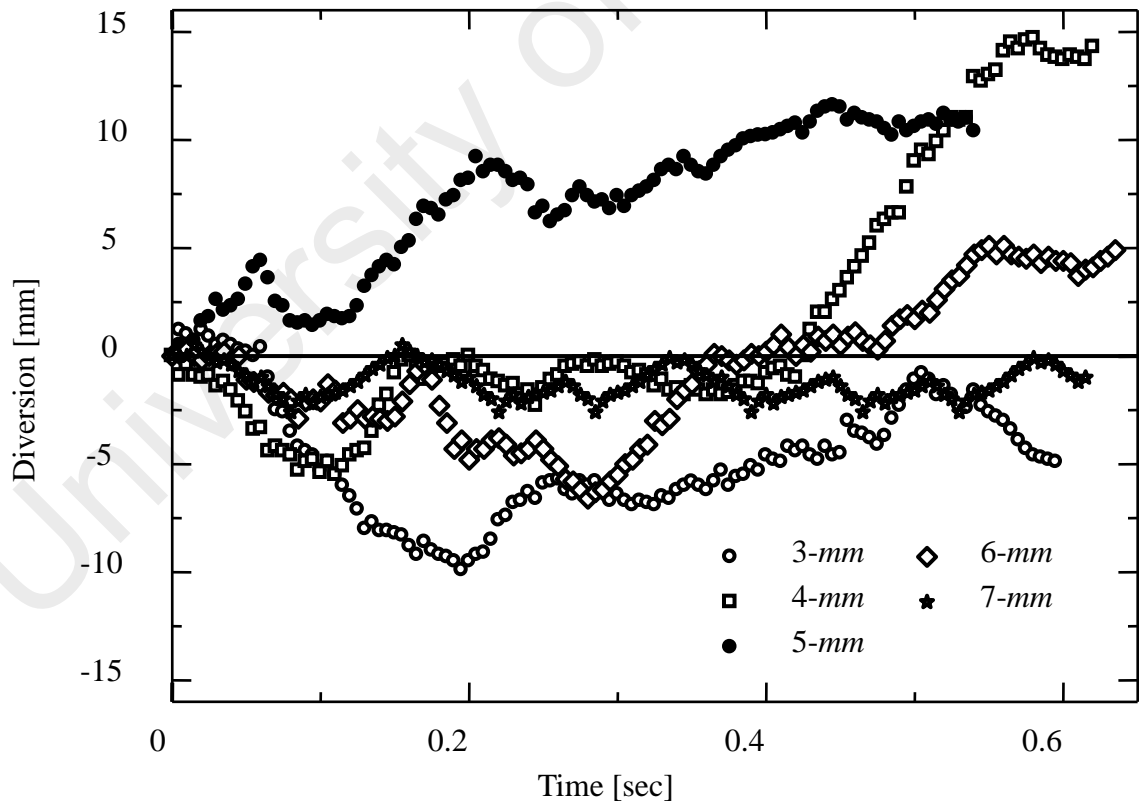


Figure 4.7 : Trajectories of bubbles with different diameters under the effect of vibration with mode M3

4.3.3 Rising Velocity

In this study, bubbles with diameter 3 to 6 mm were seen to have a similarity of terminal velocity at around 0.2 m/s as well as presented by Krishna and van Batten (1999), and Tomiyama et al.(2001), which the result is shown in figure 4.8. This result confirmed that the current experiment agreed well with the work conducted by those two researchers. Therefore, a further investigation on the vibration effects onto the rising velocity of single bubbles with the same diameters can be conducted and the results can be compared with the one displayed in figure 4.8. The effects of bubble sizes also can be observed in this figure where the rising velocities differ with the sizes showing the smaller sizes having higher velocity but however they are settled around the same value in the upper part of the travel, showing a considerable terminal velocity with the current diameter range.

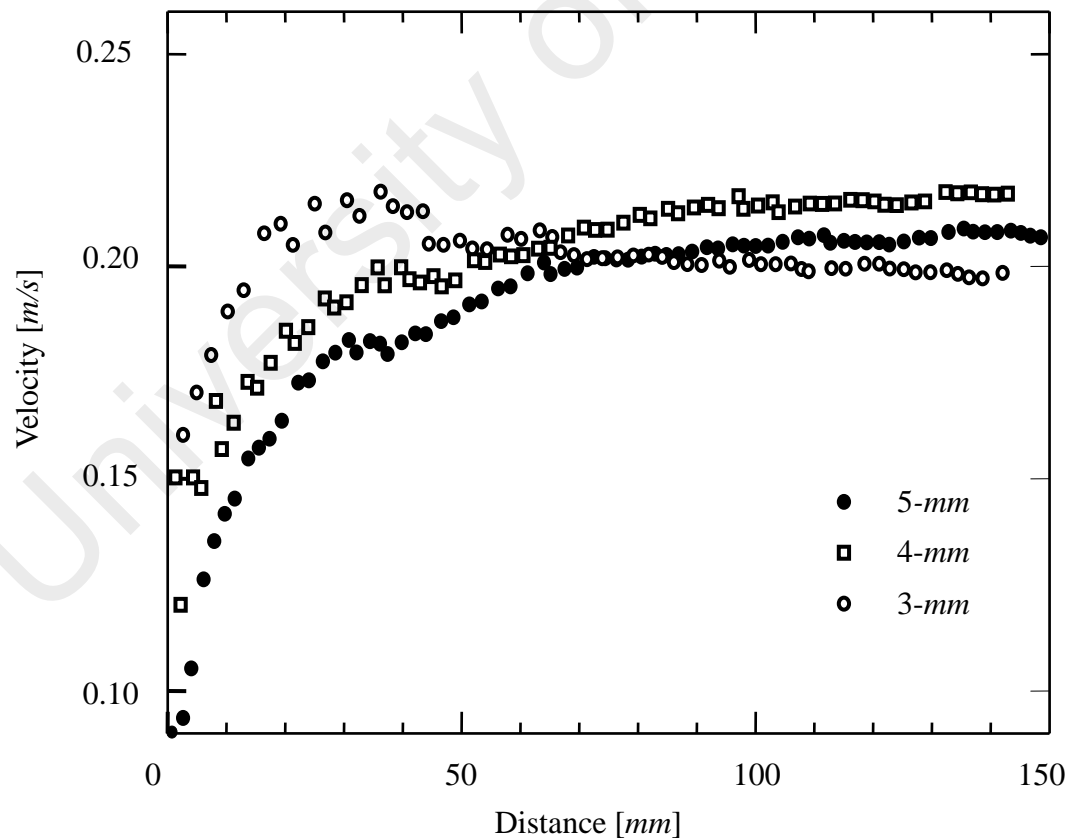


Figure 4.8 : Rising velocities of single bubbles with different diameters

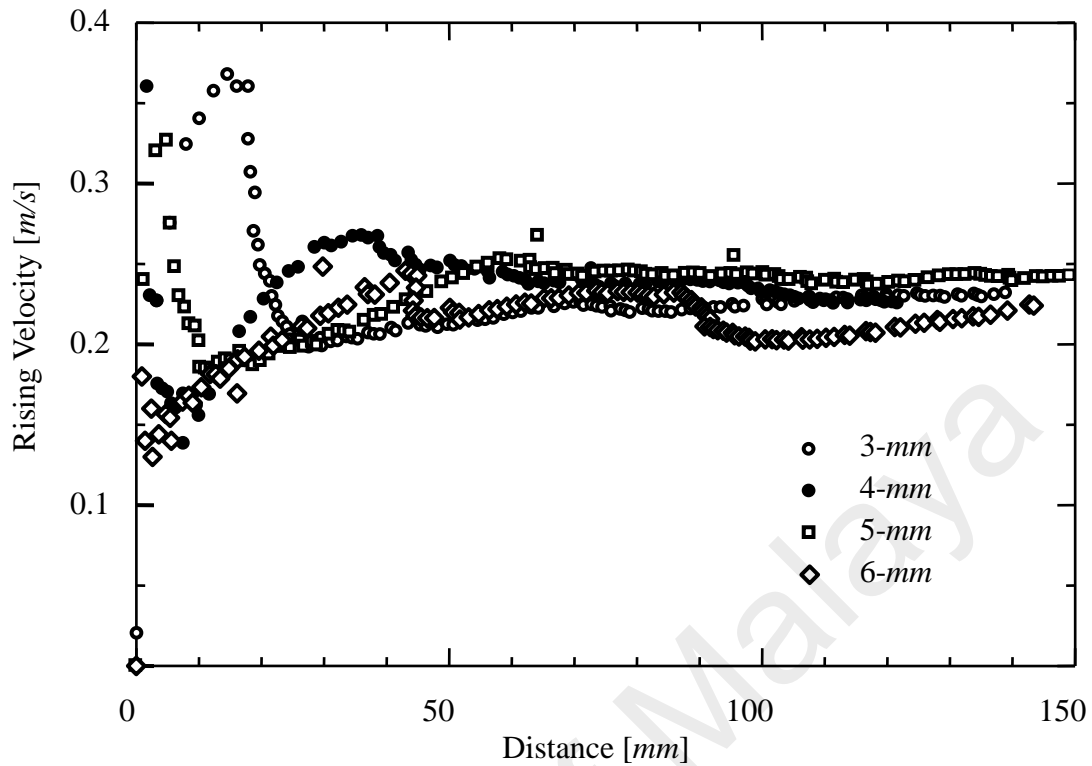


Figure 4.9 : Rising velocities of single bubble with different diameter under the effect of vibration with mode M3

Figure 4.9 shows the fluctuation of the rising velocities for bubbles with four different diameters under vibration with mode M3. Small diameter bubbles were seen to be shot out with high velocity, which is believed to receive the influence from the external forces and drop down to achieve nearly the value during the normal condition. For bigger bubbles, since they experienced bad shape oscillations, they move slowly upward and achieve the ordinary value. However, during the rising, all these bubbles were seen to have a velocity fluctuation, particularly for 6-mm bubble, which drop below 0.2 m/s in the upper region of the rising. This result gives an implication of influence of vibration on different bubble size where the smaller bubble can be swung easily since they have lower mass. The bigger bubbles however, due to their higher mass, was uneasy to retain the momentum when drag down in a vertical motion of vibration, and therefore dropped in term of terminal

velocity since they were struggling under the higher mass of substance that drag them.

In figure 4.10, the effects of vibration modes are shown where the bigger scale of vibration, which also having higher vertical accelerations, seem to slow down the rising speed of the bubble. In this case, it can be predicted that the higher ground acceleration would contribute to more drag force in the fluid even though the surface level was fixed, that surely will drag down the gas bubble together. As a result, with the struggle of gas bubble under higher mass and density substance as discussed above occur, making the bigger bubble losing the rising speed as can be observed here. However, in the future, more specific relation between the rising velocity and the acceleration should be presented.

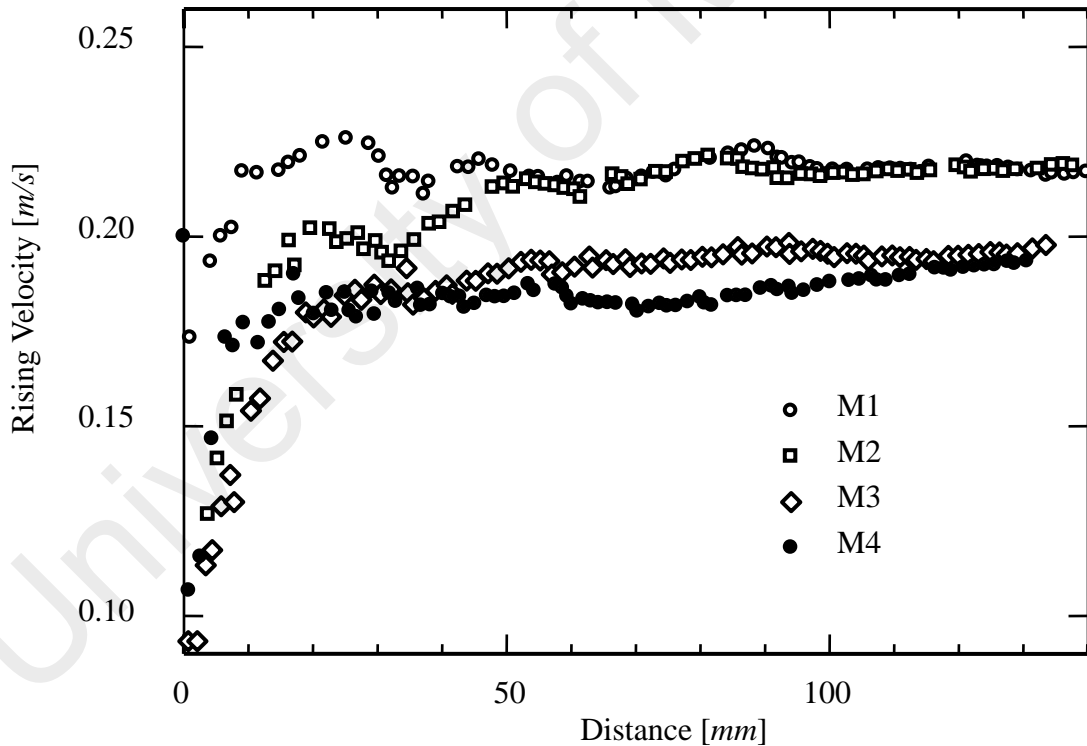


Figure 4.10 : Rising velocities of single bubble with 4-mm diameter under the effect of various scales of vibration

4.3.4 Bubble Interactions

With a constant flow rate of the air, the interval of bubble formation at the nozzle might be stable in the normal condition (without vibration). However, with external forces from the huge shakes, this formation is disturbed with tendency of smaller or bigger interval depending on the timing of the bubble releases and fluctuation of the accelerations.

As observed so far, bubble that formatted from injection of low flow rate and rise in the normal condition would be very difficult to coalesce with each other to form a bigger bubble. Some experimental results obtained previously Zainon et al. (2001) shows that the bubble coalescence is easier under vibrated condition by addition of extra forces as same as applied in the current study.

Another phenomenon that could also be an interest is the clustering of two bubbles for a certain period of time and break up to divert far from each other as well as from their original path. This phenomenon happened when two bubbles are released in a close gap and with the vibration effect they perform an unusual act unlike under normal condition where they try to avoid each other, which can be observed from rising characteristics of swarm bubbles as reported by Krishna and van Batten (1999).

Figure 4.11 gives the snapshots of the incidents that happened during this phenomenon. The results shown in these pictures are interaction between two bubbles with diameter 6-*mm* (the front bubble) and the 4-*mm* (rear bubble). Here, these bubbles were clustered at a concise period and moving upwards together before split up and divert far away from each other. The trajectories of this incident are shown in figure 4.12 where the paths after the split were recorded. The reason why this phenomenon is highlighted in this report is that it is always observed in this series of experiments. Whether, they were influenced from the timing of oscillations of acceleration or coincidentally by interaction of two bubbles with different volume are not yet investigated.

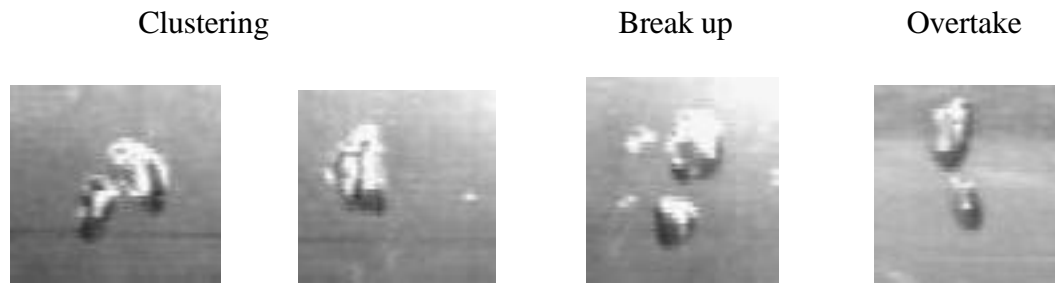


Figure 4.11 : Snapshots of interaction of the two bubbles with different sizes

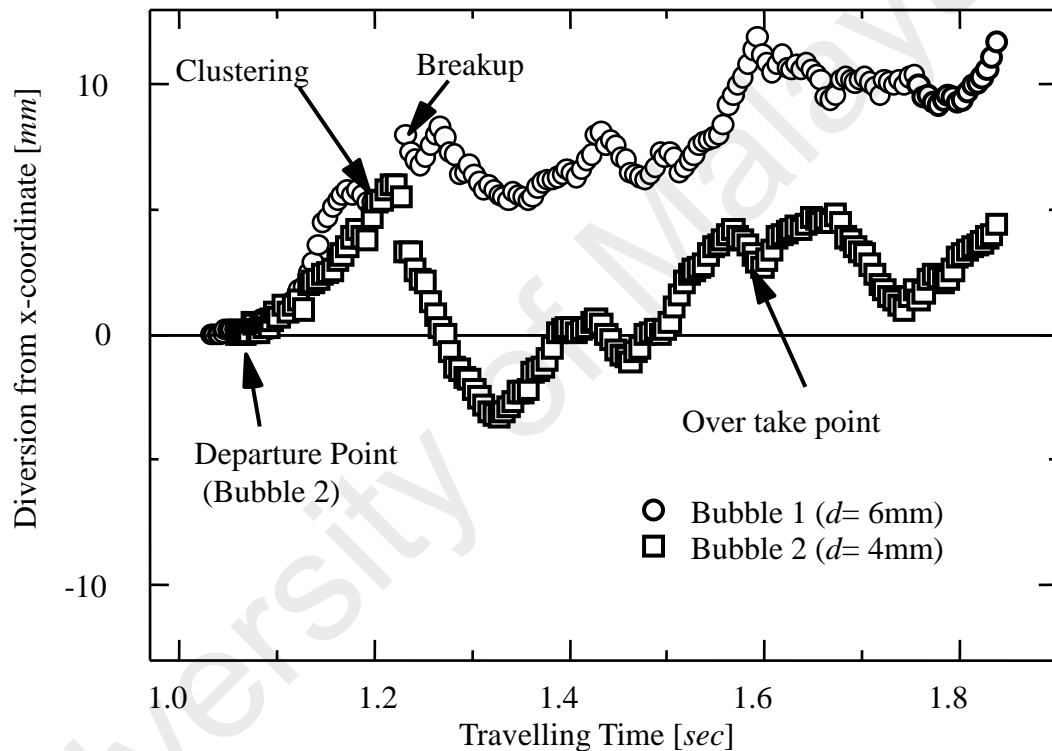


Figure 4.12 : Trajectories of interaction of two bubbles released at close gap

The results presented so far are very interesting where the bubble behavior, in terms of rising velocities, shapes and trajectories were strongly affected by the vibration. In the application of pool boiling such as BWR, it would be more dangerous if vibration took place where phenomena as observed here would strongly affect various parameters and as a result might contribute to unexpected accidents with catastrophic consequences.

5.1 Introduction to Two-phase Flow in Annular Channel

Industrial applications such as chemical processing, oil refineries and power plant involve many piping systems and sometimes are in very complicated arrangements. Those piping systems transporting many kinds of fluid with various types of flow including the two-phase flow and the studies in this field have been conducted from a long time ago (Wallis, 1969). In many power and processing plants also the orientation and arrangement of the pipe flow differs due the applications and the design of the plant. The orientation normally can be classified as horizontal, vertical and inclined. All of these orientations will thus contribute many other phenomena which differ from one to another. In the current work, the analyses of two-phase flow in pipe are focused on the vertical arrangement. The working fluids in this two-phase flow system are air and water flowing co-currently in an annulus transparent pipe. The next subsection will discuss on the characteristics of air-water two-phase flow in general as the knowledge for the preparation of this study.

Some major problems in two-phase flow systems are including the prediction and measurement of the volumetric gas-liquid rate (void fraction), pressure distribution along the pipe and thickness of the liquid film on the wall of the pipe. These three parameters are the most significant factor in order to ensure the safety of the equipment or plant. While pipes leakage and burst due to inappropriate treatments of two-phase flow are very common in many sectors. This will lead to serious disasters to humans and environment and some time with results of casualties. Leakages due to unpredictable pressure distribution caused by the drilling shakes and current flow in oil recovery plant are one of the major problems for oil producers as well and even in the inland pipe transport (Rueters, 2011).

Similarly, Mishima and Ishii (1984), found that the pipe failure in the nuclear reactor occurred due to the two-phase flow induced vibration which also happen during the fluid hammer phenomena in ordinary thermal power plant (TNB, 2006), (Bergant et al., 2006). In a high temperature condition, measurement of liquid film thickness is very important (Serizawa, 1972), (Fukamo, 1998) in order to avoid the phenomenon such as the Loss of Coolant Accident (LOCA), where dried liquid on the heating wall will cause the melting of heating element or sometime termed as core meltdown (Appendix 5.1).

Therefore, in association with the design of many industrial equipment, engineers would also face challenges dealing with high temperature fluid and it will be more complicated if the system involves the two-phase flow. These works are including the design and manufacturing the heating element such as cooling systems, various types of heat exchangers and in bigger scale like steam generators and nuclear fuel rods. Many more parameters are needed to be considered such temperature, heat flux, mass flow rate etc in order to optimize the design as discussed above.

Measurement of heat transfer in the two-phase flow of air-water, steam-water, or any mixtures involve, including the air-oil or gas-oil flow will be very essential (Bergles et al., 1981). Many researchers paid much attention on heat transfer problem in flow channel, and measured temperature using the modern or conventional method in order to get accurate information on the wall condition. These can be referred to works by Saha and Zuber, (1974), Celata et al. (1997), Kureta (1997) and many more. These experimental measurement results were always compared with those for pure liquid flow where many of non-heated two-phase flow experimentations are conducted to replicate the case of heating condition.

With complicated situation in the two-phase flow, the first thing that should be considered is the flow patterns. This factor is very important since it govern the whole situation in the flow channel.

5.2.1 Flow Patterns

When gas flowing in a stationary or moving liquid in pipes, the two-phase flow is formed with bubbles existence and they are in many shapes, and therefore the whole flow structure will form various patterns. The patterns can be called with different names depend on the behavior and position of the pipes with many geometrical and parametrical effects. For the vertical pipes, the usual names of pattern including bubbly flow, slug flow, churn flow and annular flow and also, the intermediate flow patterns are frequently encountered. The horizontal also have specific calling name such bubbly flow, stratified flow, wavy flow, slug flow, plug flow and annular flow.

The knowledge of the flow patterns is required in order to model the physical phenomenon as closely as possible and therefore easier to be able to understand the problems of two-phase flow. The determination of flow pattern will lead to the process of prediction of the characteristic in two-phase flow. Therefore, in order to conduct the simulation of two-phase flow whether through the experimental or the computational studies, understanding of the flow pattern and the flow transition are the intolerable requirement.

In general, the two-phase flow will involve the transfer of heat (if any) and mass, and also the inter-phases momentum and energy which are related to the velocity, viscosity and other parameters such as pressure and temperature. On the other hand, the characteristic of heat, mass and momentum transfer in a two-phase flow are strongly depending on its flow patterns. Therefore, the identifications of these regimes are very important because of their significant influence on many phenomena in fluid flow including the heat and mass transfer, flow transition and chaotic behavior. The classification of types of flow is very useful but it is still highly qualitative and often very subjective.

Many different regimes have been defined and a various names have been used. The definitions given in the following discussion are chosen for their relative generality of acceptance. Identification of the flow regime can be performed by using the experimental studies; with developing a suitable method and it also provide sufficient information for two-phase flow studies.

Therefore, as discussed shortly above, the determination of flow pattern is very important in order to predict the characteristic of the flow, where it may contribute information to solve any problem occurred. A lot of considerable factors must be taken into account in the two-phase flow system including the type and size of channels, mass flow rate, phase properties, flow direction and gravity factors.

5.2.1 Types of flow patterns in vertical pipes

The flow patterns or regimes give a big impact on some behavior of the flow such as velocity profile, pressure fluctuation and heat transfer conditions. The classification of types of the flow regime is useful but sometime it become very subjective to define. Many different regimes have been defined by researchers and varieties of names have been given with suitable definitions based on the acceptable behavior of the patterns and shapes of the bubbles in those patterns. There are a lot of definitions given for each type of flow pattern or flow regime, depending on the flow direction for the two-phase flow. The various regimes for co-current vertical upward flow of gas-liquid in a vertical pipe are defined by Hewitt and Robertson (1969) as follows:

(1) Bubble flow or bubbly flow

This is a normal pattern that formed at the lower part of the flow channel. In this case, some spherical and nearly spherical shapes of bubbles exist in the

liquid flow when gas phase is dispersed uniformly. It is always in the form of discrete bubbles at various sizes but are always much smaller than the channel diameter in the continuous liquid phase.

(2) Bubbly-Slug Flow

At a higher part of the channel, or with an increasing mass flow rate of the gas, more bubbles are formed, distributions become disorder and rapid coalescences occur to form bigger bubbles with spherical cap. Some of these bubbles will further develop to become bigger and longer.

(3) Slug Flow

As the gas flow rate is further increased, the spaces for bubbles to move become very limited and they start to collide and coalesce with each other forming larger in diameter size as well as the length. A new shape of bubble normally called the bullet shaped is formed with characteristic of hemispherical nose and various shape of tail. They are also called the Taylor bubbles and moves up with very thin liquid film surrounded follow by some trailing small bubbles from behind.

(4) Churn Flow

With much higher mass of gas flow in the same channel diameter, the velocity of gas phase will also increase. During this time the stability of slug flow is disturbed and flow structure will become unsteady in an upward direction. This is due to the effects from gravity and shear stress on the liquid film that try to bring it down. This unstable slug will break off and form various shape of distorted big bubbles usually dispersed unevenly in the flow channel. The

churn flow is also recognized as an intermediate pattern between the slug and annular flow. However, in small diameter tube, churn flow may not be able to form at all since this intermediate regime is pass by the annular flow that change directly from slug flow. In many practical applications, churn flow is the pattern to be avoided because of its chaotic and unstable behavior.

(5) Annular Flow

With the same flow channel and increasing mass flow rate, the gas velocity become higher enough to surpass the effect of gravitational force on the liquid film, with more higher interfacial shear forces. The liquid will be removed from the center flow and it will only flow on the tube wall as a thin layer and formed an annular ring of liquid and the gas flows dominantly at the center. Interfaces between gas and liquid is then agitated by high ripples and surface frequency waves that make the fraction of liquid to entrain in the core of gas flow in form of tiny droplets and then deposit back to the liquid film as the gas squeeze the droplet from its path. Normally, this flow pattern is stable and for some applications, it may be the desired condition.

(6) Wispy Annular Flow

In the same condition of the annular flow, with an increase of the liquid flow rate, the number of droplet entrainment will also increase, making a higher concentration in the high velocity gas flow. With this high rate of entrainment, the droplet will coalesce with each other to form larger droplet or lumps or wisps flowing together in the gas core with higher rate of droplet deposition rate as well. This is one of the characteristics during the high mass velocity of both phases.

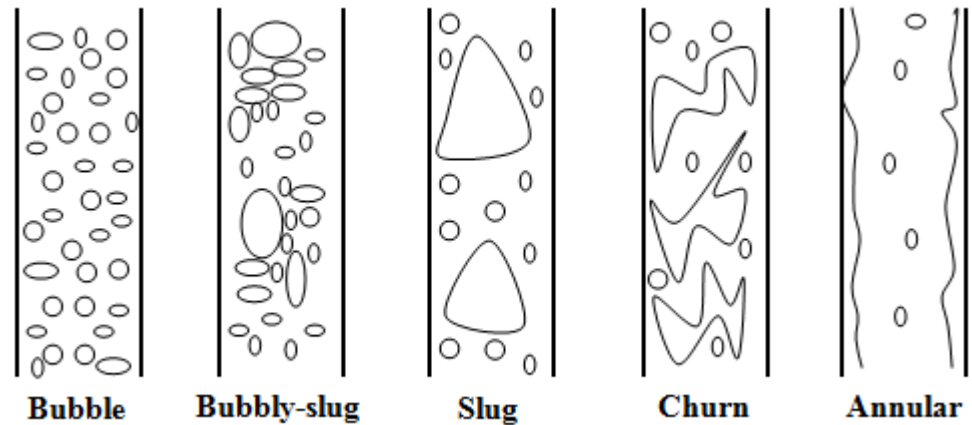


Figure 5.1: Gas-liquid two-phase flow pattern in vertical upward flow

5.2.2 Identification Techniques of Flow Patterns

Industrial application involved the two-phase flow as discussed above, normally having the flow transfer in many arrangement of piping system. Most of them are not visual-able, since they are not in transparent tube. The complexity of two-phase flow patterns however need to be identified for gaining more information in a particular application. Therefore, the detection, monitoring and full description of flow patterns is required since it contribute to many influences on the flow parameters. This can be carried out via the experimental works with proper monitoring elements and must be documented in a proper manner. It involves full measurement of various parameter distributions in space and time, such as, velocity, density and pressure (Keska and Williams, 1999).

(i) Visual Observation

There are quite a few techniques that have been developed and applied to identify the flow patterns and visual observation is a very easy and common. Generally, the information of the flow pattern is often acquired by photographic images of the flow. This technique has been used by Taylor et al. (1970) to study the flow pattern

inside a transparent tube. Many researchers use this technique since it is straight forward method and with recent technologies enable to record the moving flow and examined carefully after the experiment. It will be a lot easy for co-current flow but a little challenging for counter current, as Kim et al. (2003), presented some results based on this method on flow pattern with results also contribute to the measurement of rising velocity of slug.

A high-speed photography technique is essential in order to visualize the high velocity flows. On the other hand, for high pressure and high temperature flows other unique techniques were used. The major disadvantages of the visual observation technique is that as the light passes through the flow was subjected to a complex series of refractions, thus the produced images are often confusing thus making it difficult to interpret the flow pattern information. The visualization technique system needs high technology cameras that have a high shuttle speed, and for video visualization, high frame rate video capture is required. A good lighting system is also very important during the visual observation to capture a high quality pictures or videos.

(ii) X-radiography technique

X-radiography technique has been developed in order to overcome the refractions issue in visual observation. x-ray images can offer more useful information on the nature of the flow as the images produced from the x-radiography depends only on absorption and more information on the flow characteristic can be acquired from such images. Jones and Zuber, (1975) applied an x-ray beam passed through the flow and its resultant intensity determined in the detector. The output signal as a function of time is measured from the instantaneous void fraction and the probability density is used as a function for void fraction determination.

Heindel et al. (2008), implemented an x-ray imaging method where they were able to differentiate and measure some flow characteristics in a large vertical pipe with a maximum internal diameter of 32 *cm* and height at 4 *m*. Their facilities include the x-ray radiography and stereography imaging technique that enable the visualization of a 3D flow structure in an opaque channel with multiphase fluid flows with the rate of 60 frames per second and they used the digital detector to digitalize the film radiography.

(iii) Conductance probe

Early Conductance probe technique has been developed and used by Barnea et al. (1980) to characterize the flow patterns. A full insulated needle probe is inserted into the flow and the conductance between the needle probe tip and the tube wall is measured as a function of time. They obtained the characteristics of flow pattern by displaying the response detected from the flow on the oscilloscope. This method still has the disadvantage and does not provide accurate information as the contacts between the needle probe and the flow can occur in all flow patterns. Yoneda et al. (2002) applied this technique for high temperature flow of steam–water in a vertical large diameter pipe with an internal diameter of 155-*mm*. The experiments were carried out with a wide range of flow rate and boundary conditions to investigate the bubble characteristics and structure of the flow with concerning the developing state of the flow.

(iv) Electrical Resistance Tomography

It is a form of direct current method where the measured data does not require the reconstruction of a cross-sectional image with the distinctive of reflection that is able to characterize the gas and liquid phases. This technique has been used by Tan et al. (2007) for flow pattern investigation on gas-liquid flow in a vertical arrangement.

Nowadays there are many more advanced methods that have been used in monitoring the flow pattern.

5.2.3 Effects of Flow Patterns in Two-phase Flow

Apart from the methodologies, various works also being carried out on flow patterns for various applications and studies on effects in the two-phase flow. Those works include types of fluids, properties, channel and flow condition, and location in the flow channel. Yang et al. (2001) found that the flow transitions are strongly affected by the fluid properties after comparison of two-phase for air-water and refrigerant R-134.

Ohnuki et al. (2000) investigated the dependency of gas-liquid two-phase flow on pipe scale. The experiment conducted based on vertical 200-*mm* diameter tube to see the effect of axial position on the transition characteristic of flow pattern and phase distribution. Their flow patterns is shown in Appendix 5.2.

The same work also performed by Shen et al. (2005) that divided the result for phase distribution as wall peak and core peak which actually give an image of the position of bubble crowing at the wall or at the core of the flow.

At higher temperature condition, more difficulties would be faced for determination of flow patterns since condensation might rapidly happen along the pipe and turbulent effects will be more significant, with many parameters fluctuate such as temperature and pressures. Petritsch and Mewes (1999) investigates the flow patterns in hot leg of a pressurized water reactor to simulate the Loss of Coolant Accident (LOCA) using comparison of a small and a large size plant. It appears that flow patterns are easier to be predicted by using the small scale plant and usually a fully developed flow can be achieved.

As also being discussed in the beginning of this section, the parametric effect on the two-phase flow will contribute to different patterns even at the same position and the same flow conditions; many parameters should also be studied in order to recognize the flow pattern in pipe. One of the parameter that is in the interest is the liquid viscosity and this has been studied by Furukawa and Fukano (2001) in the vertical upward air-liquid flow in 19.2-*mm* inner diameter tube with height of 5.4 *m*. They observed the flow pattern using the high speed video recorder and still photography as well.

Other effect on the flow patterns would be the surface tension and gravitational force. There are number of studies as discussed above involving the gravitational force effect but there are also application of two-phase flow in the absent of this force. As a reference, a study by Zhao and Hu (2000), in the microgravity should also be put into account. It is obviously revealed that the surface tension has a dominant role under the microgravity condition.

In the following chapters, the current study will however, discuss on the effect of higher ground acceleration effects on the two-phase flow patterns.

5.2.4 Transition of Flow Pattern

The transition of the flow pattern is the phenomena which the changing situation from one pattern to the other pattern. The example of the transition of the flow pattern is the change from bubbly to slug in vertical upward or from bubbly to plug flow for the horizontal flow.

The pattern transition depends on a few factor such as the flow velocity, the pipe size, length of the pipe and the flow condition such pressure and temperature. All these aspect give an impact to the flow pattern and also to the flow transition pattern. External factor such as external vibration can affect the pattern of the flow as well.

Since the transition flow also appears to be significant in some of the flow conditions, some indicator might be very essential in determining this phenomenon as well. Hervieu and Seleglim (1998) approached a technique for this purpose with an assumption that flow during transition would be more energetic than the established regime.

During higher liquid velocities, the flow in the vertical and horizontal is less affected by the gravitational force, and therefore, a considerable analysis can be made in the same manner for the both cases. This is particularly in the transition during the bubbly-slug flow transition, where bubbles coalesce together to form bigger bubbles and for sometimes develop a fully slug flow.

Lewis et al. (2002) describe this transition in internal flow structure using the hot-film anemometry technique within the scope of intermittent nature of slug flow. They have shown that a single probe can be used for identifying gas and liquid phases and for differentiating the large elongated bubble group from the small bubbles present in the slug flow.

In many cases, the mechanism of transition and formation of other flow patterns is very important to be described since the flow pattern will give a lot of influences on equipment and machineries.

Formation of slug is one of the most important topics and being studied in very deep interests in vertical gas-liquid two-phase flow. The slug will be formed by the increase of void fraction waves where more bubbles will congregate and coalesce in the transient bubbly flow (Sun et al., 2002). Violent flow from turbulent effects will however slow down the formation of Taylor bubbles and therefore, even in larger diameter pipe with low flow condition, Taylor bubble can be observed, an effect of void fraction waves. In addition, in high flow condition no slug will be formed due to less coalescence of bubble since they have more space to move.

Mi et al. (2001) obtained many characteristics of slug bubbles such as length, formation probabilities, void fraction and velocity using electromagnetic flow meter coupling with impedance void meter. They also developed correlations for slug void fraction from this study.

5.3 Flow Patterns Mapping

For a vertical upward two-phase flow, particularly the cases that involve boiling phenomena, has a significant engineering application. To illustrate the flow pattern in such condition, it is the best to refer to flow boiling in vertical annulus by Collier (1981) as shown in figure 5.2 that represents a whole structure of flow boiling from the boiling incipient to dryout.

The flow patterns begin with bubbly flow at the early stage during onset of boiling bubble nucleation particularly with the effect of subcooling. At this point, bubbles were generated (nucleated) within the superheated thermal boundary layer on the wall of the heated surface but later on condense in the core of the flow. Sometime, the onset of nucleation might happen in a poor manner or delayed due to low vapor qualities and low heat flux in subcooled boiling and slug waves formed after the bubbly flow as discussed in the previous section as well.

As the flow boiling reach the upper part of the heated surface, the liquid receives enough energy to change the phase in more frequent rates. As a result, annular flow regime is formed with thin liquid film flow on the wall, vapor in the core of the channel, and droplet entrainment with alternate deposition flow along in the vapor core. All the transition of flow regime as discussed above can be explained or estimated for prediction studies using the flow patterns map. It is a complete diagram that shows the interchange of boundaries between patterns.

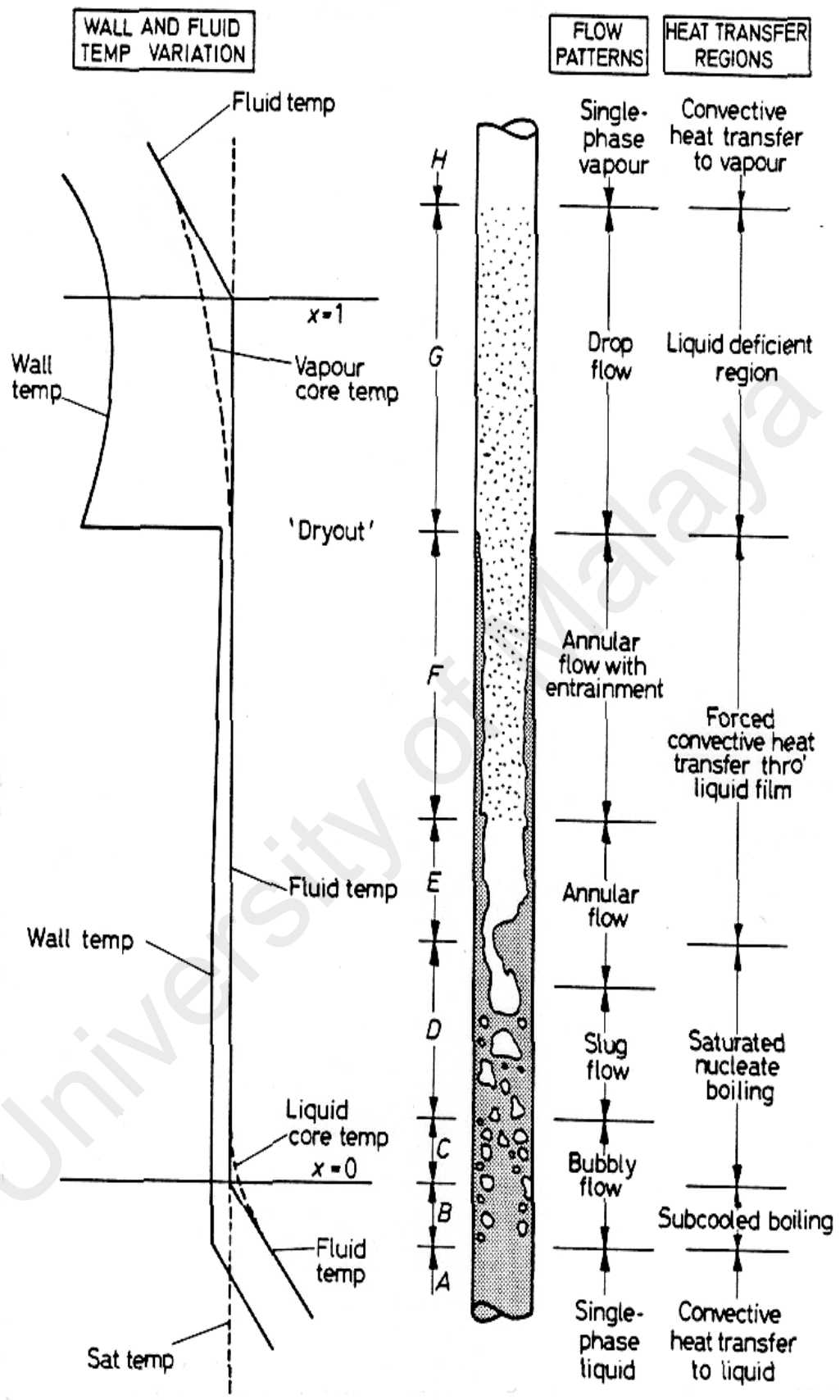


Figure 5.2 : Flow boiling in vertically heated annular tube (Collier, 1981)

A lot of argument also underwent in the two-phase studies on the selection of fair and appropriate parameters to be presented in the flow pattern maps particularly on the scaling of the transition boundaries. Generally, it can be displayed using dimensionless parameter representing the superficial velocity of liquid and gas, in the form of normal scale or in the log-log axis.

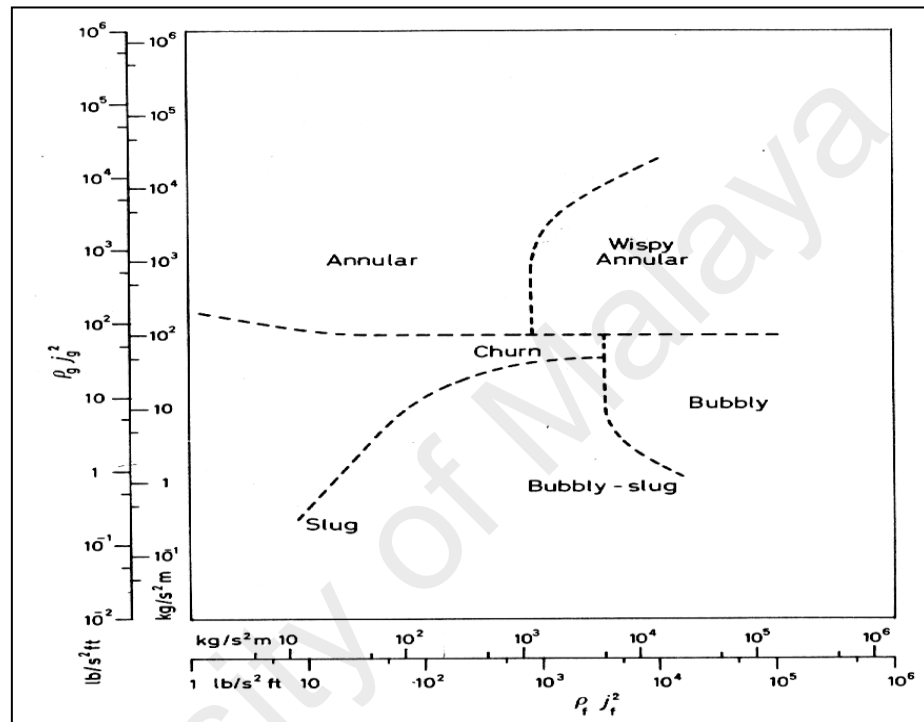


Figure 5.3: Two-phase flow pattern maps for vertical flow
(Hewitt and Robertson 1969)

One of the famous examples of flow pattern maps is such as and Hewitt and Robertson (1969) for vertical flow as shown in figure 5.3. This map represents the results for small flow channels but there is also a non-dimensionalized pairs of parameters such as by Fair (1960) depicted from Dalkilic and Wongwises (2010) as shown in figure 5.4 that can be applied to all conditions regardless of channel diameter and other diameter applied in the experiments.

Another popular flow pattern map is the one presented by by Taitel and Duklear (1976), as shown in figure 5.5. In all of these maps, the transition curves can be read as the transition of patterns or transition zone that give analogy of transition between laminar and turbulent flow as well. As shown in figures 5.3 ~ 5.5, the parameters used by scholars differ from one to another.

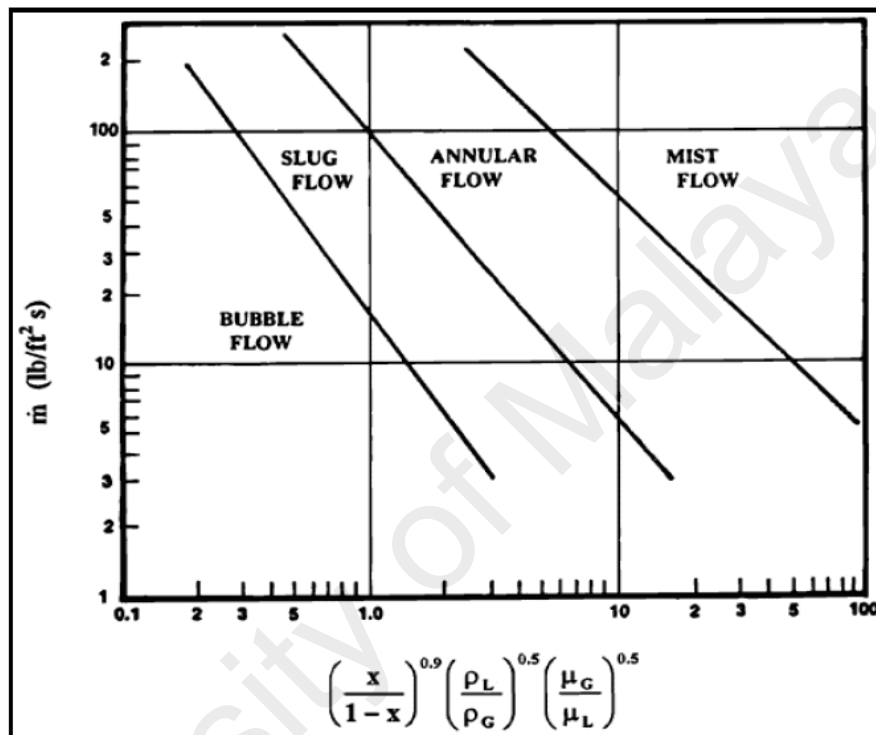


Figure 5.4: Two-phase flow pattern maps for vertical flow (Fair, 1960)

To utilize the Fair (1960) map, our information at hand should be the superficial velocities of gas and liquid on x -axis and mass flow rate on y -axis. The two-information are then to be matched vertically and horizontally to reach the intersection on the graph. The same procedure applies in order to utilize the Hewitt et al. (1969) map but with different parameters should be prepared at hand.

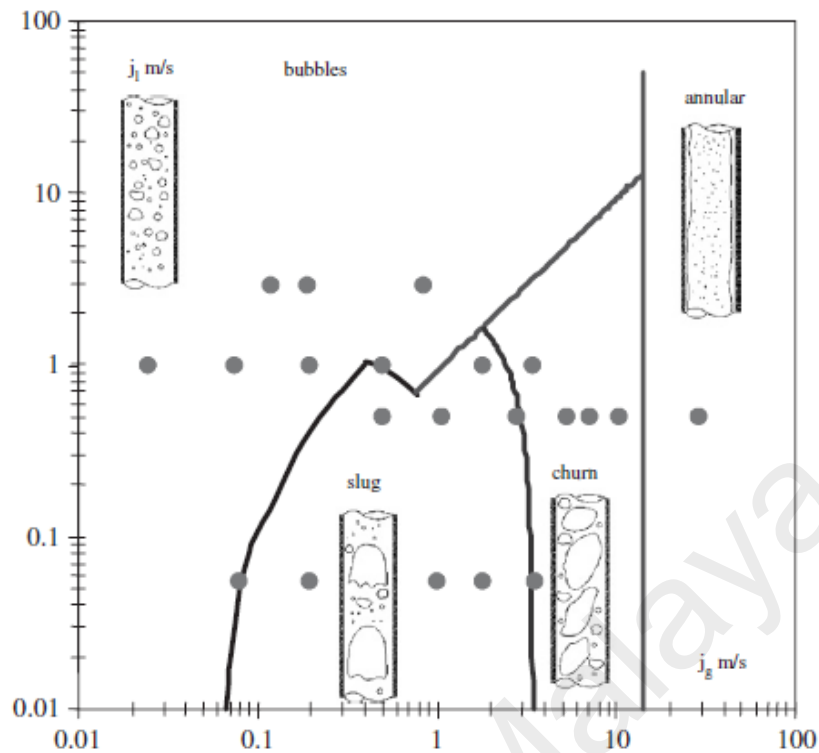


Figure 5.5: Two-Phase Flow Pattern Map for Vertical Flow (Taitel and Duckler, 1976)

As works in the two-phase flow progressed, many more flow pattern maps were developed with many more information can be obtained from those maps such as comprehensive treatment provided by Barnea et al. (1985) and more complete information on fluid viscosity by Furukawa and Fukano (2001). Kattan et al. (1998) and Zurcher et al. (2002) presented the flow map for wide range of parameters such as, vapor qualities, mass velocities and heat fluxes. This map also provides the information on estimation of dryout point at the upper side of the tube for evaporation and extended for other fluids, refrigerants HFC-134a, HFC407c and R717 (ammonia).

For the current work, flow mapping suggested by Taiteland Duckler (1980) and Furukawa and Fukano (2001) will be applied as reference since the flow conditions in these two maps are in the range of the current experimental works.

5.4 Void Fraction

5.4.1 Definition and Models

Void fraction is the volumetric gas rate in the liquid flow and can be considered as the most important parameters in analyzing the two-phase flow. In more detail explanation, it can be described as ratio of the gas volume (the voids in the flow channel) to the total volume of the flow channel. Let us consider an adiabatic case with a mass flow rate, \dot{m}_L of liquid, with density, ρ_L and a mass flow rate, \dot{m}_G of gas, with density, ρ_G are flowing upwards in a vertical pipe with diameter, D_C , length z , and cross sectional area, A_C .

Then by considering that equilibrium has been achieved, the parameters in both phases can be treated as the following assumption referring to figure 5.6. In this case, the liquid mean velocity can be represented as v_L and the gas mean velocity as v_G , while the cross sectional area of the core of the flow channel that filled by the gas phase represented as A_G and its diameter as D_G .

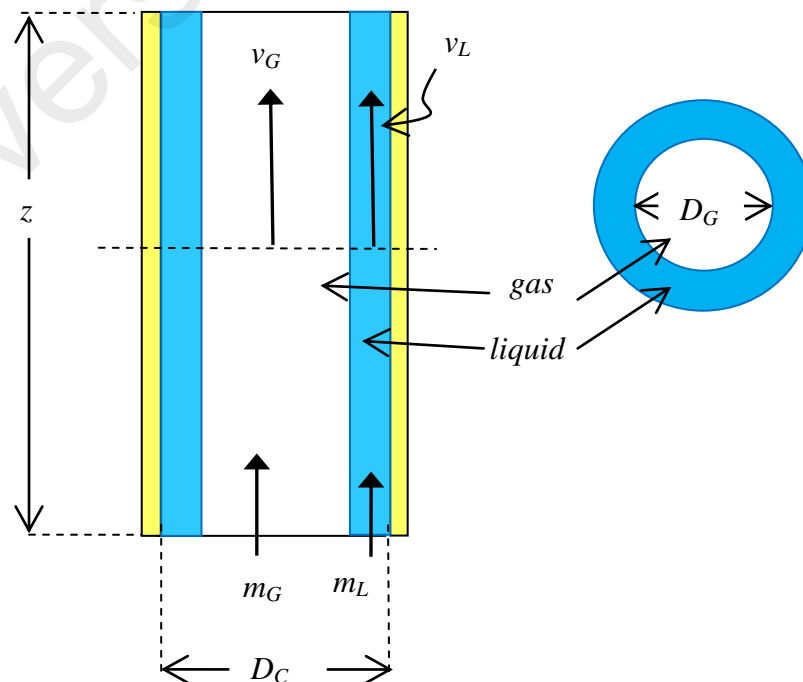


Figure 5.6: Fundamental depiction of void fraction

Information from figure 5.6 can be expressed into the mathematical form as follows, where the volume or area ratio representing the void fraction,

$$\alpha = \frac{A_G}{A_C} = \frac{1}{\left\{1 + \frac{m_L \rho_G v_G}{m \rho_L v_L}\right\}} \quad (5.1)$$

Or simply,

$$\alpha = \frac{A_G}{A_C} = \left(\frac{D_G}{D_C}\right)^2 \quad (5.2)$$

Homogeneous flow model

In one-dimensional method, a fundamental assumption can be carried out as a steady state has been established in the flow channel. Here the velocity of each phase is assumed to be constant even though some variations exist, but they are negligible. Therefore, average parameters are assumed over the cross-section and this model is termed as the *drift flux model* as suggested by Zuber and Findlay (1975).

For simplicity of the equation, the force, F can be treated as one of the parameters described above and the governing equation for this assumption can be written as follows,

$$\langle F \rangle = \frac{1}{A} \int_A F dA, \quad (5.3)$$

The weighted mean value for F can be expressed as,

$$\bar{F} = \frac{\langle \alpha F \rangle}{\langle \alpha \rangle} = \frac{\frac{1}{A} \int_A \alpha F dA}{\frac{1}{A} \int_A \alpha dA} \quad (2.4)$$

Applying the volumetric flux, j and, j_G and j_L as the superficial velocities of gas and liquid phase respectively, the average gas velocity can be written as,

$$\langle v_G \rangle = \langle j \rangle + \langle v_{Gj} \rangle \quad (5.5)$$

and the weighted mean velocity for gas flow can be expressed as,

$$\bar{v}_G = \frac{\langle j_G \rangle}{\langle \alpha \rangle} = \frac{\langle \alpha j_G \rangle}{\langle \alpha \rangle} = \frac{\langle \alpha j \rangle}{\langle \alpha \rangle} + \frac{\langle \alpha v_{Gj} \rangle}{\langle \alpha \rangle} \quad (5.6)$$

Where, v_{Gj} is the drift velocity of gas phase relative to j , the total flow velocity

While expression for superficial velocity in one-dimensional model, can be written as,

$$j_{GL} = \alpha v_{Gj} \quad (5.7)$$

And therefore, equation 2.4 can be witten as,

$$\bar{v}_G = C_0(j) + \frac{\langle \alpha v_{Gj} \rangle}{\langle \alpha \rangle} \quad (5.8)$$

Where,

$$C_0 = \frac{\langle \alpha j \rangle}{\langle \alpha \rangle \langle j \rangle} = \frac{\frac{1}{A} \int_A \alpha j dA}{\frac{1}{A^2} \int_A j dA \int_A \alpha dA} \quad (5.9)$$

Similarly the weighted mean liquid velocity is given by,

$$v_L = \frac{\langle j_L \rangle}{\langle 1-\alpha \rangle} = \frac{\langle j-j_G \rangle}{\langle 1-\alpha \rangle} = \frac{\langle \alpha j \rangle}{\langle \alpha \rangle} + \frac{\langle j \rangle - \langle j_G \rangle}{\langle 1-\alpha \rangle} \quad (5.10)$$

And the slip ratio given by

$$S = \frac{j_G}{j_L} = \frac{\langle 1-\alpha \rangle}{\frac{1}{C_0 + \frac{\langle \alpha v_{Gj} \rangle}{\langle \alpha \rangle \langle j \rangle} - \langle \alpha \rangle}} \quad (5.11)$$

In the case of no local velocity difference (slip velocity) between phases, $u_{Gj}=0$:

$$S = \frac{\langle 1-\alpha \rangle}{\frac{1}{C_0} - \langle \alpha \rangle} \quad (5.12)$$

For $C_0 \neq 1$, the slip ratio is not unity, even though the phases are travelling at the same velocity at each point in the channel. This arises because of differences between the distribution of velocity and void fraction. If v_{Gj} is constant across the channel, then equation 5.8 can be converted into a void-quality relationship of the form:

$$\langle \alpha \rangle = \frac{j_G}{C_0 \langle j \rangle + v_{Gj}} \quad (5.13)$$

This equation shows that $\langle \alpha \rangle$ can be determined if C_0 , v_{Gj} and the average gas or vapor volumetric flux $\langle j_G \rangle$ are known for a given flow regime; i.e., bubbly, slug churn-turbulent. Noting that v_{Gj} and C_0 are flow-pattern dependent quantities then any void fraction predictions based on equation 5.13 would reflect the flow-pattern effects on the void fraction. In fully-developed bubble and/or slug flow, C_0 is usually of the

order of 1.1 ~ 1.2. It is often convenient to correlate data for void fraction in terms of the parameters C_0 and v_{Gj} . An extensive empirical correlation in this form is that of Chexal and Lellouche (1991). However, the evaluation of C_0 based on those correlations is not in the scope of the current work.

Suggested expressions for C_0 and v_{Gj} and other flow-pattern dependent void fraction correlations are presented in Table 5.1 based on the work of these investigators.

Table 5.1 : Drift flux suggested values

Flow regime	C_0	v_{Gj}	References
Bubbly	$1.2 \sim 0.2 \sqrt{\frac{\rho_G}{\rho_L}}$	$1.4 \left[\frac{\sigma g \Delta p}{\rho_L^2} \right]^{\frac{1}{4}}$	Ishii and Zuber (1979) Wallis (1979)
Slug	1.2	$0.35 \left[\frac{g \Delta p}{\rho_L} \right]$	Collier (1981)
Churn turbulent	1.0 ~ 1.3	No recommendation	-

Therefore, the entire void fraction measured will be evaluated based on the drift-flux models since it has been used in many application of gas-liquid two-phase flow. Furthermore most of thermal-hydraulic analysis codes that have been developed in the nuclear and other industries to analyze behavior of systems during a wide variety of transient conditions also based on this model.

5.4.2 Measurement Techniques of Void Fraction

Even though the two-phase flow is used widely in industrial plant, piping system, and in some equipment of close system, in real situation, there is no opportunity to observe a real flow of two-phase mixtures inside the pipe. In relation to this problem, many researchers put on their efforts to overcome this shortcoming. They have

proposed many techniques as will be discussed in the following sections for many purposes such as void fraction measurement, flow patterns identifications, velocity measurement and other parameters. These developments were supported by studies on relationship and many correlations in the two-phase flow in order to determine the flow characteristics of a particular system. Therefore, efforts on laboratory experimentations are always the best way to provide some view of insights and valuable quantitative information of the phenomena in the two-phase flow system. Appendix 5.2 shows a direct measurement of void fraction for a large scale of application such as BWR.

(i) Neutron Radiography (NR)

This method has been applied by many researchers such as Mishima and Hibiki (1996), Takenaka et al. (1998) and Harvel et al. (1999). The advantage of this method is that it can differentiate the concentration of substance and deliver those images through an opaque or mostly black body channel and deliver them into the optical images via scintillator. The disadvantages include the unnecessary triggering signal system, long recording time and difficult setup.

(ii) Conductance Probes

The early and most common method to measure the void fraction is by using the resistance probes. These types of measurement method were used by many researchers such as Serizawa (1974), Song et al. (1998) and Yang et al. (2003). The tube wall is connected to the full insulated needle probe except its tip through the fluid. The conductance between the needle probe and the wall varies depending on the phase of the flow which is either in gas phase or liquid phase.

Another conductance method void fraction measurement was done by Fossa (1998), which used plate and ring-shaped electrodes to measure the fluctuation of

electric voltage due to conductance in gas-liquid flow. A pair of electrodes is placed in the flow channel and electric current is supplied in the water flow to obtain the voltage during the single phase flow. When the gas is injected to the liquid flow, some voltage fluctuation will occur and these fluctuations are detected by the ring sensors installed flushed to the inner side of the flow channel. The differences between the two voltages during single and two-phase therefore provide the reading for the void fraction.

(iii) Impedance Void Meter

Costigan and Whalley (1997) measured void fraction in a vertical 32-*mm* inner diameter tube with flow pattern ranging from bubbly to annular flow, where they also have conducted good calibrations, the same method used by Ma et al. (1991) which is an impedance probe that connected to a signal processing circuit which gave a linearized output with fast response. While Cheng et al. (2002) conducted void fraction measurement using this technique for 28.9-*mm* diameter with liquid constant velocity of 0.356 *m/s* with four different bubbles to study the patterns transition due to changes of bubble sizes.

(iv) Electrical Resistance Tomography and Capacitance Tomography

Electrical Resistance Tomography (ERT) was also used by Tan et al. (2007) for identification of flow pattern, also works as void fraction measurement technique. The measured data does not require the reconstruction of images to characterize the two-phase flow. Capacitance tomography is a system consists of stand-alone long electrodes which objects are illuminated from five projections.

The luminous intensity of the object is measured and changed into discrete signals but it is reconstructed based on the matrix algorithm. Void fraction measurement

using this system has been performed by Ismail et al. (2005) for horizontal gas-oil and Rzasa (2008) for air-water two-phase flow in vertical arrangement.

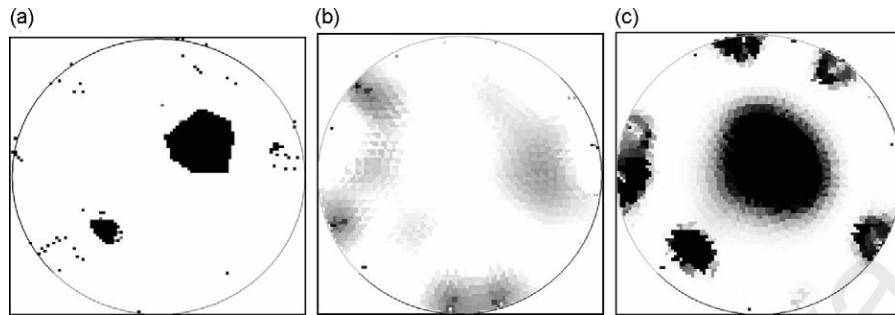


Figure 5.7: Comparison of the measurement results for tomography method:

(a) from the optical tomography

(b) from the capacitance tomography for LBP method

(c) from the capacitance tomography for IBP method (Rzasa, 2009)

(v) Other methods

An attempt has been made by Cha et al. (2002) to apply the electromagnetic flow meter on the measurement of parameters in two-phase flow using the alternating current. They have done the calibration using non-conducting rod as void simulator to examine the effect of bubble position and signal from the flow meter that they designed and fabricated, and then compared with visual observation of flow patterns. The results turned to be very good and they concluded that this electromagnetic flow meter can be applied in determination of flow regime of two-phase flow.

(vi) Prediction Methods

Assessment of many correlation related to void fraction is very important in order to predict the void fraction in wide range of flow conditions. The Zuber-Findlay model, as the most famous drift-flux model was examined by Coddington et al. (2002) using 13 different correlations of which the void fraction data were taken from

variations of 9 experimental results performed in 15 years around the world's famous experimental institutes. They compared the algebraic slip calculation and the differential slip equation for slip velocity and found out that the drift-flux approach can be applied in analysis of rapid transients.

One of the prediction works was carried out by Rivière et al. (1999a) and the result shows that void peaking near wall and the velocity profile modification has capability to induce the wall shear stress and if compared to single phase flow at the same flow rate of liquid, it would be in several folds. Comparison made in other work by experimentations, Rivière et al. (1999b), satisfied this prediction and also shows that frictional mechanism also play an important role interfacial transfer in the two-phase flow.

5.4.3 Relation of Void Fraction, Measurement Techniques and Other Parameters

For the flows that develop and change the patterns, the effects of axial location are found to be quite important. Many researchers have studied this effect to investigate the interfacial area transport by using analytical and simulation or by experimental works. For the analytical studies, the development of constitutive relation regarding this matter must be supported by an appropriate experimental data. Hibiki et al. (2001) performed a vertical upward flow of air-water and made a systematic investigation on the effects of three location of axial position.

Double sensor probe also used by Hibiki (2003) for measurement of local parameter in vertical upward of air-liquid system in double annulus with pipes of 19.1-*mm* in a 38.1-*mm* inner diameters. Interfacial velocity, area concentration and void fraction were measured with liquid velocity and turbulence intensity were measured by the laser Doppler anemometer where they managed to validate the proposed constitutive

equations (Hibiki et al. 2001) with the current experimental data for local parameter measurement.

In order to investigate the velocity of bubbles in a liquid flow, a lot of analyses are required. This can be carried out by the theoretical, simulation and experimental studies. Jameson (1966) proposed the theory on motion of small bubble in an inviscid liquid which is in forced oscillation. It predicts that the bubble will oscillate at fixed point with the distance of movement at about three times of the imposed amplitude on the liquid. However, this argument is just a rough idea and only agreed at some point with the experimental data. However, with the effects from viscous forces it is believed that the bubble will be held stationary by the vibration if a proper experiment is conducted.

Measurement in two-phase flow is very important in many aspects of applications. For a rectangular channel, for high velocity flow, the turbulent effect is a very important factor to be considered. Panidis et al. (2000) demonstrated experiments to study the two-phase grid turbulence structure and used the Laser Doppler Velocimetry (LDV) to measure the liquid phase velocity. They also applied the hot film anemometry and optical probe to measure the local void fraction and estimated the velocity and size of the bubble using the photographic method. The results show that inhomogeneities in flow property distributions and void fraction are strongly affected by the dispersed phase in the turbulence field.

5.4 Two-Phase Flow Boiling

In many cases, the two-phase flow always associated with heat transfer and phase changes in the flow channel. Therefore, some analysis as fundamental information was carried out in this study to obtain more firm relationship with the current experimental works. As replication to many cases in flow boiling, two-phase flows with non heated channels were always being a good choice to endeavor into some fundamental findings. In view of this, the concern is always in the form of maximum heat flux that is permitted on a particular heating wall, the critical heat flux, (CHF).

Serizawa (1983) formulated a model to predict the burnout characteristics during a power increase with analytical description of the model built upon visual and photographic observations of the vapor-liquid configuration near the maximum heat flux reported by other investigators. He gave broad conclusion that the maximum heat flux occurs because of the balance between the consumption of a thin liquid layer form between a vapour blanket and a heated surface and the supply of liquid during the postulated transient and also found that the liquid thickness layer is the primary influence on the transient burnout behaviour as well as the liquid supply to the layer.

Suzuki et al. (1983) employed a simple model for the wave effects on momentum, heat and mass transfer, and the theory proposed for the calculation of heat transfer coefficient and flow characteristics of two-phase two-component annular flow. This theoretical result agreed reasonably well with the experimental data obtained for a wavy-laminar thin liquid film heated at low heat flux.

Even though the ideal results would be obtained from experimentations, easier methods such as theoretical and computational offer good approach as well. Kataoka and Serizawa (1997) analyzed the structure of subcooled boiling two-phase flow based on basic equations of mass, momentum and energy conversion of each phase and conservation of turbulent kinetic energy. In boiling two-phase flow, bubbles are

generated from heated wall and these bubbles considerably alter the turbulent structures of laminar sublayer and turbulent boundary layer. Therefore they did modelling on the effects of boiling bubble on turbulence generation, the structure of laminar sublayer and turbulent mixing length, based on the previously analysed turbulent structure of non-boiling air-water two-phase flow. A renewed model from this work was obtained for laminar sublayer due to boiling bubble and analyses on velocity profiles in laminar sublayer have also been performed. From this work, the results show that the turbulent kinetic energy distribution has a high peak value near wall due to the wall void peak and bubble induced turbulence which is similar to the analytical results for non-boiling bubbly flow under the same condition. Average velocity distribution has less effect of subcooled void near wall and it revealed that turbulence structure of subcooled boiling two-phase flow is sensitive to the period of bubble generation. This whole structure of flow again is very similar with the current experimental flow conditions and set up and therefore will be a good reference for future works as well.

On the other hand, Zainon (1997) conducted extensive studies on prediction of this parameter and suggested combinations of correlations for two- and three fluid models based on DNB (departure from nucleate boiling) models by Weisman-Pei (1983) and Katto (1996). This method is similar to the combination of gas and liquid superficial velocities in a non-heated channel as replication to a heated flow channel to obtain various flow patterns as discussed in section 1.7. Similar works were also carried out by Kawara et al. (1999) to study mechanism for DNB- and dryout CHF.

While Celata et al. (1994) presented the CHF analysis based on sublayer dryout mechanism, which is the phenomenon happened when the liquid film depleted from the tube wall during the non-heated experiments. Their predictions shows good agreement with 1888 data points for water that experimentally investigated by many scholars previously.

5.5 Bubble Velocity in a Vertical Annulus Channel

Theoretical calculation by Ruckenstein (1970) using the velocity distribution function, shows that at low oscillation frequency, the mass transfer coefficient will decrease proportionally to the decreasing frequency of translational bubble velocity and vice versa.

Most researchers use the Laser Doppler Velocimetry (LDV) to measure the liquid and gas velocity in two-phase flow. This technique offers to different amplitudes for the velocities of the two phases. Vassallo (1999) used this technique and found out that the increase of void fraction will reflect the increase of the velocity of gas phase and they confirmed this result using the hot film anemometry and images from high speed video camera.

Suzuki et al. (2002) carried out experimental investigations in a vertical counter-current for void fraction less than 7% to measure velocity profile around the bubble using Ultrasonic Velocity Profile monitor. Using this technique, they can obtain an instantaneous velocity profile along its measuring line across a channel. They plotted the results in the form of non-dimensional velocity profiles with wide ranges of flow conditions. It shows that the velocity field around a bubble has a similar structure to the turbulent boundary layer on a solid wall. This result is discussed with comparison to other scholars' model, that applied an assumption of a spherical bubble move steadily while rising in liquid, and on the relation between these two structures of boundary layer.

Zhang et al. (2003) developed a mathematical model to predict the interactive spherical bubbles behavior on the velocity while rising in an intermediate Re , based on different forces acting on the bubbles. They compared the prediction results with measurements made by other scholars and found out that the model incorporating both the wake effect and the bubble acceleration effect. It is also traced that if both bubbles

are kept in distance, the rise velocity of the trailing bubble can be well predicted by adding the mass and Basset force.

In theoretical analysis done by Hibiki et al. (2003) for large diameter pipe, and based on comparison on experimental data and correlations proposed by many scholars, they recommended that the drift–flux velocity for vertical upward flow for churn and annular flow can be predicted well by using the correlation proposed by Ishii (1977) and for cap bubbly flow the velocity can be predicted using correlations developed by Kataoka–Ishii (1987).

On the other hand, Hayashi et al. (2012) suggested that the fluid surfactant will also contribute to the rising velocity in vertical pipe. They used the interface tracking method, a CFD tool to track the rising of Taylor bubble in vertical channel occupied with contaminated water at low Morton number and simulations were conducted at various Eötvös number. The results show that the increase of terminal velocity will be affected strongly by reduction of surface tension and at high Eötvös number, no effect of surfactant is found, however at low Eötvös number surfactant effect is found to be quite important.

Shawkat et al. (2008) conducted investigation on the characteristics of bubbly flow in a large diameter vertical pipe by applying the hot film anemometry to measure the turbulent of liquid phase and optical probe to identify the bubble behavior. With range of liquid superficial velocities of $0.2 \sim 0.68 \text{ m/s}$ and $0.005 \sim 0.18 \text{ m/s}$ for gas superficial velocity they gained the void fraction of 1.2% to 15.4% where wall peaks were found at the low void fraction flow and core peaks slowly show up with the increasing void fraction. As the void fraction profile moved from a wall to a core peak, the average liquid velocity and the turbulence intensities were found to be less uniform. In more detail analysis, the turbulence intensities will increase when the bubble are introduced into the flow. With low void fractions of maximum 1.6%, and at high liquid

superficial velocities, turbulence suppression was observed close to the wall. Based on the dimensionless group and the force ratio, a non-dimensional map was proposed for void fraction in bubbly flow with two conditions of wall or core peak.

Using the Particle Image Velocimetry (PIV) and fluorescent tracer particles, Fujiwara et al. (2004) measured the liquid phase velocity in vertical upward driven bubbly flow to study the effects of dispersed bubble size on turbulence modification. They performed experiments at low void fraction of 0.5% and 1.0%. They found that bubbles strongly accumulate near the wall (wall peak) that as a result accelerates the liquid phase and fluctuation of liquid velocity intensity is reduced by high concentration of bubbles.

Velocities of elongated bubbles were studied for various flow rates and pipe diameters by van Hout et al. (2002), using the optical fiber probe and image processing. These measurements were compared with the appropriate correlation. For small elongated bubble the velocities were well predicted and in continuous slug flow, they were under-predicted.

Clark et al. (1990) performed some alteration in the drift-flux model so that it can be used for prediction in the low velocities and large diameter pipes. Using some data obtained from experiment in 152mm diameter pipes, computer simulation has been performed to establish new values for drift-flux profile constant when it is influenced by buoyancy effects. The recommended value for can be in the range of <1 to >10 for some outermost cases.

Lucas et al. (2011) applied the four sensor probes to measure the bubble velocity in bubbly flow of air-water and oil-water flows. They proposed the arrangement of new probe and calibration methods and presented that this new technique performed well for the particular purpose. The same approach was carried out by using a double sensor

probe also by Wu et al., (2001) for bubble velocity measurement in a vertical two-phase flow channel.

Revellin et al. (2008) also measured the length of elongated bubble but using different fluid, the refrigerant R-134a to study the effect of viscosity and the effect of subcooling in micro-channel. With small variation of subcooling (2 to 5 °C) and variation of evaporator length (30 to 70 mm), no effects are found on the bubble length. However, bubble length and the bubble velocity both show the increment during the decreasing of saturation temperature, which the effects of decreasing vapor density.

Celata et al. (2007) examined many correlations proposed by many scholars on terminal velocity of rising bubbles and assess the degree of accuracy of these correlations using wide range of data set. A simple experimental apparatus for this purpose was constructed and tested and the data of bubbles shapes and velocities taken from high speed video camera were compared with available correlations as mentioned. The comparison revealed that shapes of bubbles were well correlated by the Tadaki number and the Weber number and the terminal rising velocity were agreed well with correlations by Tomiyama et al. (2001).

5.6 Vertical Upward Two-phase Flow and Vibration

Dillon et al. (2005) studied the effects of wall gas injection and channel vibration on the pressure drop in two-phase flow through experiments in a thin annulus. They examined the effects of lateral mechanical vibrations that worked on the center of test section with frequencies of 5–400 Hz and amplitude of 0.034 ~ 0.2 mm and 5 ~ 400 Hz and found that the effects from the vibration on the pressure drop were generally small.

Some works have been conducted by Ellenberger et al. and Krishna et al. (2002-2007) and Vandu et al. (2004) on the effects of vibration in a bubble column with investigations in many aspects such as, the liquid height due to bubble levitation, bubble

intensification and improvement of mass transfer rate. They applied the bubble column reactor and with low frequency vibration in the range of 40-120 Hz. The bubbles were generated from a specific gap using 12 capillary nozzles and vibration was excited to the liquid phase from the piston at the bottom of the reactor. They found that the application of vibrations to the liquid phase contribute to a better homogeneous bubbly flow regime and at the same time delay the progression of flow pattern of churn-turbulent regime. The experimental values for height of liquid, h were found to be in good agreement with the theoretical model developed by Baird (1963). In term of mass transfer rate, it was also confirmed that the vibration effect helped in improving the gas-liquid distribution through the channels and hence better mass transfer rate was obtained.

In relation to the enhancement of mass transfer rate in the processing industries there are also works conducted by number of scholars such as Fand (1965), Li (1967), Iida, (1992) and Bonekamp (1997), using the ultrasonic vibration. Kim et al. (2004) investigated the possibility of enhancing the heat transfer in pool boiling chamber and the natural convection. Their experimental facilities include the platinum wire as heating element and the temperature controller in both cases. They observed the cavitation behavior and bubbles from boiling nucleation using the high speed video camera.

These experiments show that different heat transfer regimes receive different influences from the ultrasonic vibrations with association of cavitation effects. Behavior of cavitation bubbles found to be strongly influenced the degree of heat transfer enhancement in the natural convection and subcooled boiling regimes. However, in saturated boiling, no cavitation occurs and the heat transfer enhancements are due to acoustic streaming and the reduced sizes of nucleation bubble.

As comparison, the highest enhancement ratio is obtained in natural convection regime. At this point, the effect of ultrasonic vibration is manifested through violent motion of cavitation bubbles.

Another effect of vibration to the flow channel is by its natural frequencies. Gorman et al. (1998) described the theoretical analysis of the effect of natural frequencies of a pipe on the annular two phase flow due to undamped vibration. From the nature of application, they studied this effect both for the cases where fluids are flowing inside and outside the pipe. The model of the pipe was set as cylindrical shell and is fixed at both ends and the fluid is non-dimensionalized. The results show that in the internal flow, the natural frequencies decrease with the increasing density ratio, i.e. in a stabilized annular flow where the density ratio of gas-liquid is small, the natural frequencies will be much greater. The external flow has similar effects as the internal flow only differ when the fluid is not in contact with the pipe.

Most numbers of the works that associating vibration and two-phase flow would be the flow induced vibration. Huda (1998), Hibiki et al. (1998) and Sasakawa and Serizawa, (2005) are among the scholars who worked on this issue. Khushnood et al., (2004) reviewed more than 100 literatures on the flow-induced vibrations particularly on the known models and experimental research. They concluded that there is some agreement in the general conclusions despite of the considerable differences in the models and experimental results.

For experimental base, most of the works carried out are in wide range of investigations being the general examinations on local flow parameters for many applications such as rod bundles, u-tube steam generator, incline pipes and so on. Hibiki et al. (1998) for example conducted the experiments using the vibration and non-vibration as reference. In their facilities, the reference was fixed in a very tight manner in order to achieve a zero vibration effect and the vibration experiment was set to be a

loosen test rig to enable the effect of vibration. Bubbles coalescences were found to be rapidly occurring during the low superficial liquid velocity due to flow-induced vibration but were easily breakup by the influence of turbulent energy in the liquid. This effect leads to an increase of Sauter diameter and decreasing of interfacial area concentration.

The effects of flow-induced vibration also changed the void fraction profile from wall peak to core peak or transition, which increased distribution parameter in the drift-flux model. Flow induced vibration; on the other hand enhanced the liquid turbulence in the high superficial velocity condition and the two-phase flow developed a dominant a shear-induced liquid turbulence. Therefore, the effect of flow-induced vibration can be concluded as very low in the high superficial velocity if compared to low superficial velocity of liquid.

Other than the natural phenomena of flow induced vibrations and natural frequencies from pipe flow, there are very little works being conducted to study the vibration effects on the two-phase flow particularly with the scale of vibrations which occur during the natural disaster such as earthquake and tsunamis. Therefore this study endeavored in a new challenge to investigate the effects of this scale of vibration on the vertical upward gas-liquid two-phase flow. The analyses were carried out in many aspects as described in the following chapters.

6.1 Introduction

Gas-liquid two-phase flow in pipes are widely encountered in many engineering applications such as in processing and power plant industries, which comes with equipment such as the evaporators and condensers, gas-liquid reactors and also in combustion systems. The two-phase flow is in fact a difficult subject principally because of the complexity of the form in which the two-fluid exist inside the flow channel, and they are divided in scientific term as the regime.

A detail discussion has been carried out in Chapter 5 on various phenomena occurring in vertical upward gas-liquid two-phase flow such as the change of flow patterns and transition from one pattern to another from the effects of the various parameters and flow conditions. In the two-phase flow, the concept of holdup is very important where it defines the relative fraction of one of the phases in a particular flow channel. This is not necessarily equal to the relative fraction of that phase while the entering fluid mixture. This indicates that the measured value of velocity, pressure, temperature and other parameters of each phase might differ before and along the mixing section. As one of the most important parameters that always play an important role in the determination of flow conditions, the velocity of each phase is termed as the superficial velocity.

All the above information is very important in order to develop the experimental facility for any purpose of application. The current study however is an endeavor in a new phenomenon that is very important in the application of the two-phase flow. The effects of vibration were studied on the flow structures and dynamics of two-phase flow. In view of this, vertical ground accelerations in wide ranges of scales were applied, particularly to investigate the effects of heavy disaster shakes such as earthquake onto the gas-liquid two-phase flow.

In order to conduct such investigations, a scale down two-phase flow experimental rig was developed and experimentations were carried out for wide range of flow conditions. This experimental rig was equipped with high end of measurement technologies and reliable sensors developed based on previously obtained successful results by other scholars.

6.2 Development of Two-phase Flow Rig

The current studies on vertical two-phase flow were concentrated on four parts; the flow patterns, flow mapping, void fraction and instantaneous bubble velocities. In order to conduct all the four elements of work, a vertical two-phase flow rig was constructed. It consists of a 1.2-*m* length of transparent pipe with inner diameter of 20-*mm* and an implanted void sensor on the inner wall. The construction of the current facilities is shown in figure 6.1.

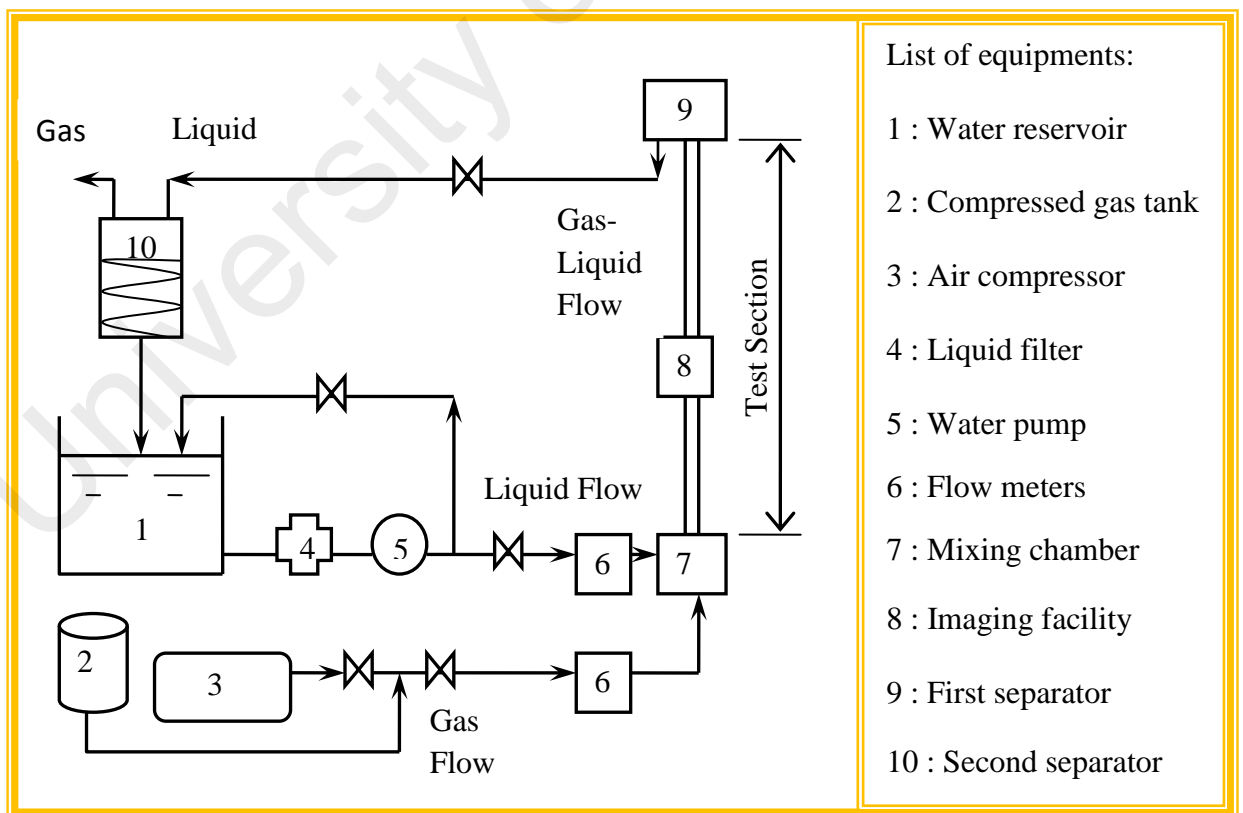


Figure 6.1 : Experimental apparatus for vertical upward two-phase flow

6.2.1 Basic Principle of the Facilities

The working fluids for the current work are air and water as mentioned in the previous chapters. As shown in figure 6.1, water was supplied from tap source into the 500liter capacity reservoir and filtered before pumped into the loop. The liquid flow rate was measured before it enter the mixing chamber with Kofloc digital water flow meter and based on the 20-*mm* inner diameter flow channel, the liquid velocity was listed next to it for a reference during the experimentations. The water temperatures were also recorded via digital thermometer placed at the reservoir and throughout the experimentations, it was maintained at 27 ~ 30°C.

In order to achieve the two-phase flow, the air is injected into the system from the compressed tank and flow through the gas pipe into the mixing section and the flow rate was measured by two different Kofloc, Japan gas flow meters for low and high mass flow rate. The tip of the gas line was covered with porous cap with very fine holes in order to produce very fine small bubbles into the test section. At the mixing section, the gas and liquid mix together and the gas bubbles move upward co-currently with the liquid flow.

The upper end part of the test section was constructed with small separator to allow the gas bubble separate from the liquid and was connected with flexible tube that will deliver both the gas and liquid into a bigger separator at the top of the flow loop. The liquid is then channelled back into reservoir and recirculated again into the flow loop.

Since the current studies focus on the effects of the vibration onto the two-phase flow in the pipe, all the test section part was placed on the vibration platform that specially developed for this study as disussed in chapter 3. This test section was connected through the flexible pipes to the main loop to allow the flexible movement during the vibration and also to avoid the leakage due to these aggressive motions.

6.2.2 Experimental Apparatus

For flow pattern investigations, systematic observations were conducted using a high speed camera and proper lighting system of two halogen lamps. The same Canon fast-cam Rabbit as used in the bubble column experimentations was also used for this purpose. This camera was fixed at the middle of the test section to shoot the bubble shapes and motions as a method to investigate the flow patterns in the two-phase flow channel. It was placed on the vibration platform as well and move together with the flow channel without changing its position and therefore the real changes of bubble motion can be captured.

After the recorded flow patterns were analyzed, the flow mapping processes were then being carried out. The flow patterns transition at the same location was carefully examined and these data were recorded on the graph sheet, differentiating all the flow pattern according to the variations of both liquid and gas superficial velocities. For both the flow patterns investigations and flow patterns mapping, only the rapid significant changes were recorded and the comparison of patterns during the steady state and vibration were carried out.

The effects of axial location on the void fraction distribution were also investigated, and therefore, this flow channel was divided into three sections where at each section the void sensor was installed. The first void sensor was placed in the Section I which is at 400 *mm* from the bubble injection and the section II starts with the second void sensor at 300*mm* from the first sensor and followed by another section with another 300*mm* gap making the third section. In between sections II and III another sensor was placed in the middle. The void fractions data were taken from all the four locations of void meters, with more concentration were paid on the upper three since the flow patterns will be more stable in these sections. The detail configuration for test section is shown in figure 6.2

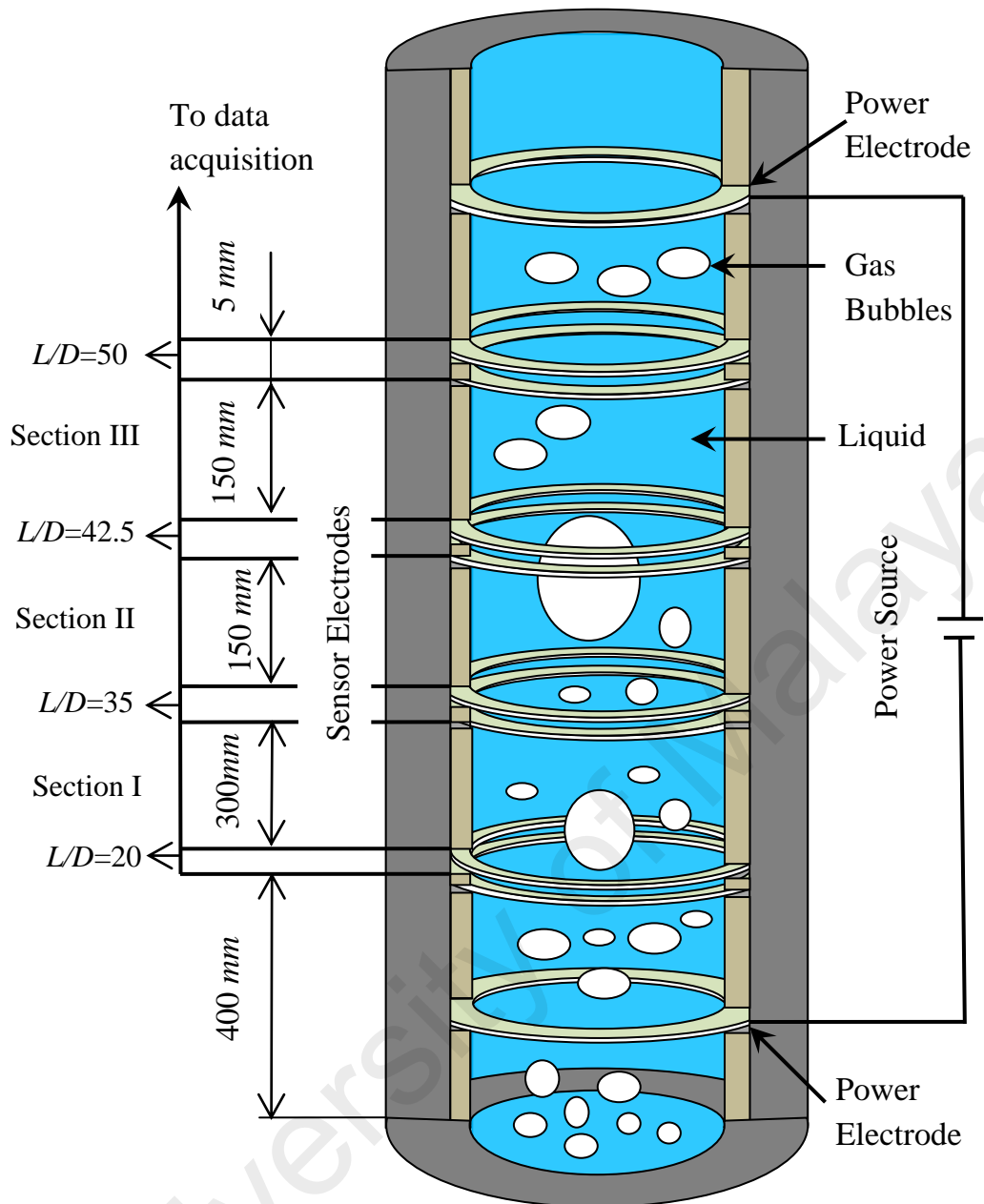


Figure 6.2 : Detail configuration of the test section for vertical upward two-phase flow

6.2.3 Analytical Flow Chart

The actual process of this work is explained in the flow chart provide in figure 6.3. This framework is with an objective to clearly show the experimental process and in a systematic arrangement. Apart from the development of the vibration platform, in

this part, the works were divided into three major divisions; constructions of two-phase flow loop, preparation of the apparatus, and void fraction measurement facility.

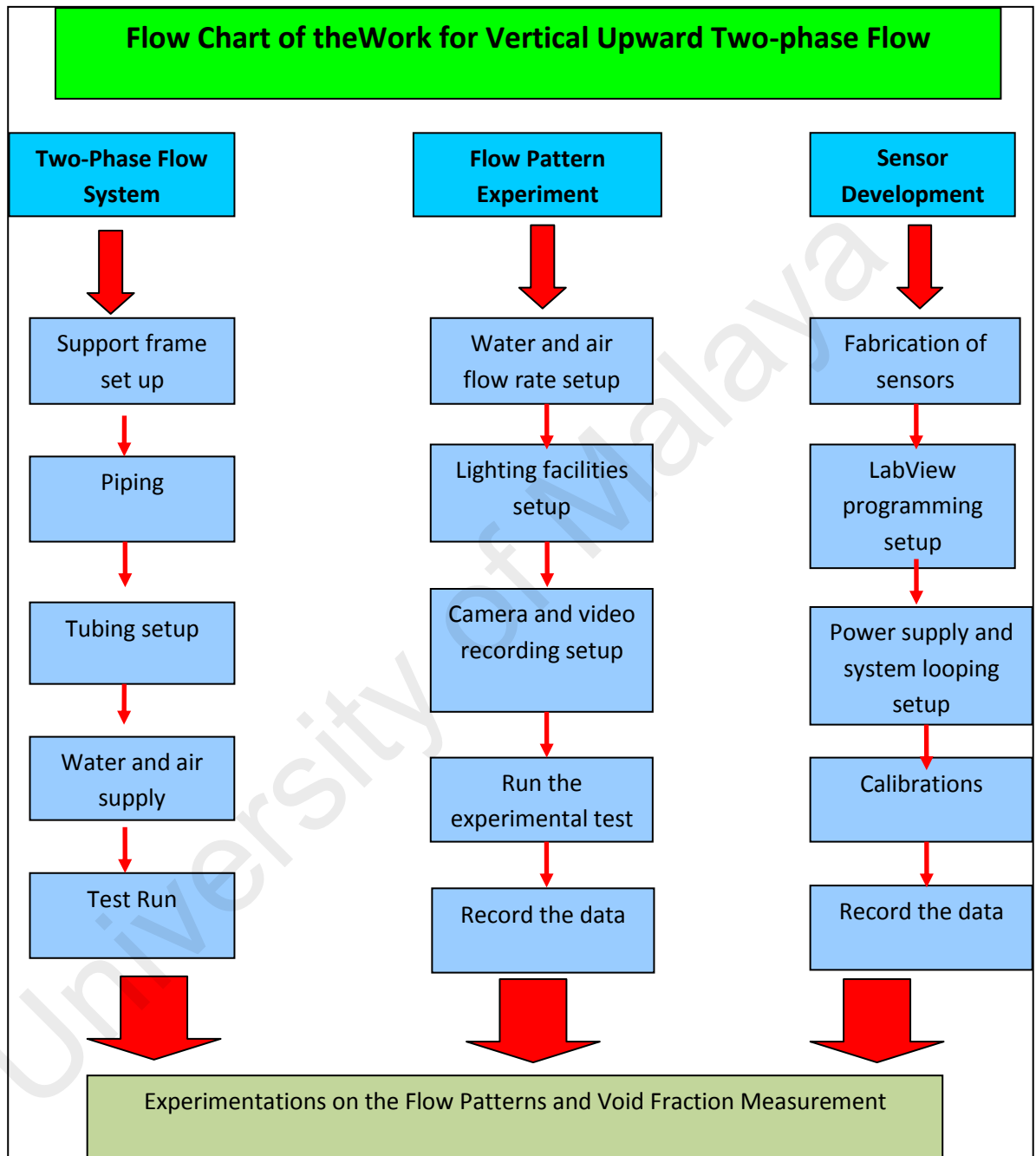


Figure 6.3: Flow chart for vertical upward two-phase flow experimental procedures

The actual experimental facility is as shown in figure 6.4. Here, the test section was placed on the vibration platform where the water flow into the system through the flexible tube from the bottom part of the test section and form two-phase flow mixture in the flow channel. The upper part of the test section was also connected with the flexible tube to deliver back the gas-liquid two-phase flow into the separator and flow back into the reservoir for recirculation into the loop.

All the numerical data from voltages fluctuation during void fraction and the vibration measurement were recorded real time and process by the two personal computers. The images of bubble flow in the flow channel were recorded using high-speed video camera and processed by the image processor in the PC. Close up of this facility is shown in Appendix 6.1.



Figure 6.4 : Actual photo of experimental facilities for vibration effects
on vertical upward two-phase flow

6.3 Development of Sensor for Two-Phase Flow Measurement

As discussed in chapter 5, there are many systematic approaches in measurement of two-phase flow parameters such as, void fraction, liquid film thickness and velocities conducted by many scholars in the history of two-phase flow. Among all, the electric conductance methods are quite famous, easy to understand and easy to be implemented as well. Nevertheless, there are varieties of electric conductance methods that being practiced such as, void impedance meter applied by Costigan and Whalley (1997), and Cheng et al. (2002), conductance probe by Mishima and Ishii (1984) and Hibiki et al. (1999) and also the constant electric current method by Fukano(1998). For the current work the Fukano method is applied since it is the most reliable so far in many experimentation carried out by Fukano (1998) and Furukawa and Fukano (2000) and as recent as Uesawa et al. (2012).

6.3.1 Constant Electric Current Method (CECM)

Outline of the Method

In this method, the composition of the system is formed by at least four electrodes. A pair of power electrodes is used to supply a constant electric current into the flow and the other pair is called the sensor electrode is used to capture the voltage fluctuation (holdup) when there is a gas bubble flow as gas-liquid two-phase flow. In the application, the position of these pairs of electrodes must be separated, where one piece of power electrode must be placed at the bottom (for vertical) or at the beginning (for horizontal) of the flow channel, and the other piece at the upper part (for vertical) or at the end (for horizontal) of the flow channel. The pair of sensor electrode is therefore must be placed in between the power electrodes.

For sensor electrodes, the space between the pieces is not fixed, where it can be arbitrarily installed depending on the application or the purpose of measurement. For

example, in the measurement of local void fraction, the space can be in few millimeters in order to capture the voltage fluctuation when the bubbles pass through. It can also be in several hundred millimeters for measurement of average liquid film thickness in a particular space in the flow channel.

The CECM method is in good priority to be applied as a two-phase flow sensor since it is independent from the power electrode because of the proper manner of its construction. The basic idea of this method can be referred to figure 6.2 and repeatedly displayed in figure 6.5 where the power electrodes are far separated, and the sensor electrodes are placed in between them. With this arrangement, the power electrodes are able to supply a sufficient density of constant electric current, making a uniform distribution along the flow channel, and therefore, at any location, as a conductance method, the voltage reading will be in the same value, and thus enable a good result for the measurement.

Therefore, there is only one pair of power electrode needed to be installed for a particular flow channel and hassles such as multi wiring and power sourcing can be avoided. The voltage output that captured by the sensor electrodes is transferred to the pre-amplified data acquisition by National Instruments. This voltage fluctuation data is then digitally transferred into a personal computer and recorded in the LabView software. In this case, the increase in voltage output with the increase of electrical resistance caused by the existence and increasing of the gas flow rate in the two-phase flow experiments is independent of the locations of the gas phase in the cross section of the flow channel. Therefore, some shortcomings encountered in other conductance method, such as the voltage fluctuation during measurement of various parameters in different flow patterns in the channel can be avoided.

The voltage fluctuations also are independent of the sensor electrodes, where these electrodes are connected to different ports on the data acquisition. Therefore, it is

possible for construction of multiple number of sensors along the flow channel, and simultaneous measurement of all sensors can be carried out; for instant as an application to measure the bubble instantaneous velocity based on data from different locations of local void fraction.

A disadvantage of this method is only on the fabrication of the sensors where very careful procedures must be carried out. On the hand, the difficulty of installation should also be taken care of since these sensors must be at flush position with the surface of flow channel. This installation method however, is very good since it does not disturb the flow. Therefore, flow agitation due to disturbance of coils or probes as faced in other methods can also be improved.

6.3.2 Basic Equations

Using an electrical resistance concept, let us consider electrical resistance during the two-phase flow, R_{TP} in a unit length of the channel as,

$$\frac{1}{R_{TP}} = \frac{1-\eta}{R_G} + \frac{\eta}{R_L} \quad (6.1)$$

where the electric resistances; R_G for gas phase and R_L for liquid phase when each of them solely occupies the whole cross section of the channel and η is the holdup or the percentage of liquid volume to the total volume of the channel. Considering V_{TP} as the voltage drop in a unit length when constant current I_0 is supplied, and for air-water two-phase flow, the resistances size should be, $R_G \gg R_L$, therefore, the holdup can be expressed as,

$$\eta = \frac{R_L}{R_{TP}} = \frac{I_0 R_L}{I_0 R_{TP}} = \frac{V_L}{V_{TP}} \quad (6.2)$$

where, V_L is the voltage output during the sole existence of liquid that occupied whole cross section of the flow channel.

6.3.3 Construction of the sensor

The electrodes as discussed in the previous section can be fabricated using any electric conductor. In the current work, they were constructed from 0.5-*mm* thickness Copper plate, with electric conductivity of a ring shape at $\sigma=5.96\times 10^7$ S/m. The fabrication of these rings were done very thoroughly to fit the inner diameter of the flow channel at 20-*mm*. They were then installed flush to the inner wall in order to avoid the problems as discussed earlier. The pair of sensor electrodes were placed at four different location along the flow channel at 150-*mm* distance between each other and the gap between the electrodes of each sensor is at 5-*mm*. The configuration of this sensor, without scale is shown in figure 6.5.

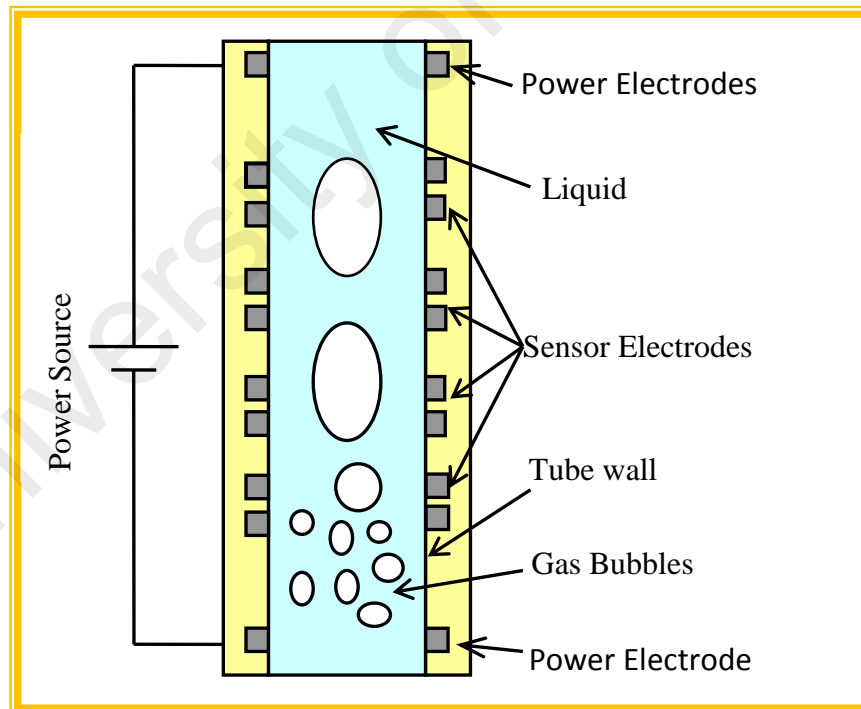


Figure 6.5. Configuration of CECM sensors

A power source by Wells-Gardner Electronics Corp. was used in this work and a constant electric current in the range of 0.1~0.3 mA was applied. A low direct electric current was considered in this work to avoid the electrolysis on the electrode surfaces to avoid any unnecessary gas bubbles in the flow channel. The output from the four sensor electrodes were sampled using data acquisition and the data were digitized to compute three main parameters in the current works; the void fraction, liquid film thickness and bubbles instantaneous velocity.

6.3.4 Calibrations

In order to validate the reliability of the measurement of this sensor, a good calibration based on proper method must be carried out. Two calibration methods were conducted for this purpose as the following.

(a) Static Calibrations

The easiest way to calibrate this sensor is by using a static method. It can be conducted by applying the electrical resistance concept; where any non-conductive material can be applied to replace the real gas bubble in the test channel in order to capture the voltage fluctuation. For this purpose, cylindrical acrylic rods with four different diameters were inserted one by one into the channel that initially filled up with water.

In order to replicate a single bubble passes through the channel flow, shorter rods of which length is longer than the sensor gap (5-mm) were used. On the other hand, for estimation of group of bubbles passing through the whole channel, longer rods with various diameters were applied. Therefore, when these rods were placed in the center of the sensor electrodes, the voltage fluctuation were recorded, and they actually differ among positions of the sensors. Hence, very careful and systematic data recording is recording in this case.

The concept of the void fraction based on nonconductive rod is as follows,

$$\alpha = \frac{A_C}{A_E} = \left(\frac{D_C}{D_E} \right)^2 \quad (6.3)$$

where A_C , A_E , and D_C , D_E are the cross sectional area and diameter of the calibration rod and the experimental flow channel respectively.

In this work, a 20-*mm* diameter flow channel and six different diameters of calibration rods were used. Table 6.1 gives the ratios of the cross sectional areas based on these rods to the experimental channel.

Table 6.1 : Area ratio based on calibration diameter

Calibration Rod Diameter, D_C [mm]	Area Ratio, α [-]
4	0.0400
5	0.0625
8	0.1600
10	0.2500
15	0.5625
18	0.8100

According to equation (6.2), when $V_L = V_{TP}$, holdup is $\eta = 1$, which implies that only liquid exist in the channel. Hence, void fraction can be expressed as,

$$\alpha = 1 - \eta = 1 - \frac{V_L}{V_{TP}} \quad (6.4)$$

when, $0 < \eta < 1$. In both cases for calibration rod tests, the radial effect (location of the rod at the radial of the channel), and the amount of constant current were also investigated. This is to check if there is any effect of the bubbles locations since the positions of bubbles in a flow channel are unexpected.

Based on equations 6.3 and 6.4, calibration tests were carried out and their curves were plotted. Figure 6.6 shows the result of the test model for calibration where four different amount of electric current supplied into the channel, which initially filled with water. Here, it is found that within these current ranges, the calibration line is fitted well with the accuracy of 2%. Hence, it can be concluded that the amount of electric current supplied into the liquid in the flow channel does not affect the measurement of void fraction.

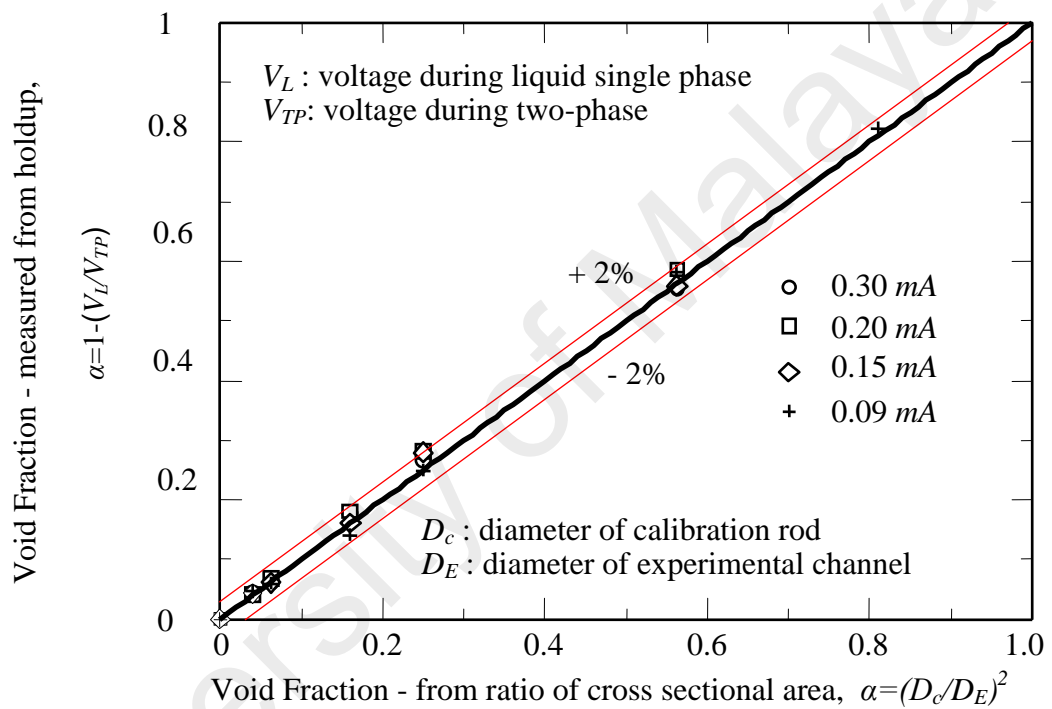


Figure 6.6 : Electric current effect on holdup

The effects of radial location on the voltage drop was investigated and the result is shown in figure 6.7. In this case, the calibration was placed in the center, left and right positions and a constant electric current was supplied into the liquid in the flow channel. Here, it also revealed that the voltage drop are almost constant regardless of the position rod in the experimental channel and therefore confirmed that there will be no effect of bubble positions for void fraction measurement using this method.

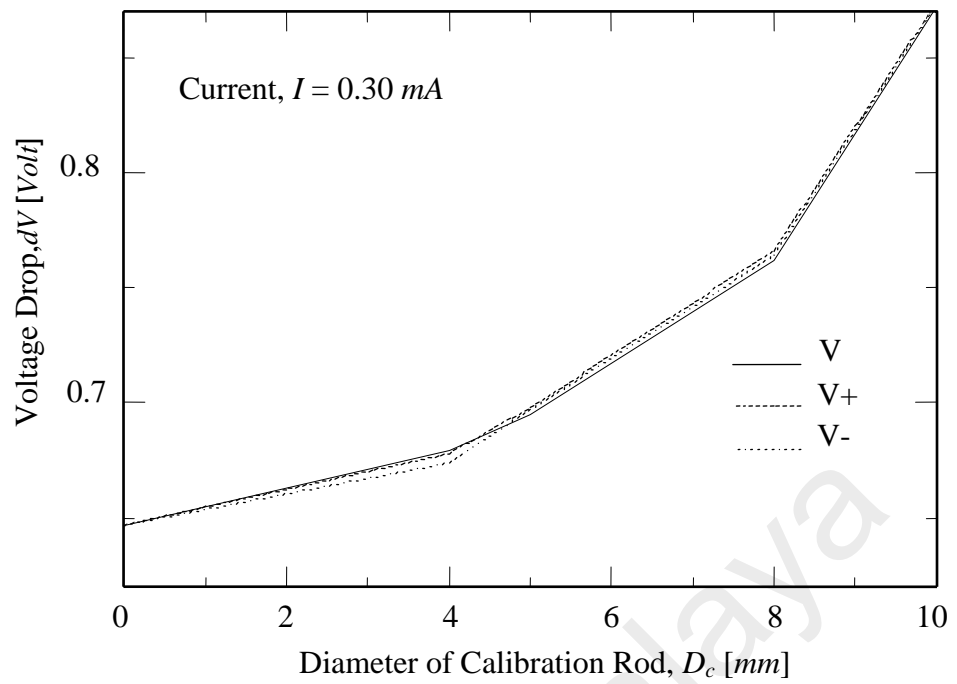


Figure 6.7 : Voltage drop by radial location

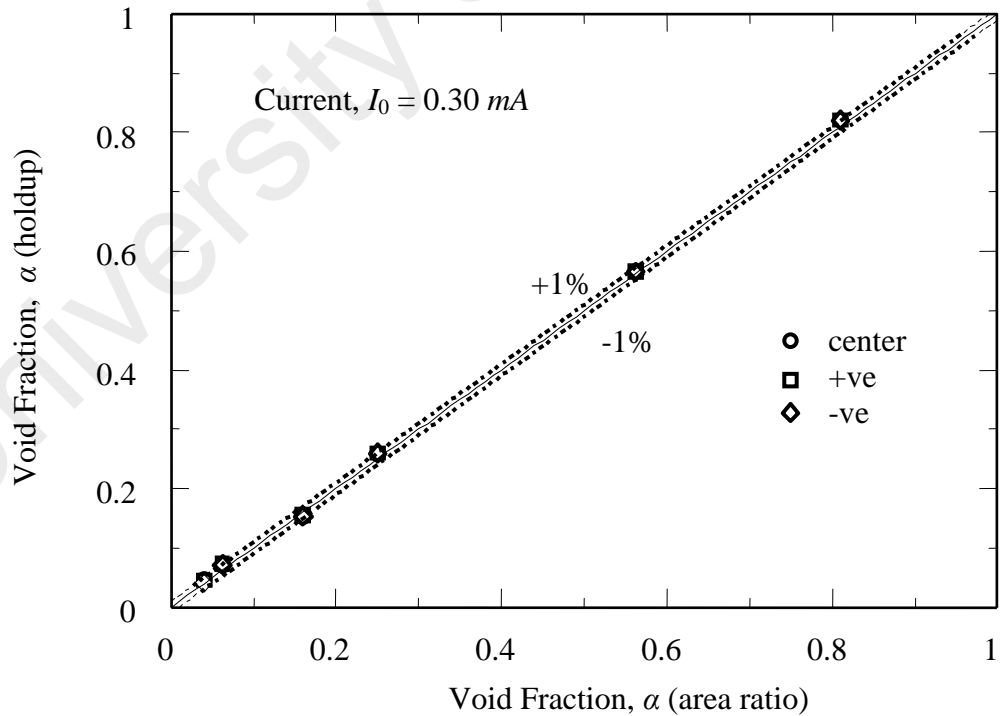


Figure 6.8 : Radial location effect on holdup

Using the same data from figure 6.6 and 6.7, the effect of the radial position of the rod during the calibration to the holdup can be pulled out and this is shown in figure 6.8. With 1% different, the accuracy is found to be very good and this reflected that the CECM method would be a reliable tool where electric resistance caused by the bubble at any radial position of the flow channel can be detected.

The calibrations for sensor electrodes on the experimental channel were conducted for four times at four axial positions based on the ratio of length, (position of the sensor from the two-phase mixer) and diameter of flow channel, L/D using both the long and short cylindrical rods and they are shown in figure 6.9. The difference of the symbols signifies the repetition of calibration, and A and B denotes the long and short respectively. Again, the similar results were obtained with good accuracy at 3%, meaning that good data for measurement can be reproducible as well.

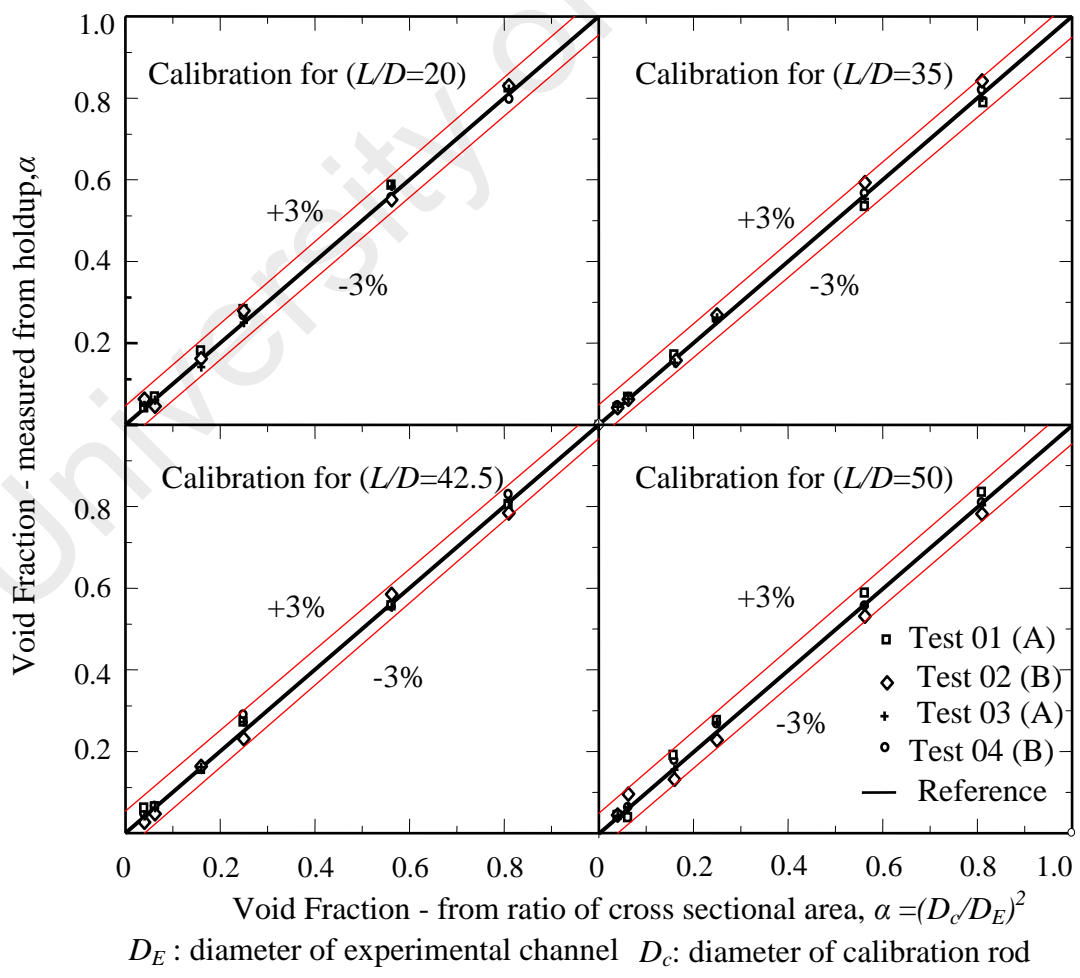


Figure 6.9 : Static calibration for CECM sensors

(ii) Dynamic Calibrations

Since the static calibration does not give the real picture of the two-phase flow due to stationary position of the calibration rod, there is a strong requirement to conduct the calibration using the real moving bubbles. In order to fulfil this requirement, the dynamic calibration was conducted by comparing the visual data from the recorded images and the measurement by the sensors. In these tests, a single air bubble was injected through the bottom of the liquid filled with water via a syringe with six different needle sizes to produce different sizes bubbles. The image of the bubble was captured by the high speed video camera, and at the same time as it passes through the sensor the voltage fluctuation was recorded. Since it was released as a single bubble, there were no trailing bubbles behind it and therefore it can be confirmed that only the captured bubble that passed through the sensor.

For continuous bubble rising, the bubbles were released from a compressed gas tank and the average areas occupied by gas bubbles were examined. The images of the captured bubbles were analyzed where the area and diameter sizes were determined with comparison to the tube diameter. The obtained sizes were then compared with the recorded data from the sensor and the same comparison as shown during the static calibration in figure 6.9 can be carried out and they are plotted as in figure 6.10.

This dynamic calibration also has been conducted at four different locations of sensors. According to this figure, there is a slight difference from the static calibration result, where this dynamic calibration gives an accuracy of 5%, which is an acceptable tolerance. In this figure, the Test 101 and Test 102 denote the calibration using single bubble of different sizes and Test 103 denotes the calibration using continuous rising bubbles. For this calibration, the liquid superficial velocities (j_L) were varied in the range of 0.25 ~ 1.0 m/s. The results show very similar accuracy as discussed above, but for the current report, calibration with $j_L=0.25$ m/s and $j_L=0.5$ m/s are presented.

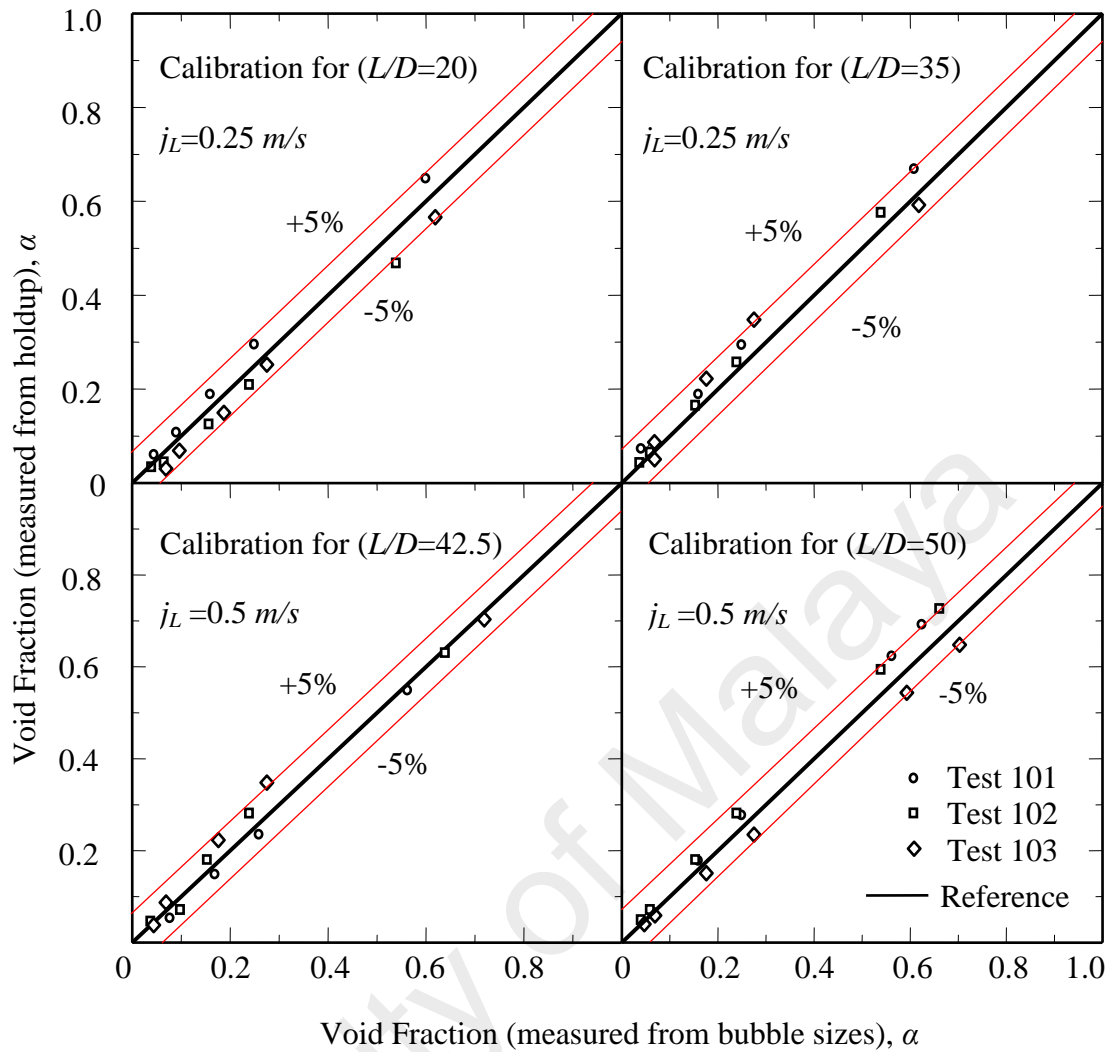


Figure 6.10 : Dynamic calibration for CECM sensors

6.3.5 Reliability Test

The fluctuation of void fraction were measured in the case of vertical upward air-water two-phase flow and their time mean values were calculated using the data obtained in quiet a long period. Figure 6.11 shows the example voltage fluctuation that was used to compute the holdup. Here, V_L denotes the voltage read during a liquid single phase occupied fully in the cross sectional area of the flow channel and V_{TP} denotes the voltage fluctuation during the two-phase flow. With a fixed V_L and variation of V_{TP} , and referring to equation 6.4, the void fraction along the channel can be easily calculated for variation of flow conditions.

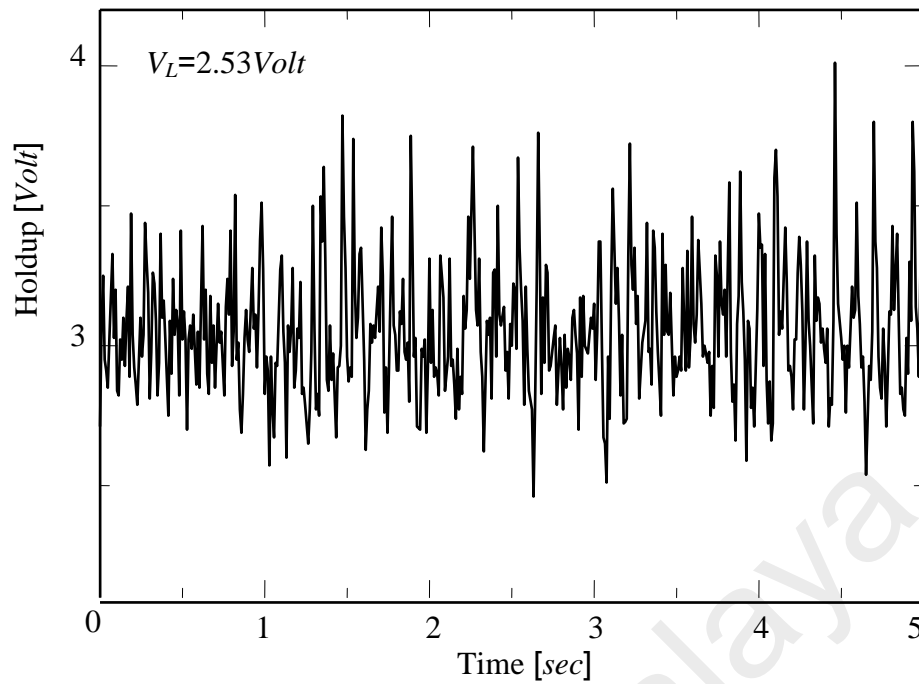


Figure 6.11 : Example of voltage fluctuation for holdup to measure void fraction

(a) Comparison of Void Fraction

As an introduction and particularly for the presentation on the reliability of the current sensor, the value of void fractions fluctuations were measured for the arrangement of vertical upward air-water two-phase flow for a fixed liquid superficial velocity, $j_L=0.1, 0.75, 1.0, 2.0$ and 2.5m/s and gas superficial velocities, j_G in the range of $0.025 \sim 0.25$ m/s. Their time mean values were calculated using the data obtained in quiet a long period and plotted against the slip ratio, j_G/j_L in figures 6.12 ~ 6.16. The current result was compared with three other data obtained previously by other scholars from 1960's and these data are used widely in the studies of two-phase flow. The current result shows very similar patterns with other data and the value of void fractions were very well obtained with acceptable range. Some results for void fraction measurement in a long vertical annulus pipe with length of 4-m also has been reported by Zubir and Zainon (2011). In their work, the CECM sensor performed very well and the measured results were in very good range with comparison to prediction method by Bestion (1990).

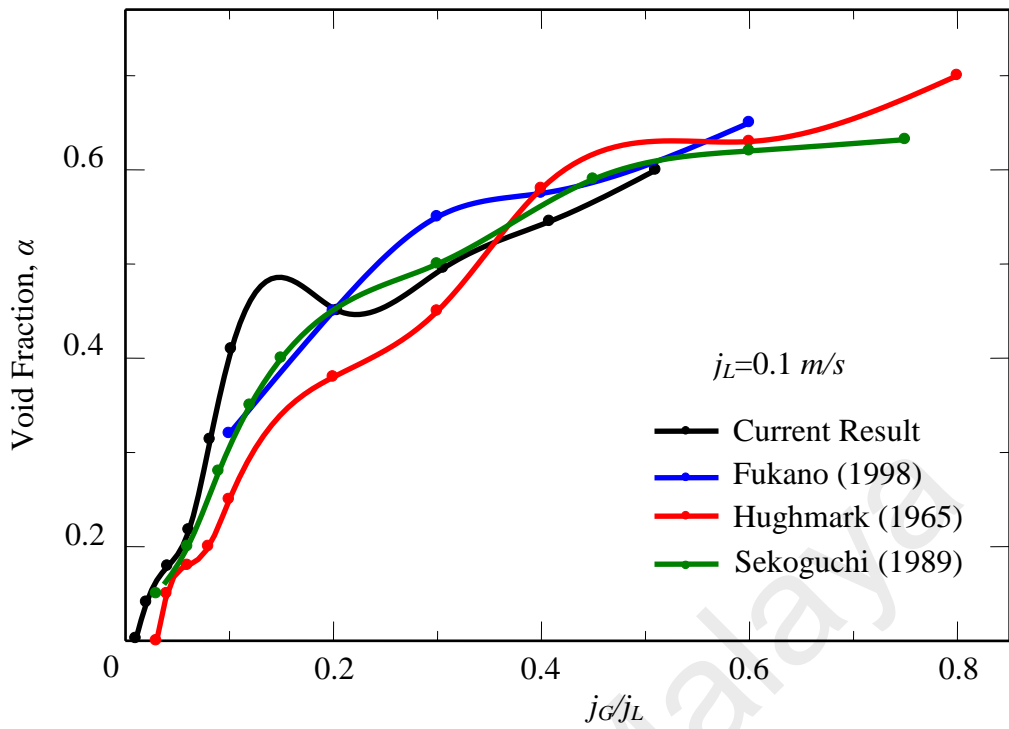


Figure 6.12 : Comparison of measured void fraction with other scholars' for $j_L=0.10 \text{ m/s}$

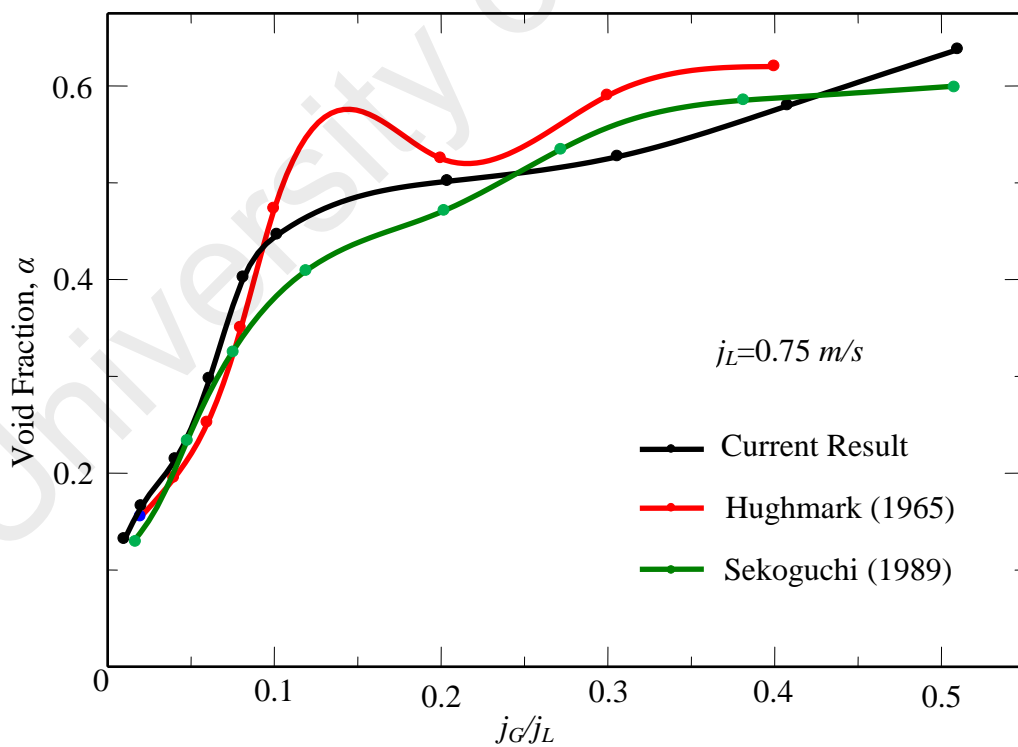


Figure 6.13 : Comparison of measured void fraction with other scholars' $j_L=0.75 \text{ m/s}$

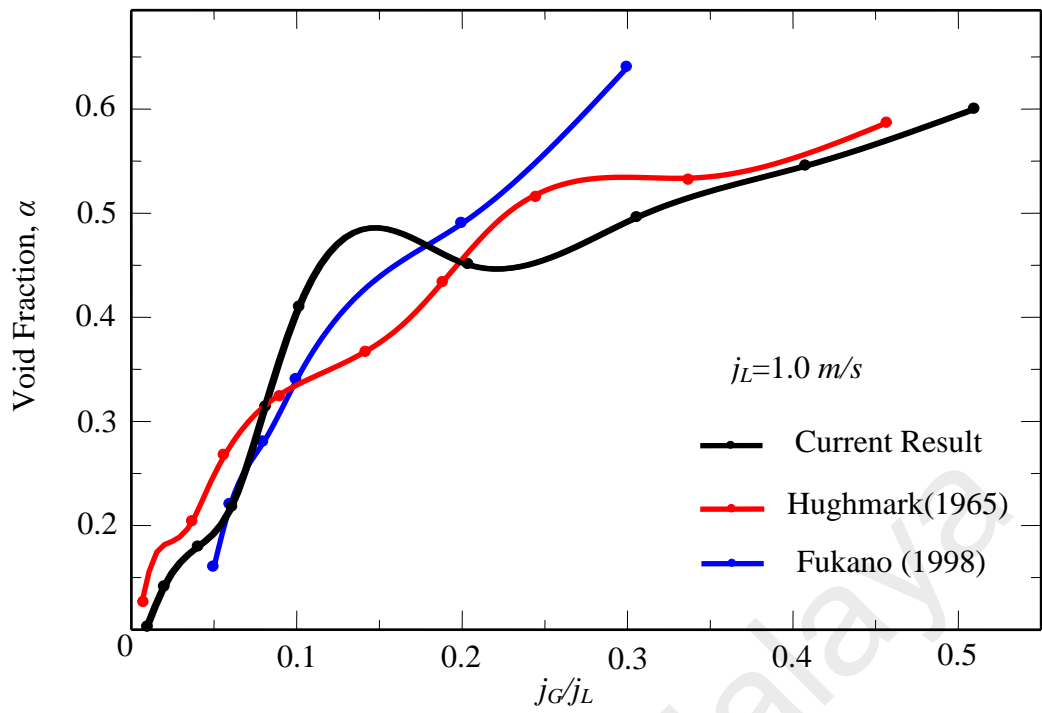


Figure 6.14 : Comparison of measured void fraction with other scholars' for $j_L=1.0 \text{ m/s}$

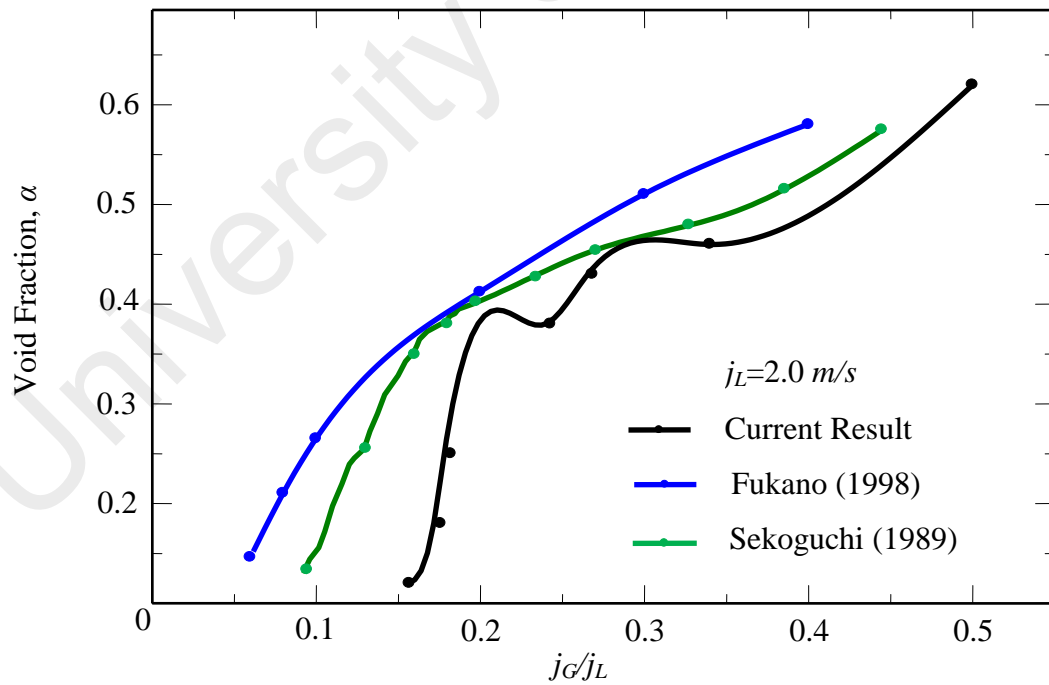


Figure 6.15 : Comparison of measured void fraction with other scholars' for $j_L= 2.0 \text{ m/s}$

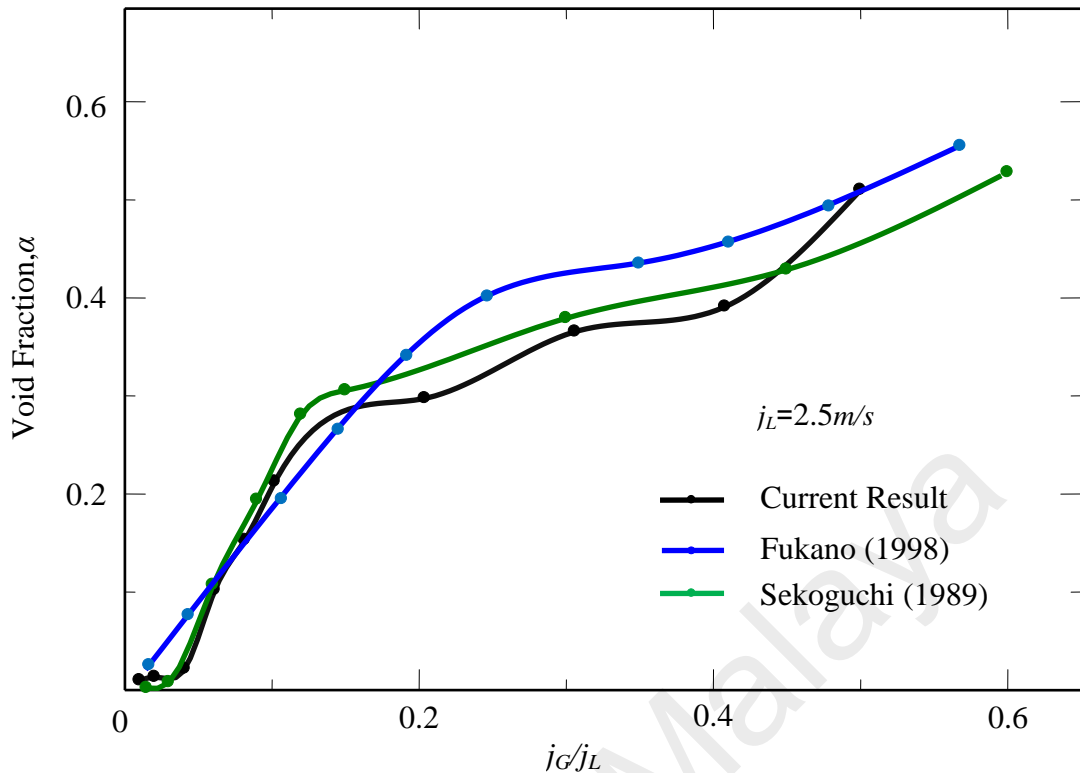


Figure 6.16 : Comparison of measured void fraction with other scholars' for $j_L = 2.5 \text{ m/s}$

(b) Comparison of Liquid Film Thickness

In the process engineering and power plant applications, the liquid film thickness represent the severance of a particular flow condition and particularly very important for the cases that involve with heat transfer such as boiling and condensation. This parameter will determine the point of dryout or burnout on the heating surfaces and therefore its measurement is very significant. Dryout is a phenomenon that occurs when the film on the heated surface disappears due to evaporation and droplet formation. While the burnout in departure from nucleate boiling (DNB) is another phenomenon that occur when the thin liquid film beneath the vapor slug completely evaporate during the passage of of slug bubble (Katto, 1992). Therefore, in order to predict the critical heat flux (CHF) for dryout and the burnout DNB, the accurate knowledge of liquid film thickness is very important.

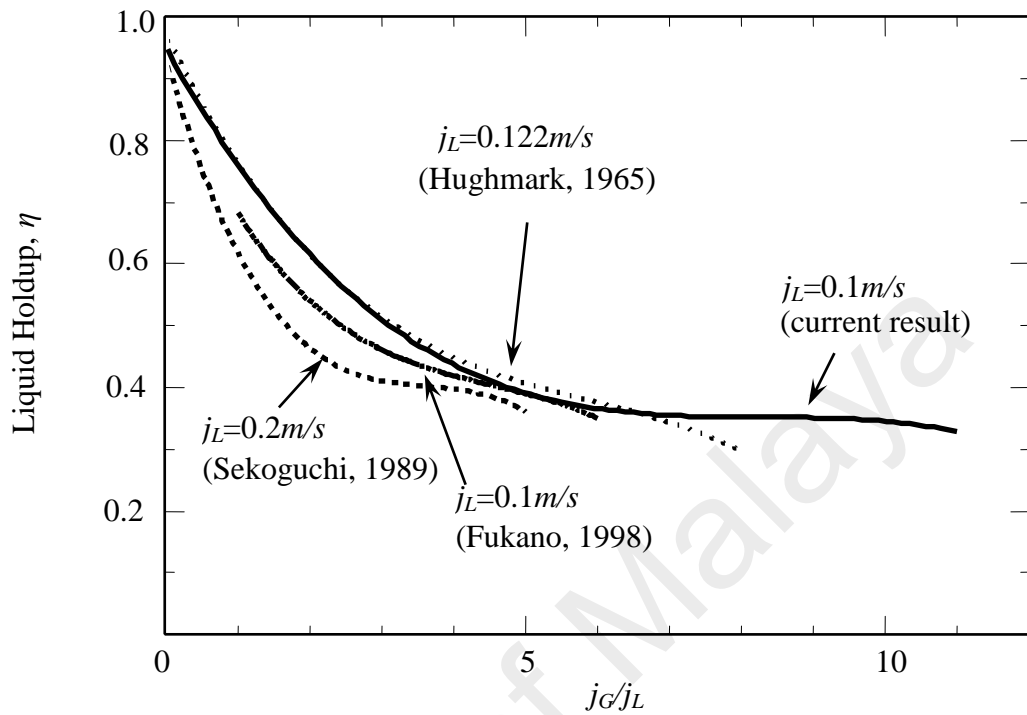
On the other hand, during the low quality boiling, the CHF was postulated by Weisman and Pei (1983) as a local phenomenon where the bubble layer builds up in thickness along the channel until it fills the region close to the wall where the turbulent eddy size is sufficient to transport the bubble radially. At the CHF location, the bubbly layer assumed to be at the maximum thickness. DNB is considered to occur when the average void fraction in the bubble layer just reaches a certain limiting value, α_{limit} . In all of the cases discussed here, the liquid film thickness and void fraction are both very important to be considered and must be well measured. These models are presented in Appendix 6.3.

There are also several method developed to conduct this measurement such as, laser extinction method, (Utaka et. al., 2007) and ultrasonic transmission technique, (Kamei and Serizawa, 1998) as well as theoretical method (Bretherton, 1961). However, these techniques are limited to measurement of film thickness and not suitable for the other parameters, therefore requires additional sensors for the others. Furthermore, they can only be applied for certain cases of flow condition.

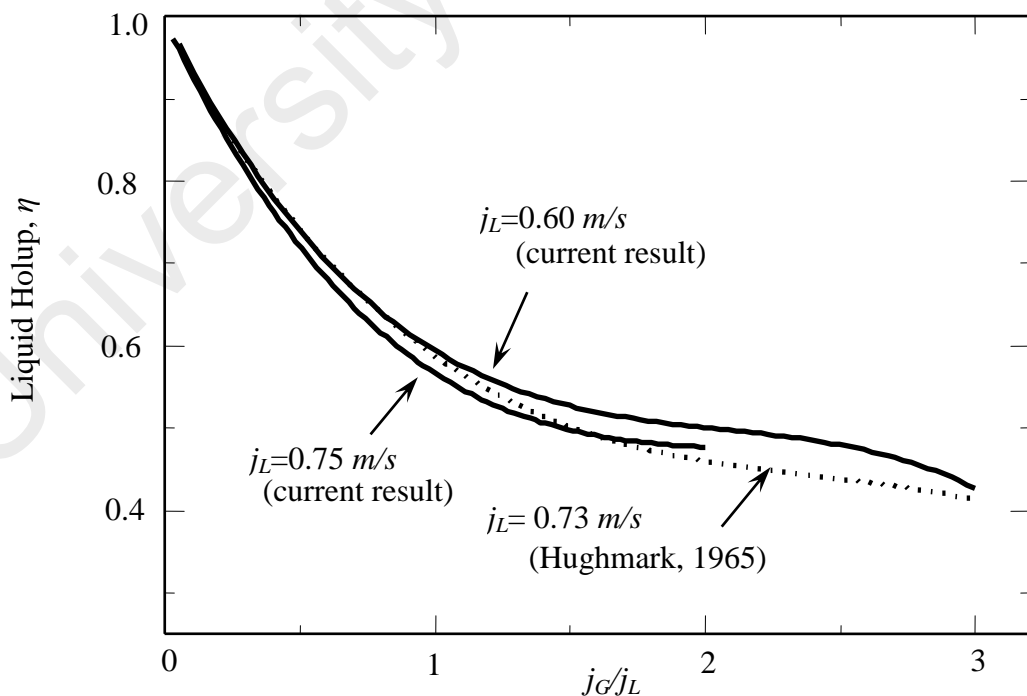
An attempt has been carried out to test this sensor on the measurement of liquid film thickness for wide range of flow conditions, with liquid superficial velocities, $j_L=1.0\sim 2.0$ m/s and gas superficial velocities, $j_G=0.5\sim 2.0$ m/s. The current results were compared with Fukano (1998), Hughmark (1965), and Sekoguchi and Takeishi (1989) as in figures 6.17 and 6.18 where they show very good agreement. These results however, still very limited for the current comparison, and more works regarding this matter need to be carried out to ratify this sensor and examine the limit of its performance.

As a result, it can be concluded that the sensor developed in this study which is based on the Constant Electric Current Method, has very good capabilities in

measurement of various parameters in the gas-liquid two-phase flow. It is very reliable and performed very well in wide range of flow conditions.

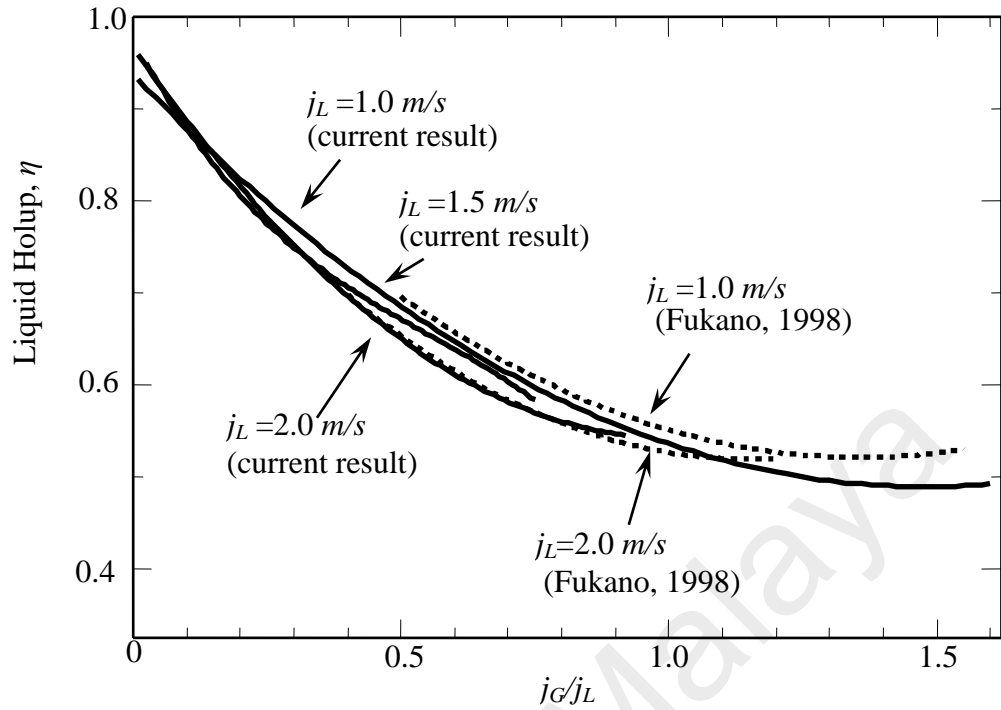


(a) Liquid film thickness comparison for $j_L=0.1 \sim 0.2 \text{ m/s}$

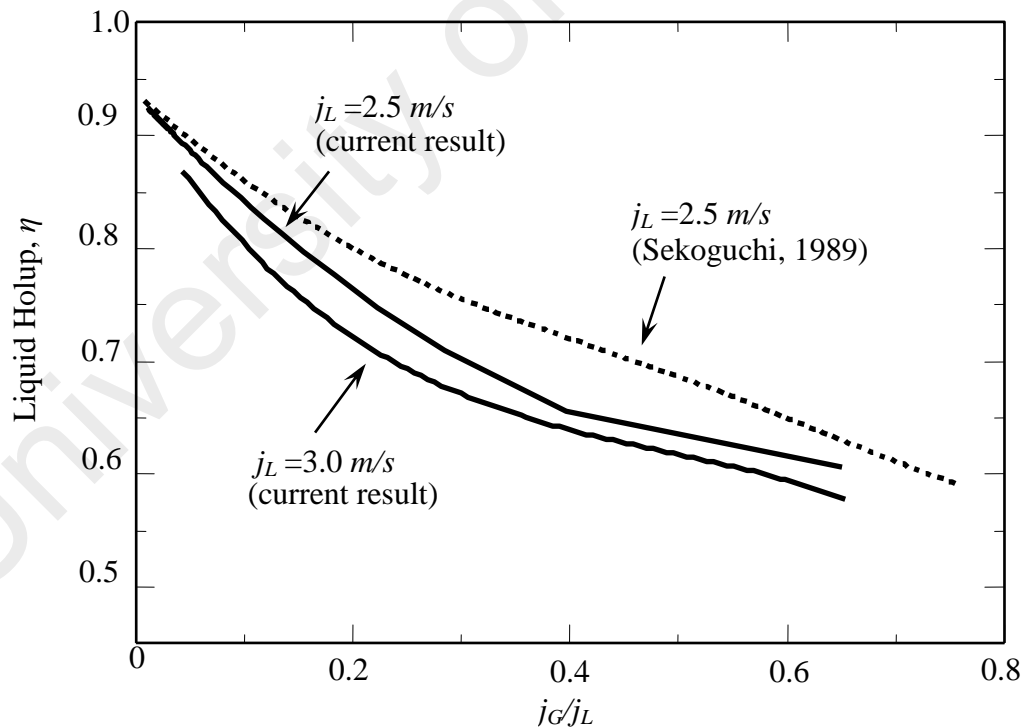


(b) Liquid film thickness comparison for $j_L=0.6 \sim 0.75 \text{ m/s}$

Figure 6.17 : Comparison of liquid film thickness (low liquid superficial velocity)



(b) Liquid film thickness comparison for $j_L = 1.0 \sim 2.0$ m/s



(b) Liquid film thickness comparison for $j_L = 2.5 \sim 3.0$ m/s

Figure 6.18 : Comparison of liquid film thickness (high liquid superficial velocity)

7.1 Outline of the Analyses

This chapter will present and discuss the results for four categories of investigations on the flow structures and dynamics of gas-liquid two-phase flow in a vertical upward arrangement in an annulus tube under the influence of vibration. The investigations can be categorized as the following:

- (i) Flow Patterns
- (ii) Flow Mapping
- (iii) Void Fraction
- (iv) Instantaneous Bubble Velocity

The experiments for each of the category were performed for both the steady state and transient condition. Steady state refers to the controlling experiments during no vibration and the transient condition refers to the conditions where the vibrations effects take place. The details of comparisons are presented in every section of these categories.

In section 6.2, it has been mentioned that the flow patterns were investigated using the visual observation techniques. The information from the photographic and video-graphic data were analyzed and lead to the flow mapping processes. Both of these investigations were varied by combination of different gas and liquid superficial velocities. The gas superficial velocities, j_G were ranged in 0.025 m/s ~ 0.75 m/s and the liquid superficial velocities, j_L were ranged in 0.25 ~ 2.5 m/s. Thus the slip ratio of the gas and liquid phases as according to equation 5.11 is in the range of 0.01 ~ 3.0.

Void fractions on the other hand, were measured using the electrical resistance concept described in sections 6.2.2 and 6.3.3 at four different locations along the flow channel with axial position, $L/D= 20, 35, 42.5$ and 50 . The first position, ($L/D= 20$) was set as the reference to check the responses of electric current in the flow and also to obtain the local void fraction at the beginning of the flow. The other three positions

($L/D= 35, 42.5$ and 50), which are in the section II of the test section as shown in figure 6.2 were used in the overall calculations for void fractions and provide the average void fraction values for further analyses in section 7.3. Variations of void fraction were also carried out accordingly to the combination of gas and liquid superficial velocities.

The instantaneous bubble velocities due to vibration effects were analyzed using the information from void fraction data using a computer programming. This code has capability to differentiate the peak values obtained from all the three locations of void sensors in time domain. Therefore, the distance traveled by the bubbles (distance of sensors = 150 mm) divide by the time taken from one location to another produce the values for velocities. Details of these results are discussed in section 7.4.

Table 7.1 : List of gas and liquid superficial velocities

Liquid superficial velocities, $j_L[m/s]$	Gas superficial velocities, $j_G[m/s]$
0.25	0.025
0.50	0.050
0.75	0.075
1.00	0.100
2.00	0.150
2.50	0.250

With the range of liquid and gas superficial velocities as in the above table, the function of slip ratio and its limit to the effects that caused by vibration can be evaluated. From equation 5.11, the range of slip ratio, $S=j_G/j_L$, will be, $0.01 \sim 3.0$, a good approach for the application on industrial scale gas-liquid two-phase flow.

7.2 Flow Patterns

From selected literatures in chapter 5, some detail discussions on the flow patterns and flow transitions in the vertical upward two-phase flow has been carried out. For the current work, the effects of vibration on the flow patterns have been investigated and this section will present the results of flow patterns based on the visual observations. As also discussed in the section 6.2, the images of bubble flow in vertical two-phase flow channel has been captured by a high speed video camera, and these photographic data have been analyzed frame by frame using the image processing software, the Pinnacle Studio. The observation took place at the center of the flow channel, and referring to experimental apparatus in figure 6.1 and channel configuration in figure 6.2, it is at the section II with two axial positions; which is between $L/D=35$ and $L/D=42.5$. Flow conditions were varied by changing the combination of gas and liquid superficial velocities as the pair listed in table 7.1. Selections of flow patterns in these analyses were based on the most extreme changes shown during the entire flow both for steady state and transient condition.

The effects of flow conditions and the vibration will be discussed in this section with the image of flow patterns are projected in the series of vibration modes started from the steady state or no vibration on the left and follow by other sequences of vibration sizes as Mode 0 to Mode 4(M0, M1, M2, M3, M4) to the right as in figures 5.3 ~ 5.20. These vibration intensities are discussed in section 3.3 and details are listed in Table 3.2 and their vibration spectra are displayed in figure 3.8. Theoretically, based on these vibration sizes, the bigger ground acceleration will contribute greater effects on the flow patterns. However, the other factor that would also affect the flow transition is the slip ratio in the flow channel. Therefore, these investigations will define the limitation of this effect with regards to the sizes of ground acceleration.

7.2.1 Liquid Superficial Velocity, $j_L=0.25$ m/s

The first investigation in the flow patterns was conducted for the lowest liquid superficial velocity for this experimental facility at $j_L=0.25$ m/s. The investigations were varied with six different gas superficial velocities at $j_G= 0.025, 0.050, 0.075, 0.10, 0.15$ and 0.25 m/s. As shown in figures 7.1 and 7.2, these flow conditions were then examined to see their changes of patterns due to the vibration sizes. Referring to these figures, the bubbly flow were developed for the above two different conditions when there is no vibration (M0). When the ground accelerations were introduced, even at the lowest value of ± 3 m/s (mode M1) the pattern straight away changed to slug flow.

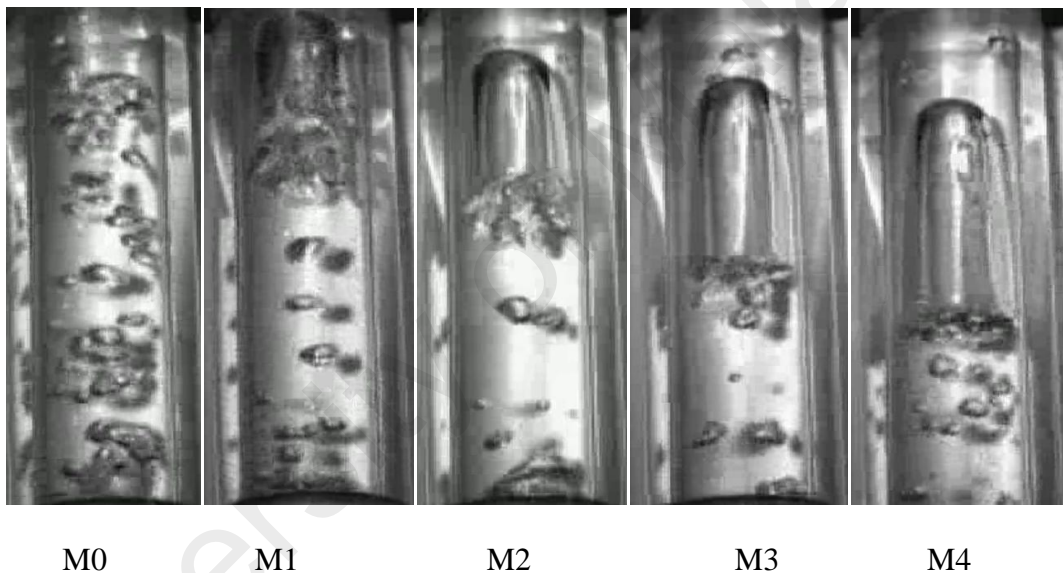


Figure 7.1 : Changes of flow patterns due to vibration sizes, for $j_L=0.25$ m/s, $j_G=0.025$ m/s

As the ground accelerations increased, the longer slugs were formed. However, during this time, the pattern was not slug formation only but they were also bubbly flow before and after the slugs which could be seen from these figures that all the slug flow were followed by the trailing bubble as well. With the changes of motions, the bubbles seems to experience up and down movement and in between were stagnant due to transition from the positive to negative accelerations which reflects the downward and

upwards travel. These kinds of motions contributed to more bubble congregations and coalescences and therefore resulting in the formation of longer slug as discussed.

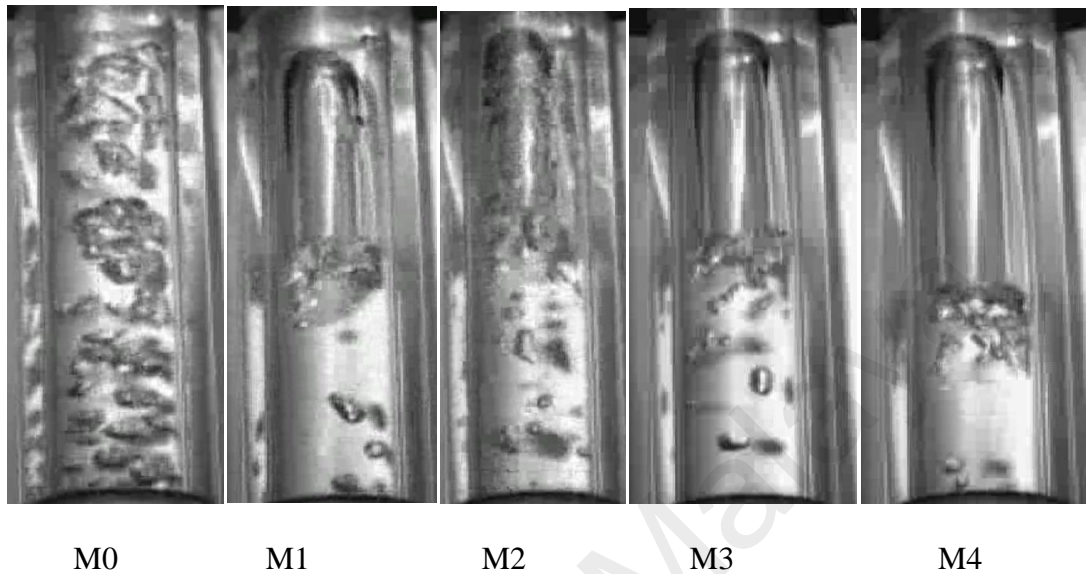


Figure 7.2 : Changes of flow patterns due to vibration sizes, for $j_L=0.25 \text{ m/s}$, $j_G=0.05 \text{ m/s}$

There was also a phenomenon of transition from slug to churn flow in these flow conditions as can be seen in figure 7.2 during the vibration of mode M2. The slug in this figure seems to breakdown into smaller distorted bubbles due to downward movement that drag the liquid holdup down which also has been discussed in chapter 5 on the transition of slug to churn flow. From this observation, it can be said that the vibration provides a strong influence in the downward slip motion of the liquid holdup, and this case may slow down the bubble motion in the two-phase flow.

In figure 7.3, a further increase in gas superficial lead to the formation of bigger bubbles with spherical caps and when hit by the ground accelerations at $\pm 3 \text{ m/s}^2$ (M1), slugs were formed. These slugs travel together with the spherical cap bubbles with distorted shapes. With bigger ground accelerations at $\pm 6 \text{ m/s}^2$ (M2) more slugs were formed in better shapes with short length, but they grow up with very nice shape with bigger accelerations at modes M3 and M4. These bigger and longer slugs were formed

due to vibrations as a result of the up and down motions sometime slow down the movement of the bubble or move backward to allow more bubble congregations and coalescences. With higher rate of acceleration, the slugs sometime are unstable and break off leaving small bubbles at their tails.

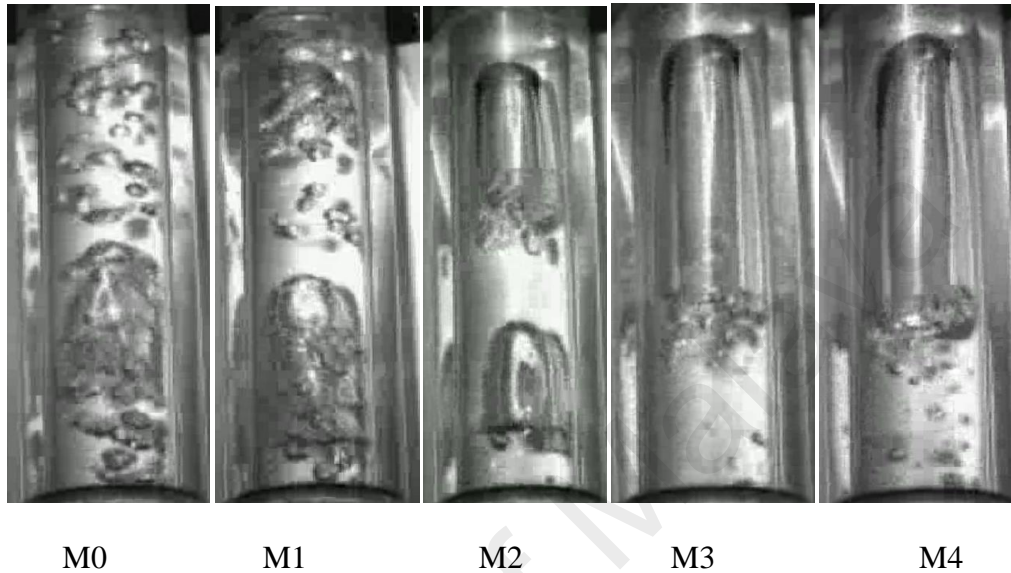


Figure 7.3 : Changes of flow patterns due to vibration sizes, for $j_L=0.25 \text{ m/s}$, $j_G=0.075 \text{ m/s}$

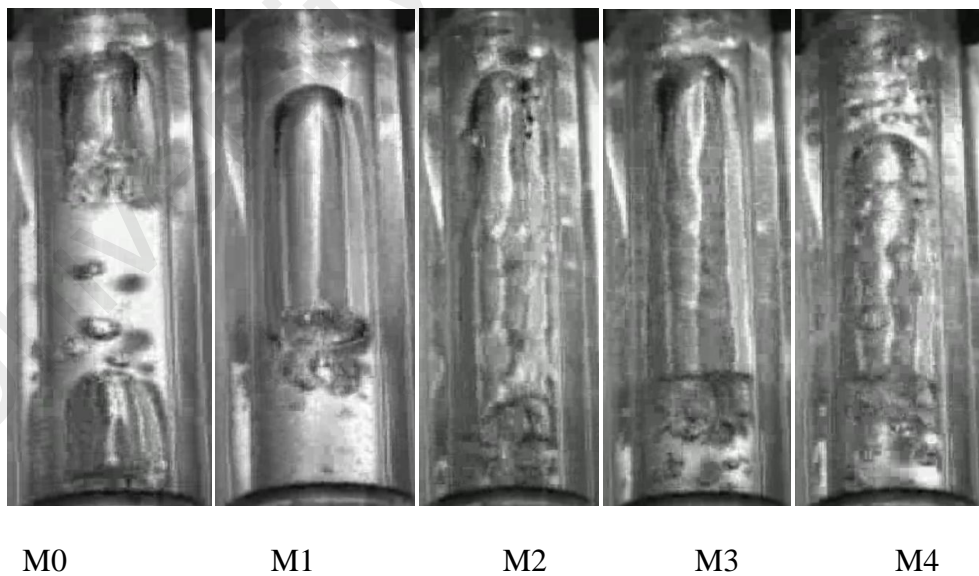


Figure 7.4 : Changes of flow patterns due to vibration sizes, for $j_L=0.25 \text{ m/s}$, $j_G=0.1 \text{ m/s}$

When the gas superficial velocity is further increased to 0.1 m/s , the flow patterns change immediately into slug flow even without vibration. At low acceleration,

bigger slugs start to form and as the accelerations increases, they become more longer but unstable. The shapes of the slugs were distorted and more small bubbles exist on their heads and tails. This is also a result from the downward flow of liquid hold up that disturbs the smoothness of slug flow, break them down into smaller bubbles where these bubbles also move downward and therefore as in figure 7.4, they can be seen surrounded the slug while travelling under the effects of higher ground accelerations.

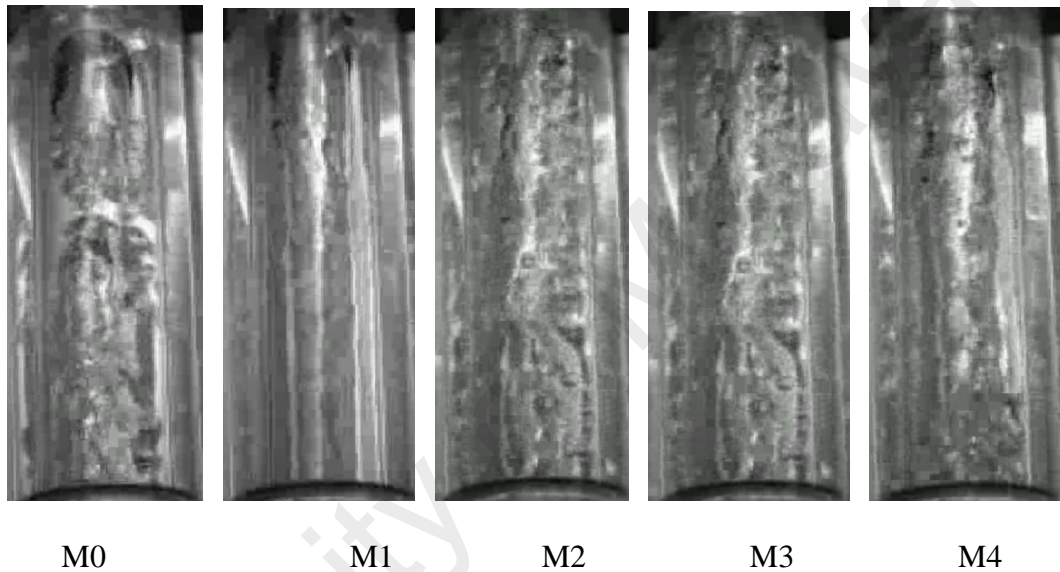


Figure 7.5 : Changes of flow patterns due to vibration sizes, for $j_L=0.25 \text{ m/s}$, $j_G=0.15 \text{ m/s}$

When the gas superficial velocities being increased to 0.15 m/s and 0.25 m/s , as shown in figures 7.5 and 7.6 respectively, a fully developed slug flow were formed with bigger sizes and longer lengths compared to the lower gas superficial velocities in the previous figures. They also look like a stable flow pattern when there is no vibration. As soon as the vibration introduced, the slugs became distorted, as the liquid holdup is moving downward. In these figures, this effect can be observed very clearly. With further increase in ground accelerations (M2 - M4), the slugs seems to coalesce with each other forming super long slug and sometime it appears like the annular flow. The patterns during these flow conditions can be stable in the form of long slugs with

distortion of shapes. In some cases, the slugs were formed for about 300 mm and this fact can be confirmed through the measurement of void fraction that will be discussed in detail in the following sections.

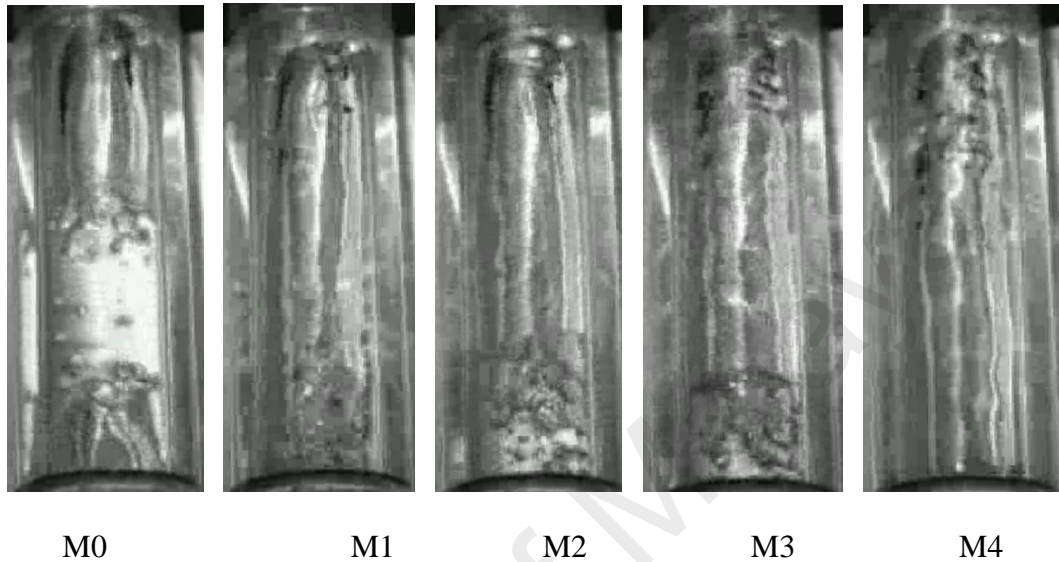


Figure 7.6 : Changes of flow patterns due to vibration sizes, for $j_L=0.25 \text{ m/s}$, $j_G=0.25 \text{ m/s}$

7.2.2 Liquid Superficial Velocity, $j_L=0.5 \text{ m/s}$

For liquid superficial velocity, $j_L=0.5 \text{ m/s}$, the same procedures as in the previous were repeated. At gas superficial velocities of $j_G=0.025 \text{ m/s}$ and $j_G=0.050 \text{ m/s}$ as shown respectively in figures 7.7 and 7.8, a steady bubble flow was formed when there was no vibration. With the effects of vibration, the bubbles start to congregate and shorten the gaps between their groups particularly in the case of very low gas superficial velocity at 0.025 m/s . In this flow condition, there was no significant change in the flow patterns except the effects of vertical motions that slow speed up and slow down the bubble flow. As shown in figure 7.7, these bubbles appeared in closed and distanced gap due to this effect but the scale of vibrations in this case does not have enough force to change flow patterns.

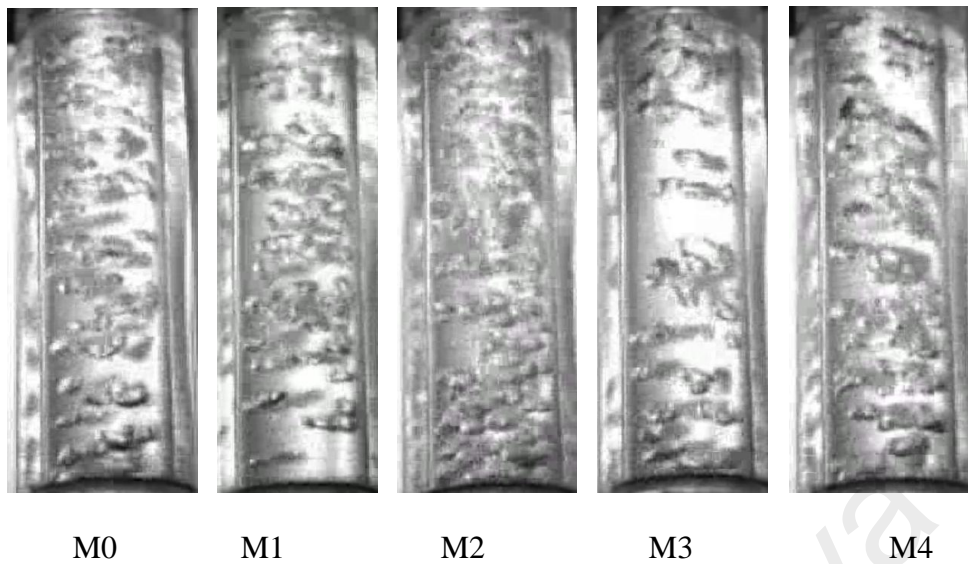


Figure 7.7 : Changes of flow patterns due to vibration sizes, for $j_L=0.5 \text{ m/s}$, $j_G=0.025 \text{ m/s}$

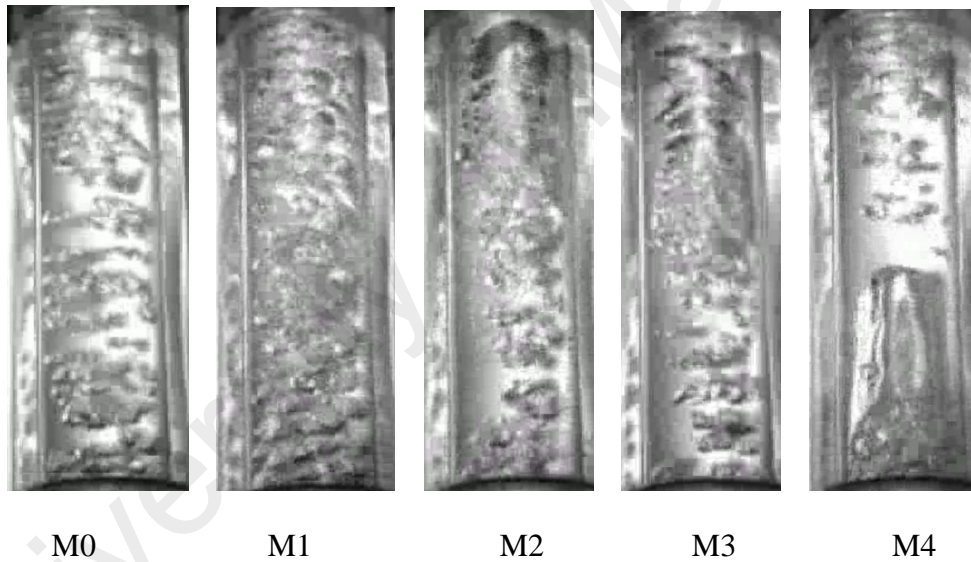


Figure 7.8 : Changes of flow patterns due to vibration sizes, for $j_L=0.5 \text{ m/s}$, $j_G=0.05 \text{ m/s}$

With gas liquid velocity, $j_G=0.05\text{m/s}$, the bubbles congregates very closely forming very firm bubble flow after receiving the influence of vertical motion of ground acceleration and of sometime naturally formed a single liquid flow after the close congregations. The flow start to change it patterns into small slug after hit by the 6 m/s^2 ground accelerations and the bubble-slug flow pattern appeared throughout the travels under higher ground accelerations at vibration mode of M3 and M4, but severely

affected by the downward liquid holdup. Therefore, in this case there was no long slug formed even though they experienced very high ground accelerations.

Further increase of gas superficial velocity to, $j_G=0.075$ m/s, resulted a flow pattern with very steady bubble flow, with bigger bubbles sizes and some of them were flapping like a bird wing as observed by Krishna and van Batten (1999). As the vibration take place, the bubble coalescence became more rapid forming bigger bubbles but not big enough to form a solid slug until bigger size vibration being introduced at mode M2. Here, the slug started to form with large amount of bubble flow as well. At mode M3, firm slugs were formed but as the previous cases, the effect of downward liquid holdup distorted their shapes. Sometimes this distortion breaks out the slugs forming smaller slugs, but not good enough to form the churn flow. At the highest ground acceleration with vibration mode M4, these distortions obviously contributed to the shapes alteration with rapid break off as well.

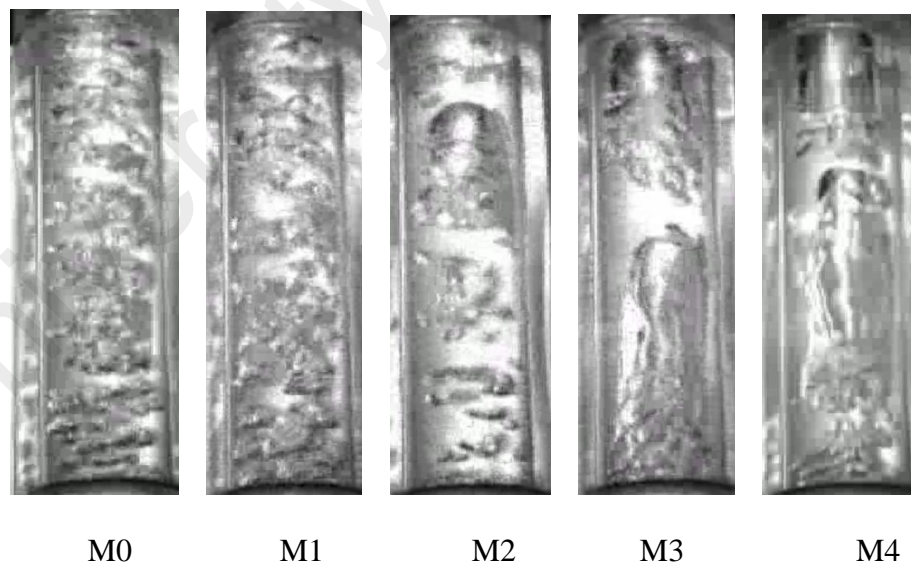


Figure 7.9 : Changes of flow patterns due to vibration sizes, for $j_L=0.5$ m/s, $j_G=0.075$ m/s

From the result obtained at this stage, the flow patterns in figure 7.9, with liquid superficial velocity at $j_L=0.5$ m/s, and gas superficial velocity at $j_G=0.075$ m/s shows a

very well manner in their changes and transitions were very clear from one mode of vibration to another. Therefore, this result will be the basic condition to study the effects of slip ratio on the changes of flow patterns due to sizes of ground accelerations in a vertical flow channel for gas-liquid two phase systems.

With higher gas superficial velocity at $j_G=0.1$ m/s, the flow pattern started with formation of slugs during the steady state condition where there was no vibration applied. The vibrations effect thus in this case, was very small due to high speed gas flow in the flow channel that surpassed the effects of downward flow of liquid holdup on the wall. Therefore, as can be observed in figure 7.10, flow patterns remain as slug flow throughout the condition. However, a notable effect that can be looked at during this condition is the thickness of liquid film on the wall of the flow channel becoming thinner as the vibration sizes increases. This effect might due to coalescences of slugs forming super big slug and it behaves like annular flow with regards to high superficial velocity of gas flow as well.

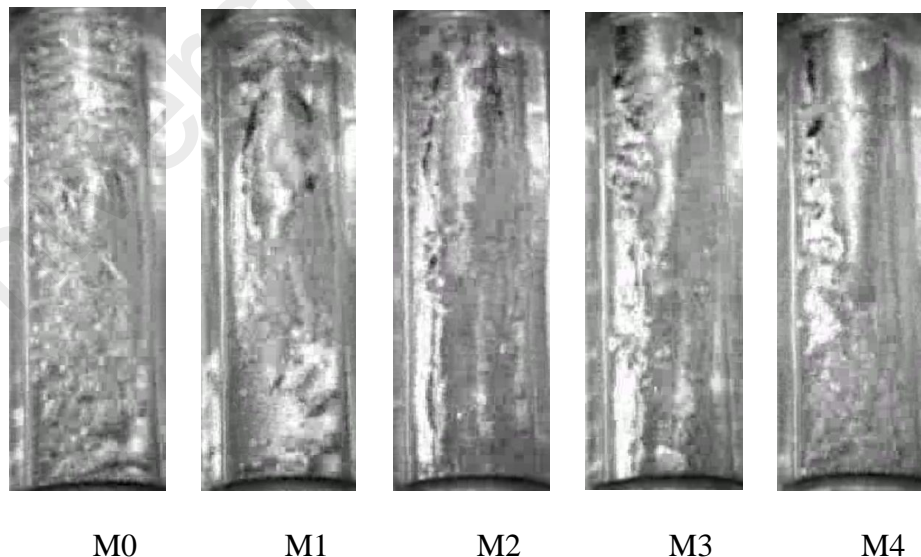


Figure 7.10 : Changes of flow patterns due to vibration sizes, for $j_L=0.5$ m/s, $j_G=0.1$ m/s

Even though the effects of vibration seem to be very small in this case, the flow pattern demonstrated in this figure is very dangerous for flow channel that operate as heating element, such as the boiling tube or evaporators. This condition may lead to dryout at undesired position and thus will easily contribute to unpredictable accidents due to the effects of vibration.

The effect of gas superficial velocities were also tested for the gas superficial velocities at higher level at $j_G=0.15 \text{ m/s}$ and $j_G=0.15 \text{ m/s}$ as shown respectively in figure 7.11 (a) and (b). Both figures show that even without vibration, the flow pattern is the churn flow with fractions of bubble flow along the channel. With vibration effects these churn flows somehow coalesce to form annular flow. At this stage the effects of vibration is very small as discussed in the previous flow condition. Again, unpredictable accident can be expected in this condition as well due to very thin liquid film for some critical applications.

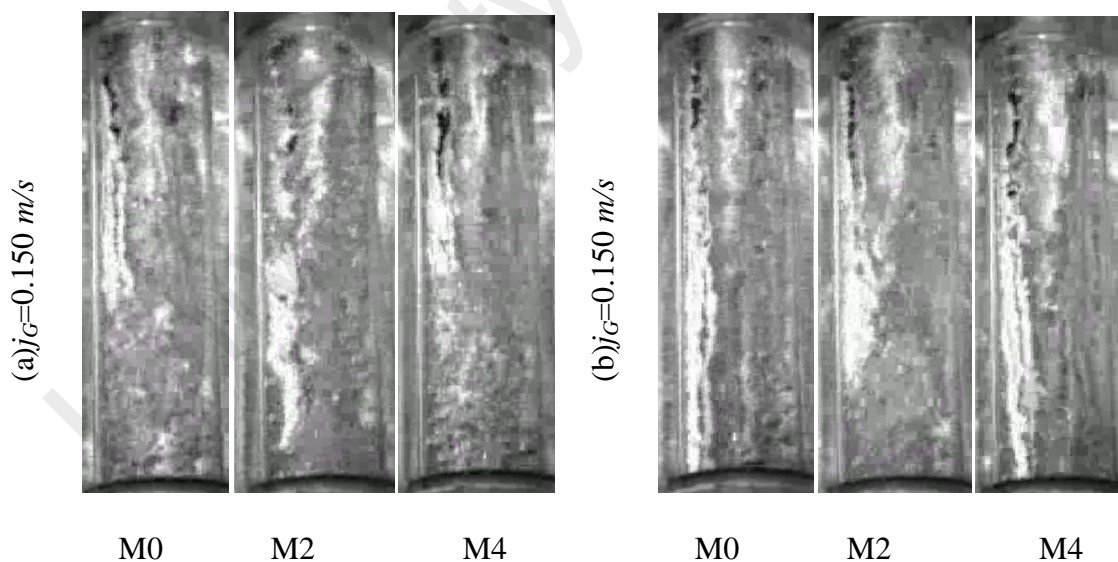


Figure 7.11 : Changes of flow patterns due to vibration sizes,

for $j_L=0.5 \text{ m/s}$, $j_G=0.150 \text{ m/s}$ and $j_G=0.25 \text{ m/s}$

7.2.3 Liquid Superficial Velocity, $j_L=0.75\text{ m/s}$

Under the condition of liquid superficial velocity at, $j_L=0.75\text{m/s}$, very stable bubble flow was formed in most of the condition for wide range of gas superficial velocities. At very low, $j_G=0.025\text{ m/s}$ (figure 7.12a), and $j_G=0.050\text{ m/s}$ (figure 7.12b), the flow pattern remain as bubble flow through out all the steady state and transient rough conditions even with higher degree of vibrations. The only observation that can be compelled is the bigger sizes of bubbles formed in this flow condition. They move upward steadily but sometime demonstrated very close gap of congregations and dispersed away from other group due to vertical motion.

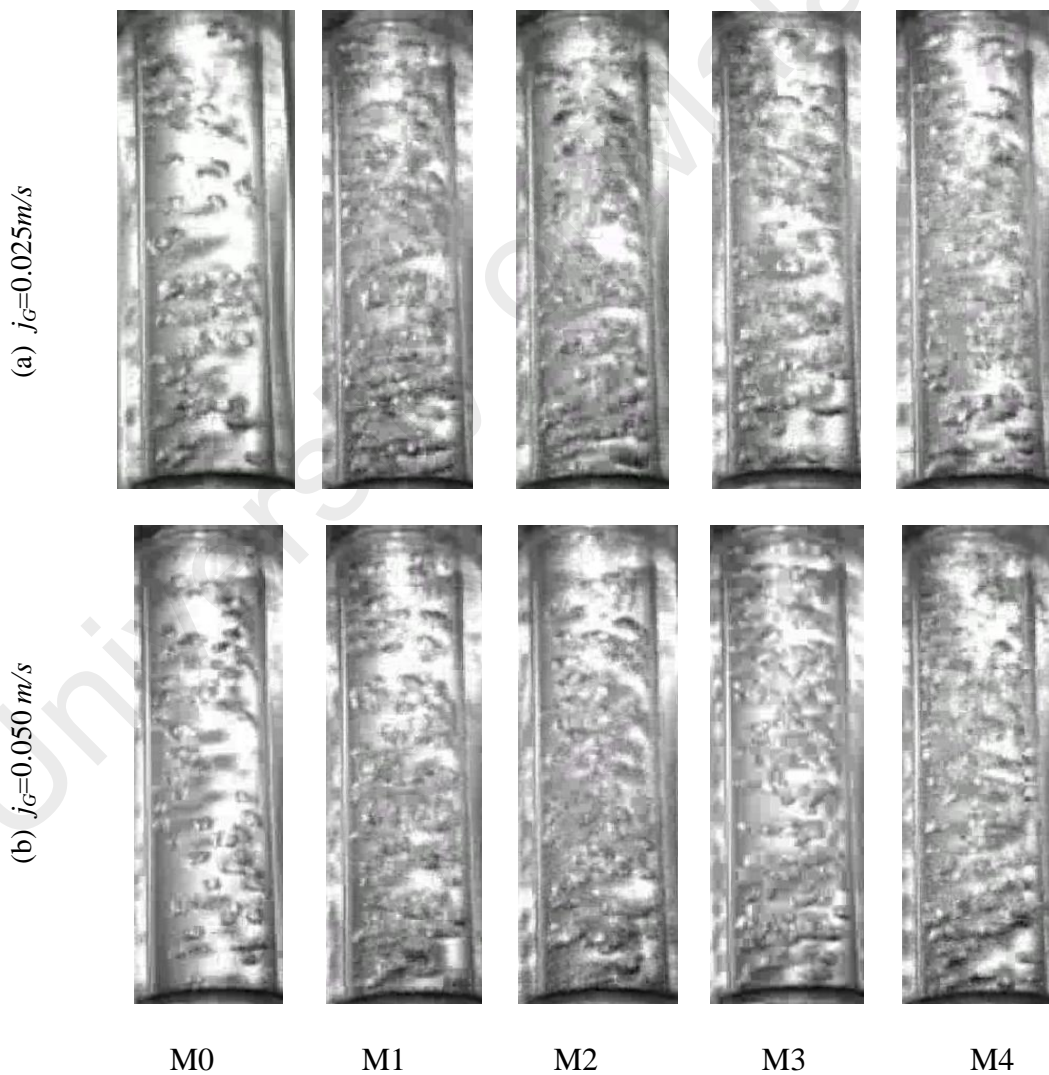


Figure 7.12 : Changes of flow patterns due to vibration sizes,
for $j_L=0.75\text{ m/s}$, $j_G=0.025\text{ m/s}$ and $j_G=0.050\text{ m/s}$

With further increase of gas superficial velocities to 0.075 m/s and 0.1 m/s , the flow pattern remains as bubble flow for steady state condition and show similar correspondent towards vibration at low degree as the previous flow conditions with close gap congregations. The bubbles start to coalesce and forming bigger bubbles with spherical caps as in figure 7.13a ($j_G=0.075 \text{ m/s}$) for mode M1 and mode M2 for figure 7.13b ($j_G=0.1 \text{ m/s}$). In both figures, bubbles flow behave as flapping wing as discussed in the previous section for $j_L=0.5 \text{ m/s}$ and $j_G=0.075 \text{ m/s}$.

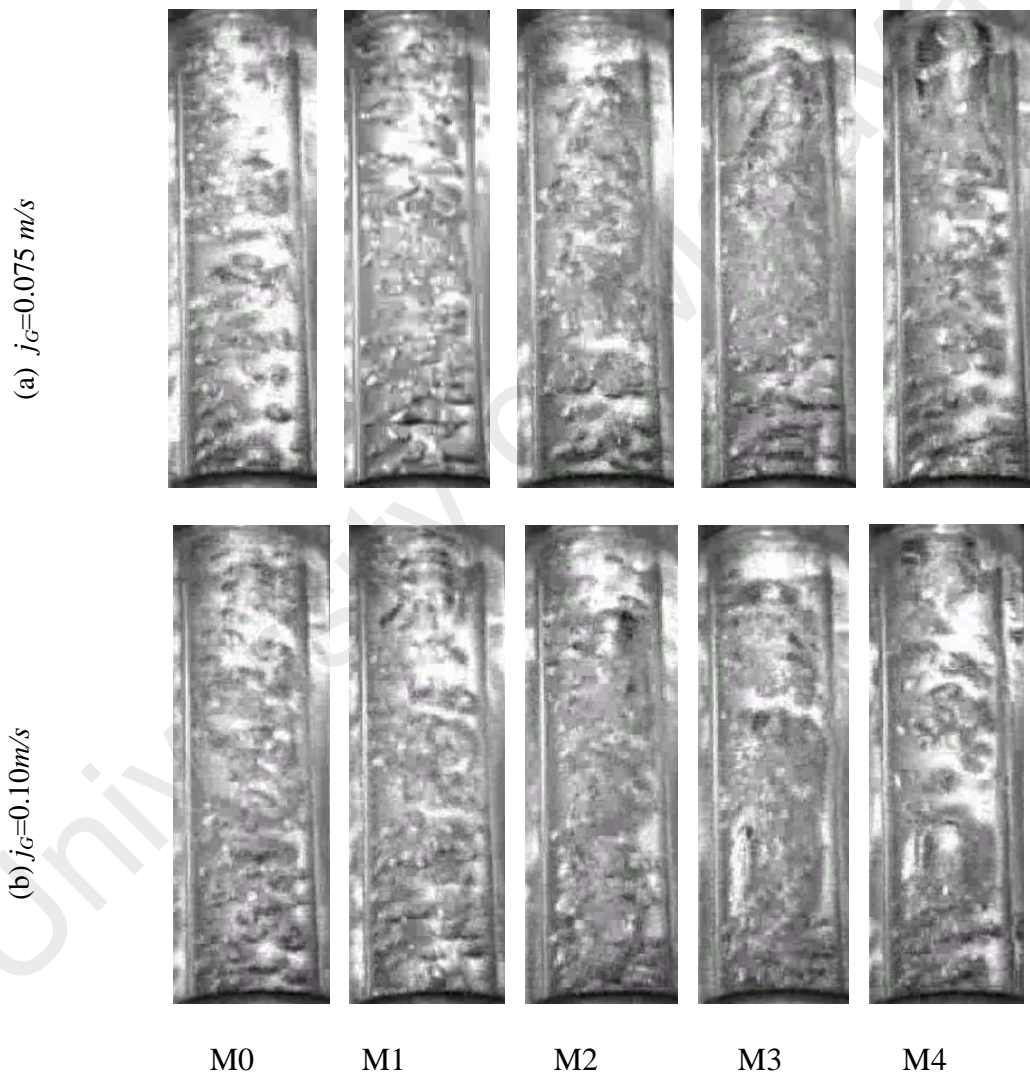


Figure 7.13 : Changes of flow patterns due to vibration sizes,
for $j_L=0.75\text{m/s}$, $j_G=0.075 \text{ m/s}$ and $j_G=0.1\text{m/s}$

Flow pattern start to change with vibration mode M3 for $j_G=0.075\text{ m/s}$ and M2 for $j_G=0.1\text{ m/s}$. At the end of higher degree vibrations slugs were formed but not in proper shape. This situation might due to imbalance interfacial forces between the vertical motion and the gas velocity in the flow channel that somehow disturbed the formation of steady slug even though the effects of downward liquid holdup considered being small.

When gas superficial velocities were increased to 0.15m/s , bubbles with spherical caps and small slug flow were formed at as low as vibration with mode M1 and bubble congregations were as in the previous cases. These slugs continue to form in higher order of vibration modes and but not with a stable shapes. In this case, as can be observed from figure 7.14, slugs flow in the channel together with small bubbles, as likely resulted from dispersed slugs and they are sometime coalesce back again at upper level of the channel.

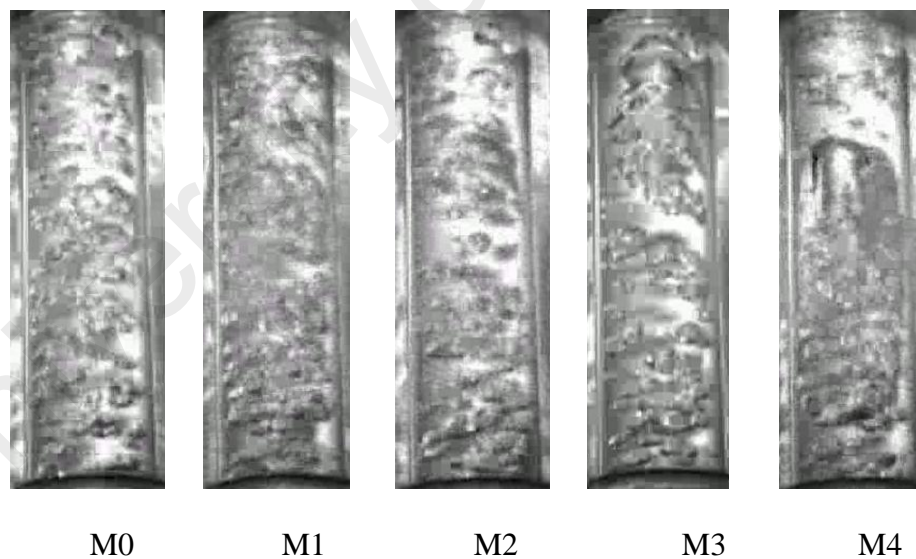


Figure 7.14 : Changes of flow patterns due to vibration sizes, for $j_L=0.75\text{ m/s}$, $j_G=0.150\text{ m/s}$

A simple conclusion that can be addressed here is again about the vertical motion that promotes a disordered bubble rising; in term of velocity and interfacial forces. Hence, in further analysis, the relation of slip ratio and ground acceleration sizes

can be remarked as having some degree of effect, but up to this stage no single conclusion can be summarized yet.

The flow pattern still show the bubble flow for gas superficial velocity of $j_G=0.25\text{ m/s}$, during the steady state condition with formation of slugs in between the bubbles. However for gas superficial velocity of $j_G=0.5\text{ m/s}$, no more bubble flow characterization can be made since bigger slugs were formed in a turbulent flow. For both of the cases, these slugs become very unstable when vibration is applied and become distorted. In figure 7.15, at $j_G=0.25\text{ m/s}$, as the size of vibration increases, these slugs with the effects of vertical motions repeatedly coalesce with each other forming much bigger slugs and damaged probably due to collision with wall of the flow channel. During these events, the flow patterns can be observed as experiencing the transition to churn and then developed into annular flow.

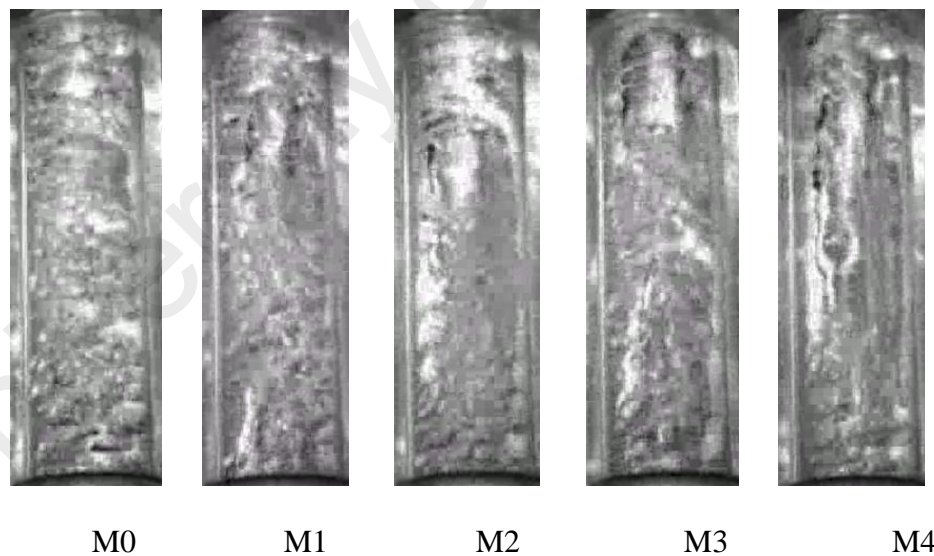


Figure 7.15 : Changes of flow patterns due to vibration sizes, for $j_L=0.75\text{ m/s}$, $j_G=0.250\text{ m/s}$

An immediate formation of slug flow during gas superficial velocity of $j_G=0.5\text{ m/s}$, only show very minimal influences receive from the vibration as shown in figure 7.16. In this case, an urgent transition occurred from slug to annular flow as vibration

take place. With high liquid superficial at $j_L=0.75 \text{ m/s}$, the liquid film still stick on the wall of the flow channel with considerable thickness. However, collision of slug and the wall sometime appeared in this condition and they sometime contribute to the same phenomena as dryout and therefore as dangerous as discussed previously.

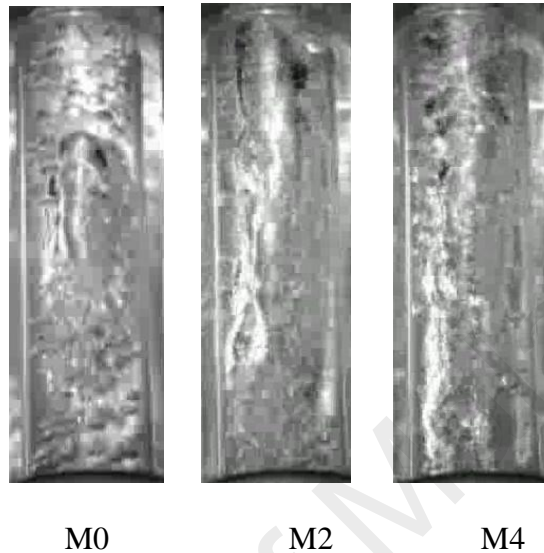


Figure 7.16 : Changes of flow patterns due to vibration sizes, for $j_L=0.75 \text{ m/s}$, $j_G=0.50 \text{ m/s}$

7.2.4 Liquid Superficial Velocity, $j_L=1.0 \text{ m/s}$

In this condition, bubble flow was observed in most of the gas superficial velocity, ranging from $0.025 \sim 0.25 \text{ m/s}$ with discrete and continuous flow in those range. The effects of vibration does not seem to be significant for gas superficial velocity in the range $0.025 \sim 0.075 \text{ m/s}$. As in figure 7.17 for 0.025 m/s , bubble coalesces occurred during the vibration mode M2 ~ M4 and in figure 7.18 and 7.18 for 0.050 m/s and 0.075 m/s , respectively coalescences occurred from as low as mode M1. However, due to high velocity of liquid flow, these coalesces were not good enough to form slug. Bubble sizes in these conditions, were much bigger compared to previous cases and rise up steadily in the flow channel. Therefore there was no drastic change in flow pattern that can be observed in these figures except the coalescences and grouping of bubble which is due to vertical motion effects.

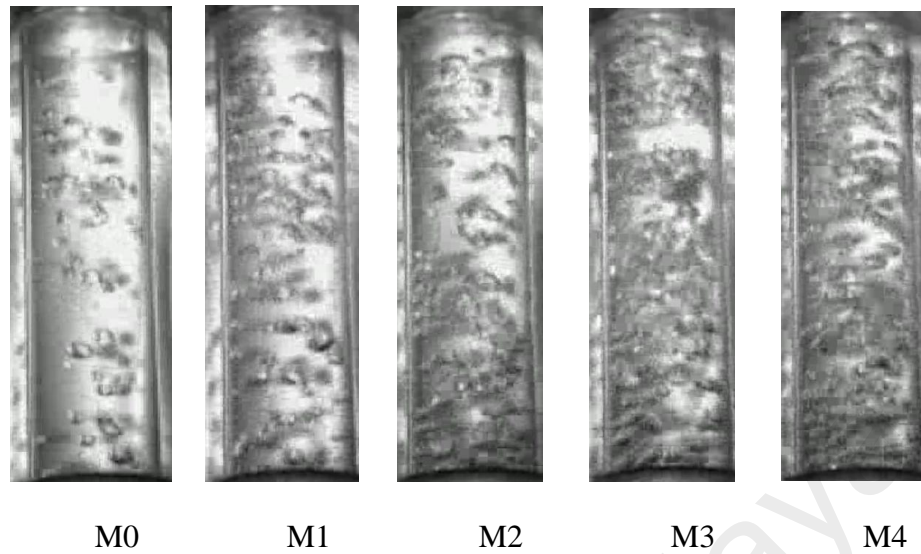


Figure 7.17 : Changes of flow patterns due to vibration sizes, for $j_L=1.0 \text{ m/s}$, $j_G=0.025 \text{ m/s}$

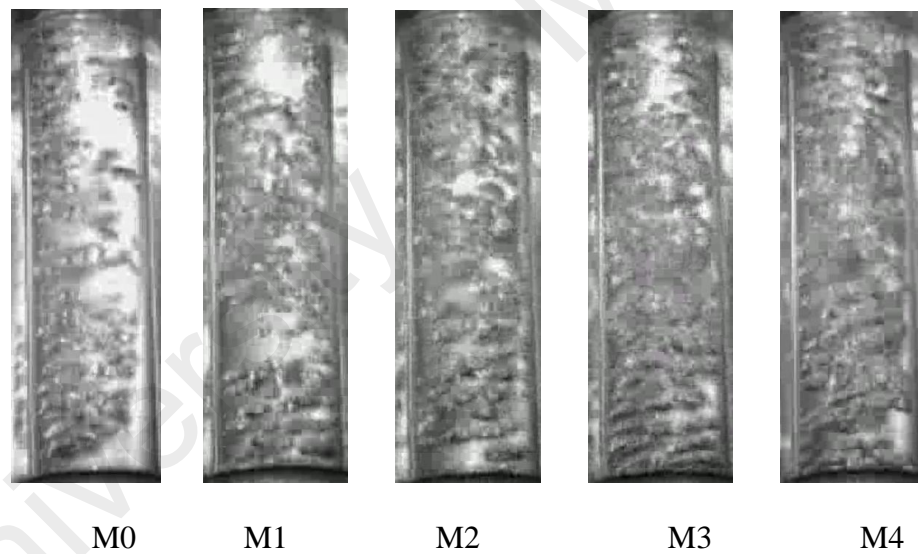


Figure 7.18 : Changes of flow patterns due to vibration sizes, for $j_L=1.0 \text{ m/s}$, $j_G=0.05 \text{ m/s}$

The flow pattern was maintained in the form of bubble flow for gas superficial velocity of $j_G=0.075 \text{ m/s}$ for two mode of vibrations M1 and M2. This indicates that at this level, the ground acceleration with range of $3 \sim 6 \text{ m/s}^2$ did not contribute to flow pattern transition. A small change is observed when the vibration with mode M3 was applied for this flow condition. Small slugs start to form due to rapid coalescences and

with higher order vibration at mode M4, a solid spherical cap bubbles were observed in the entire flow channel and lead to formation of slugs.

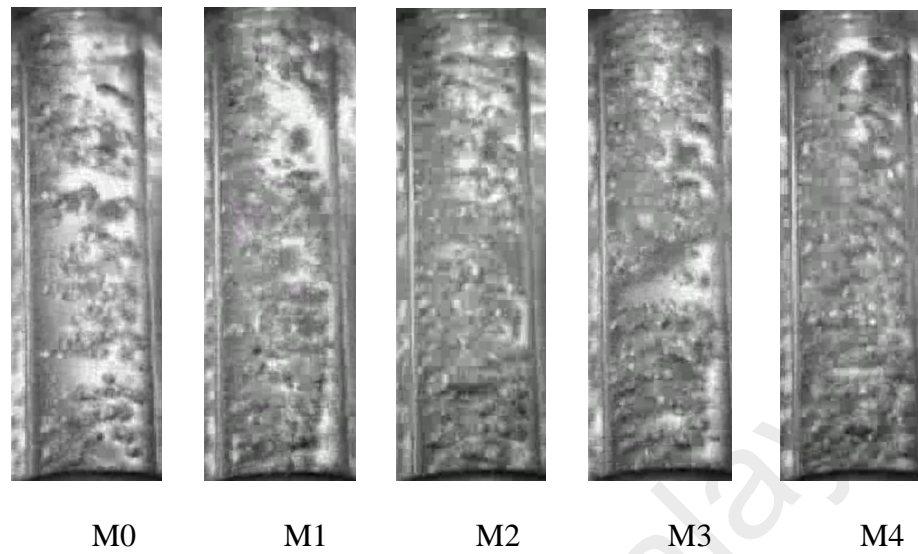


Figure 7.19 : Changes of flow patterns due to vibration sizes, for $j_L=1.0\text{ m/s}$, $j_G=0.075\text{ m/s}$

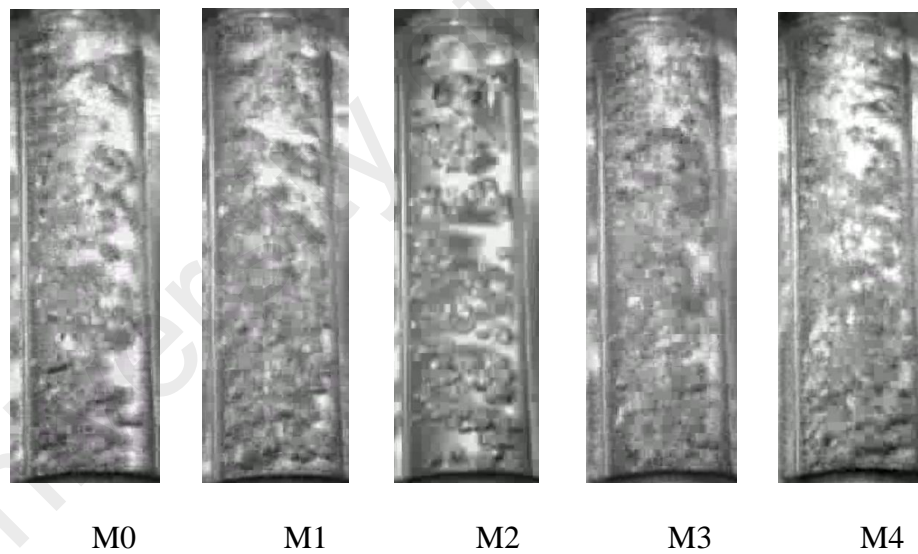


Figure 7.20 : Changes of flow patterns due to vibration sizes, for $j_L=1.0\text{ m/s}$, $j_G=0.1\text{ m/s}$

The same phenomena were observed for condition where gas superficial velocity was increased to $j_G=0.1\text{ m/s}$. The formations of slugs only take place at higher order of vibration modes of M3 and M4 but they were not fit where most of them broke up to either forming smaller bubbles or at very low chance becoming churn flow.

Coalescences of bubbles were more rapidly seen for gas superficial velocities in the range of $j_G=0.15 \text{ m/s} \sim 0.25 \text{ m/s}$. They have opportunities to form slugs during higher order of vibration at M3 and M4 but immediately break up as experiencing collision with the wall of channel flow becoming more often. The bubble rising was more stable due to their sizes and high liquid superficial velocities. Therefore, throughout these conditions and vibration modes, it can be concluded that the flow patterns remain as bubbly flow.

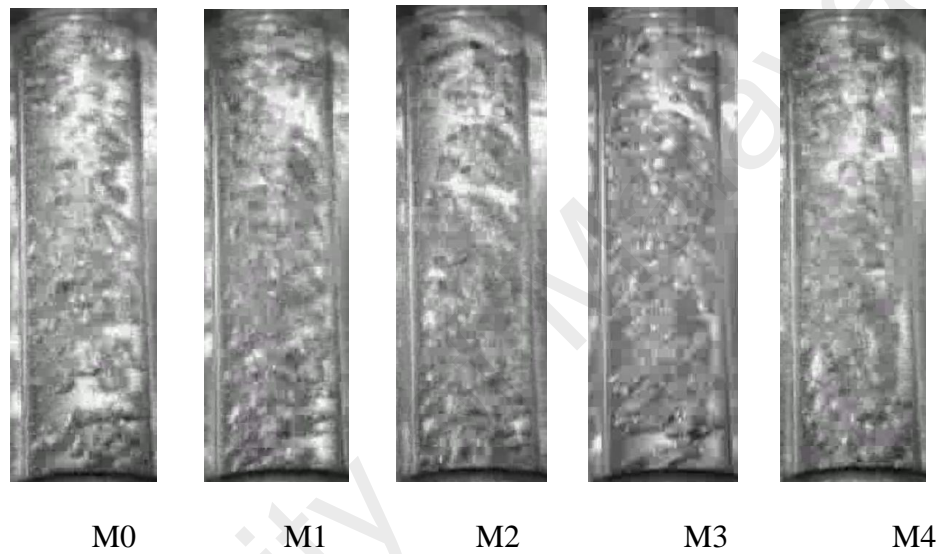


Figure 7.21 : Changes of flow patterns due to vibration sizes, for $j_L=1.0 \text{ m/s}$, $j_G=0.15 \text{ m/s}$

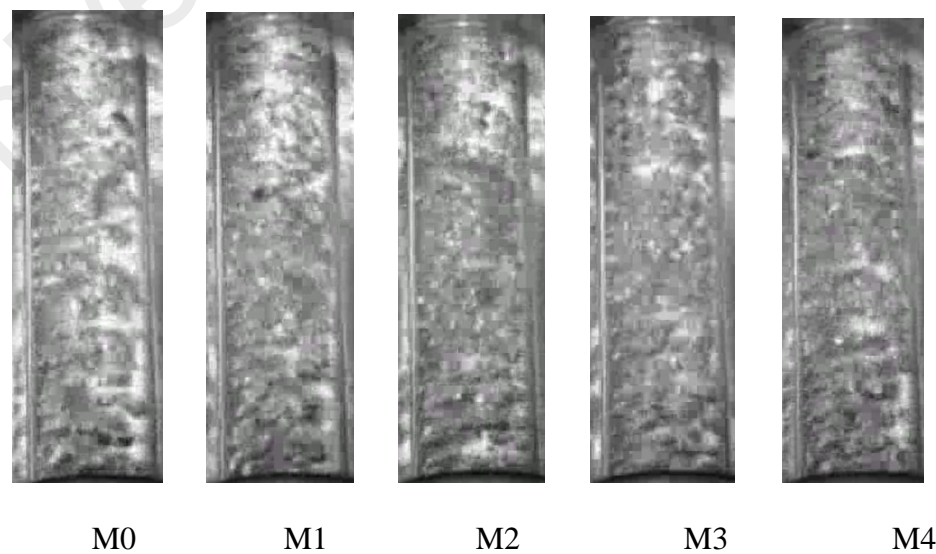


Figure 7.22 : Changes of flow patterns due to vibration sizes, for $j_L=1.0 \text{ m/s}$, $j_G=0.25 \text{ m/s}$

When the gas superficial velocity increased to 0.5 m/s , transitions of bubbly to slug flow were observed during the steady state condition as shown in figure 7.23. This is very well match with the work by Furukawa and Fukano (2001). When the vibration was applied the rising bubbles were again in a slower or faster mode depending on the direction of the accelerations. Again in this case, the effect of vertical motion with downward movement of liquid hold up show an impact to the rising bubbles and slugs even though they are at high velocity. As the mode of vibration becoming higher, the formation of bigger slugs occurred and they again underwent the break up and forming the churn flow during the accelerations at $\pm 12 \text{ m/s}^2$.

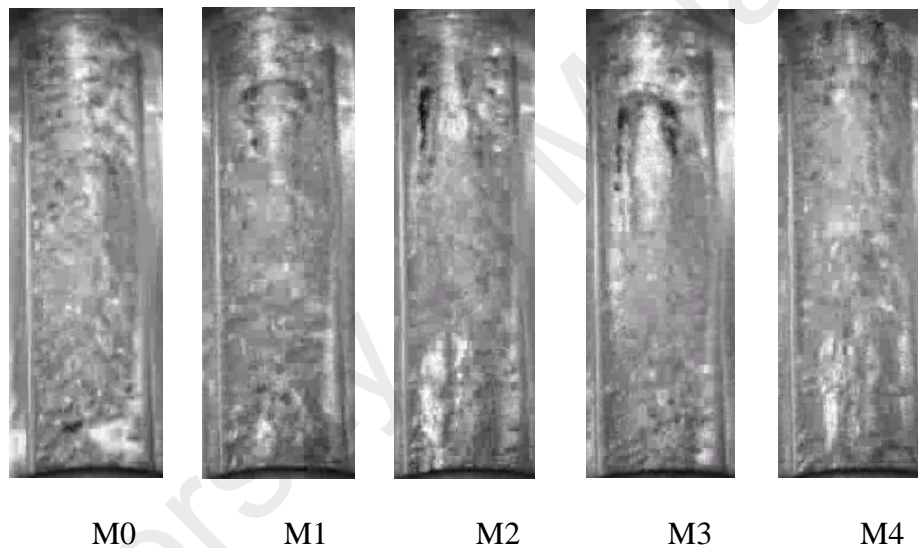


Figure 7.23 : Changes of flow patterns due to vibration sizes, for $j_L=1.0 \text{ m/s}$, $j_G=0.5 \text{ m/s}$

For more higher gas superficial velocities at $j_G=0.75 \text{ m/s}$ and $j_G=1.0 \text{ m/s}$, the flow pattern appeared as slug flow at the beginning and after sometime when more slugs were formed, coalescences become more often and they started to break up. Hence, the transition from slug to churn flow during the steady state condition was observed and after receiving the impact form the vibrations the alternately shows the transition from churn to annular flow even at very low mode of vibration at M1. When the annular flow developed, there was no more distinguish changes that being observed

except the liquid film thickness became thinner as the order of vibration getting higher as shown in figure 7.24.

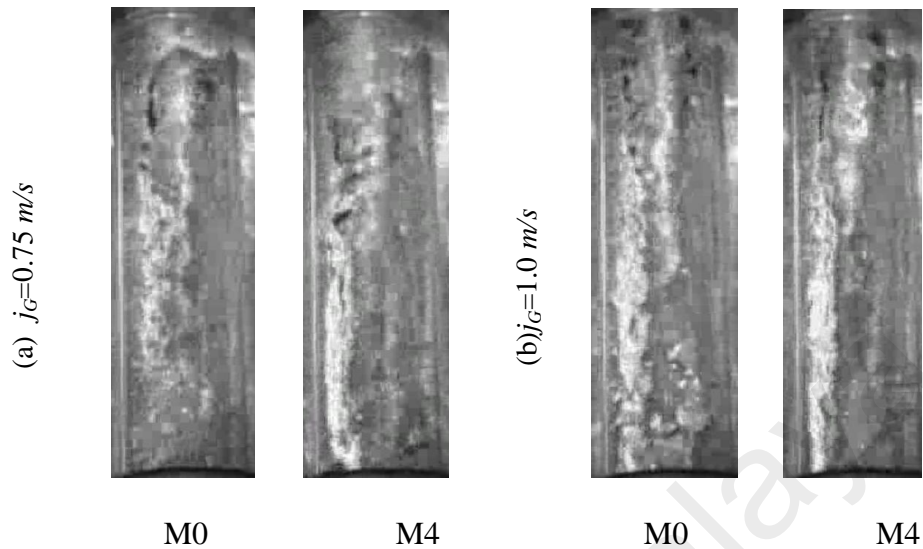


Figure 7.24 : Changes of flow patterns due to vibration sizes, for $j_L=1.0 \text{ m/s}$, $j_G=0.75 \text{ m/s}$ and $j_G=1.0 \text{ m/s}$

7.2.5 Liquid Superficial Velocity, $j_L=2.0 \text{ m/s}$

Many industrial applications operate in a wide range of liquid superficial velocities. As demonstrated in this work, these velocities were ranged for $0.25 \sim 2.5 \text{ m/s}$, which is acceptable to many engineering and processing works. Up to this point, the flow patterns were discussed for liquid superficial velocities in the range of $0.25 \sim 1.0 \text{ m/s}$. As the last discussion for 1.0 m/s , there is tendency where the ground accelerations from vertical vibration do not contribute strong impact to the flow patterns for low gas superficial velocities in the range of $0.025 \sim 0.25 \text{ m/s}$.

Again for the current size of liquid superficial velocity at 2.0 m/s , these ranges of gas superficial velocities show very small influence accepted from the vibrations. This reality can be verified in figures 7.25 ~ 7.30. All of these figures show that the flow patterns are only in the form of bubbly flow in all of the cases; the steady state conditions and for all of the vibration modes applied. The steady flow due to high liquid superficial velocity is very obvious in figure 7.25, for very low gas superficial velocity

at 0.025m/s where bubbles flow in very good manner with only very little coalescences even though the effect of downward motion is quite strong at higher order of vibration modes.

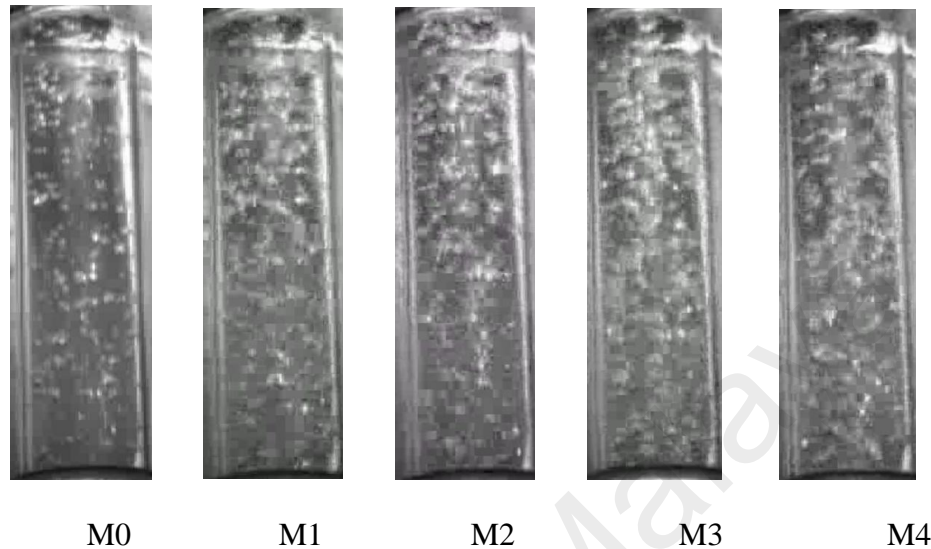


Figure 7.25 : Changes of flow patterns due to vibration sizes, for $j_L=2.0\text{ m/s}$, $j_G=0.025\text{ m/s}$

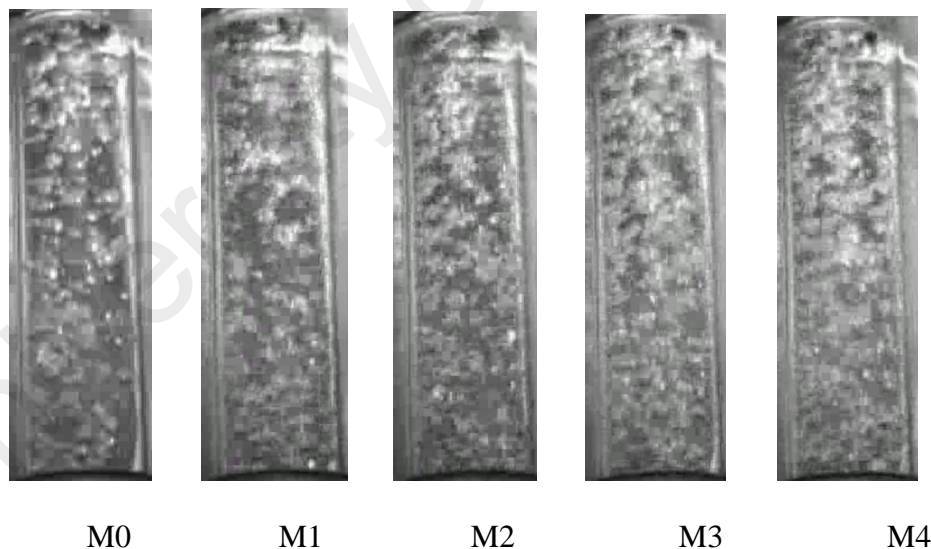


Figure 7.26 : Changes of flow patterns due to vibration sizes, for $j_L=2.0\text{ m/s}$, $j_G=0.05\text{ m/s}$

From figure 7.26, for gas superficial velocity at 0.05 m/s , a small change of flow patterns can be observed during the vibration modes of M3 and M4 where spherical caps bubbles were formed as a result of rapid coalescences but not big enough to establish a solid slug. This is again due to the effect of vertical motion with bigger force

that disturbed the interfaces of bubbles and as a result denied more coalescences to form bigger bubbles and therefore do not allow any chance of slug formation.

At higher superficial velocities of gas, for 0.075 m/s and 0.1 m/s , in figures 7.27 and 7.28, slugs formation appeared during the vibration with mode M2 and above. These slugs however, are very small and travel in between small bubbles become distorted and break up forming smaller bubbles and therefore their existence is very hard to be identified.

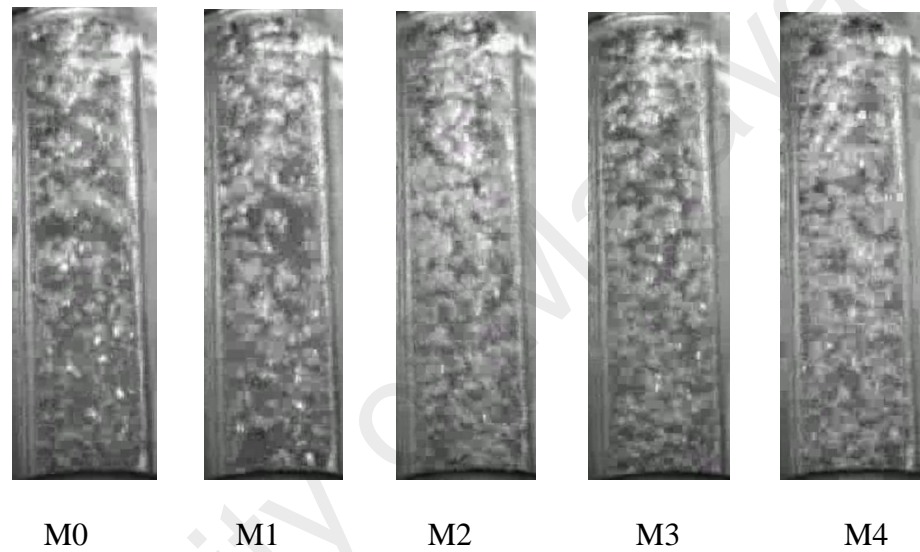


Figure 7.27 : Changes of flow patterns due to vibration sizes, for $j_L=2.0\text{ m/s}$, $j_G=0.075\text{ m/s}$

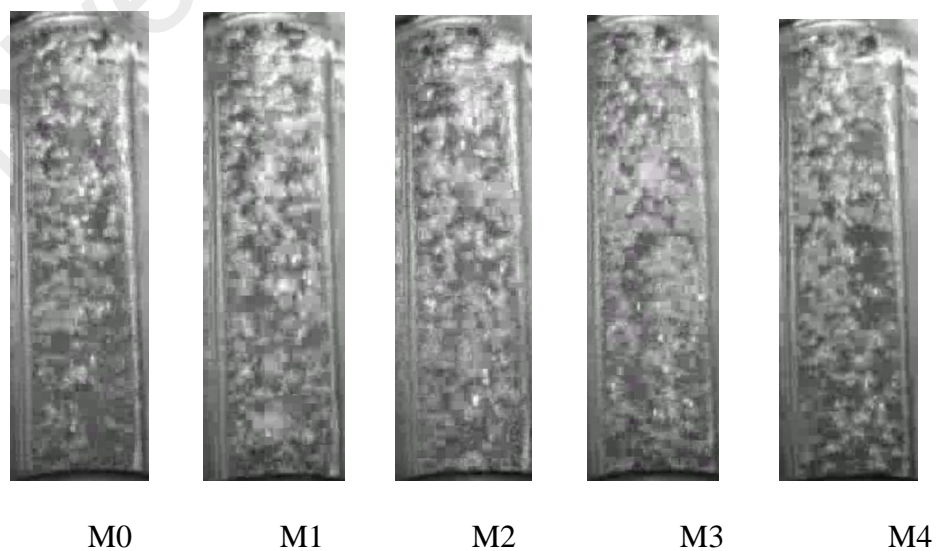


Figure 7.28 : Changes of flow patterns due to vibration sizes, for $j_L=2.0\text{ m/s}$, $j_G=0.1\text{ m/s}$

Bubble congregations were observed to be better with the increasing of gas superficial velocities as shown in figures 7.29 and 7.30 for $j_G=0.15 \text{ m/s}$ and $j_G=0.25 \text{ m/s}$, respectively. In both of these figures, in all modes close gap congregations took place and lead to coalescences where as a result forming more slugs. These slugs also travel within the bubbles and easily distorted to form smaller bubbles but there do not show any transition into the churn flow. Therefore, at these conditions, they remain as bubbly flow and sometimes demonstrated the transition of temporary slug flow except for $j_G=0.25 \text{ m/s}$ at vibration mode M4 with accelerations of 12m/s^2 , where slug flow was steadily formed (figure 7.30).

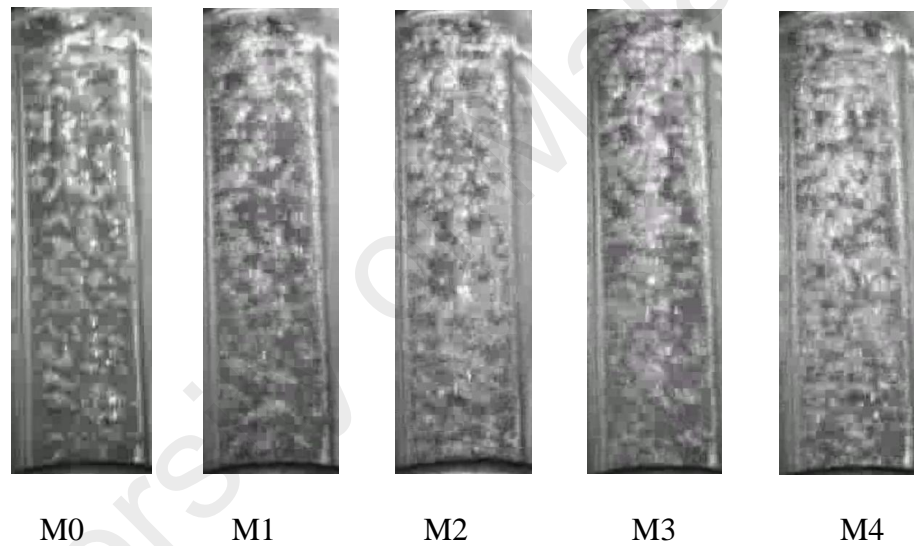


Figure 7.29 : Changes of flow patterns due to vibration sizes, for $j_L=2.0 \text{ m/s}$, $j_G=0.15 \text{ m/s}$

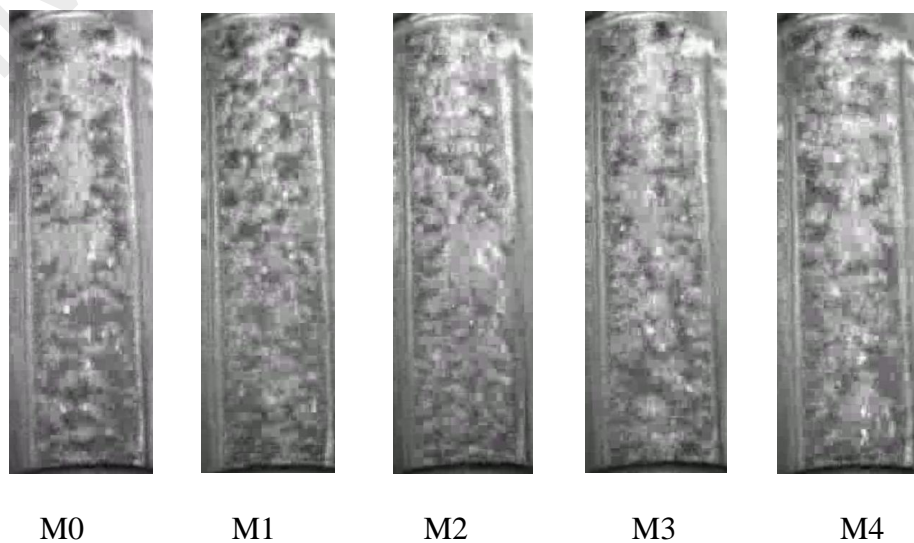


Figure 7.30 : Changes of flow patterns due to vibration sizes, for $j_L=2.0 \text{ m/s}$, $j_G=0.25 \text{ m/s}$

Figure 7.31(a) and (b) show the flow pattern for gas superficial velocities at $j_G=0.5 \text{ m/s}$. and $j_G=0.75 \text{ m/s}$. Transition from bubble to slug flow was displayed during the steady state condition and slug flow developed as the ground acceleration hit the base of the test section. The pattern then changed into churn flow as the order of vibration progressed. However, as an unstable flow pattern, the churn flow exchanging the pattern into bubble-slug as the vertical movement changes the direction. Therefore this condition can be judged as showing the transition of slug to churn and it was alternately repeated as the vibration take place during the rising of gas bubbles in the flow channel.

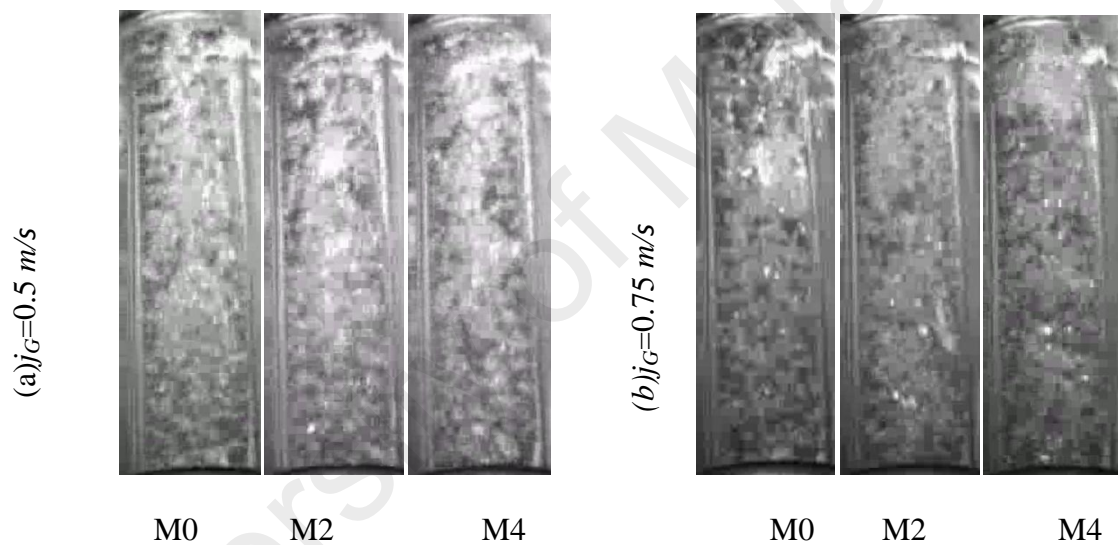


Figure 7.31 : Changes of flow patterns due to vibration sizes,

For $j_L=2.0 \text{ m/s}$, $j_G=0.5 \text{ m/s}$ and $j_G=0.75 \text{ m/s}$

For the highest liquid superficial velocity obtained in this work $j_L=2.5 \text{ m/s}$, the flow patterns remain as bubbly for almost all of the conditions as shown in figure 7.32. Therefore, a short conclusion can be addressed here is to confirm that this is the level that limit change of flow pattern for gas superficial velocity in the range of $0.025 \sim 0.25 \text{ m/s}$ or translate in the form of slip ratio as $0.01 \sim 0.1$ for the current vibrations with sizes of ground accelerations in the range of $3 \sim 12 \text{ m/s}^2$.

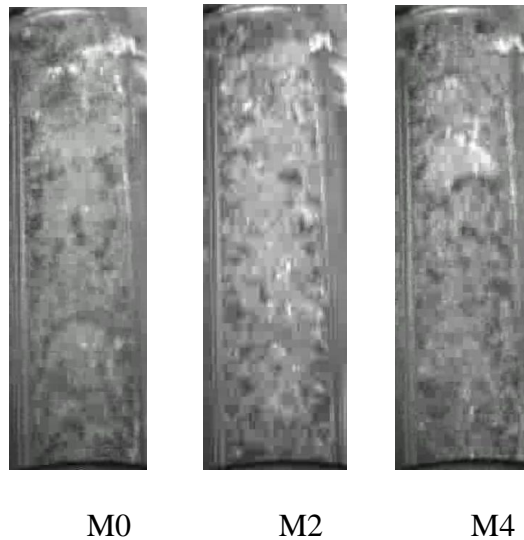


Figure 7.32 : Changes of flow patterns due to vibration sizes, for $j_L=2.5 \text{ m/s}$, $j_G=0.75 \text{ m/s}$

7.2.6 Effects of Vertical Motion

Since direct ground accelerations from vertical vibrations were associated in these investigations, the effects of vertical movements are surely very important to be considered. Some discussions were carried out on this issue along with the discussion on the changes of flow patterns in the previous sub-sections. For more concrete evident, figures 7.33 and 7.34 are used to discuss about the structures of flow during the event of vibration. The selections of these conditions were just based on the flow development that took place in these investigations which the two main patterns; the bubbly and slug flow. These flow structures were observed based on their development in time series as the vibration damped harmonically during the experiments.

Figure 7.33 shows the flow structures for $j_L=0.5 \text{ m/s}$ and $j_G=0.05 \text{ m/s}$ or the slip ratio at $S=0.1$ during vibration with mode M3. The flow started with steady bubbly flow in the beginning of the experiment and bubble congregations in very close gap were observed at $t=2.1 \text{ sec}$ when vibration was applied. During the upward movement the liquid holdup tends to be pulled or slowing down as the vertical vibration experiencing a negative acceleration. It therefore drags together the bubbles and as a result a high percentage of liquid occupied in this position at $t=2.3 \text{ sec}$. The effects of downward

liquid flow resulted in the huge congregations of bubbles and lead to easy coalescences and as a result developed the slug flow with some trailing bubbles on the tails at $t = 2.5$ sec.

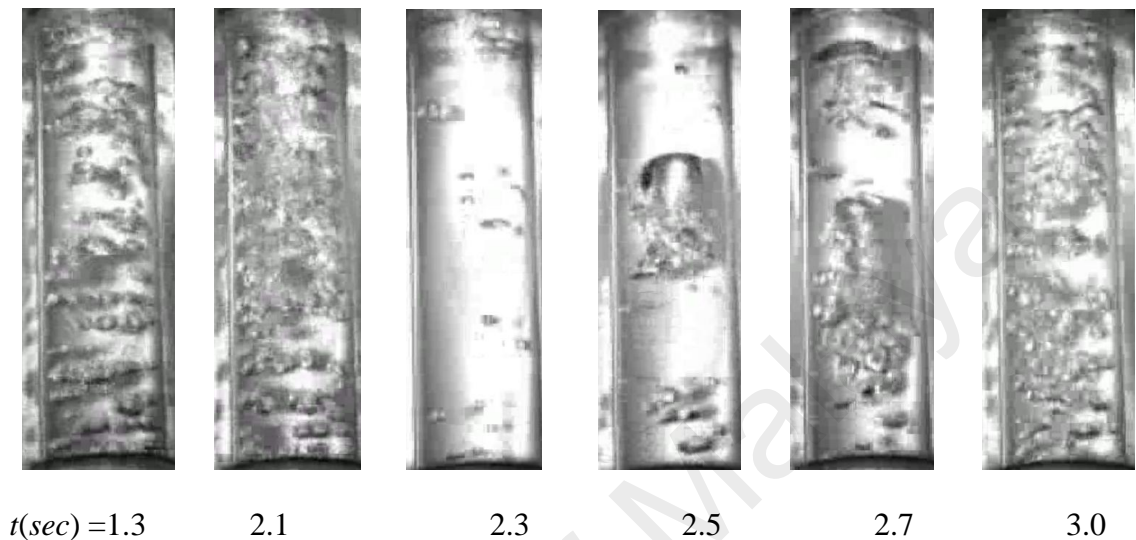


Figure 7.33 : Flow structures for $j_L=0.5$ m/s, $j_G=0.05$ m/s during vibration with mode M3

Since the coalescences happened very rapid and easy, more slugs were produced but again with the effects of downward liquid flow due to vertical motion, these slug were seen to be very unstable, distorted and breaking up forming smaller bubbles in the flow channel as at $t=2.7$ sec. This discomfort situation does not extend for long until the motion change its direction along the sinuous curve of vibration to move downward. During the downward motion, the system is then experiencing a positive acceleration and therefore accelerating the liquid flow as well. As a result, a more stable bubble flow were observed as at $t=3.0$ sec.

Figure 7.34 shows the flow structures for $j_L=0.5$ m/s and $j_G=0.1$ m/s or the slip ratio at $S=0.2$ during vibration with mode M3. The flow also started with steady bubbly flow in the beginning of the experiment with very close gap of bubble congregations and sometime allowing the coalescences. As soon as receiving the impact from vibrations, rapid coalescences occurred and forming slugs as at $t=2.0$ sec with trailing of

small bubbles at the tail and this kind of slug look like an uncompleted structure. This phenomenon is due to the downward liquid holdup that disturbs it and tearing down the surrounded liquid that hold the slug proportion.

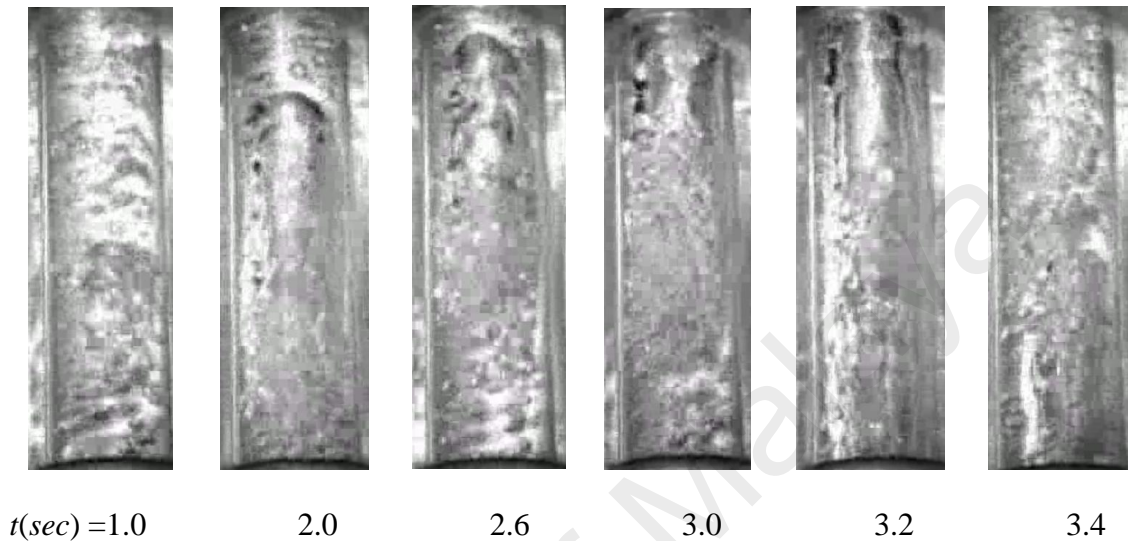


Figure 7.34 : Flow structures for $j_L=0.5$ m/s, $j_G=0.1$ m/s during vibration with mode M3

This history keep repeating and as a result, the slug structure never been established in a proper shape and rising like at $t=2.6$ sec. With further propagation from the upward and downward of liquid holdup, these long slugs break up along the travel as at $t=3.0$ sec. The effect of vertical motion also sometime forced these slugs to coalesce with other slugs forming super long slug which having a length of about 300 mm with very thin liquid film thickness. With this length, they are sometime behaving as or misinterpreted like an annular flow as at $t=3.2$ sec. Again with continuous vertical motion effects as they break up again forming a very unstable flow regime as a churn flow at $t=3.4$ sec.

Therefore, from this investigation, it is observed that vibration can easily change the flow patterns into varieties of flow pattern with the same gas and liquid superficial velocities, but the effect is limited during higher velocities of both phases.

7.3 Flow Patterns Mapping

Mapping of flow patterns is very important in order to predict the behavior of two-phase flow in a channel under a particular flow condition. For example, as discussed in section 7.2, the gas-liquid two-phase flow exhibits different patterns under different flow conditions, such as transition from bubbly to slug to churn to annular flow. There are a lot of argument that also underwent on the selection of fair and appropriate parameters to be presented in the flow pattern maps particularly on the scaling the transition boundaries. However, for the current studies since the investigations were merely involved with the combination of gas and liquid superficial velocity, the flow patterns maps presented in this thesis are on the scale of these parameters for x - and y - axis.

In this section, the flow patterns maps are presented based on the results obtained from photographic data as discussed in the previous section. These data were analyzed for various set of flow conditions which are the combination of gas and liquid superficial velocities (j_G and j_L). They are expressed to show the vibration effects on the total map with comparison to the steady state condition. The types of vibration that applied in this case are also the same as in the previous cases, which are modes M1 ~ M4. This vibration however, is actually limited to very short period of time, normally about 5 ~ 6 seconds, since they are the damped harmonic vibration that decelerate according to damping factor of the spring. This condition does not enable the flow patterns to fully develop even though they exhibit some changes.

Furthermore, for a practical important such as, chemical processing that requires a longer period of shakes, analysis with extended time of vibration would be a good investigation to be carried out (Ellenberger and Krishna, 2002 and 2003). Taking an account for this purpose and disaster shakes as well, the continuous vibration as introduced in the previous section also applied in this investigation and they are

extended to the full mode of vibration scale which uses the whole range of available amplitude 10 ~ 40 mm. Therefore, the continuous vibration as in figure 3.9 was applied.

Before proceeding to further analyses, as a calibration or references for the current work, flow patterns map developed by other researchers were compared with the current result. As shown in figure 7.35, flow patterns map by Furukawa and Fukano (2001) and Hughmark (1962) were selected and compared with the current result. From this figure, and comparison with the flow patterns map by Taitel and Duckler (1976) in figure 5.5, it can be observed that the gas-liquid two-phase flow changes the patterns from bubbly to slug flow at combination of $j_G=0.025 \text{ m/s}$ and $j_L=0.1 \text{ m/s}$, or in other word at around slip ratio, $S = \frac{j_G}{j_L}=0.25$. The boundary of this flow pattern transition for this range of flow condition, which is in this case, $j_G=0 \sim 0.1$ and $j_L=0 \sim 1.0$ is nearly following the linearity of the reference line (the dashed line). Hence, this figure confirmed that the current result agrees well with flow patterns map developed both by Furukawa and Fukano (2001) and Hughmark (1962), and in the range of map developed by Taitel and Duckler (1976).

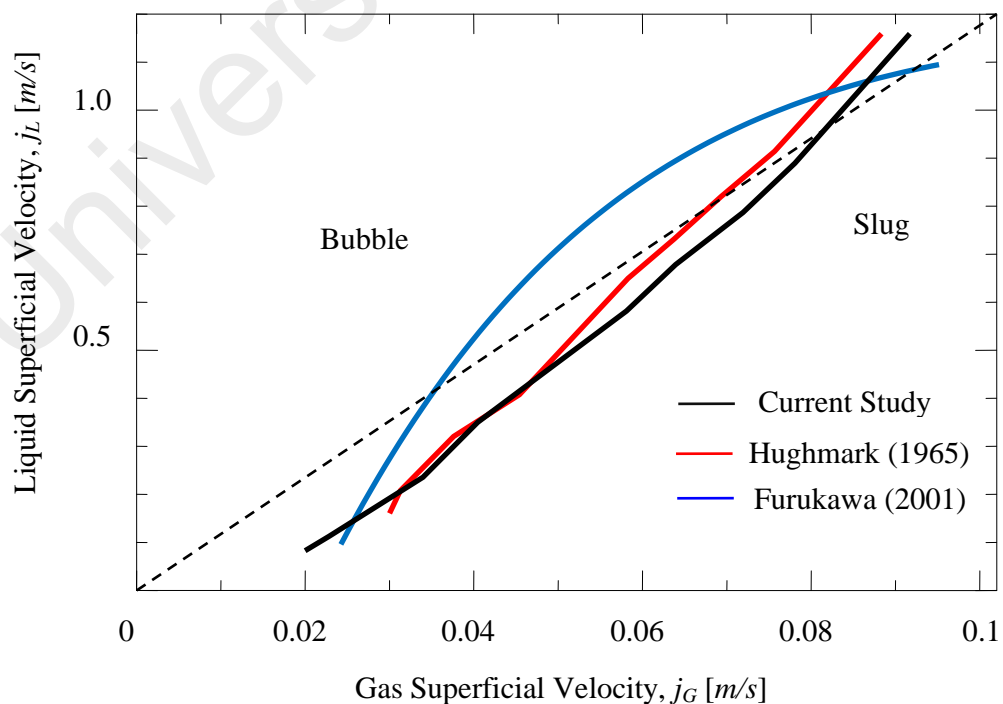


Figure 7.35 : Comparison of flow patterns maps with other scholars

7.3 Flow Patterns Mapping based on Modes of Vibration

Since the transition from bubbly to slug is the most commonly encountered in most of the flow conditions with combination of low gas and liquid superficial velocities, and again referring to figure 5.5, this transition extended to the combination of $j_G=1.0 \text{ m/s}$ and $j_L=1.0 \text{ m/s}$. There is also a probability of same patterns that will be obtained for higher value of j_G and most probably the same pattern as bubbly flow will be obtained as well if the extension of liquid superficial velocity goes beyond 1.0 m/s . Therefore all the analysis for flow patterns map in this study were carried out only for the range of gas and liquid superficial velocities as, $j_G=0 \sim 0.15 \text{ m/s}$ and $j_L=0 \sim 1.5 \text{ m/s}$. In addition, the current experimental facility also has a limitation of maximum gas and liquid superficial velocities, of which the both respectively limited to $j_G=1.0 \text{ m/s}$ and $j_L=2.5 \text{ m/s}$. The details of composition of the flow pattern during the steady state for the current work, is presented in figure 7.36.

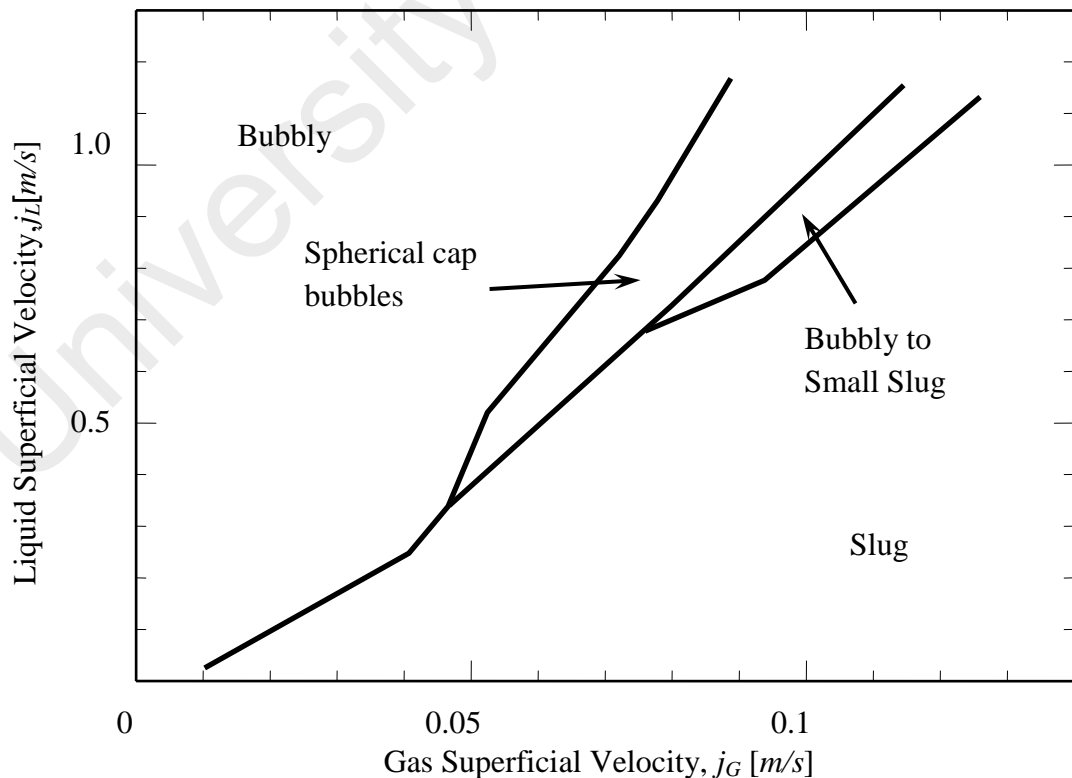


Figure 7.36 : Flow pattern map during steady state condition (mode M0)

As shown in this figure, the boundary between bubbly and slug is quite clear, following the almost the same line as projected in figure 7.35. Since the interaction between bubbles resulted in coalescences that promote small bubbles to form bigger bubbles, the composition in bubbly flow are mainly of small bubbles of various sizes at several millimeters and some bigger bubbles with spherical caps and mushroom shapes at various sizes as well. These bubbles stay stable and do not change pattern along with the boundary lines but they start to develop another form of structure on combination of the higher gas and liquid superficial velocities.

At the boundary of flow transition, particularly on the higher velocity of both phases, the bubbles start to interchange the shapes from spherical head to small slugs when rapid coalescences occurred. Slug flow, on the other hand, following the rules of nature, start to occur even a low gas superficial velocity with liquid velocity as low as 0.2 m/s or in specific measure, from low value of slip ratio, $S=0.2$. Even though the formation of slug during the low value of slip ratio was not really significant, it increases as j_G increases particularly when j_L is small, and this result indicates that the formation of slug is very much easier at high j_G and low j_L .

With the same behavior exhibits by the current study as the above comparison, it is very safe to conduct the analysis of vibration effects on the flow patterns maps with concerning on the transition of each pattern due to the combination of j_G and j_L . Figure 7.37 shows the flow patterns map of gas-liquid two-phase flow of the current work under the influence of vibration initiated from 10-mm amplitude that produces ground accelerations in the range of $\pm 3\text{m/s}^2$.

The same behavior presented under the flow condition with combination of very low j_G and j_L that formed only bubbly flow along the flow channel. The spherical cap bubbles were formed at a very stage and under the influence of vibration, the amount of

types of bubbles increased forming about 50% of total bubbly flow. The same event also occurred for early transitional from bubbly to slug flow and the formation of slugs also become more intense.

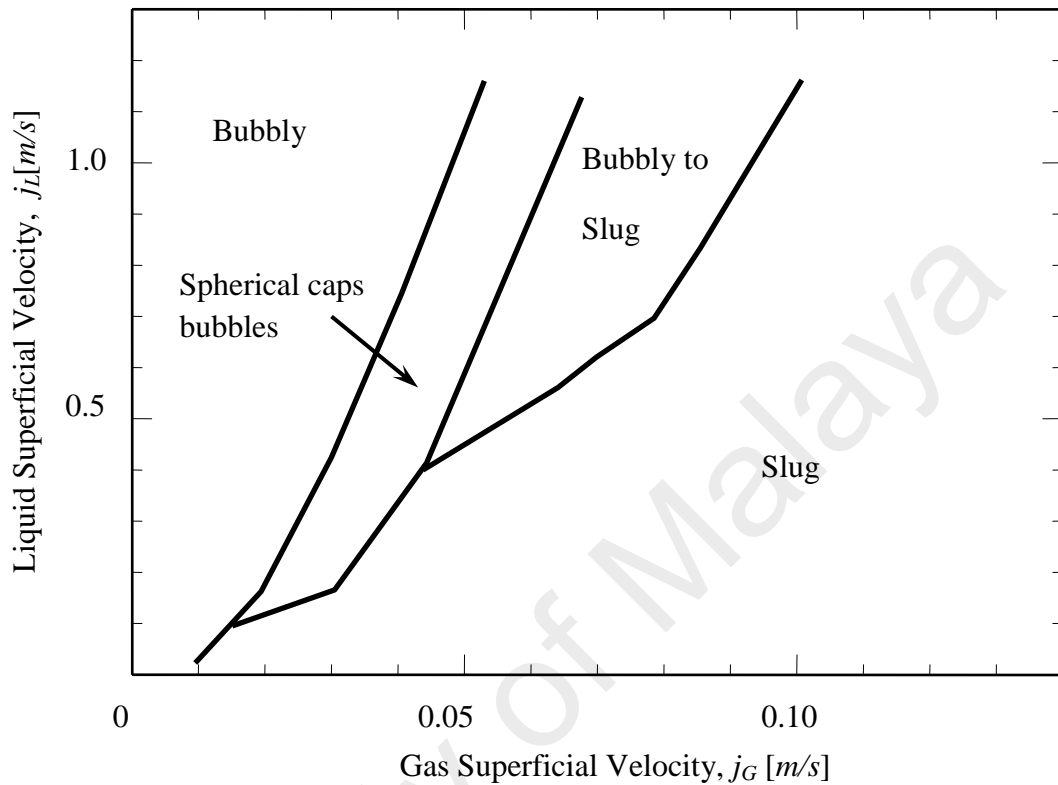


Figure 7.37 : Flow patterns map for damped vibration with mode M1

Comparison between figure 7.37 and 7.38 which are respectively for vibration with modes M1 and M2, reveal that with higher vibration mode, the flow patterns map is completely transformed into different composition. In figure 7.38, there are only three main regime can be mapped, which are the bubbly to slug, short slugs and the slug flow. The bubbly to slug pattern in both figures is actually the development from spherical caps bubbles that experienced rapid coalescences forming more short slugs. In figure 5.48, the bubbly flow was mostly in the form of spherical caps at bigger sizes and there were also mushroom type bubbles dominated this flow regime and they were both developed to become short slugs.

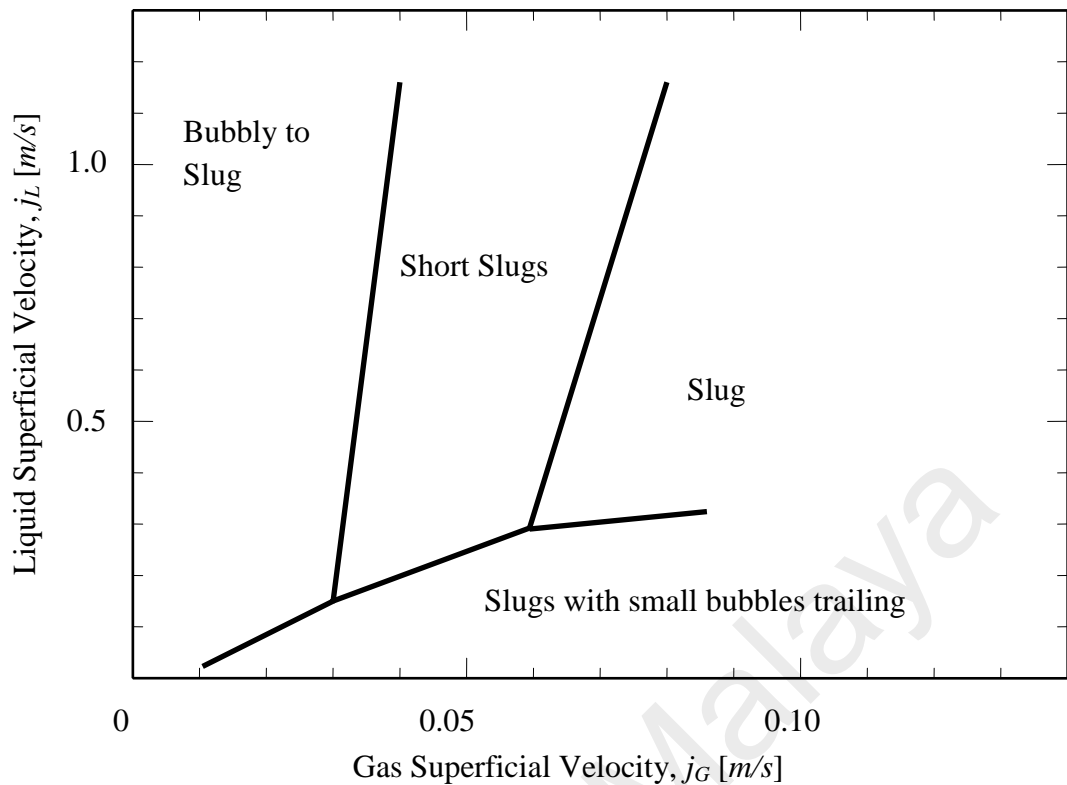


Figure 7.38 : Flow patterns map for damped vibration with mode M2

With further increase of gas superficial velocities, this short slugs becoming more stable and flow in very high volume in the flow channel. The extra force from vibration alleviates more congregations and making it easier for these short slugs to coalesce to form solid slugs in the flow channel. In figure 7.38 also, it can be observed that with a low liquid superficial velocity and increase of gas superficial velocity, slug formation was quite easy. However, since the flow was comparatively not stable compared to the one in higher j_L , the slug formation was still in progress where most of these slugs were associated with many trailing bubbles from behind in various sizes. This flow pattern progress with time and with more forces from vibration, some of the slug break up into short slugs and again coalesce to form solid slugs with the increase velocity of both phases.

It is also very clear that the volume of combination of short slugs and slugs is much higher under this mode of vibration compared the lower mode in figure 7.37, and a rough observation may be calculated 50% of solid slugs, 30% of short slugs and only 20% of bubbly flow. Therefore, as a short conclusion, it can be said that vibration with mode M2 or in other words ground acceleration with range of $\pm 6 \text{ m/s}^2$, can contribute to a totally different flow pattern when compared to steady state condition as in figure 7.36. This is a very serious alteration to the normal flow patterns and therefore attention on this subject must be paid in order to predict any hazardous possibility in an event of any two-phase flow facilities that undergo the same situation.

Figure 7.39 representing the maps of flow patterns when the current flow channel experienced the vibration with mode M3 or with ground acceleration with scale of $\pm 9 \text{ m/s}^2$. This figure displays more distinguish composition of flow regime compared to the previous two modes of vibration. Here, for the two-phase flow that underwent this mode of vibration, there are three different regimes which are the bubbly to slug flow, slugs, and longer slugs the one that looked like churn and annular flow. In this case, there is the bubbly flow in the flow channel, but mostly as the same in the two previous cases, where this regime only exist during the lower gas superficial velocities and higher liquid superficial velocities. The composition of this regime again is very similar with previously discussed, the spherical caps and the mushroom types bubble but they are very disordered, distorted and sometime broke up into smaller bubbles. The formation of short slugs occurred soon after the congregation of bubble at various sizes took place and compared to the previous two cases, the volume of short slugs is very much higher.

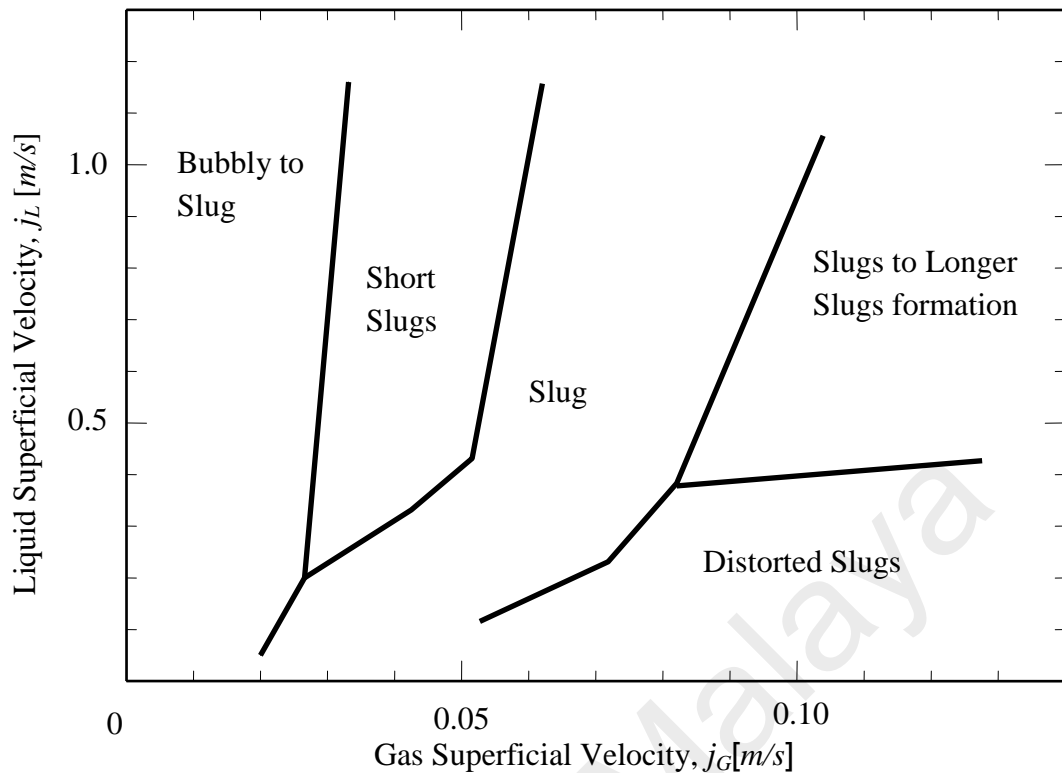


Figure 7.39 : Flow pattern map for damped vibration with mode M3

The same phenomena repeated in the process of solid slugs formations where the short slugs with higher mass and assisted by the vibration, coalesce well with their counterparts. However, with this scenario, the slugs were found to be easily form and break up. As shown in this figure during the low liquid superficial velocities region, and with low gas superficial velocities, there are huge volume of slugs but they are distorted and break up, forming very distinctive shape, looked like the churn flow. These slugs however, coalesce back with each other and forming longer slugs. This incident happened when the vertical movements due to vibration, speed up the motion of these slugs and they coalesce with each other, and during the negative acceleration, slowed down to collide and break them up into small pieces with the mentioned shapes.

With higher velocities in the both phases, more slugs were formed, where more collision and coalescences occur making longer and bigger slugs' formation as the most common phenomenon in this regime. Domination of slugs is very obvious during this

mode of vibration, where can be observed from figure 7.39, the slugs composed around 70 ~ 80% of the whole population, which reveal another interesting development yet very dangerous assumption in the event of heavy disaster shakes.

The same composition can be seen when the flow channel being hit by another scale of vibration at mode M4, or with ground acceleration at $\pm 12 \text{ m/s}^2$ as shown in figure 7.40. About the same rate of bubbly to slug flow transition can be observed in this figure, with also the same composition of spherical head and mushroom types bubbles in more heavily distorted shapes and with various sizes as well. Formation of short slugs also with the same process as in the previous cases and as the transition of bubbly to slug is much easier in this case, the formation of short slugs sometime jumped into a proper shape of solid slugs. Therefore, with this condition, it does not require much effort for these small and short slugs to form solid shape slugs where in this figure, they were developed shortly after the small volume of short slugs domination in the flow channel, even at low gas superficial velocity in the high velocity of liquid phase. The volume of this slug regime only occupy 30 ~ 40% of entire population.

However, the most significant changes under the influence of this mode of vibration are the development of slug flow in the upper region of gas superficial velocities. As seen in the previous case for mode M3, where with low liquid superficial velocity, the slugs broke up and forming the churn flow shape, this phenomenon also repeated under this vibration size. At the higher velocity of both phases, very much longer slugs were formed and the flow pattern during this time looks like the annular flow.

However, the classification of the annular flow still cannot be carried out for this case since these slugs were in their shape, and sometime because of their sizes collide with the wall of the flow, and break up, becoming as the same condition for lower region of gas superficial velocities. These breaks up were then refilled by another long

slugs and this condition continuously repeated forming a very unstable flow pattern and making the most chaotic regime which can be considered in a very critical and hazardous condition particularly if the system involve the heat transfer such as boiling and condensation.

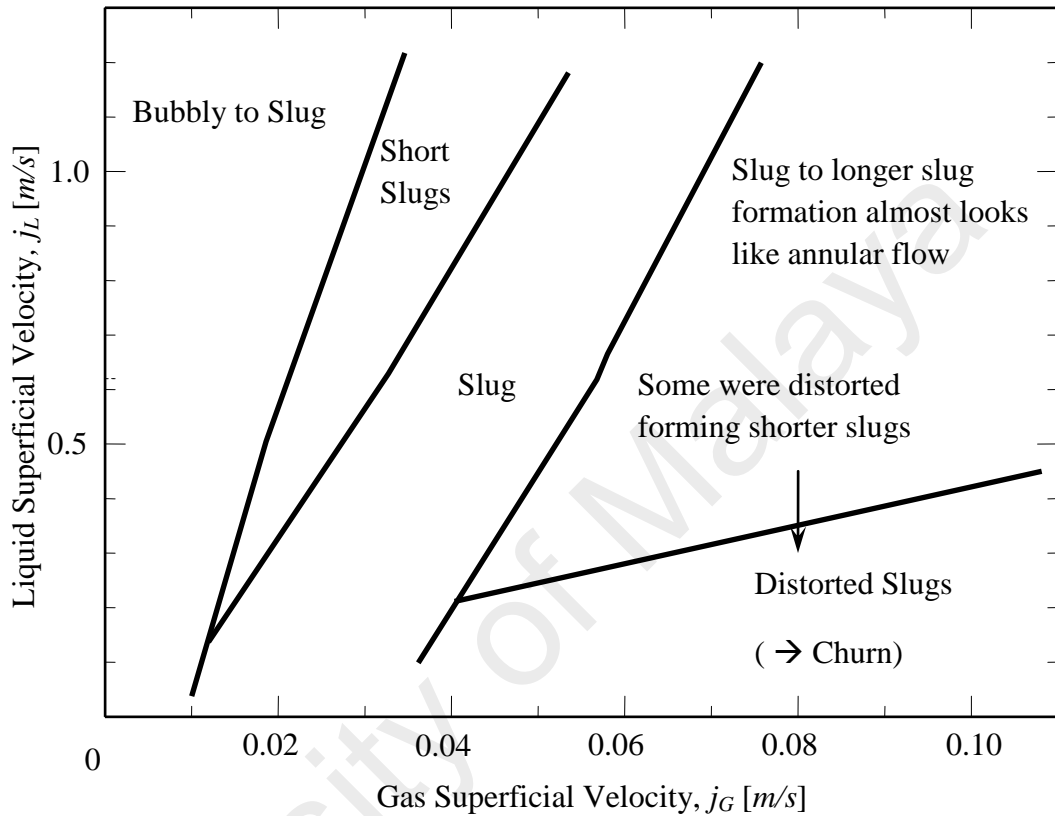


Figure 7.40 : Flow patterns map for damped vibration with mode M4

The flow patterns map for the current study under the influence of continuous vibration at 20-mm amplitude or continuously vibrate under the ground acceleration of $\pm 6 \text{ m/s}^2$ is shown in figure 7.41. Similar to the maps for vibration with modes M3 and M4, the composition of flow regime under this vibration effects consists of bubbly to slug flow, short slugs, stable slugs and longer slugs. In this case, the continuous vibration under this scale of ground acceleration contribute to the effects between mode M3 and M4, as can be seen in the figure where the volume of slugs is very much the same as the two cases.

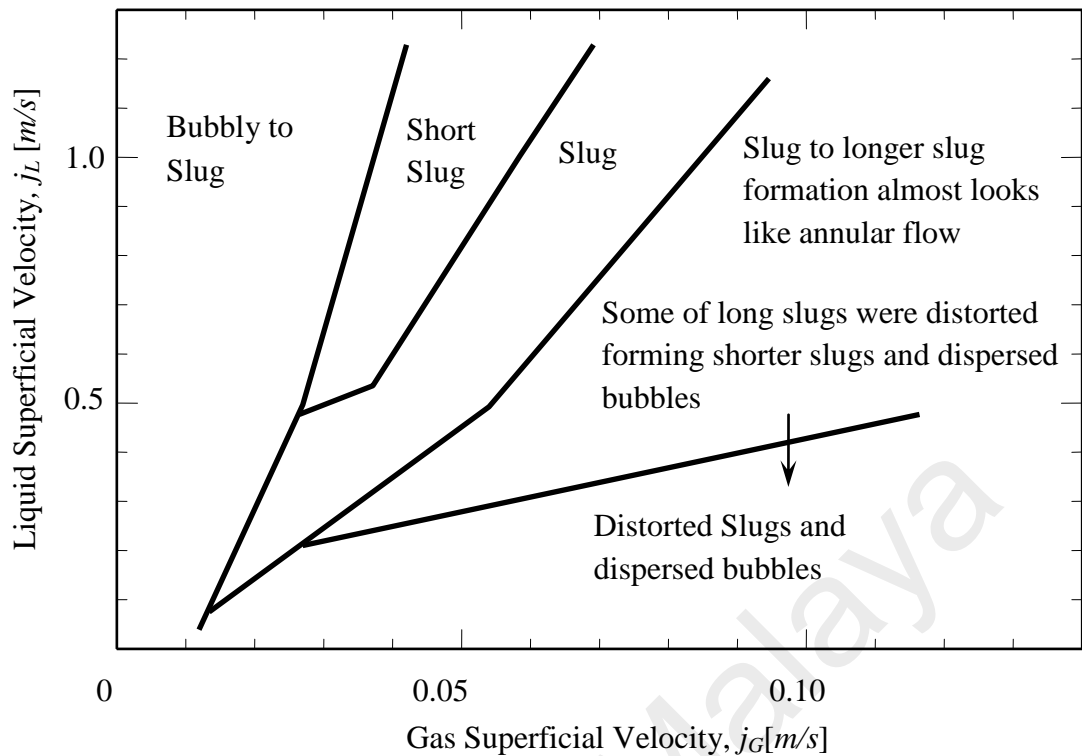


Figure 7.41 : Flow patterns map with continuous vibration with amplitude 20-mm

The combination of higher velocity in both phases with continuous vibration leads to more collision among bubbles and the wall of the flow channel, making the break up more frequent and those big bubbles dispersed into smaller bubbles with different shapes and sizes. Longer slugs of which more stable in form of shapes and structure were broke up into shorter shapes. Some of these shorter slugs with huge diameter were easily move toward the wall of flow channel coalesce with smaller bubble that crowding on the wall forming slightly bigger slugs and move back to the core of the flow, collided with the incoming slugs from the bottom and move upward together in a longer shape. The processes of flow patterns mapping is shown in Appendix 7.1. From the data distribution in this sheet which is generated from high speed video images, the discrete bubble distribution analyses can be carried out as in the following section.

7.3.2 Discrete Bubble Distribution

Under the influence of vibration, the bubbles were very easy to be swung to any side of the flow channel and they were also being pulled up and down very frequently due to the vertical motion under the nature of the degree of freedom of this vibration. These bubbles will therefore can be seen anywhere in the flow channel, and they were particularly populated in very high density after the breakup of bigger bubbles and slugs. In the free space, they tend to attract to bigger bubbles and slugs due to their small sizes and lower mass. This makes the trailing bubbles behind big bubbles and slugs occur everywhere in the flow channel, which as a result very difficult to identify a specific flow pattern at a particular flow condition.

The vibration effects resulted in an abnormal behavior of bubbles flow in the channel where the congregations of bubbles as discussed throughout this section is a very important characteristic to be analyzed as well. This is due to the uncertainty of movement as the vertical motion took place, disarranging the bubble position to be anywhere, regardless of flow condition as they might follow in either core peak or wall peak as described by Hibiki (1998), Shen (2005) and Shawkat (2008).

In this case, since the bubbles were dispersed and congregate everywhere, the coalescences were found to be much easier to occur, and this condition contribute to formation of longer and bigger slugs which happened even under the low order of vibration mode. With the flow patterns maps displayed in this section, the most important factor to be looked into is therefore the composition of the regime in these maps that completely altered due to the vibrations. It may leave very a bunch of homework to be completed in order to minimize the hazardous possibility in dealing with two-phase facilities flow that have possibility to undergo the scale of heavy disaster shakes as discussed in this work.

7.4 Void Fraction

Vertical upward two-phase flow is a very important subject to be studied since they are widely used in many engineering practices, analyses and design of equipments. In the previous sections, results on the flow patterns and flow mapping under the influences of vibration have been carried out to describe the behavior of two-phase during those events. The dynamics of two-phase flow can be more exclusively expressed by the direct measurements of the parameters involved. During the experimentations, the gas and liquid superficial velocities can be determined using the relation of volumetric or mass flow rate and the channel diameter, but these parameters has limitation to draw the characteristic of the two-phase flow. Therefore, the actual rate of gas existence in the flow channel or systematically termed the void fraction is the best parameter that would fill in the hole of this incomplete event.

7.4.1 Measurement and Procedures of Analyses

Using the same experimental facility and test section, the measurement of void fraction has been carried out. In section 6.2, the preparation, calibration and test of void meter has been discussed. This void meter was used to measure all the void fractions in this work with liquid superficial velocities in the range of 0.25 ~ 2.5 *m/s* and varied with gas superficial velocities in the range of 0.025 ~ 0.25 *m/s*. In order to investigate the effect of vibration on fluctuation of void fractions, these flow conditions were then varied for according to the modes of vibrations as practiced in the previous sections which are the M1, M2, M3, M4, as well as the control experiment during no vibration. Therefore, the ground accelerations can also be listed in the range of $\pm 12 \text{ m/s}^2$.

Beside the measurement for those four modes of damped free vibrations, another mode of vibration was added in this investigation, which the continuous mode, C as same as that has been conducted for flow patterns mapping in section 7.3. This mode

serves as a reference for the case where the vibrations occur for quite a long period, for example about 10 seconds and continuously produce a sinusoidal motion without damping. As shown in figures 7.37 ~ 7.41, the flow patterns show different trends during damped free vibrations and the continuous vibrations, the same effects would be presented for the void fractions.

Furthermore, the void fraction measurements were conducted at three different locations along the test sections to study the effects of axial locations (L/D), which are at the $L/D = 35, 42.5$ and 50 . In chapter 5, the discussion on the Drift-Flux Model has been carried out for the analyses of void fraction. This model will determine the effect of superficial velocities of both phases on the fluctuation of void fraction in vertical upward two-phase flow. In this investigation, the Drift-Flux Model was applied and it was used to observe the changes of void fraction due to vibration modes and therefore give more detail description on the effects of ground acceleration sizes.

Since the fluctuation of the void fractions are in very wide range, the average of void fraction does not reflect the real situation in the flow channel. In view of this, the peaks of the void fractions were chosen from the spreadsheet maximum and minimum values. These peaks and valleys will therefore give information as the repeated situation happens in the flow channel or the frequencies of highest and lowest void fraction at a given flow condition and vibration modes. Therefore, the analyses on measured void fractions were carried out for two different ways, the overall average and the differences between the maximum and minimum of local values at two different positions. The methodology of this analysis can be referred to flow chart in figure 7.42.

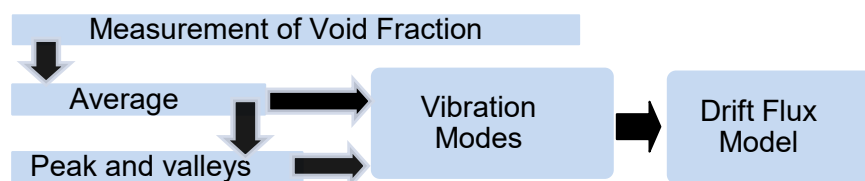


Figure 7.42 : Flow chart of void fraction analyses

7.4.2 Basic Measurement

(a) Effects of Vibrations

Some of the examples of the measured void fractions can be referred to figures 7.43 ~ 7.47. A typical graph of measured void fraction distribution is shown in figure 7.43, where in this case the flow condition was set at $j_L = 0.5 \text{ m/s}$, $j_G = 0.025 \text{ m/s}$. In this example, measurements were carried out for Mode 1 and Mode 3, as well as the control experiment for the steady state where no vibration is applied. This figure shows that as the modes of vibration become higher or as the ground accelerations increase, the void fraction also increases and it goes as high as 0.8 which represent 80% of gas and only 20% of liquid at a particular situation. It also shows that this rate fluctuates steadily for sometimes until it settled down to be as the same rate during the steady state condition. This fluctuation only happened for around 5 ~ 7 seconds which is the same time taken for the harmonic vibration to take place using the current shaker which is about 5 seconds as discussed in chapter 3 and figure 7.44 describe in detail about this event.

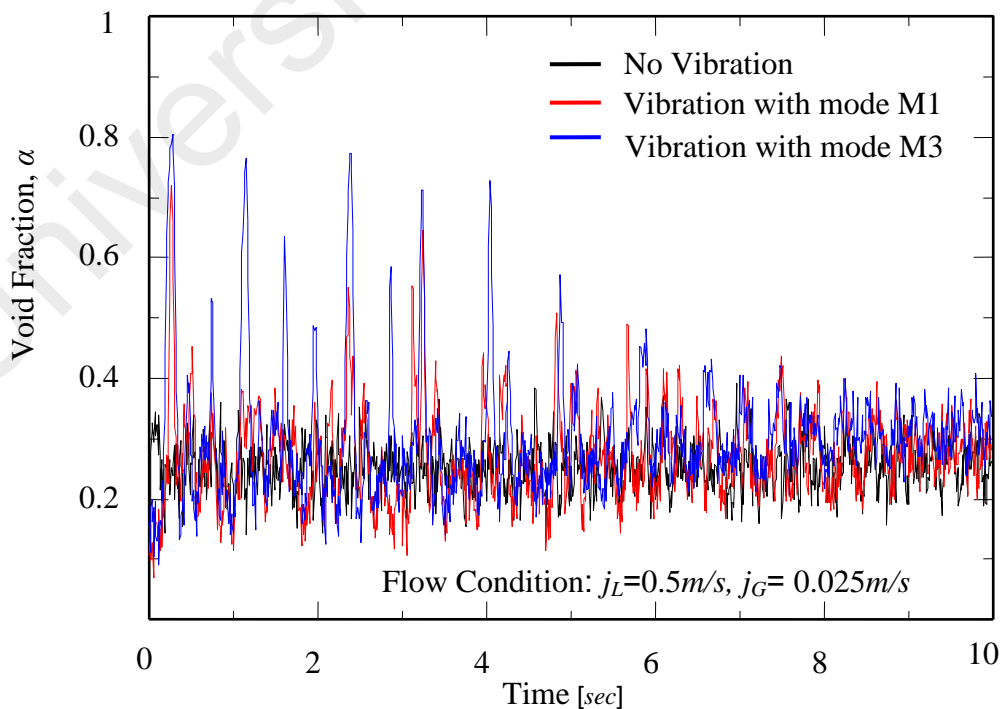


Figure 7.43: Fluctuation of void fraction due to scales of vibration

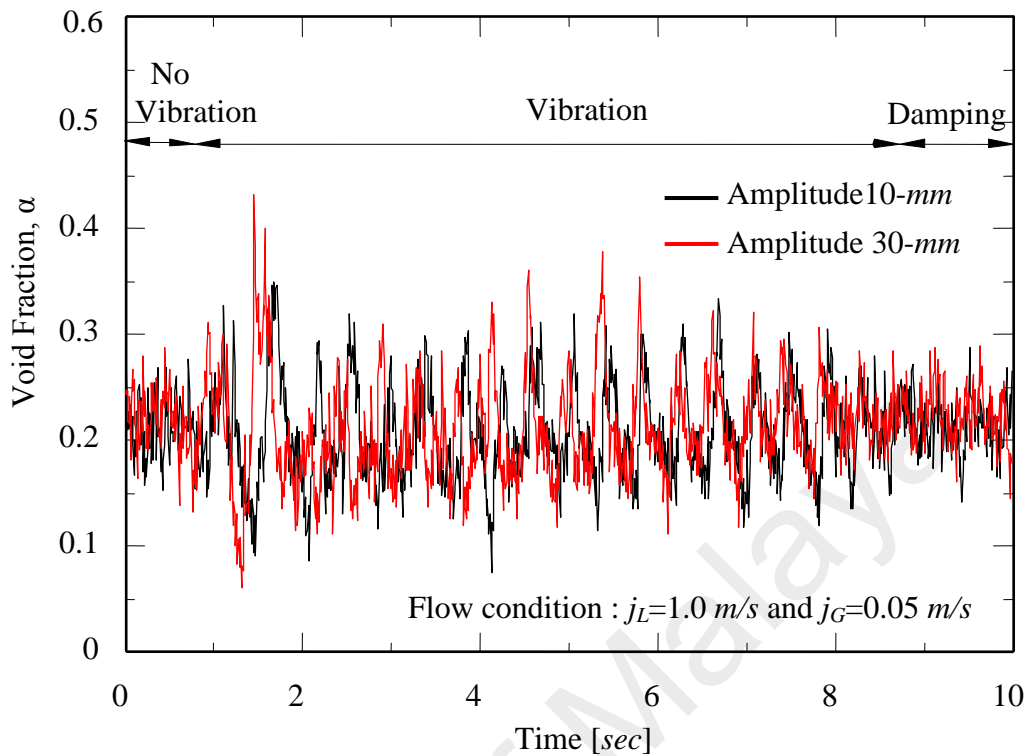


Figure 7.44 : Fluctuation and damping of void fraction due to vibration

A further analysis as can be referred to figure 7.45, which a close up of the above figures, but using a slightly different flow condition at $j_L = 0.5 \text{ m/s}$, $j_G = 0.05 \text{ m/s}$. It shows that the fluctuation is also very similar to the sinuous curved produced by vibration and is follows exactly the same frequency of the vibration. This fluctuation can be compared to the steady state condition in figure 7.43 and also on the same graph here, where it does not have the same typical peak and valley frequency and the fluctuations varies irregularly without any fixed pattern. Therefore two simple conclusions can be drawn from this analysis; when vibration hit any two-phase flow system, the fluctuation of void fraction will follow the vibration frequencies and divert from its original value only during the time of the vibration taken place.

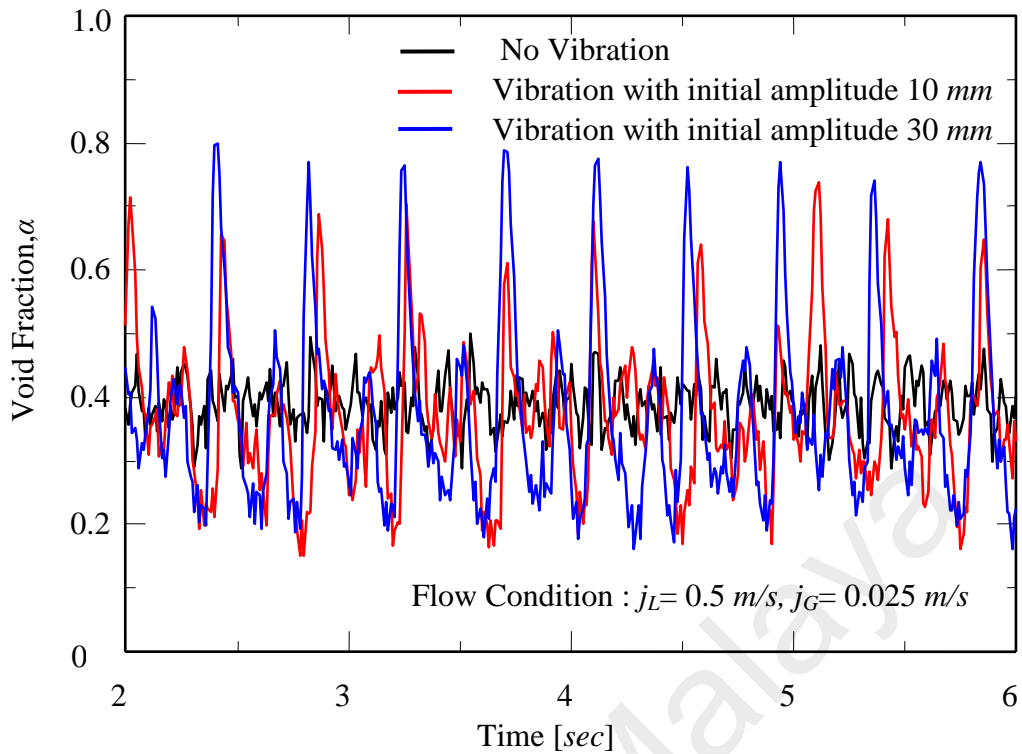


Figure 7.45 : Void peaks show the frequency similar to vibration frequency

As shown in the above figures, the fluctuations of void fractions during vibration have a very wide range in values, and also show very large differences if compared to the steady state condition. For example, during mode M3 vibration, the maximum value is 0.8 and the minimum value is 0.2; and compared to average at steady state condition at 0.4, reveals that the fluctuation is about double of the normal value. This analysis is very important, particularly for process engineering to optimize the operating condition and furthermore in some of the boiling and condensation equipment, fluctuation of very high void fraction might lead to early burnout phenomenon which is a very dangerous situation. Therefore, it is very important to conduct a further analysis on the maximum and minimum value of void fraction or the local void fraction in addition to the average void fraction analysis during the vibration in order to investigate the possible hazardous problem in a particular flow condition.

(b) The effects of liquid and gas superficial velocities

The effects of liquid and gas superficial velocities can be summarized as in figures 7.46 and 7.47 respectively. One comparison can be carried out for same modes of vibration at M1 and M3 with gas superficial velocity at 0.025 m/s and different liquid superficial velocities such as shown figure 7.45 with $j_L = 0.5 \text{ m/s}$, and figure 7.46 with $j_L = 1.0 \text{ m/s}$ reveal that the effect of vibration is very low for higher liquid superficial velocity. The same approach was also applied to test the effects of gas superficial velocities with respect to the vibration. With comparison between figure 7.43 and 7.47, the effect of vibration become very low for higher gas superficial velocities. However, these results would be different with different combination of gas and liquid superficial velocities. As the current work applied the range of gas superficial velocities at $0.025 \sim 0.25 \text{ m/s}$, the effects of this parameter in the form of slip ratios, S were investigated as well and they are reported in the further sections.

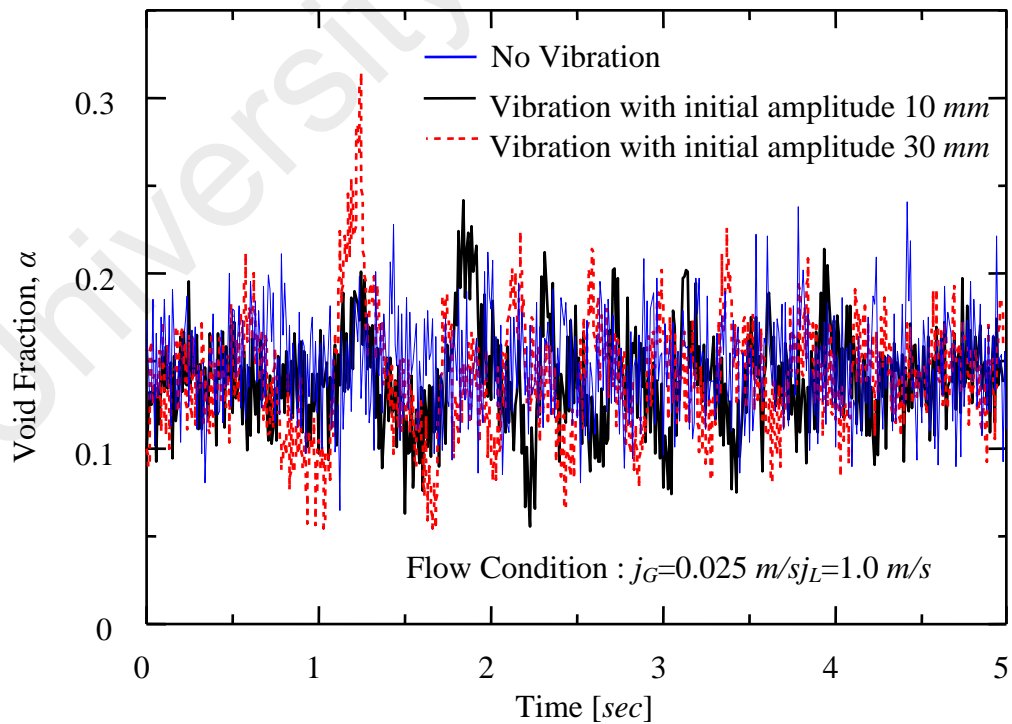
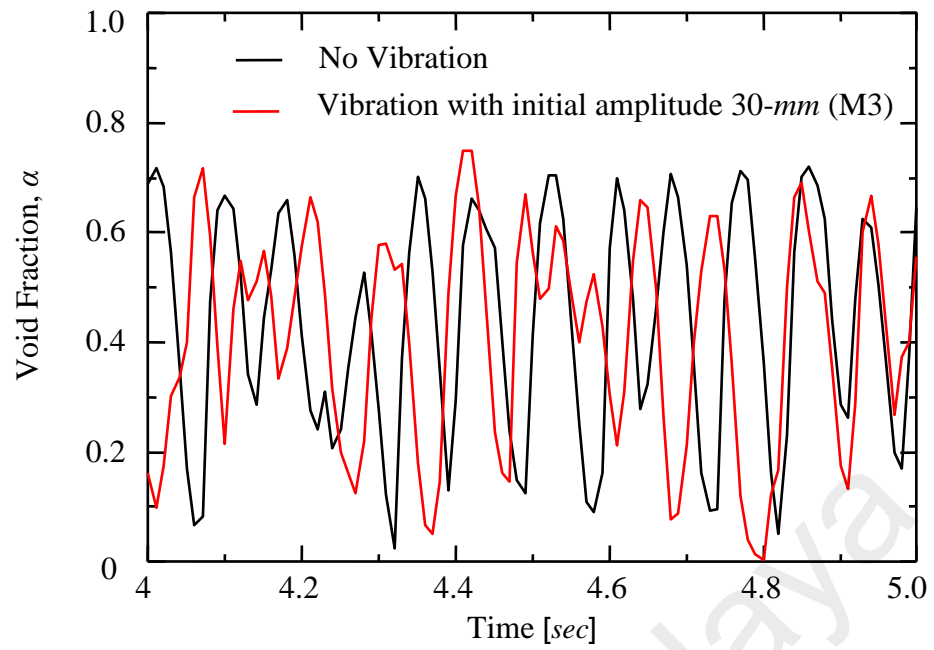
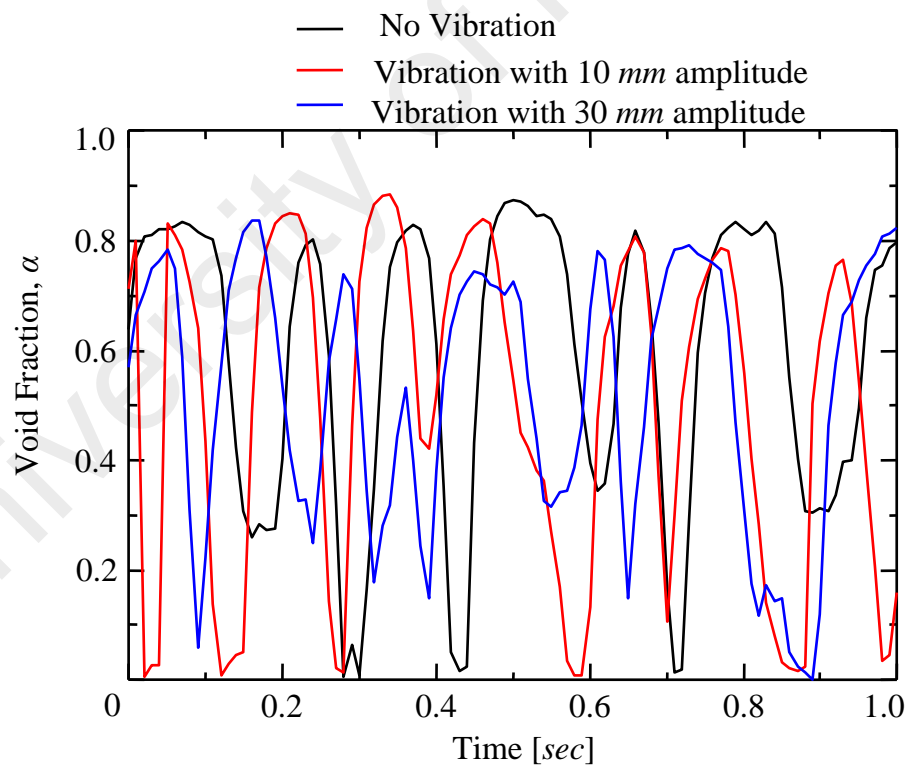


Figure 7.46: Low vibration effect during high liquid superficial velocity



(a) Flow condition : $j_L = 1.0 \text{ m/s}$, $j_G = 0.75 \text{ m/s}$



(b) Flow condition : $j_L = 0.5 \text{ m/s}$, $j_G = 0.75 \text{ m/s}$

Figure 7.47: Low vibration effects during high gas superficial velocities

7.4.3 Vibration Effects on the Fluctuation of Void Fraction

In this section the effects of vibration on the average void fraction along the 300-*mm* length test section will be discussed. As described in the previous sections, the modes of vibrations applied throughout the void fraction investigations are the same as in the previous sections with modes M1 ~ M4 or the range of ground acceleration of $\pm 12 \text{ m/s}^2$. With range of liquid superficial velocities at 0.25 ~ 2.5 and gas superficial velocities in the range of 0.025 ~ 0.75, the slip ratios were obtained in the range of 0.1 ~ 3.0. The data for void fraction was taken for 1000 sample for 10 seconds with frequency of 100 for three different locations of void sensors. These measurement was taken for the steady state and repeated for four different modes of vibration plus an additional mode of continuous vibration with accelerations in the range of $(\pm) 6 \sim 9 \text{ m/s}^2$. The vibration effects on average void fraction are shown in figures 7.48 ~ 7.54. In these figures all they were illustrated in the form of increment of void fraction with respect to the increase of gas superficial velocities (j_G) at fix liquid superficial velocities (j_L) and the effects of damped harmonic vibration modes (M1 ~ M4) are shown in six different lines that represent the sizes of vibrations that affecting the void fractions increment. The other two legends M0 and C are respectively representing the steady state where there is no vibration and the continuous vibration at mode M1.

Total Average Void Fraction

The first result for average void fraction is for liquid superficial velocity, $j_L=0.25 \text{ m/s}$ as shown in figure 7.48. According to this figure, the increases of vibration modes contribute to higher void fraction. The data for average void fraction were only calculated for the slip ratios in the range of 0.04 ~ 0.4. In this case, the average void fraction increased for about 25% compared to the steady state condition and the developments of this increment are nearly linear. This might be due to very low liquid

superficial velocity where the gas flow dominated the flow channel. With this linear development, it is enough to table the data for average void fraction were only calculated for the slip ratios in the range of 0.04 ~ 0.4, and further increase of the slip ratio also will show the same trend of result. The dotted line represent the continuous vibration at the accelerations of (\pm) 6 ~ 9 m/s^2 as comparison to the damped harmonic vibrations reveals that the continuous vibration just shown a little higher value of average void fraction as other modes of vibrations at around 0.38.

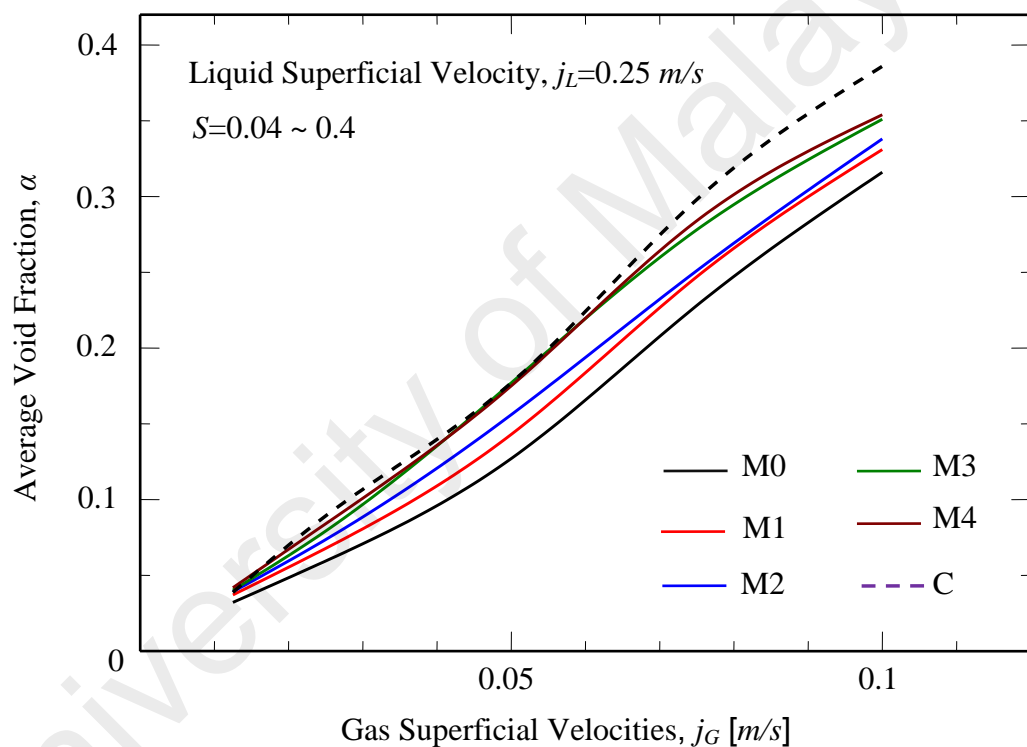


Figure 7.48 : Effects of vibration on average void fraction for $j_L=0.25 m/s$

The average void fraction for a higher liquid superficial velocity, $j_L=0.5 m/s$ shown in figure 7.49 shows a little different phenomenon where it not as linear as the previous case. It started as linear at the beginning of the flow condition with slip ratio, S around 0.05 ~ 0.15 and started to be up and down until reach $S =0.2 (j_G=0.1 m/s)$. It linearly growing up again and beginning to decrease at around $S =0.4 (j_G =0.2 m/s)$ and

the void fraction value settled at around 0.3. The effects of vibrations also demonstrate a different trend where, during this range vibrations seem does not contribute much to the increment of average void fraction. From $S = 0.4$ ($j_G = 0.2 \text{ m/s}$), the void fraction shows some decreasing value and it might increase again as the gas superficial velocities. During this range, the vibrations show the same trend of effects as in the previous case where as the mode of vibration increases, the value of void fraction also increases. On the other hand, the continuous vibration also shows the void fraction at around the same value as the other modes of vibrations. As a comparison with the previous case, vibration still play a role in the increment of void fraction value as the slip ratio for the current flow condition is still around 0.05 ~ 0.5.

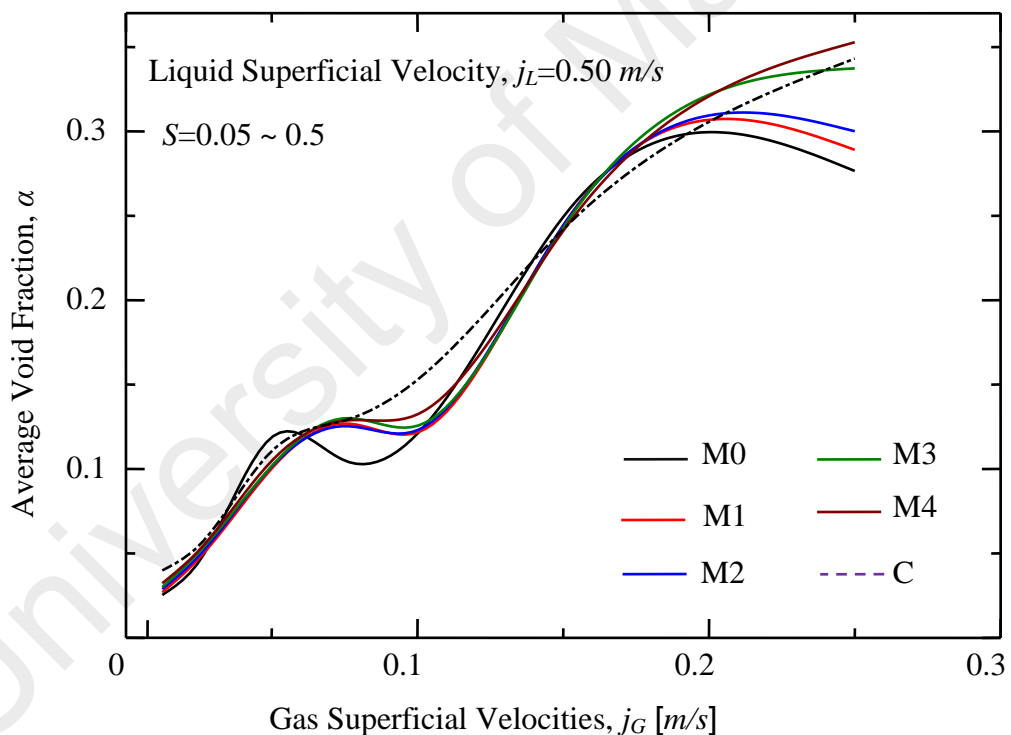


Figure 7.49 : Effects of vibration on average void fraction for $j_L = 0.5 \text{ m/s}$

With further increase of the gas superficial velocity to 0.75 m/s , the same range of slip ratio is maintained at maximum of 0.5 as shown in figure 7.50. The trend of void fraction increment is as about the same as represented in the case of $j_L = 0.5 \text{ m/s}$ where

there are linearly increase and settled at some range of slip ratio around $S = 0.13 \sim 0.2$ ($j_G=0.1 \sim 0.15 \text{ m/s}$) and then linearly increased again to achieve the maximum average void fraction value of 0.275. The value is a little lower and it is due to the effects of higher liquid superficial velocity with shows that higher mass flow rate of liquid phase start to dominate the flow channel. The effects of vibration still exist in this flow condition and as shown in this figure, the same effect of higher modes contribute to higher rate of void fraction and these curves suggest that with further increase of gas superficial velocities, the void will surely increase but the effect of vibration seem to be weaker.

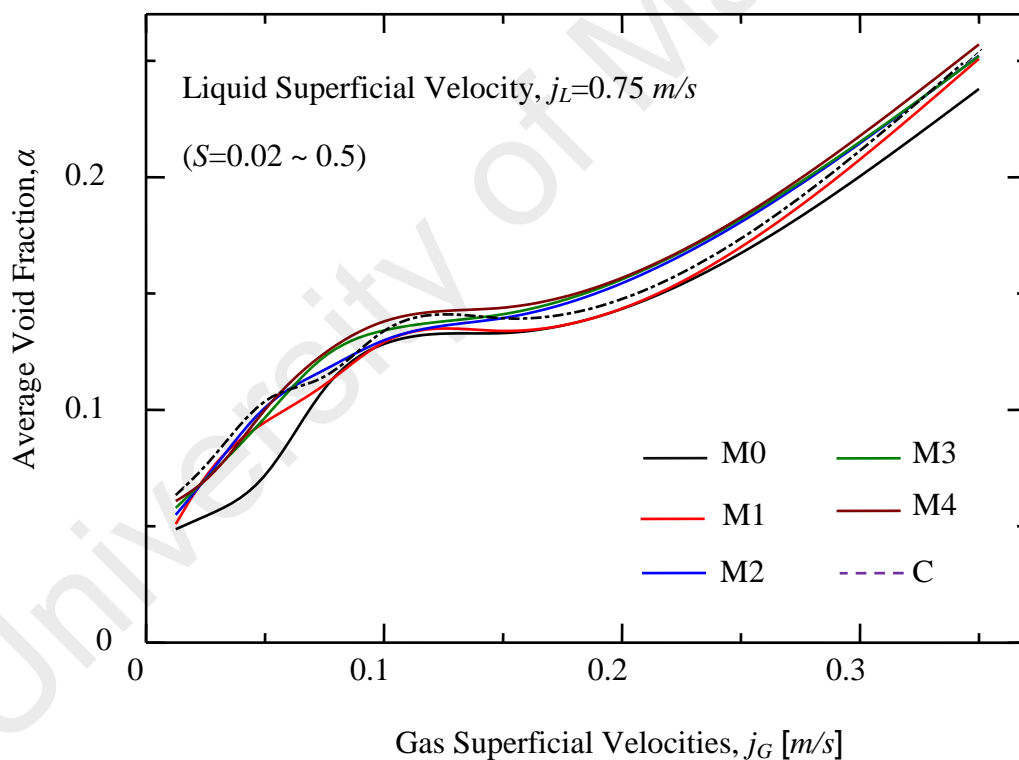


Figure 7.50 : Effects of vibration on average void fraction for $j_L=0.75 \text{ m/s}$

The average void fractions for higher liquid superficial velocity $j_L=1.0 \text{ m/s}$ were analyzed as in figure 7.51. From this figure, the void fraction increment is having the same trend as the increments demonstrated by the previously discussed flow conditions.

This is particularly obvious when the gas superficial velocities increase around 0.1 ~ 0.2 m/s ($S= 0.1 \sim 0.2$). Later on the void fraction increase as nearly linear until it reach the value of 0.35 at slip ratio of 0.5 which almost the same as the previous three cases. With this flow conditions, the effects of vibration still in play with most of the situations shown in this figure demonstrate that the change of vibration modes slowly altered the value of average void fraction.

The continuous vibration also shows about the same value of void fraction in between mode M3 and M4, a similar occurrence as the previous cases. Overall, the percentage of void fraction increment due to vibration as recorded in this figure can be analyzed and up to this stage this value is maintained at about 25%. This shows that this increment is constant with range of slip ratio up to 0.5.

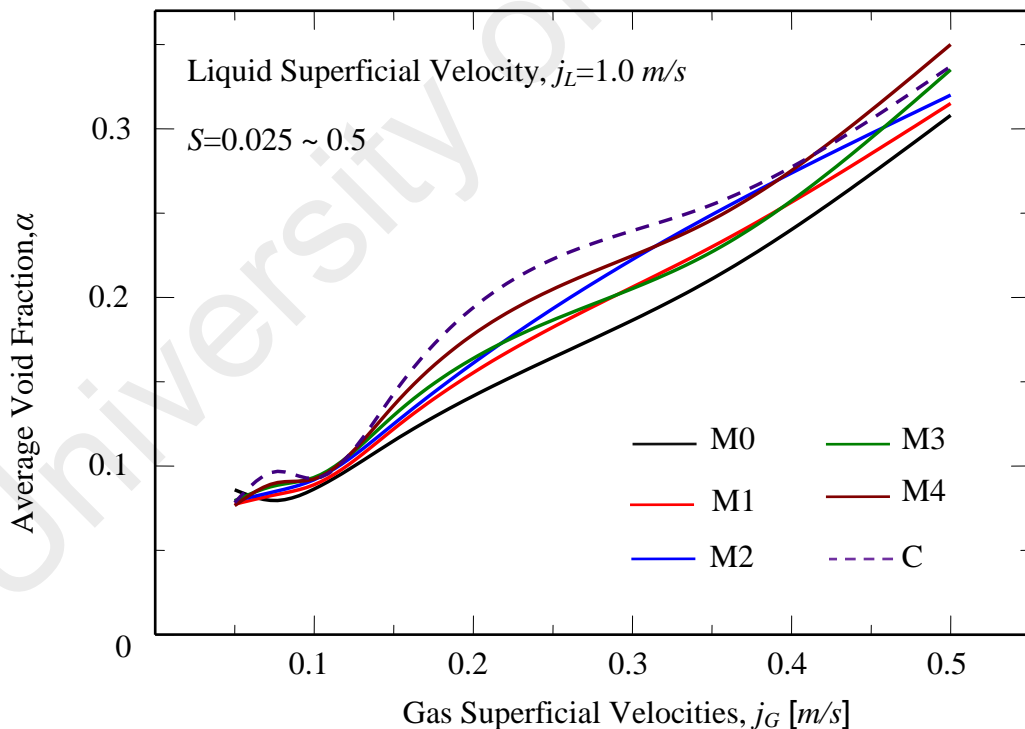
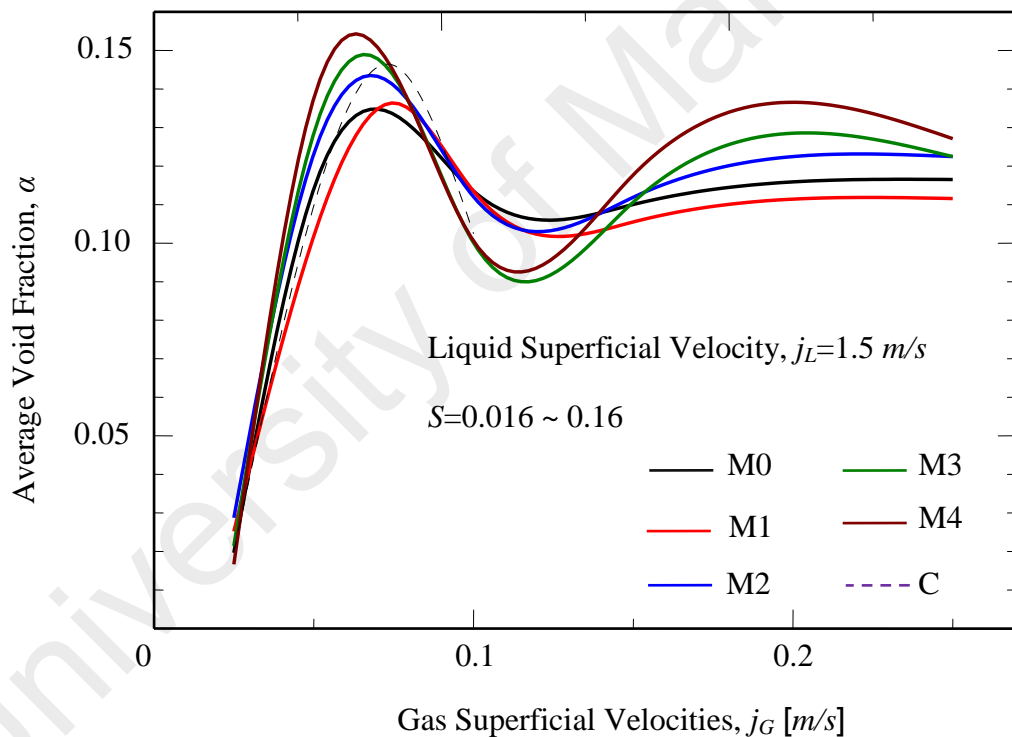


Figure 7.51 : Effects of vibration on average void fraction for $j_L=1.0$ m/s

The previous four flow conditions show the result for a constant slip ratio up to 0.5. In this case for liquid superficial velocity of 1.5 m/s as in figure 7.52, the analyses concentrated on the lower parts of slip ratio which is around 0.016 ~ 0.16 to see if there is any significant changes in void increment and the effects of vibration onto this flow condition. In this case, all modes of vibration as well as the steady state condition show the linear increment for slip ratio of 0.016 ~ 0.05 ($j_G = 0.025 \sim 0.075$ m/s) and when reached the value of 0.15, the start to decrease with the higher vibration modes still affecting the value of void fraction. The decrement was adjusted from $S=0.08 \sim 0.13$ ($j_G = 0.125 \sim 0.2$ m/s) where they start to increase again and settled at 0.1 ~ 0.125.



7.52 : Effects of vibration on average void fraction for $j_L = 1.5$ m/s

These fluctuations are exactly the same as presented in the previous cases, and therefore regardless of the scale of the liquid superficial velocities, the increase of void fraction follows the same order. In term of vibration sizes, the same conclusion can be drawn and they are still in the range of 25% increment.

The average void fraction for superficial velocity, $j_L=2.0 \text{ m/s}$, is shown in figure 7.53. In this case, again the same void fraction fluctuations are in the form of almost straight line particularly during $S=0.01 \sim 0.05$ ($j_G=0.025 \sim 0.1 \text{ m/s}$) and as they achieved the maximum value of 0.14, the decrement start to occur around $S=0.05 \sim 0.2$ ($j_G=0.25 \sim 0.4 \text{ m/s}$). All these void fraction curves were then settled at around 0.08 \sim 0.11 at the end of the calculation with slip ratio 0.4.

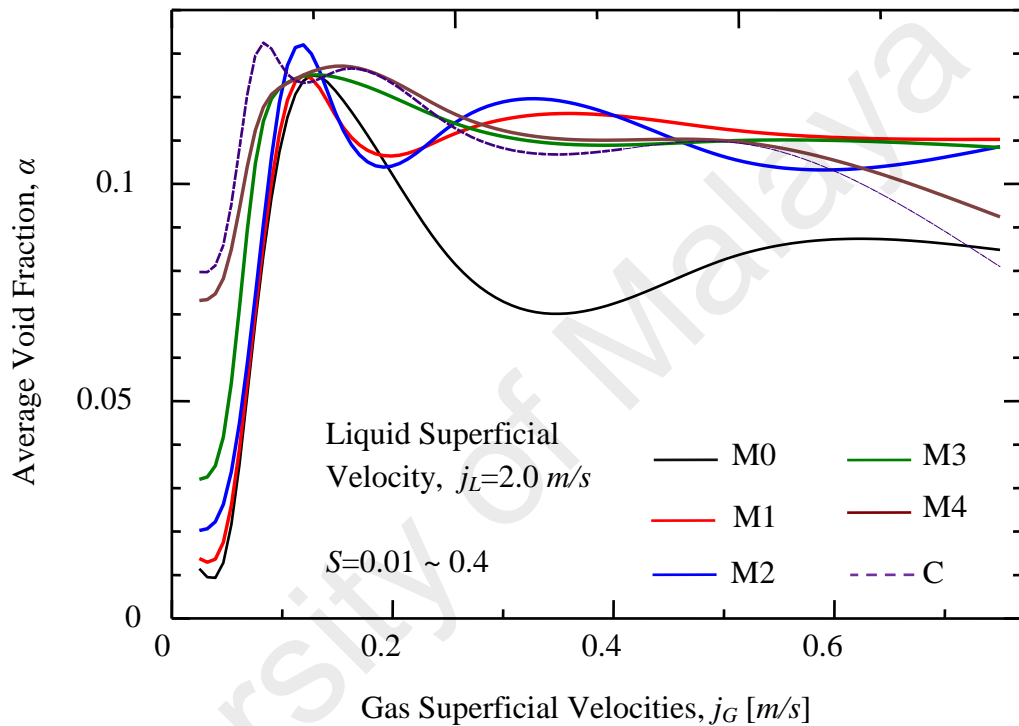


Figure 7.53 : Effects of vibration on average void fraction for $j_L=2.0 \text{ m/s}$

The increment of void fraction in this case is about 37%. This phenomenon is very hard to understand but it might probably due vertical motion of the flow channel associated with high liquid superficial velocity that disturbed the bubble motion. As also discussed in section 7.1 on the flow patterns, where the disturbed bubble motion will therefore create more congregation of bubbles, making close crowding and this will occur regardless of the degree of vibration. Therefore, as shown in this figure, the even

at highest mode of vibration M4, the value of average void fraction is lower than the value for vibration with lower mode such as M1, M2 and M3.

The final case study was conducted for flow condition with liquid superficial velocity of 2.5 m/s . As shown in figure 7.54, the fluctuations of average void fraction value are very obvious and they seem cannot be settled at any fixed point. However, they show very same trend of curve but the effect of vibration is totally different compared to all of the previous cases. In this flow condition, as the flow progressed, the effect of vibration is lowering down leaving the value of void fraction during the steady state condition to be the highest among all. The only conclusion that can be taken is on the chaotic behavior during turbulent flow in the channel where it eliminated all the vibration effect on the two-phase flow. Again referring to section 7.1, the flow patterns during this flow condition are almost unchanged regardless of the increasing gas superficial velocities.

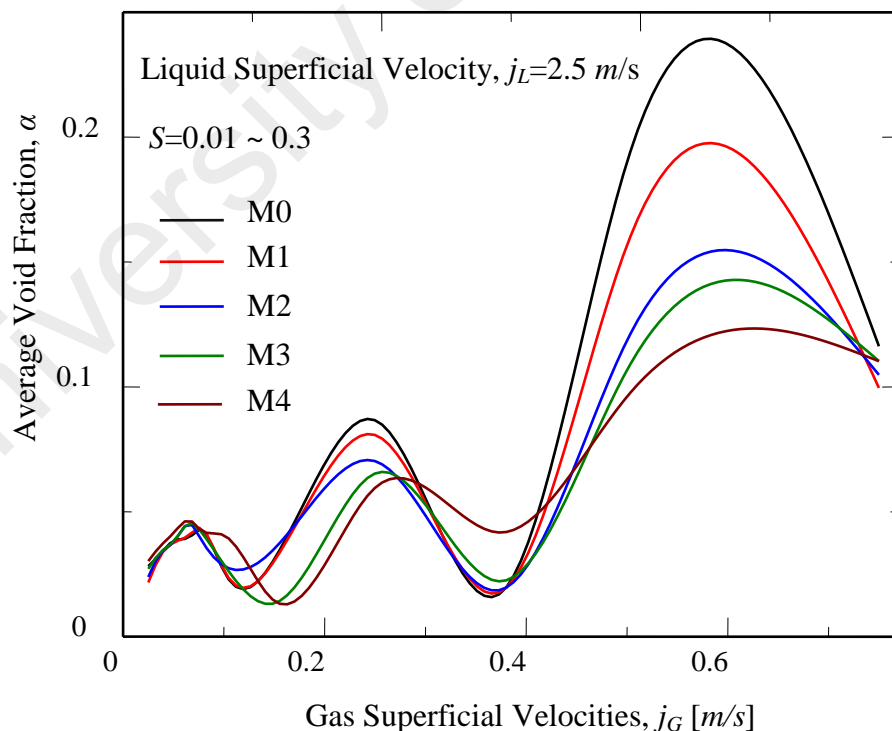


Figure 7.54 : Effects of vibration on average void fraction for $j_L = 2.5 \text{ m/s}$

Effects of Slip ratio

Therefore, as short judgment for this section, it can be said that the effect of current slip ratio with respect to vibration onto the average void fraction stop when the superficial velocity reaches 2.5 m/s. However, the maximum void fraction or the peak of value of void fraction of each case of flow condition and with respect to the vibration effect should also be considered for further analysis to confirm this statement.

7.4.4 Effects of Vibration and Axial Position on the Void Fractions

The analyses in this section were focused on the effects of axial position since it is very important in the void fraction measurement where it governs the value of void fraction in addition to the effects of flow condition where these two influences will change the flow patterns or demonstrate different patterns. In a vertical upward two-phase flow, the higher the position, the gravitational effect will offer significant contribution to the change of flow patterns and therefore might contribute to different value of the measured void fraction. This is very important in the boiling analyses as discussed in Chapter 2, and particularly when referring to the flow patterns transition in flow boiling in an annulus by Collier et al. (1981) and repeatedly discussed by Kawara et al. (1998), Celata et al. (1998) and others where very different flow patterns were observed from bottom to the top of flow channel. These phenomena is very important to be considered where types of boiling can be predicted for a particular flow condition in order to conduct the safety analyses of various power plant equipment such as heat exchangers, condensers and other components as well (Zainon, 1997).

In this section, the effect of axial position were evaluated for the position of $L/D=50$ and $L/D=35$, where L is the length of the flow channel and D is the channel diameter. This effect will be discussed in detail with comparison on the fluctuations of void fraction at local averages and peaks.

These two cases can be explained separately as follows :

- (i) Local average void fraction, $\alpha_{avg(l)}$

The averages void fraction for a pair of flow condition (j_G and j_L) refers to the average of all the void fraction values measured during the 10 seconds period of time for all of the vibration modes (M1 ~ M4) and the continuous vibration (C) as well as the steady state (M0) as presented in the previous section.

- (ii) Local maximum void fraction, $\alpha_{max(l)}$

The peaks of void fluctuation or the highest void fraction for a pair of flow condition (j_G and j_L) was picked for all of the vibration modes (M1 ~ M4) and the continuous vibration (C) as well as the steady state (M0) as presented in the previous section.

They are again illustrated in the form of graphs for increment of void fraction due to the increase of gas superficial velocities (j_G) at fix liquid superficial velocities (j_L). Since the focus is to see the effects of the axial position, the analysis differentiate the percentage of overall value for a flow condition with increasing gas superficial velocity at a particular vibration mode. The flow conditions are as the same as has been discussed in the previous sections.

(a) Local Average Void Fraction

The first analysis is as usual with liquid superficial velocity, $j_L=0.25$ m/s as shown in figure 7.55. According to this figure, most of the void fraction for the position of $L/D=50$ are in linear increment and for the position of $L/D=35$, there are a slight polynomial curve of increment. During the steady state (M0), the difference of values for both of the average void fraction is 10.8%. When vibration was applied the difference becoming higher as during modes M1 and M2 show nearly the same degree of differences at 14.6 ~ 14.7 %. As the ground accelerations increase to 9 – 12

m/s^2 during modes M3 and M4 the differences of void fraction fluctuate to about 15.3%. On the other hand, when the whole test section receives continuous vibration with mode M2, the differences of average void fraction for both locations increase to about 20%.

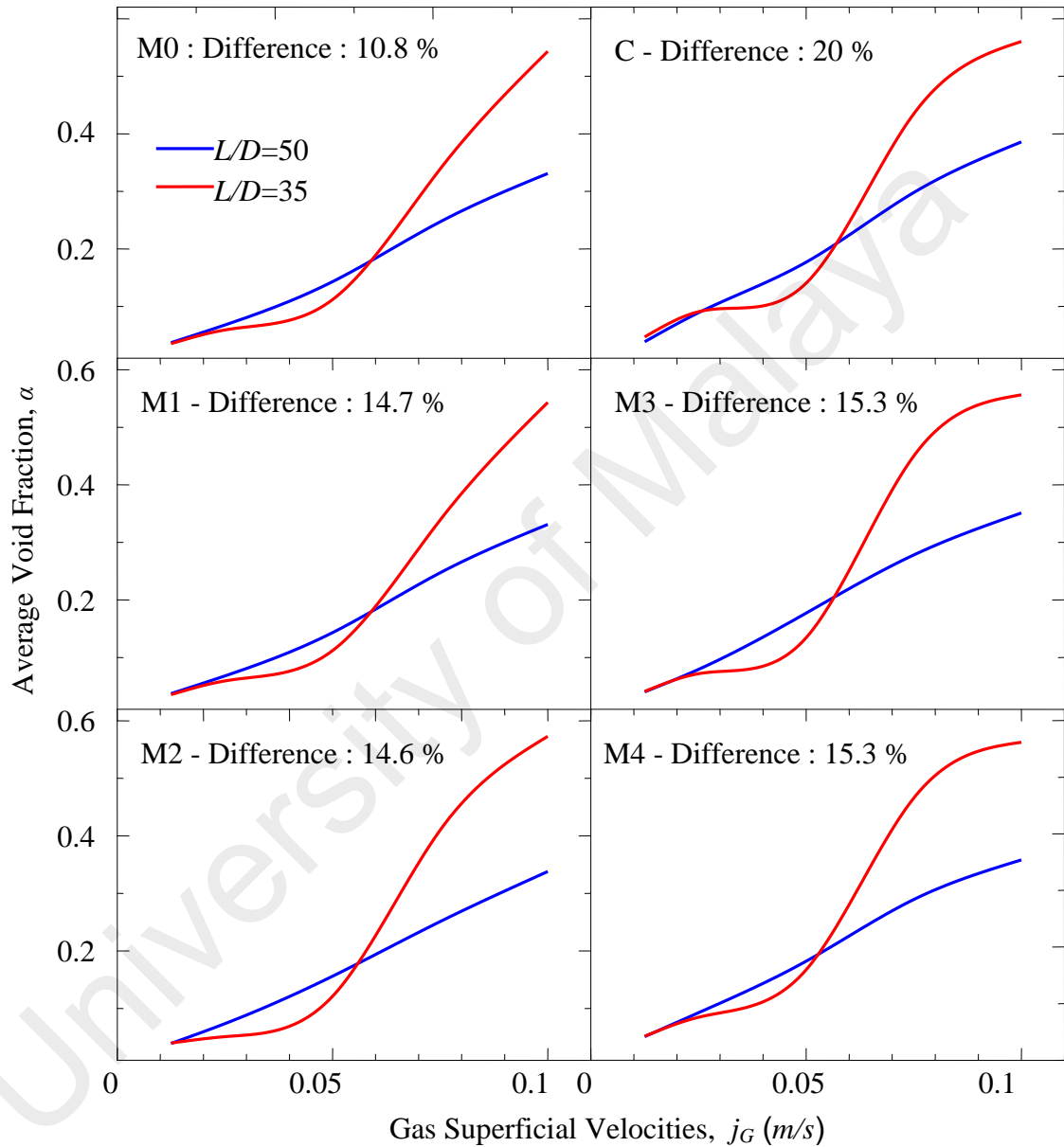


Figure 7.55: Effects of vibration and axial position on the fluctuation of average void fraction, for $j_L=0.25$ m/s

This phenomena show that when the gas superficial velocity increases during very low liquid superficial velocity, more bubbles collide and coalesce to form bigger

bubble and as a result forming slugs and bigger slugs. As has been discussed in section 7.2, when the flow patterns changes, the void fraction also will demonstrate different values. With higher order of vibration modes, bigger slugs were formed and during the travel upward of the flow channel, the vertical motion effect take place making bubble concentration differs heavily along the flow channel. Therefore, there will be a location that has high void fraction and otherwise demonstrating the high and low of the void fraction reading for both of the positions as in this analysis. Furthermore, when the channel receives continuous vibration (mode C), and even with lower mode, the congregation and segregation of bubbles become more serious and therefore shows very big difference of average void fraction for both positions.

This result suggests that the longer the vibration take place, the change of flow patterns also will becomes very frequent with concentration of bubbles differs significantly among locations in the flow channel. In conclusion, the difference of void fraction for both positions under this flow condition for the entire vibration modes is around 5% when compared to the steady state. In term of the maximum value, the highest void fraction were obtained as high as 0.6 and they are at most of the vibration modes and occurred at the position of $L/D = 50$, the higher position of measurement.

The effects of axial position on the average void fraction for liquid superficial velocity, $j_L=0.50 \text{ m/s}$ is presented in figure 7.56. The same trend of void fraction differences was demonstrated for the entire vibration modes showing the increase of difference percentage with higher order of vibration modes. However, in the entire vibration modes, they shows quiet high spread of value for both of the measured positions, where always also happened in the previous case, the steady state condition shows the minimum disagreement. The spread increase from lower mode to higher modes of vibration with M4 being the largest disagreement between the positions.

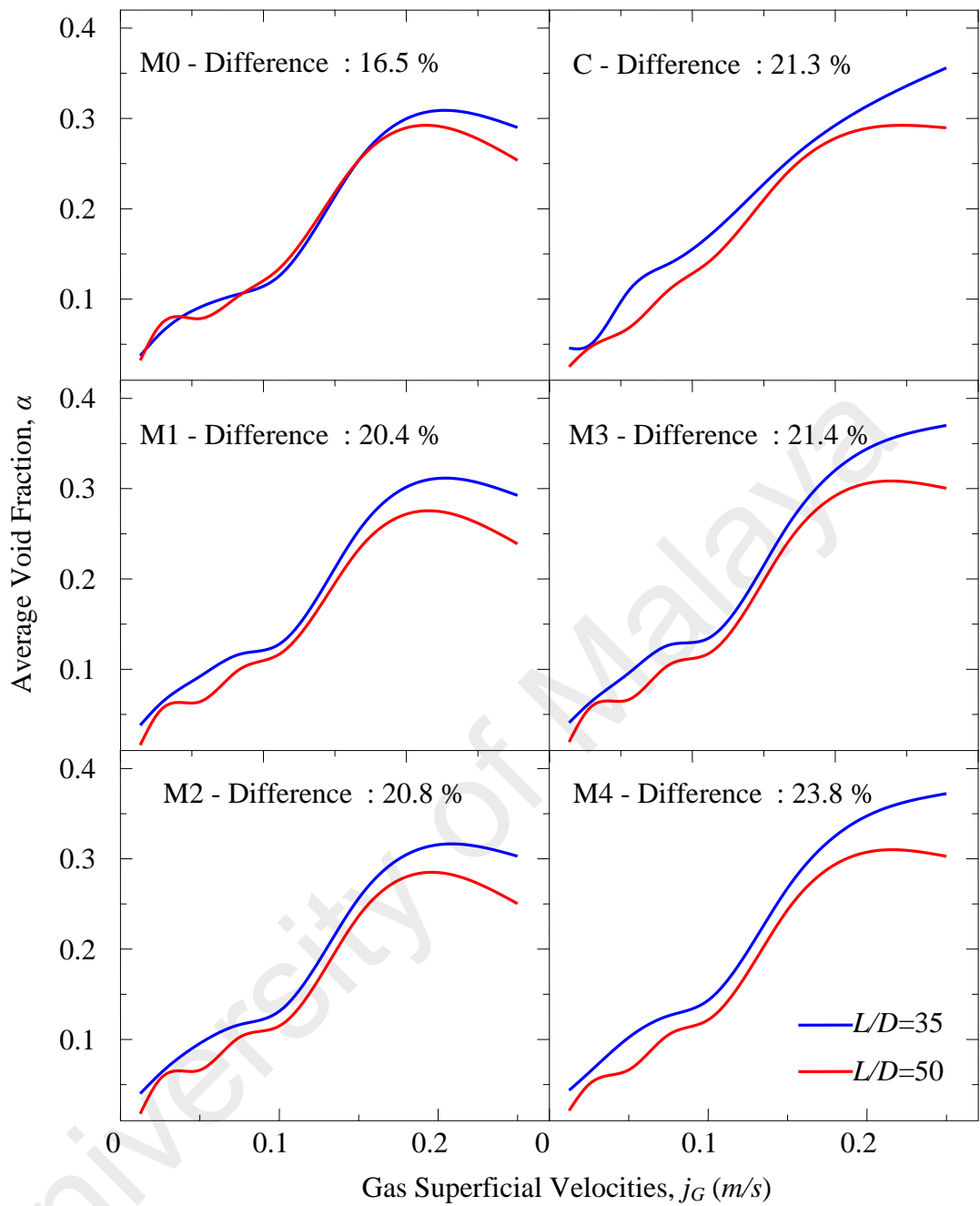


Figure 7.56 : Effects of vibration and axial position on the fluctuation of average void fraction, for $j_L=0.50$ m/s

In this case, however, the continuous vibration did not demonstrate much higher differences as in the previous case, where the disagreement lies between the M2 and M3 or even more close to M3. Again, the result reveals that a longer time for vibration will contribute to more significant disagreement in the value of void fraction between

locations due to formation of different flow patterns. With a slightly higher liquid superficial velocity, $j_L=0.50 \text{ m/s}$, the highest average void fraction obtained under this flow condition is $\alpha_{\text{avg(max)}} = 0.375$, with vibration mode M4 at location $L/D = 50$, much lower value compared to $j_L=0.25 \text{ m/s}$ in the previous case. This again reveals that the rising velocity of gas bubble becoming slightly higher due to higher liquid superficial velocity that does not help bubbles to perform rapid coalescence as during the low liquid flow.

For a higher liquid superficial velocity, $j_L=0.75 \text{ m/s}$, the effect of axial position was analyzed as in figure 7.57. In this figure, the difference of average void fraction for steady state shows around 16.4% and lower order of vibrations at mode M1 and M2 having differences of about 15.2 ~ 15.5% while the higher order vibration at modes M3 and M4 have differences respectively at 14.2 and 13.5%. On the other hand, the continuous vibration shows difference of 25.5% for both of the positions analyzed.

One common behavior demonstrates by the void fraction under this flow condition is the spread of void fraction value is very slim during the low region of gas superficial velocity, j_G and increase gradually as the j_G increases except for the continuous vibration mode (C) that does not really follow this trend. However, contradict to the previous two cases, the spread does not really increase as the mode of vibration change to the higher order, but it is in the reverse increment, with the continuous mode (C) being exceptional. The overall spread as to this level of flow condition still limited below 20%.

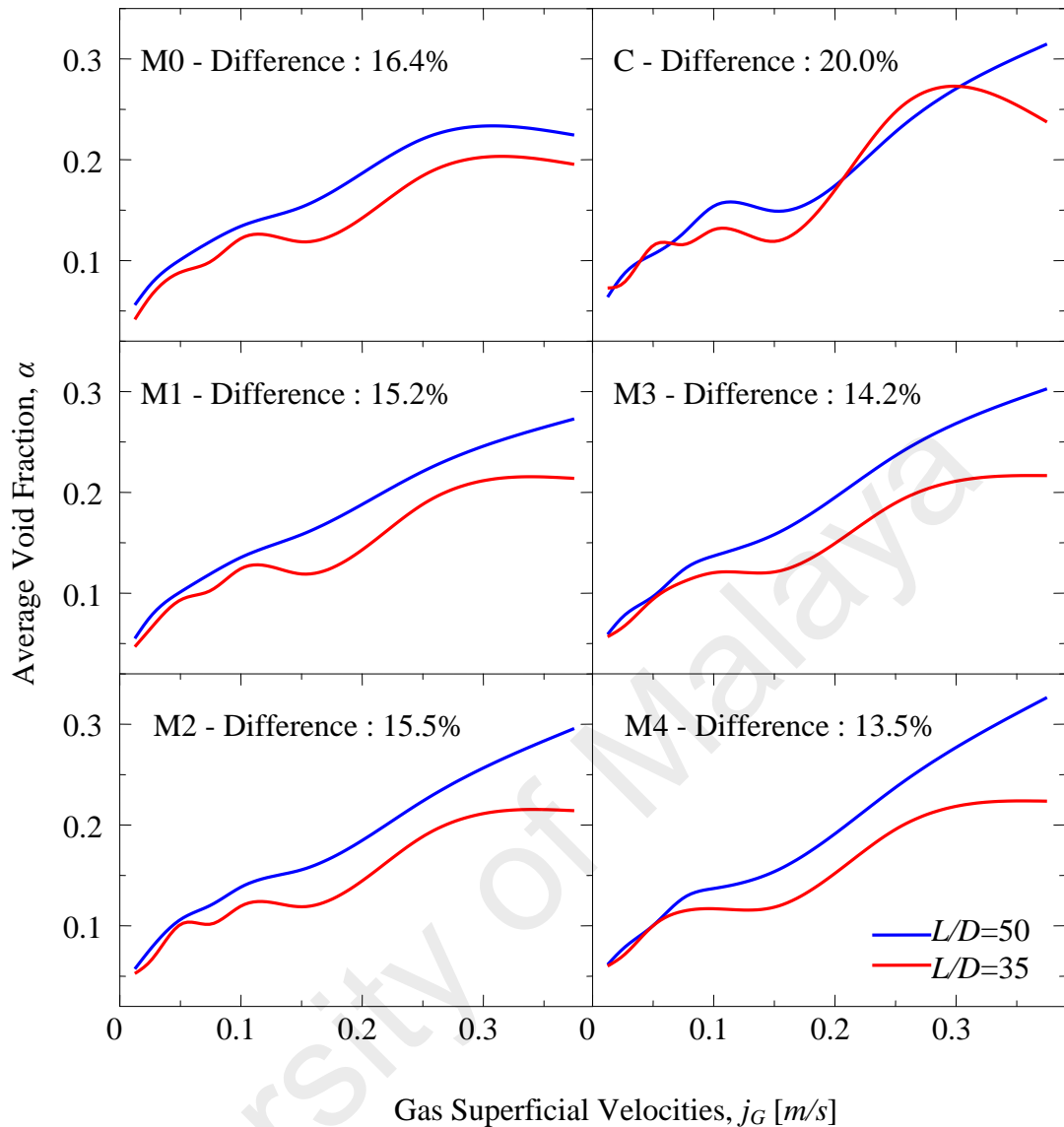


Figure 7.57 : Effects of vibration and axial position on the fluctuation of average void fraction, for $j_L=0.75$ m/s

The maximum value of average void fraction in this case is around, $\alpha_{\text{avg(max)}} = 0.325$, again at location $L/D=50$ under vibration mode M4, lower than both of the previous two cases. This is also due to an increase of liquid superficial velocity associated with vibration drastically change the flow pattern as discussed in figures 7.12 ~ 7.16 in section 7.2 where in this case it does not form bigger slugs as in the previous two cases and therefore lowering the value of void fraction.

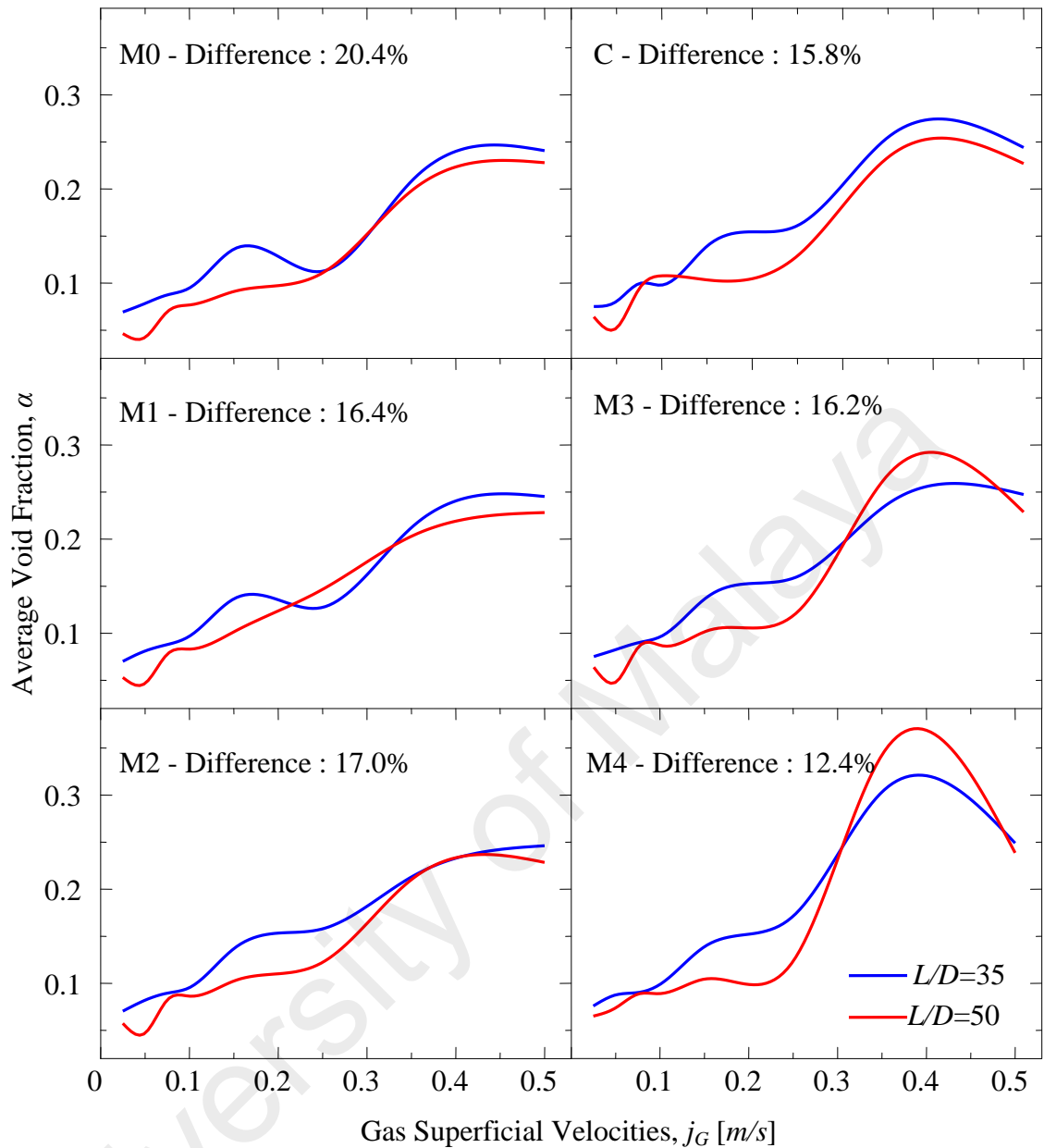


Figure 7.58: Effects of vibration and axial position on the fluctuation of average void fraction, for $j_L=1.0$ m/s

Increasing the liquid superficial velocity to $j_L=1.0$ m/s, shows another phenomenon in the variation of void fraction in this section. The significant spread is longer in the case with vibration but it is rather during the steady state. In figure 7.58, this biggest spread of void fraction for both location is at 20.4% during the steady state and it seem to decrease as the vibration applied and as the order of vibration increases,

the spread becomes slimmer. It is exceptional however for mode M1 and M2 but they differ in very acceptable range at 1%. In mode M3 and M4, the average void fraction value reach the maximum value and decreased as the gas superficial velocities increases. Under this flow condition, the axial position demonstrates different affect on the void fraction value. The higher position that so far dominated higher void fraction does not show the same behavior anymore. As can be seen in all of the vibration modes, the void fraction value transverse between these two position and the two highest values obtained at $\alpha_{\text{avg(max)}} = 0.3$ and 0.35 under modes M3 and M4 respectively, both at the position, $L/D = 35$.

This phenomenon might be due to higher liquid superficial velocity that does not allow a well manner flow patterns to be formed. It alternately change form one pattern to another and therefore varied the value of void fraction along the flow channel. Again referring to section 7.2 and particularly in figures 7.17 ~ 7.24, the flow patterns that formed under this flow condition are bubble and slug flow. However the slug flow in this case is not as solid as during lower liquid superficial velocity ($0.25 \sim 0.75 \text{ m/s}$), where the slugs still formed under the condition of crowding bubble and very easy to break up. In addition, since they travel under the effects of vibration these slugs will be distorted, change shapes and sizes regardless of the position, and therefore the variation of void fraction value can be seen in this case and in the close range of liquid superficial velocities like $j_L=0.75 \text{ m/s}$ and $j_L=1.5 \text{ m/s}$.

Figure 7.59 shows the result for a higher rate of liquid superficial velocity, $j_L=2.0 \text{ m/s}$ with range of gas superficial velocities are the same as in the previous cases. The odd situation here compared to lower liquid superficial velocities performed so far, is a very high differences of void fraction value in the entire cases. During the steady state condition, the spread is at 44% and even it gradually decreasing,

it still has a difference of 27.4 % during the vibration with mode M4 and becoming 23.2% as during the continuous vibration mode (C).

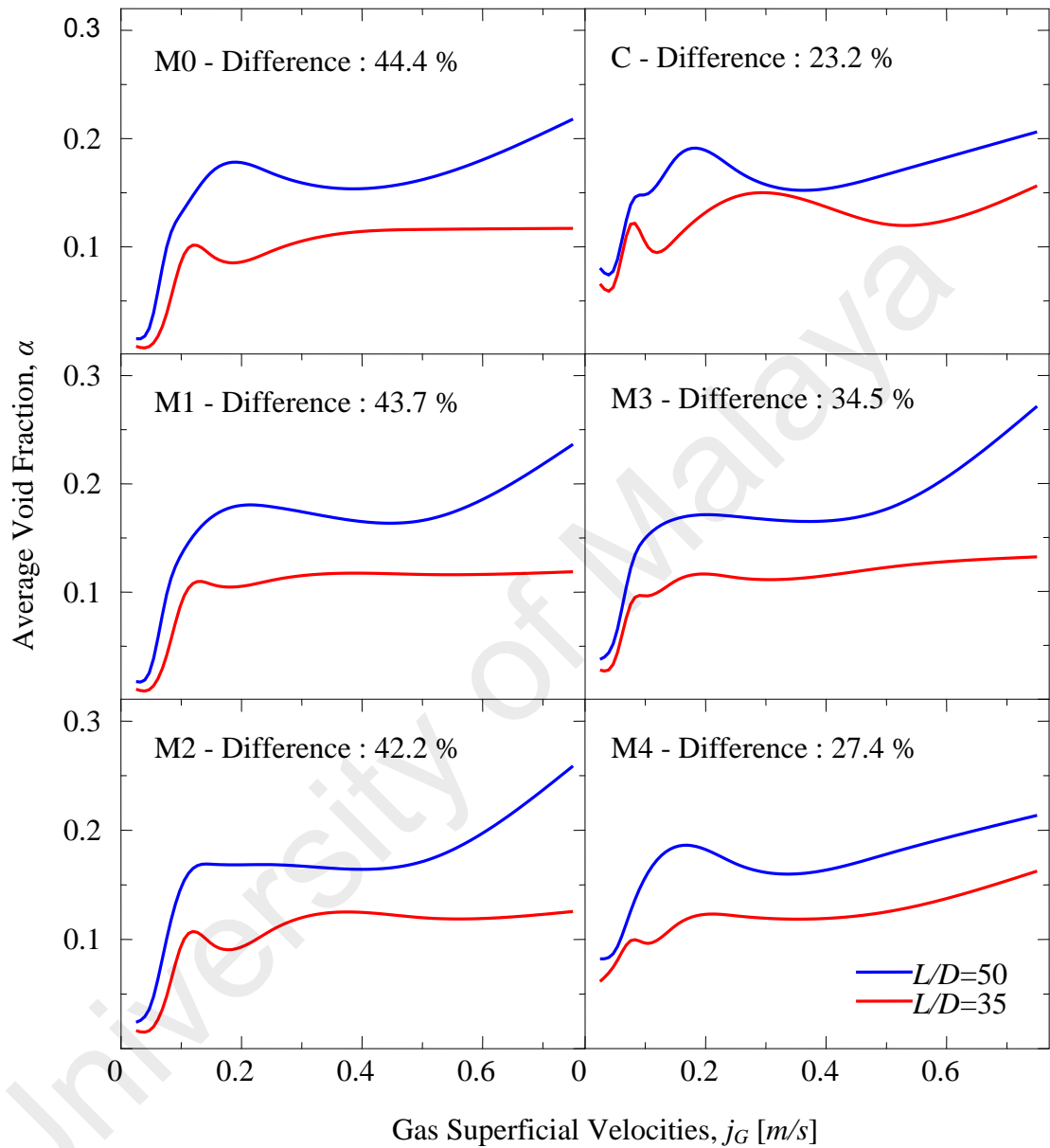


Figure 7.59 : Effects of vibration and axial position on the fluctuation of average void fraction, for $j_L=2.0$ m/s

Theoretically it can be said that with this rate of liquid superficial velocity, the bubbles do not have chance to become slug at lower part of the flow channel where they only congregate without coalescence even with the help from vibration. Therefore the

reading of void fraction was only recorded at around 0.1, which is a total bubbly flow and at the higher part a little higher around 0.2 which is the transition from bubbly to slug flow pattern as summarized by Kushnood et al. (2004). In term of maximum average void fraction, the highest value recorded was 0.25 during vibration with mode M2 at position $L/D = 35$ and this value does not differ much from the steady state condition at 0.22 also at the same position.

The final result for examination on the effect of axial location on the local average void fraction was performed for the condition with liquid superficial velocity, $j_L=2.5 \text{ m/s}$ as shown in figure 7.60. In this case, the spread of void fraction value is very slim in all of the condition and they are not in the uniform pattern, but somehow show the ascending and descending changes. During the steady state condition, the difference is about 7.2% and the decrement of this spread occurred during the vibration with mode M1 and M2 at 6.6 and 5.0 respectively. Higher order of vibration mode at M3 and M4 show the increment of differences from 7.4 to 9.0%. On the other hand, the continuous vibration shows a total spread of 11%, the highest among all.

This situation reflects the flow patterns as discussed in section 7.2 where in figure 7.32 at all flow and vibration condition, the flow pattern is the bubbly flow, with variation of bubbles sizes flow in a high liquid superficial velocity. Therefore as can be observed in this figure, the spread is very small and regardless of the position, the void fraction value transverse as they increase due to increasing gas superficial velocities. The maximum value for local average void fraction under this flow condition is 0.18, again as referred to Kushnood et al. (2004), the flow pattern is totally bubbly flow with a little chance to form slugs. However, due to high liquid superficial velocity, no slug is able to form, leaving the entire flow channel with discrete bubbles.

Furthermore with this flow condition, the effect of vibration is very weak and does not promote bubbles to coalesce even with the vertical motion that sometimes

delay the motion of rising bubble. As shown in this figure as well, only vibration with higher modes at M3 and M4 affected the spread of local average void fraction value but still in a very low percentage. The continuous mode of vibration (C) again in this case shows the highest performance, the same as in all of the cases studied so far. Therefore in term of process engineering that require mixing and mass transfer phenomena, longer vibration time might promote a better process with appropriate flow condition.

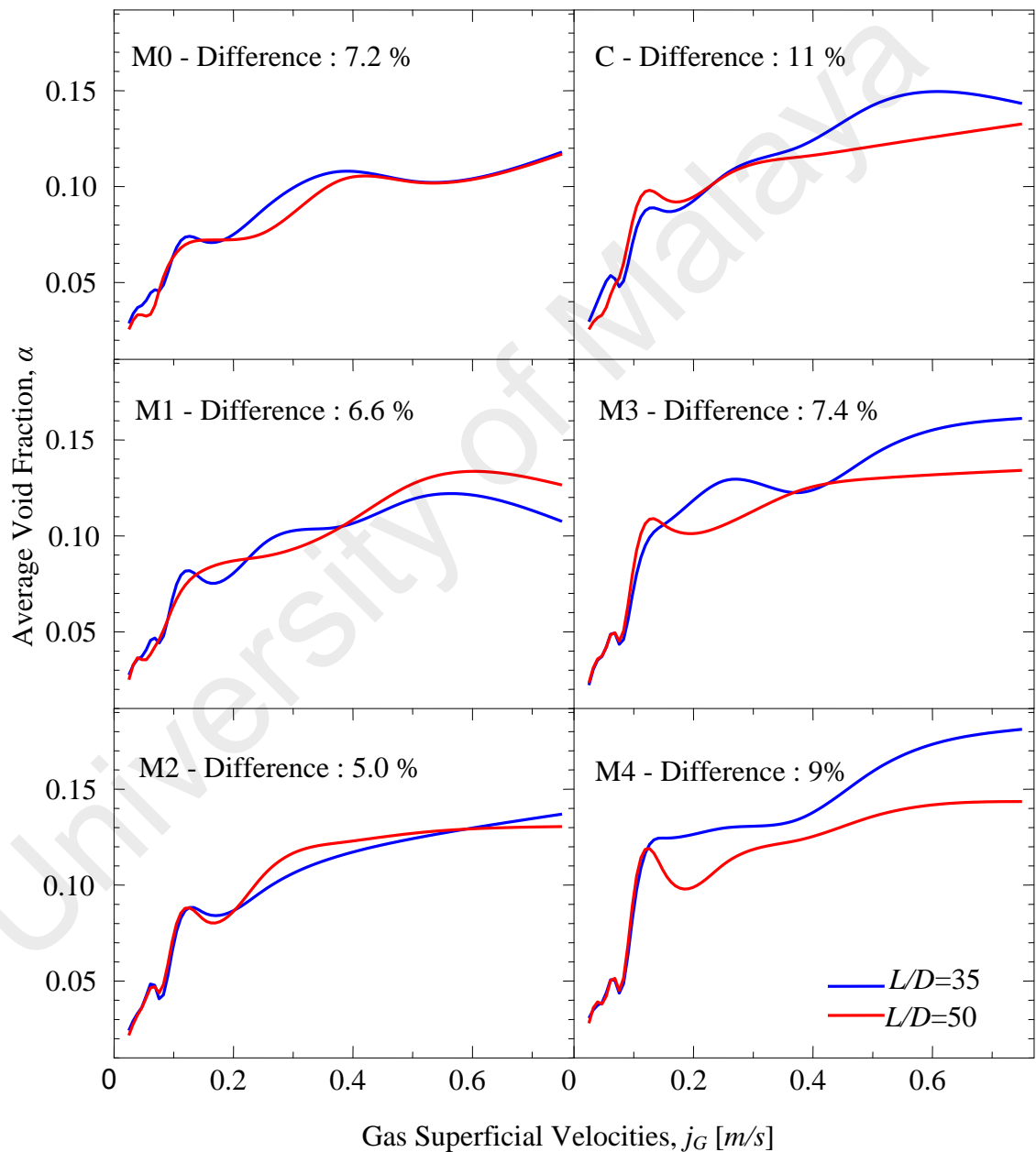


Figure 7.60 : Effects of vibration and axial position on the fluctuation of average void fraction, for $j_L=2.5$ m/s

(b) Maximum Local Void Fraction

The objective of this section is to manifest the real situation happened in the flow channel by examining the maximum void fraction, and to describe how this peaks behave at two local positions in the flow channel, $L/D=35$ and $L/D=50$. The evaluations of maximum void fraction were conducted based on comparison with overall average void fraction in Drift Flux model and local average void fraction from the previous analyses.

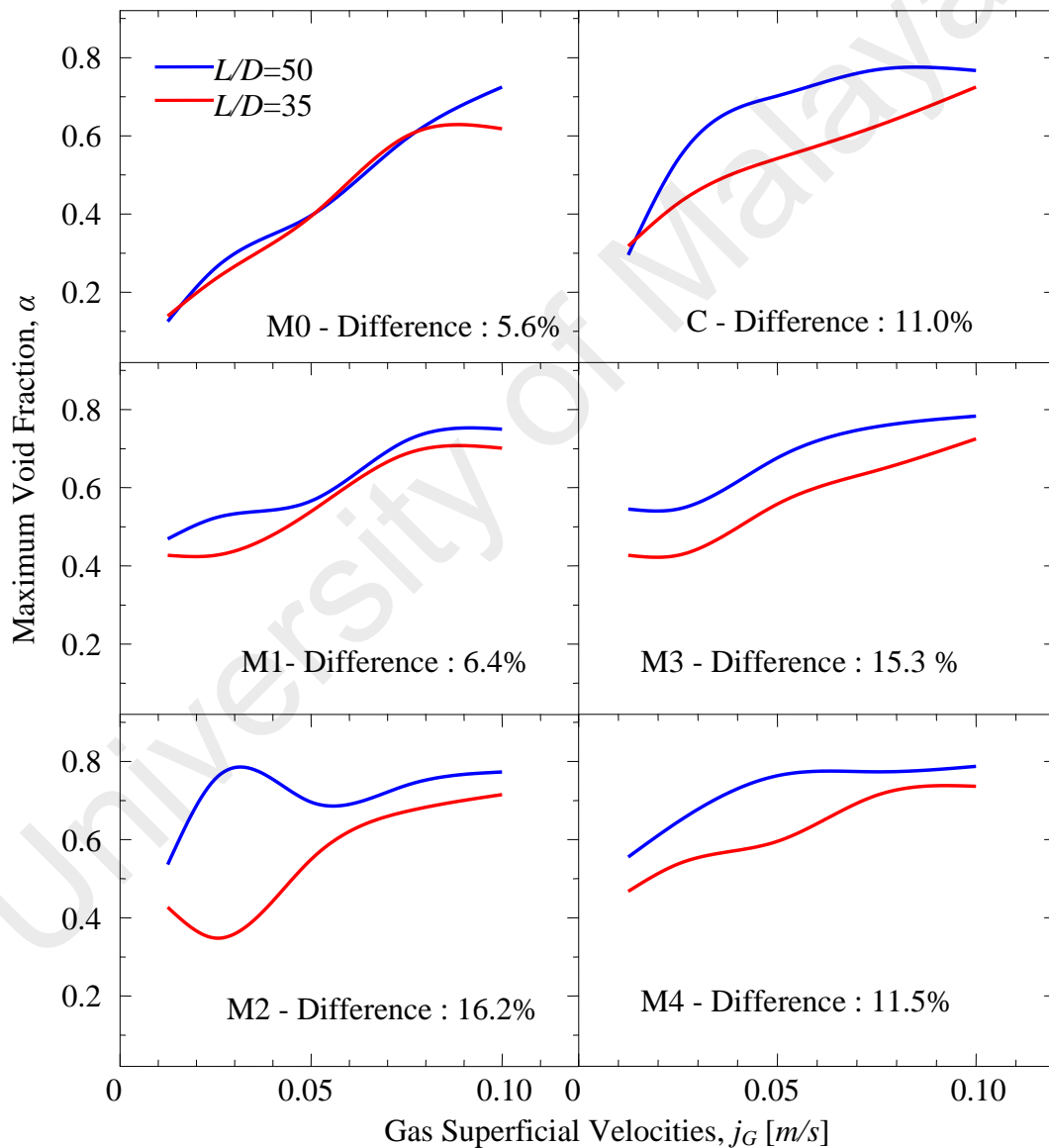


Figure 7.61 : Effects of vibration on maximum void fraction for two different axial position, for $j_L=0.25$ m/s

The first analysis started with flow condition at $j_L=0.25$ m/s as shown in figure 7.61. From this figure, with the same range of gas superficial velocities, the void fraction during the steady state increased from 0.1 to 0.7, is in good order with the increase of gas superficial velocities. The difference between both locations recorded very small at 5.6%. As the vibration applied, the difference increased to 6.4% for mode M1 and having very high increment with mode M2 at 16.2% and mode M3 at 15.3%. With the highest mode of vibration or moving under the ground acceleration of 12 m/s², the spread between the two positions become slimmer at 11.5% about the same range of gap when the continuous vibration (C) took place.

The highest void fraction ($\alpha_{avg(H)}$) under this flow condition is about 0.8, very much higher than the overall average void fraction in the flow channel (α_{avg}) which recorded at 0.35, and differs about 30% compared to local average void fraction ($\alpha_{avg(l)}$) which recorded at 0.6. Higher initial void fraction during the lowest gas superficial velocity can be seen in all modes of vibration where the peak void fraction recorded around 0.4 compared to 0.1 during the steady state. In all vibration modes as well, the maximum void fraction settled around 0.7 ~ 0.8, and mode M4 recording the highest.

From this initial result, it can be addressed that there is a remarkable change on differences or spread of value among types of void fractions. The effects of vibration on the spread of void fraction in two-phase flow is therefore very important to be analyzed in order to receive a clear picture of variation of void fraction under a certain flow condition and so far they are mostly determined by the size of accelerations in the vibration.

This analysis is further continued by the flow condition under the liquid superficial velocity, $j_L=0.50$ m/s, as shown in figure 7.62. The trend of increment is about the same as in the previous flow condition under the liquid superficial velocity, $j_L=0.25$ m/s, but differ in term of differences percentage, where in this case, the entire

vibration modes exhibit about 40% larger in gaps for maximum void fraction between the two locations, making the spread between 12.2 ~ 22%.

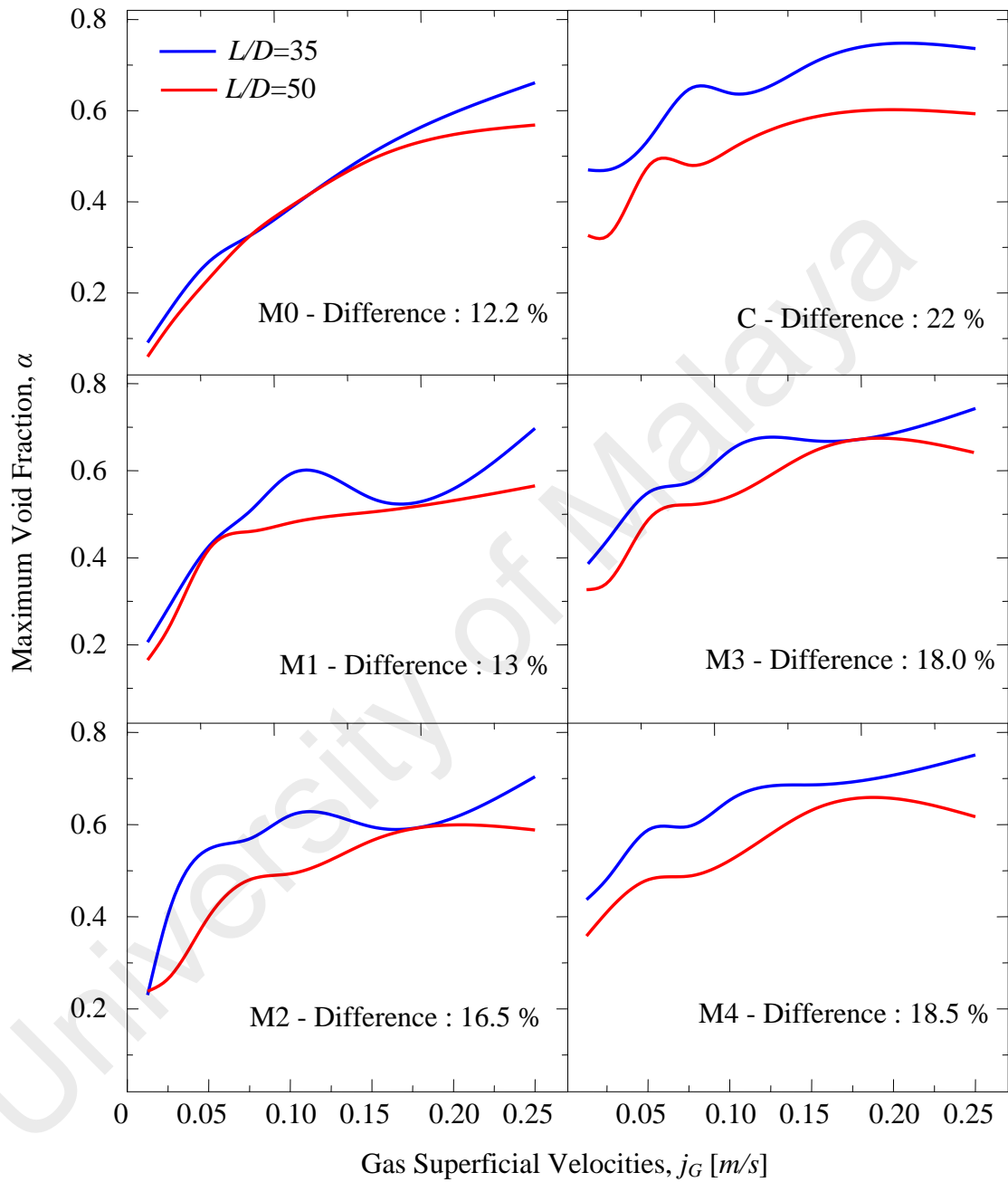


Figure 7.62 : Effects of vibration on maximum void fraction for two different axial position, for $j_L=0.50$ m/s

For this case, the steady state condition shows 12.2 % of spread and gradually increases as the mode of vibration move into higher order as where mode M1 shows 13%, mode M2 with 16.5%, mode M3 making 18% and mode M4 spread of 18.5%. On the other hand, this flow condition recorded the highest spread during the continuous vibration (C), at 22%. This trend however differs from the spread increment for the local average void fraction in the previous section. In term of value, the void fraction is very low in the lower part of gas superficial velocities and they are below 0.1 during the steady state condition and become higher with the order of vibration mode giving the mode 4 having the lowest maximum void fraction at 0.35.

On the other hand, the maximum value for average of total void fraction as shown in figure 7.49 is 0.35, suggests that this value is the lowest value maximum void fraction with the highest order of vibration. This result again verified the statement given in the analysis of previous flow condition where the maximum value obtained for average of total void fraction does not really reflect the real situation of the two-phase flow. Therefore it is very important to note that under a particular flow condition, even though the average void fraction is very low, the vibration effect will totally change the behavior of the flow. When the flow became rough and chaotic, void fraction will increase up to very high value which resulting a hazardous condition particularly for the cases involving high temperature flow such as flow boiling and condensation.

Maximum void fraction analysis for flow condition with superficial velocity, $j_L=0.75$ m/s is presented in figure 7.63. All the polynomial curves for increment of void fraction against the increasing gas superficial velocity show very similar trend with the curves for local average void fraction under the same flow condition as presented in figure 7.57. The differences of percentage of void fraction between both positions are also in the same range but they definitely differ in term of real value since this analysis selected based on the maximum value and the other one calculated for averages. Here,

under this flow condition, the lowest maximum value for steady state condition are about the same for both cases and this value increases as the vibration modes move into higher order where it reached 0.25 during the vibration with mode M4. The highest maximum void fraction for this case recorded at 0.65 also with mode M4 and the distribution of void fraction value are not segregated for a particular position. Therefore, as can be seen in the figure, the value transverse at many points along the two curves.

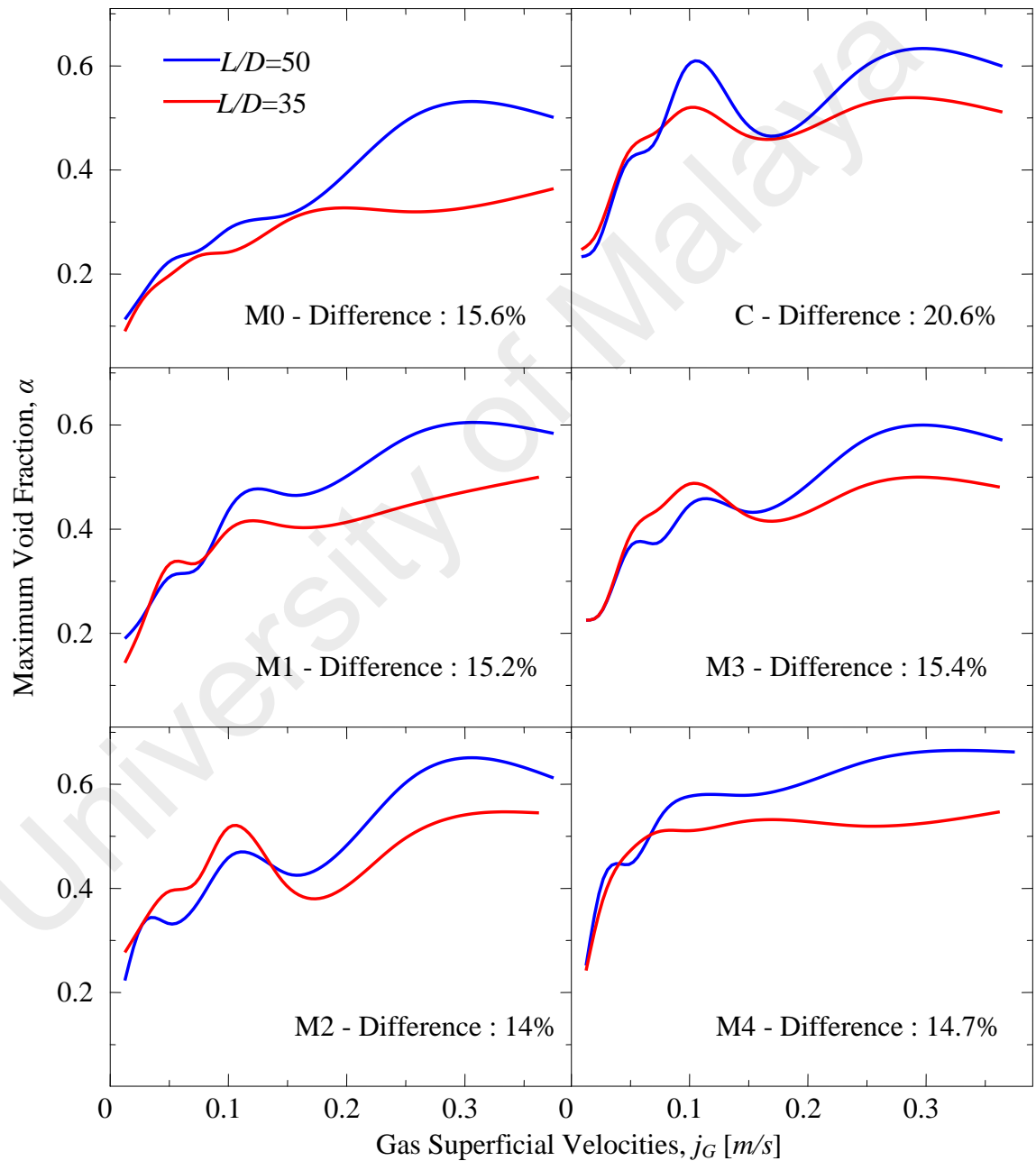


Figure 7.63 : Effects of vibration on maximum void fraction for two different axial position, for $j_L=0.75$ m/s

The transverse phenomenon also can be seen under flow condition with $j_L=1.0$ m/s, as also seen in figure 7.58 for local average void fraction analysis and figure 7.64 describe this phenomenon in detail. The difference of values between these two positions also considerably high around 23 ~ 30 %, a little lower than the result in figure 7.65.

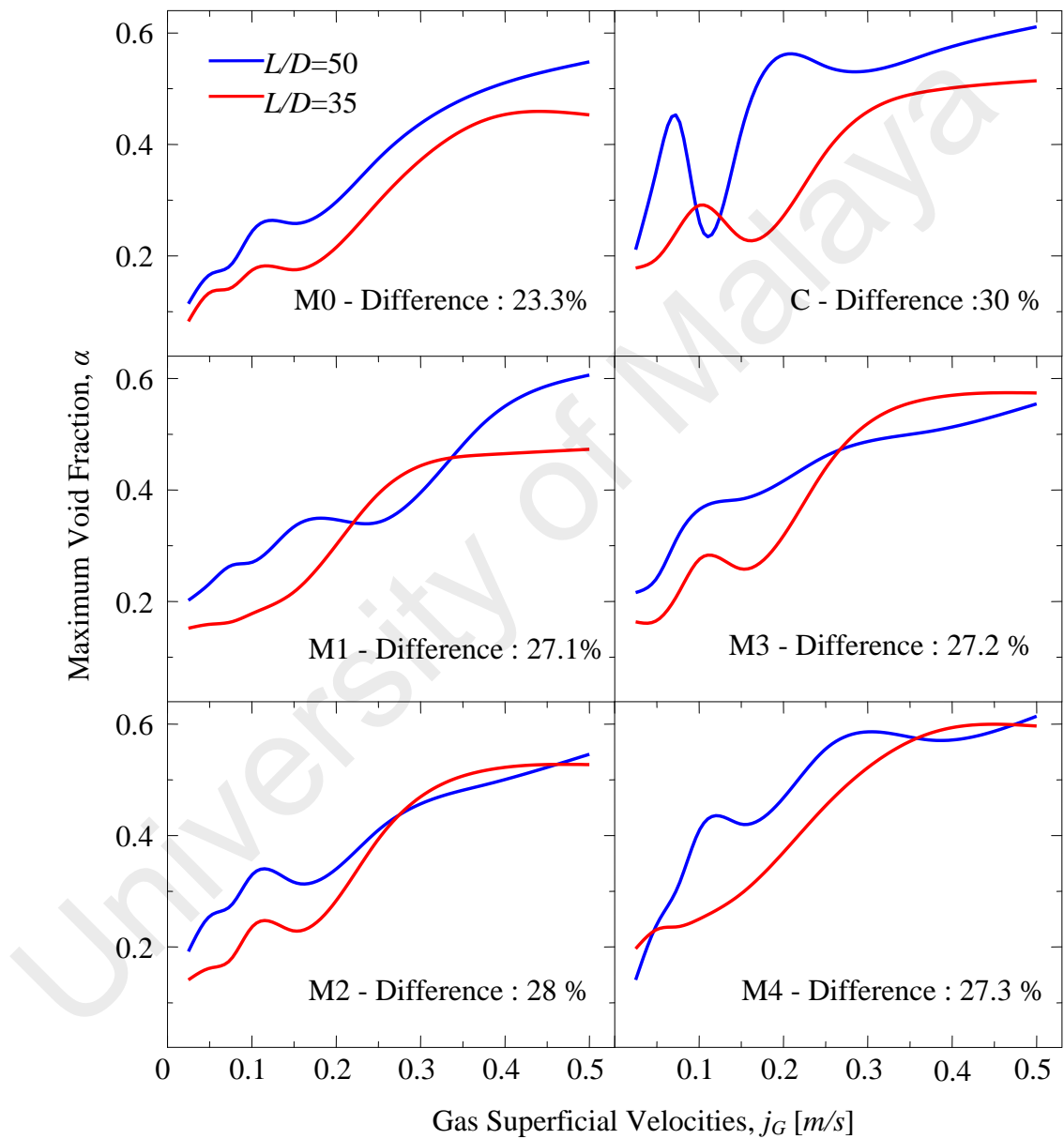


Figure 7.64 : Effects of vibration on maximum void fraction for two different axial position, for $j_L=1.0$ m/s

This suggests that the flow starts to establish a fix pattern in the flow channel, as a moderate liquid superficial velocity at $j_L=1.0$ m/s reducing the formation of slugs and details of this description can be referred to figure 7.23 ~ 7.28. The highest maximum void fraction under this flow condition was recorded around 0.6 about 40% differ from the total average void fraction in the flow channel which shown in figure 7.51, where $\alpha_{avg}=0.35$. In term of differences from steady state condition, this case recorded 8.3% disagreement.

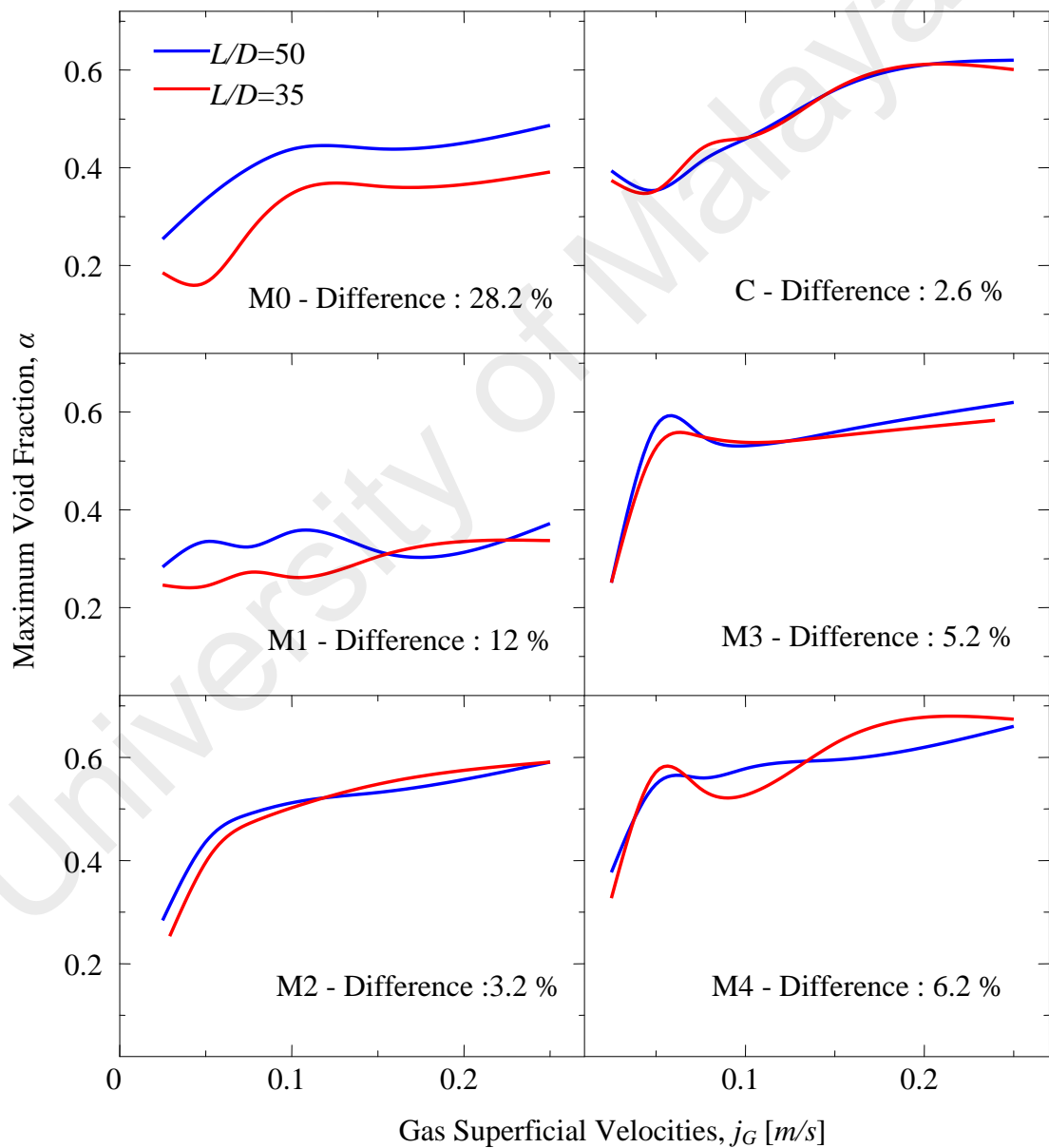


Figure 7.65 : Effects of vibration on maximum void fraction for two different axial position, for $j_L=1.5$ m/s

Even though the difference between positions are considerably high for $j_L=1.0$ m/s , these maximum values transverse at many points the same as presented in figure 7.64. A similar pattern also demonstrated by flow condition with liquid superficial velocity, $j_L=1.5$ m/s , as shown in figure 7.65, where this range of velocities (0.75 ~ 1.0 m/s ,) can be considered as medium class throughout experimentations conducted in the current work. For $j_L=1.5$ m/s also, the spread for steady state is much larger than during the entire modes of vibration where the continuous vibration made very small differences at 2.6%.

The analyses for considerably high liquid superficial velocity were conducted for two cases as in the previous cases as well. This range of flow condition is very important as well since it is applied in many engineering works such as high energy flow in processing and power generation. Hence the following analysis is for flow condition at $j_L=2.0$ m/s and is shown in figure 7.66.

The trend of results in this figure agreed well with the result for local average void fraction as discussed previously based on figure 7.59. They have big spread during the steady state condition and as the vibration modes move into higher order these differences become smaller vary between 6.0 ~ 18.7% with continuous vibration mode (C) shows the slimmest spread. The value of maximum void fraction during the vibrations move between 0.125 ~ 0.5 and the steady state condition recorded the range of 0.025 ~ 0.375. Comparison of these conditions give a very high fluctuation during the low gas superficial velocity region at around 80% (lowest maximum void fraction, $\alpha_{max(L)}$) and a notable rate of fluctuation for the higher region of gas superficial velocity region (highest maximum void fraction, $\alpha_{max(H)}$) of about 25%. Another important comparison is between $\alpha_{max(H)}$ and $\alpha_{avg(H)}$ in figure 7.53 which recorded around 0.125, that simply differ about 66.6%. This result will be discussed in detail at the end of this section.

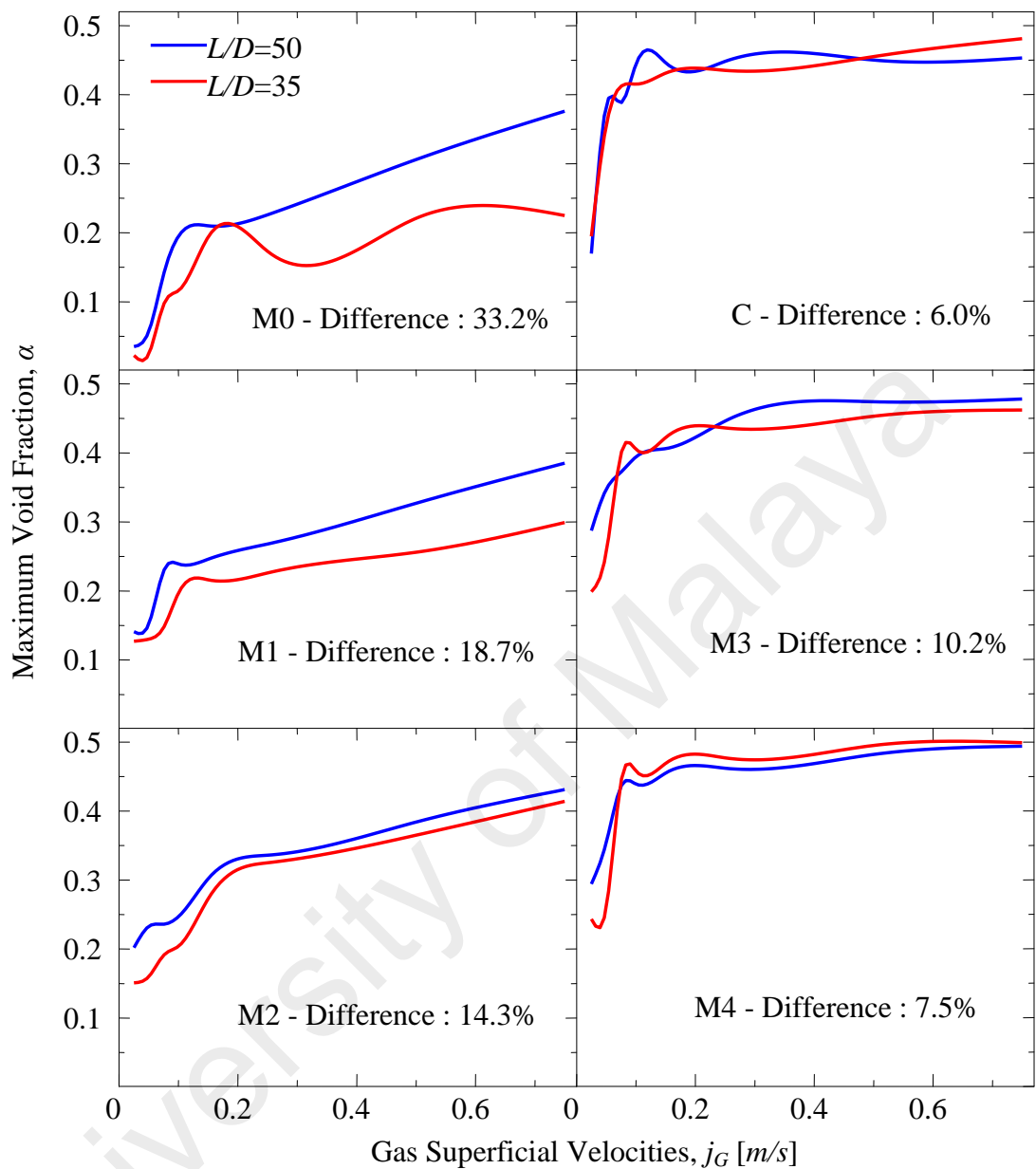


Figure 7.66 : Effects of vibration on maximum void fraction for two different axial position, for $j_L=2.0$ m/s

In figure 7.67, the results for analysis on flow condition at $j_L=2.5$ m/s is presented. The increment of void fraction due to increasing gas superficial velocities is very much similar with the previous case, with polynomial curves and very close gap of void fraction value between two positions. For steady state condition, the lowest maximum void fraction ($\alpha_{max(L)}$) was recorded around 0.025, and increase to the highest

value of $\alpha_{max(H)}=0.225$ with the spread of values about 18.3%. When the order of vibration getting higher, the spread getting slimmer and move down between 12.5 ~ 7.2 %, making the continuous vibration (C) contributing to the lowest gap. The same comparison between the $\alpha_{max(H)}$ and $\alpha_{avg(max)}$ in figure 7.54 for total void fraction which shows the difference about 44%.

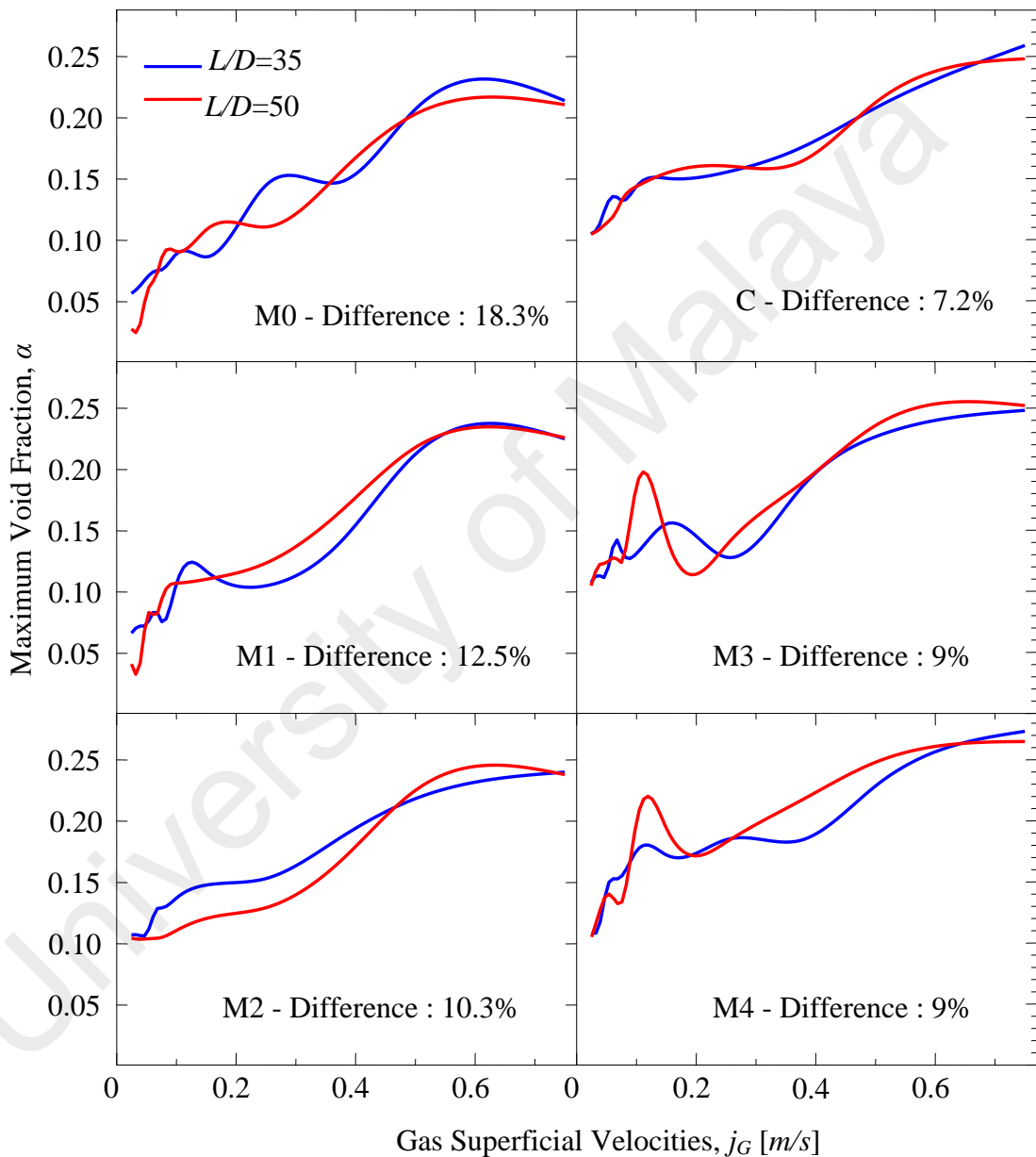


Figure 7.67 : Effects of vibration on maximum void fraction for two different axial position, for $j_L=2.5$ m/s

Considering the effect of vibration, with simply summarizing the entire modes, the above two results for a considerably at high liquid superficial velocity reveal that as this velocity increases, the maximum void fraction becoming lower. In many literatures that report the role of axial position to margining the value of void fractions in the flow channel during the steady state condition (Serizawa, 1974), (Ishii, 1979) and others, also weakening as the scale of vibration increases. This can be referred in the results for the spread of void fraction values between these two positions that decrease as the mode of vibration move into higher order. Furthermore, if the flow channel received a continuous vibration, for example as in the current work about 10 second or more, the gap of these values also will be decreasing. This result also shows that with higher liquid superficial velocity, there will be difficult for the bubble to coalesce to form another flow pattern and therefore, the effect of vibrations also will be weaker.

7.4.6 Drift Flux Analysis on Void Fraction due to the Effect of Vibration

(a) Relationship of Void Fraction, Slip Ratio and Vibration

It has been reported in many literatures in the history of two-phase flow for example, Butterworth (1975), and Revankar et al. (1992) that the void fraction will increase with the increasing gas superficial velocities (j_G) for a fix liquid superficial velocity (j_L). The ratio of these two velocities in the flow channel is called the slip ratio, ($S = \frac{j_G}{j_L}$) as discussed in section 5.3. For the current work, this relationship has been conducted and evaluated based on the Drift Flux Model where the j_L is in the range of 0.25 ~ 2.5 m/s and j_G is in the range of 0.025 ~ 0.75 m/s, which actually gives the slip ratio in the range of 0.01 ~ 3.0. However, due to the limitation of the current experimental facilities, investigations for flow condition with slip ratio above 0.5 also very difficult to obtain. An example datasheet is supplied in Appendix 7.3.

Furthermore, with high slip ratio, most of the flow patterns will become slugs and will develop further to becoming annular flow, which actually eliminate the effects of vibration as discussed in section 7.3.2 and for more specific with reference to figures 7.43 ~ 7.47. Therefore, along the analysis in the current work, the investigation for void fraction and the slip ration relation with flow condition above 0.5 has not been conducted. It is also more reasonable to compare the differences between the average void fraction and maximum void fraction recorded due to vibration effects. This is very important in order to constitute the rapid changes of flow patterns i.e. the fluctuation of void fraction for a given flow condition in of the two-phase flow that undergo a vertical motion.

The following outcomes discuss about the relationship between void fraction, slip ratio and vibration in the current work with focus on comparison between the average void fraction, (α_{avg}), average void fraction at a local position, ($\alpha_{avg(l)}$) and the maximum void fraction at a local position, ($\alpha_{max(l)}$). As also discussed previously, the α_{avg} is the average void fraction or sometimes refers as mean void fraction between position $L/D=35$ and $L/D=50$, the $\alpha_{avg(l)}$ and $\alpha_{max(l)}$ are the average and maximum value of void fraction at position $L/D=50$ respectively. Here, the effects of vibration are also evaluated in the same methodology with the previous cases as well.

Figure 7.68 shows the result for average void fraction plotted against slip ratios with the effects of vibration modes conducted in this study. During the low slip ratio, the differences of average void fraction between modes of vibration are not so obvious, where they are in the range of 0.01 ~ 0.15. As the slip ratio increases, the value of α_{avg} also increases and as a control experiment, the value of average void fraction for steady state condition reached around 0.25. With extra forces from the vibration, the increment of void fraction become more obvious where it reached around 0.375 for the case of continuous vibration (C) at slip ratio, $S=0.375$ and 0.325 for mode M4 under a further

increase of slip ratio. This result indicates that, the average void fraction follows the simple rule as discussed above, which is increasing with the increase of slip ratios.

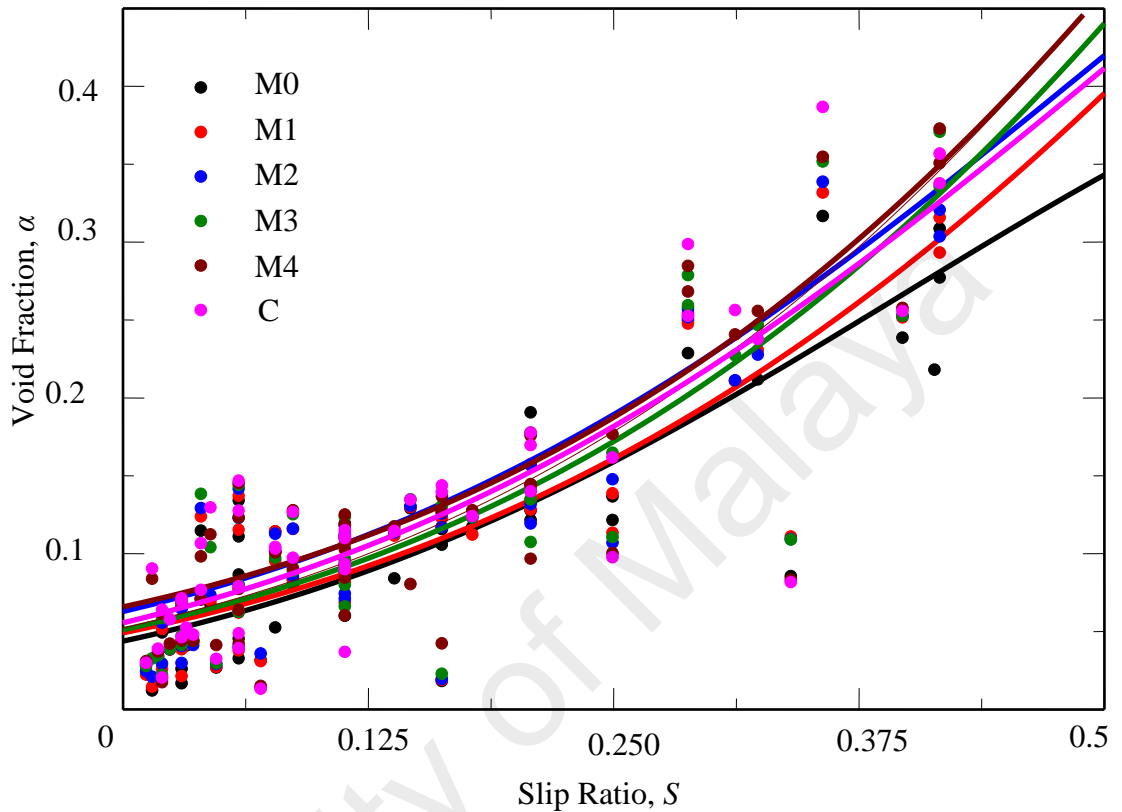


Figure 7.68: Drift flux analysis - effects of slip ratio and size of vibration on the total average (mean) void fraction, α_{avg}

(b) Local Average Void Fraction

At the same time the average void fraction will also increase as the mode of vibration move into higher order. The same results also can be observed for the average of local void fraction as shown in figure 7.69. In both figures, the spread of void fraction values is almost constant. Up to this level, the modes of vibration still show strong effect on the value of void fraction, or in other words, as the ground accelerations becoming higher, the average void fraction in a flow channel will also increase.

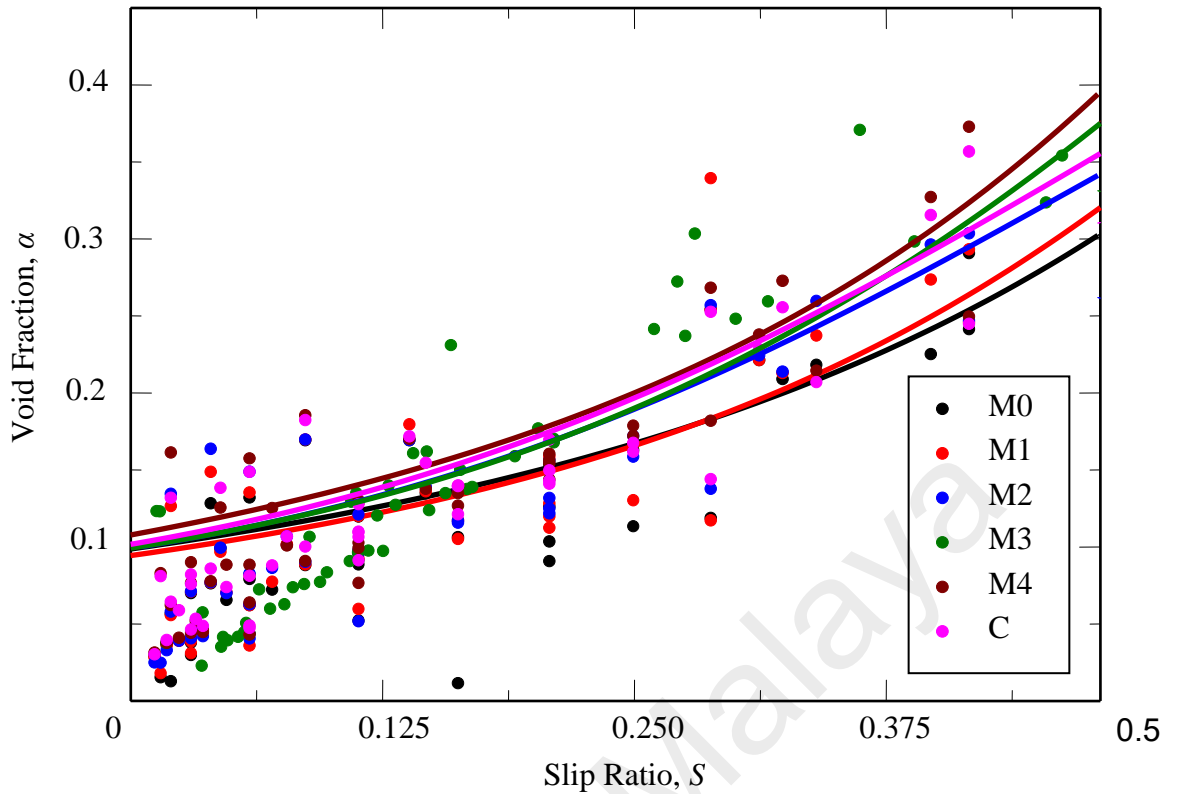


Figure 7.69: Drift flux analysis - effects of slip ratio and size of vibration on the local average void fraction, $\alpha_{avg(l)}$

(c) Local Maximum Void Fraction

However, figure 7.70, shows some other interesting results. In this figure, at low slip ratio, the spread of maximum void fraction is very big, ranging in 0.025 ~ 0.85. This phenomenon also has been discussed from the result in figure 7.67. The lower void fraction values were particularly contributed by the steady state condition and followed by low order vibration modes. As the slip ratio becomes higher the void fraction value also increases, following the law of nature but the effects of vibration in spreading the value of void fraction becoming weaker and from the figure, it can be observed that the spread gets slimmer. From the above analysis, it can be concluded that during the low slip ratio region, vibration plays a very important role to spread the void fraction value for local void fraction, the $\alpha_{avg(L)}$ and $\alpha_{max(L)}$ but contribute quiet small effect on the overall average void fraction, α_{avg} in the entire channel.

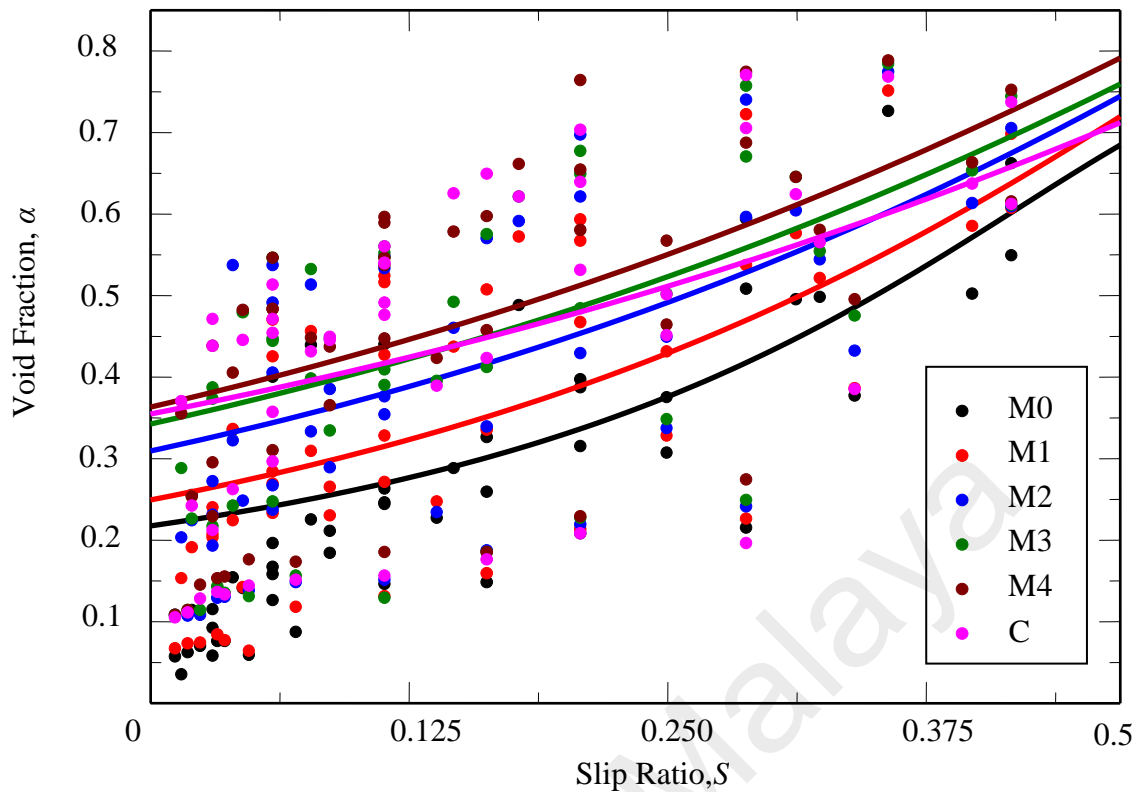


Figure 7.70 : Drift flux analysis - effects of slip ratio and size of vibration on the local maximum void fraction, $\alpha_{max(l)}$

As the slip ratio increases, the void fraction also increases and the spread are almost constant for all the cases, particularly for entire average and local average void fraction suggesting that the vibration plays very important role in void fraction fluctuation. However, even though the value of maximum void fraction keep increasing, the spread of void fraction value between modes of vibration becoming slimmer; suggesting that in the high slip ratio region most the flow have almost established a fixed pattern, that contribute to almost fix number of maximum value of void fraction.

Therefore, analyses on both of maximum and average void fraction is very important in order to have a clear picture of the whole phenomena happened when a particular flow channel receives extra forces such as vibration, as studied in this work.

7.5 Instantaneous bubble velocity

7.5.1 Analysis of Instantaneous Bubble Velocities

The instantaneous bubble velocity, v_b is one of the important parameters in two-phase flow where it will contribute to the transition in flow patterns. There are many factors that affect the value of this parameter as well. It is a function of average volumetric flux, j , the pipe geometry, the fluid properties and the body force field. In almost every case, the bubble length is not found to be an important variable since the dynamics of the nose and tail of the bubble govern the motion entirely. Another form of describing the velocity of the bubble is the drift velocity, v_{Gj} which is actually the average velocity of the phase or also referred as axial drift velocity since the phase of the fluid defined are assumed to be moving along a pipe. It is the difference of bubble velocity and the overall volumetric flux, where these three parameters are in the relationship as the following,

$$v_{Gj} = v_b - j \quad (7.1)$$

Hence the drift velocity is also independent of void fraction and depends on overall volumetric flux, j and not on j_G and j_L independently. Figure 7.71 shows the depiction of a unit cell for slug flow analysis, which illustrates the relationship of bubble velocity and the average volumetric flux, j .

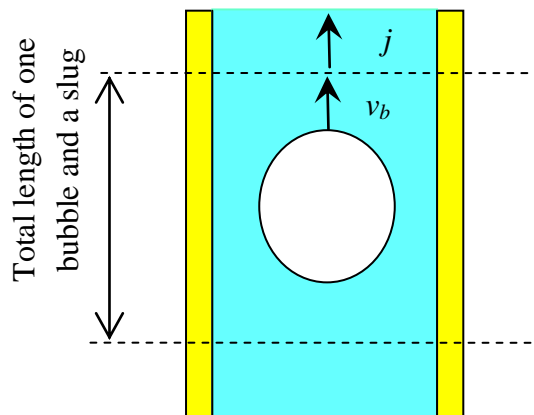


Figure 7.71 : Unit cell for bubble and slug flow analysis

On the other hand, the void fraction, α can be derived as equation 5.13 if the bubble velocity and the gas flux are known and simplified as,

$$\alpha = \frac{j_G}{v_b} \quad (7.2)$$

However, for one dimensional flow with no wall shear effects, the drift velocity is independent of j but is a function of void fraction, α . The only way these condition can be both satisfied is for v_{Gj} to be a constant. This constant can be evaluated by choosing the special case of single bubble in stagnant liquid for which the drift velocity having the same value as the terminal velocity v_∞ , for which,

$$v_{Gj} = v_\infty \quad (7.3)$$

Therefore, for all value of α ,

$$j = \alpha v_\infty \quad (7.4)$$

And thus, the bubble velocity where there is net flow is,

$$v_b = j + v_\infty \quad (7.5)$$

From the relationship as the above (equations 7.1 ~ 7.5), and the void data as obtained and discussed in the previous section, a simple method can be derived to calculate the instantaneous bubble velocity during the vibration. This measurement is very important in order to investigate on how the bubble velocity changes due to the vibration effects since this vibration accelerate in the vertical motion. The interchange of positive and negative acceleration are predicted to affect the bubble velocity as discussed in the previous section where the vertical motion sometimes slow down the rising bubble and at certain stage due to downward flow of the liquid holdup.

Even though the current experimental work used a 20-mm diameter pipe, flow characteristics such as the liquid recirculation induced that always been encountered in comparatively larger diameter pipe was also considered. Since the liquid recirculation may affect the liquid velocity profile and promote the formation of cap or slug bubbles,

the distribution parameter and the drift velocity in a large diameter pipe can be quite different from those in a small diameter pipe where the liquid recirculation may not be significant (Hibiki et al., 2003). In order to validate the result obtained from the current work, a list of drift velocities were selected and compared as in Table 7.2.

Table 7.2 Drift velocities estimated by various correlations

Investigator	Flow Regime	v_{Gj} [m/s] for $D=0.05m$ at $p=0.1 MPa$	v_{Gj} [m/s] for $D=0.02m$ at $p=0.1 MPa$ (Current Result)
Ishii (1977)	Bubbly Flow	0.124	0.156
Ishii (1977)	Bubbly or Churn	0.231	0.255
Ishii (1977)	Slug Flow	0.247	0.275
Kataoka and Ishii (1987)	Flow in pool	0.295	Not available
Hirao et al. (1986 and 1990)	Flow in Large Diameter Pipe	0.231	0.286 (different experiment using the same facility)

The result from the above table shows that the current experimental apparatus produces the drift velocities within acceptable range as compared to other investigators. Therefore, using the current void data, a safe evaluation on the bubble velocities, particularly as they vary during the vibration can be carried out. For the current analysis, example of the evaluation method are shown for the case of very low flow condition with combination of low liquid and gas superficial velocities. For the effect of increasing j_G , the j_L was set at 0.5 m/s with all modes of vibration (M1-M4) and j_G was set at 0.05 m/s for the variation of j_L with mode of vibration fixed at M3.

7.5.2 Evaluation of Bubble Velocity due to Sizes of Vibration

As a reference for all of the cases that will be discussed in this section, bubble velocities during the steady state condition are determined using the time varying void fraction fluctuation and they are displayed in figure 7.72. A time lag, Δt of the bubble to travel between two different sensors can be measured shown as the different of time between the two peaks as in this figure. Since there are four different location of sensors placed on the wall of the channel, the distance of the travelling bubble can be determined using two different axial of positions and in this case as applied in the previous sections for void fraction analyses, they are at $L/D=45$ and $L/D=50$ with 150 mm gap, can be expressed as Δz . Therefore, the bubble velocity can be generated using the relationship as the following,

$$v_b = \frac{\Delta z}{\Delta t} \quad (7.6)$$

The measurement results from equation 7.6 were then compared to the theoretical result as discussed above using equation 7.2 since the void fractions data also directly available from this figure. An example of datasheet for this calculation can be referred to Appendix 7.4.

In this analysis, the selections of peaks were carried out via a very thorough inspection on the pattern of void fluctuation spectrum. They were selected for the same patterns demonstrated for spectrum at the two different locations of sensors in order to ensure the same bubble to be analyzed. Therefore, as in the figure, they were scale down to a very short time, where in most of the cases, the analyses were carried out to evaluate the bubble velocities within the range of 2 seconds. This time frame was taken due to the highest impact from the vibration that take place around the first 2 ~ 5 seconds before it damped and faded.

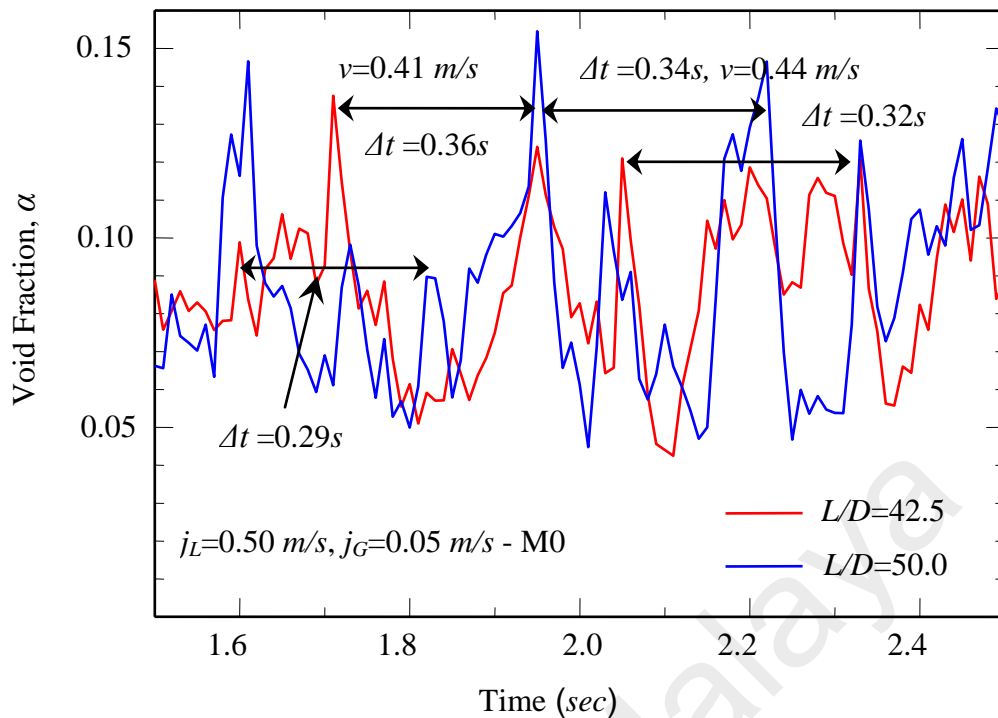


Figure 7.72 : Evaluation of bubble velocity using the void peaks for steady state condition (M0) with flow condition at $j_L=0.50 \text{ m/s}$, $j_G=0.05 \text{ m/s}$

From figure 7.72, the time lags are mostly constant around 0.3 seconds, which as a result give the bubble velocity to be around 0.4 m/s . This is a very acceptable result where as compared to the theoretical value they are about 6% higher.

Using the same concept the bubble velocity during the vibrations can be evaluated and for the first case with vibration mode M1 as shown in figure 7.73. In this case, the void peaks were tracked down to the vibration spectrum in order to investigate the effect of magnitude of vibration onto the bubble velocities as mentioned above. However, it is very difficult to select only one direction of acceleration for a particular case, since they bubbles were not at all the time travel to the next location within the same direction of vertical motion.

The result from this figure shows that the effect of vibration is quite significant where the bubble velocities were in some range differ from those evaluated during the steady state condition. With the influence from the ground acceleration they were

delayed and accelerated as well depending on the direction of the motion. However, on average, they have shown a little increase of velocity compared to the steady state condition and with higher void fraction. This is somehow contradict with equation 7.2, where the bubble velocity will inverse proportionate with void fraction. The following investigations on vibration impact will explain this phenomenon.

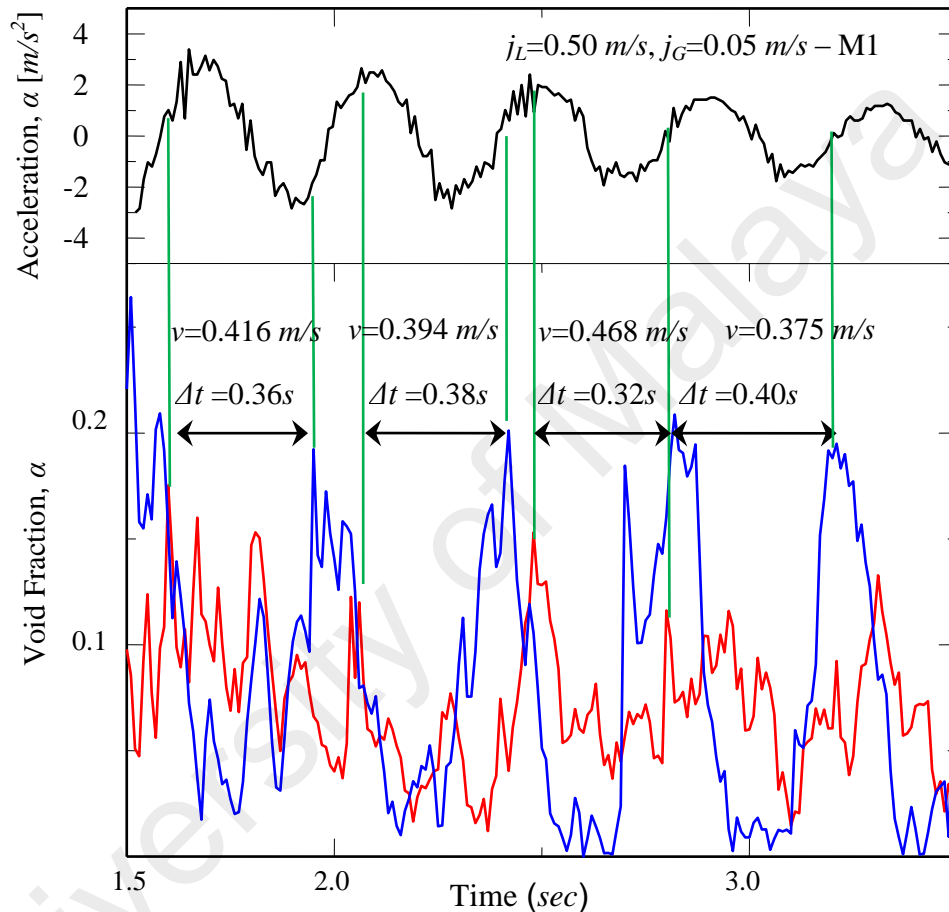


Figure 7.73 : Evaluation of bubble velocity using the void peaks for vibration with mode(M1) under flow condition at $j_L=0.50 \text{ m/s}$, $j_G=0.05 \text{ m/s}$

Figure 7.74 shows the evaluation of bubble velocities under the same flow condition as the above case with vibration mode M2. Again in this case they were travelling in both directions of vertical accelerations and the same effect from vibration can be observed, where the average bubble velocity increased around 5%. One significant finding from this figure is that when the bubbles were travelling, they

experienced an accelerated vibration and then underwent the decelerated vibration before reaching the next position as can be seen in the first three time lags. Here, they have taken almost the same duration of time with the same experiences to travel in the same distance. In the last time lag, since it travels in a complete cycle of up and down of ground accelerations, it took a longer time to travel.

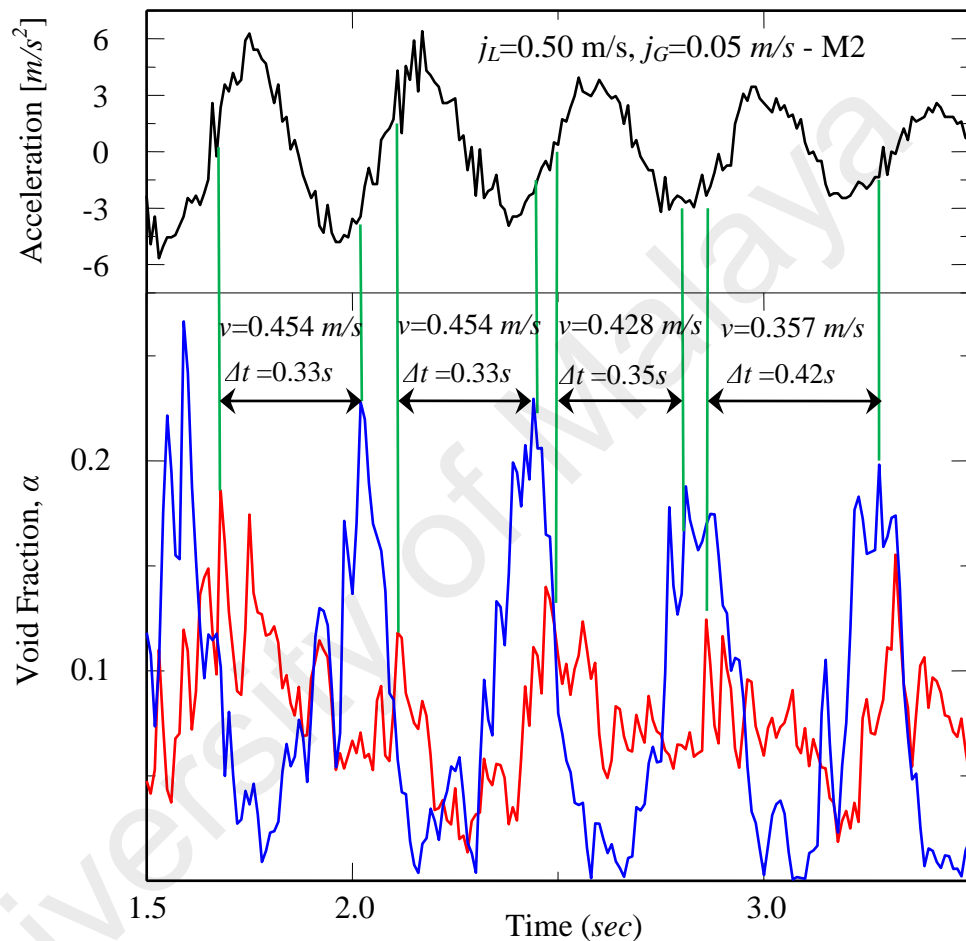


Figure 7.74 : Evaluation of bubble velocity using the void peaks for vibration with mode (M2) under flow condition at $j_L=0.50 \text{ m/s}$, $j_G=0.05 \text{ m/s}$

The same phenomenon also repeated in this case where, by receiving the ground acceleration in the range of $\pm 6 \text{ m/s}^2$, the time average void fraction also increased but it does not delayed the motion of the bubbles. Instead, the gas bubbles in this case were speed up to about 2-3% compared to the case with vibration mode M1 and about 5% compared to the steady state condition. This is again does not follow the rule as

suggested by equation 7.2 and so far, with two contradiction cases, the effect of vibration might have contribute to this changes. In all of the cases of bubble velocities evaluated for this range of accelerations, they experienced the downwards accelerations that theoretically might have slow down their motion, but they performed higher movement compared to the previous cases; of low ground accelerations and non-vibrated condition as well.

The next evaluation was conducted for the case of vibration with mode M3 as shown in figure 7.75. This figure somehow contributes an answer to the previous puzzle about the accelerated motion of gas bubbles even though the void fraction increases.

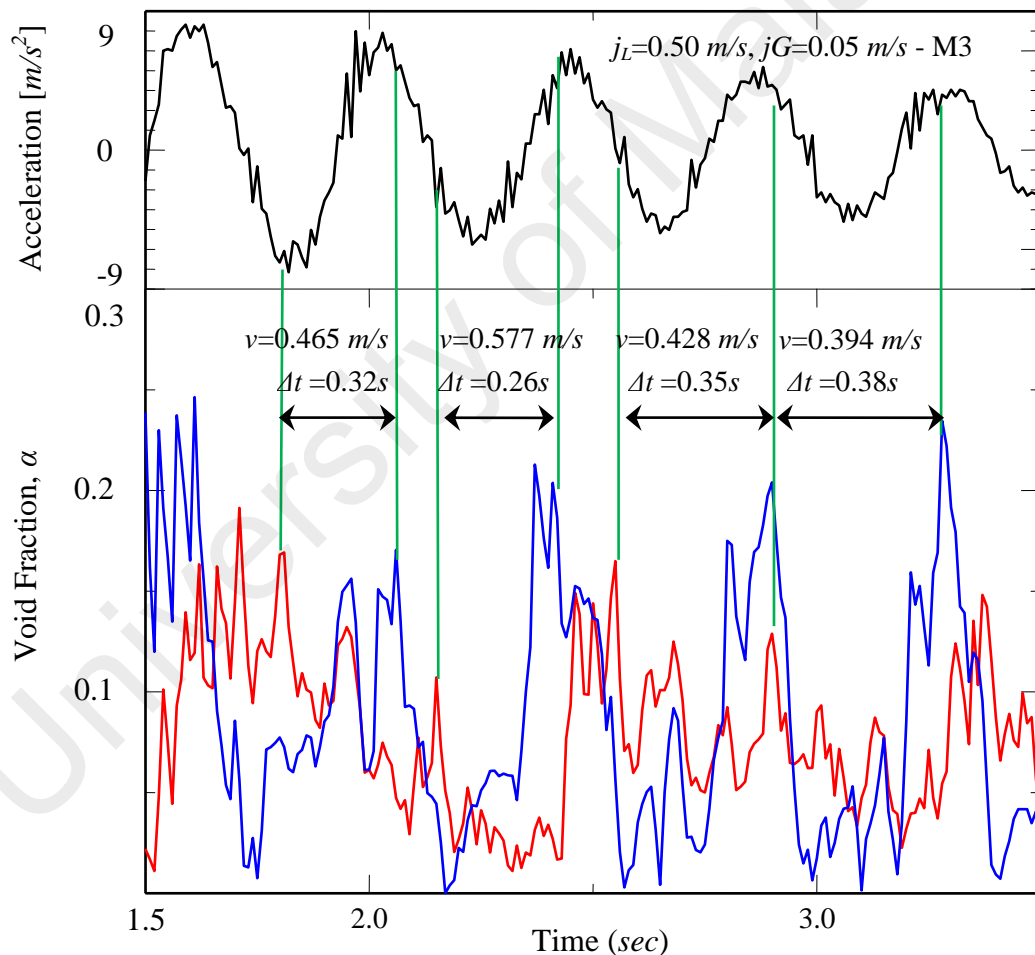


Figure 7.75 : Evaluation of bubble velocity using the void peaks for vibration with mode(M3) under flow condition at $j_L=0.50 \text{ m/s}$, $j_G=0.05 \text{ m/s}$

As shown in this figure, as the ground acceleration increased to the range of ± 6 m/s^2 , the void fractions also produced higher peaks, which mean that they are having higher maximum value. At the same time, the void fractions also having lower minimum value as the valley of the void fluctuation curve went deep down and nearly reached zero. This indicates that there are times when the voids are super high and extremely low, which actually suggests that there are variations of proportion of gas bubbles along the flow channel during the vibration which has been discussed in section 7.2 and can be confirmed using figure 7.33.

As discussed above that the bubble velocity is a function of average volumetric flux, j , not either the j_G or j_L , therefore, the absent or less population of gas bubbles at a particular position in the flow channel will make j_L becoming dominant. At the same time this less population gas bubbles contribute to low value of void fraction and therefore contribute to the higher bubble velocity as they were drifted away by the liquid flow. Along the travel this phenomena are repeated and therefore there are low and high bubble velocities along the channel. The vibration might affect the liquid holdup but not directly on the bubbles, as also discussed in section 7.2 where the bubble were seen accelerated due to positive ground acceleration that shoot up the motion of the liquid, surpassed the shear forces between the channel wall.

Hence, as in figure 7.76, three of the bubble velocities that evaluated here experienced positive accelerations. From this evaluation, they show an increased of velocity up to 30% different from the steady state condition. On the other hand, the initial void fraction as they travel from the first position is slightly low, which is around 0.1 ~ 0.16, but when they reach the next position the void fractions were as high as 0.2 ~ 0.25. These values show that during the travel the coalescences occur and as they becoming bigger and increase in mass, and this reveals that during the positive acceleration all the bubbles were crowding up to higher position of the channel.

With reference from figure 7.75, as the bubbles start the travel with higher mass or with having higher void fraction, and moving under the negative acceleration, the velocities are somehow decreased but not as low as during the steady state condition. This might due to the effect that as they underwent the negative acceleration, they tend to breakup and forming smaller bubbles and therefore contribute to lower void fraction and therefore do not exhibit the same behavior during steady state with more or less having constant void fraction.

In addition, with more forces from the positive acceleration that surpassed this shortcoming, the overall velocities are found to be much higher if compared to the steady state condition and particularly with higher ground accelerations that contribute more forces onto the liquid holdup which indirectly contribute to more momentum on the bubble motions. This statement can be confirmed by examining figure 7.76. According to this figure, even though the bubbles experienced the downward acceleration, they still have much higher velocities compared to steady state condition and also with other downward acceleration from figure 7.72 and 7.73. With vibration sizes in the range $\pm 12 \text{ m/s}^2$, the damp during this time frame is about the same as the initial vibration in the order of modes M3 – M2 – M1, and therefore, produced the velocities in the same range of those modes.

The bubble coalescences and breakups can be confirmed by the second velocity evaluation where it starts from with void fraction of 0.22 and increase to 0.25 during the upward accelerations and then keep decreasing during the downward accelerations. Then as it reaches the second position, the coalescences become more rapid and the void increased to 0.3. With the above discussion, the phenomenon of higher average void fraction with higher bubble velocity is therefore rationalized.

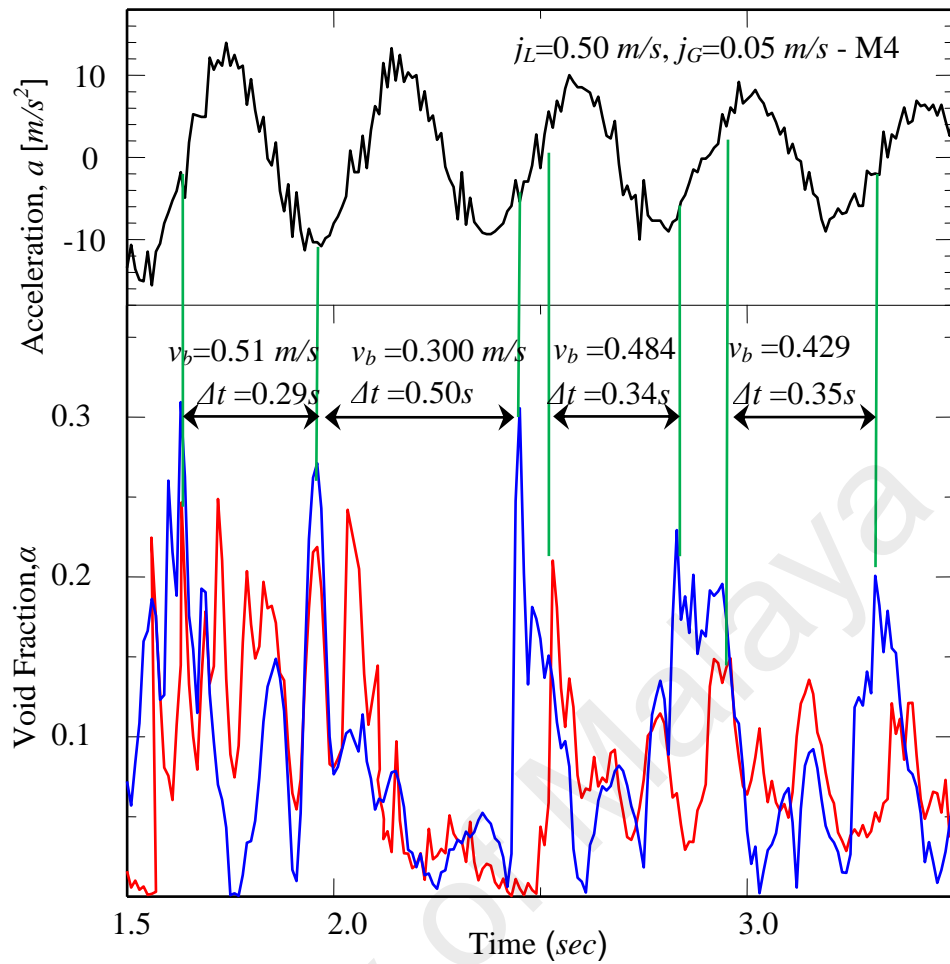


Figure 7.76 : Evaluation of bubble velocity using the void peaks for steady state condition (M4) with flow condition at $j_L=0.50 \text{ m/s}$, $j_G=0.05 \text{ m/s}$

This phenomenon indicates that there is quite a significant influence from direction of accelerations for bubble velocities. As confirmed from this analysis, bubbles that experience the positive or upward accelerations will have higher velocities and vice versa. In this case, the effect of gravitational acceleration is found to be dominant since the current result is based on the vertical vibration where the upward and downward motions produce different magnitude of accelerations. The effects of horizontal and 2-D or 3-D vibration are therefore still offer more interesting studies using the same idea as carried out in this work.

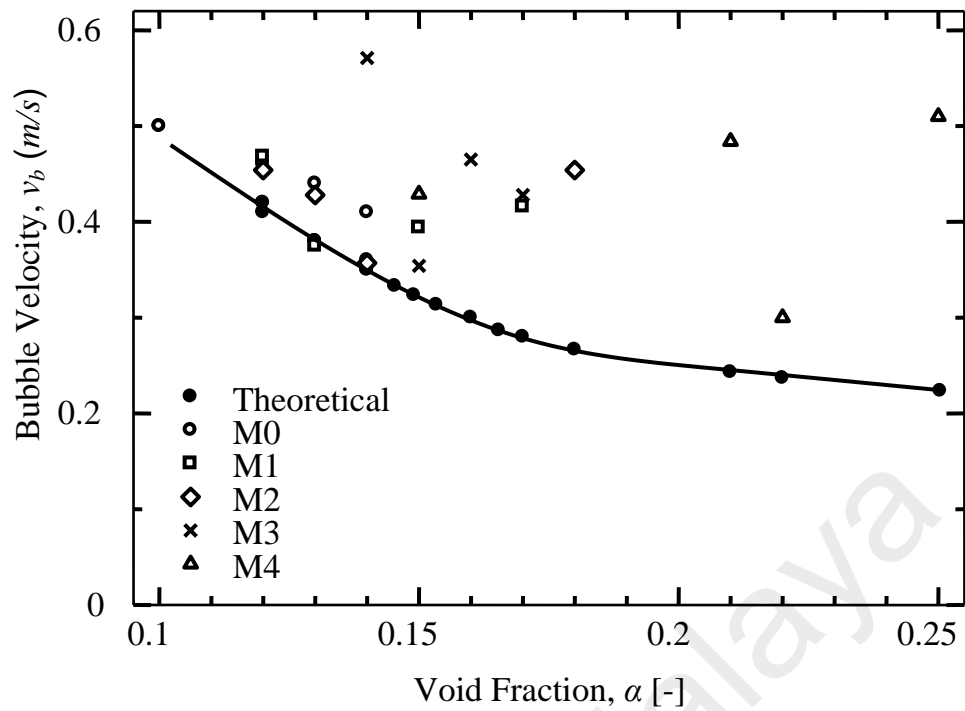


Figure 7.77 : Evaluation of bubble velocity with comparison to theoretical calculation under flow condition of $j_L=0.5m/s$, $j_G=0.05 m/s$ with all vibration modes

Figure 7.77 express the summary of the above discussion where bubble velocities were measured under flow condition of $j_L=0.5m/s$, $j_G=0.05 m/s$ with all modes of vibration were evaluated with comparison to theoretical calculation. This evaluation was carried out with regards to the void fraction value as discussed so far. Clearly in this figure, higher mode of vibration displayed higher bubble velocities and they depart far away from the theoretical value calculated by equation 7.2. The lower modes of vibration seem to follow the rule by theoretical calculation but have a slight range of differences particularly in the higher value of void fraction. This result indicates that, the normal rule of void fraction-bubble velocity relation can no longer be applied when the bubbles travel under the influence of vibrations.

On the other hand, for an application where there is only one direction of ground acceleration governs the motion of a system, it is therefore very important to know which direction of acceleration will be employed. As experienced here, different

magnitude of acceleration will cause many complicated problems caused by many strange phenomena in the gas-liquid two-phase flow system. By having this information, the direction of the flow can be rearranged in order to ensure the reliability and safety of the system.

However, since the current work has limitation on the production of higher gas superficial velocities, the discussion were concentrated on dominant effects of liquid superficial velocities in the overall volumetric flux. Beside this shortcoming, the current method to measure the bubble velocities is also very limited to low superficial velocities of both phases since the evaluations were carried out using the peaks of void fraction.

7.5.3 Effects of Liquid Flux on the Bubble Velocity

In the next analyses, the effect of liquid superficial velocities will be discussed in a little more details. As discussed earlier, equation 7.1 stated that the bubble velocity is a function of volumetric flux and equation 7.2 confirmed that the gas superficial velocities affect the variation of bubble velocities. Furthermore, from our common sense, the bubble size and velocity of gas phase will surely affect the bubble velocities; it is a necessary call to investigate the effect of liquid superficial velocities on bubble velocity and to what degree does this effect is significant. In order to carry out this investigation, four different liquid superficial velocities were examined for a constant gas superficial velocity at 0.05 *m/s* and with vibration mode M3 as shown in figures 7.78 ~ 7.80 and as well as figure 7.76 as discussed previously .

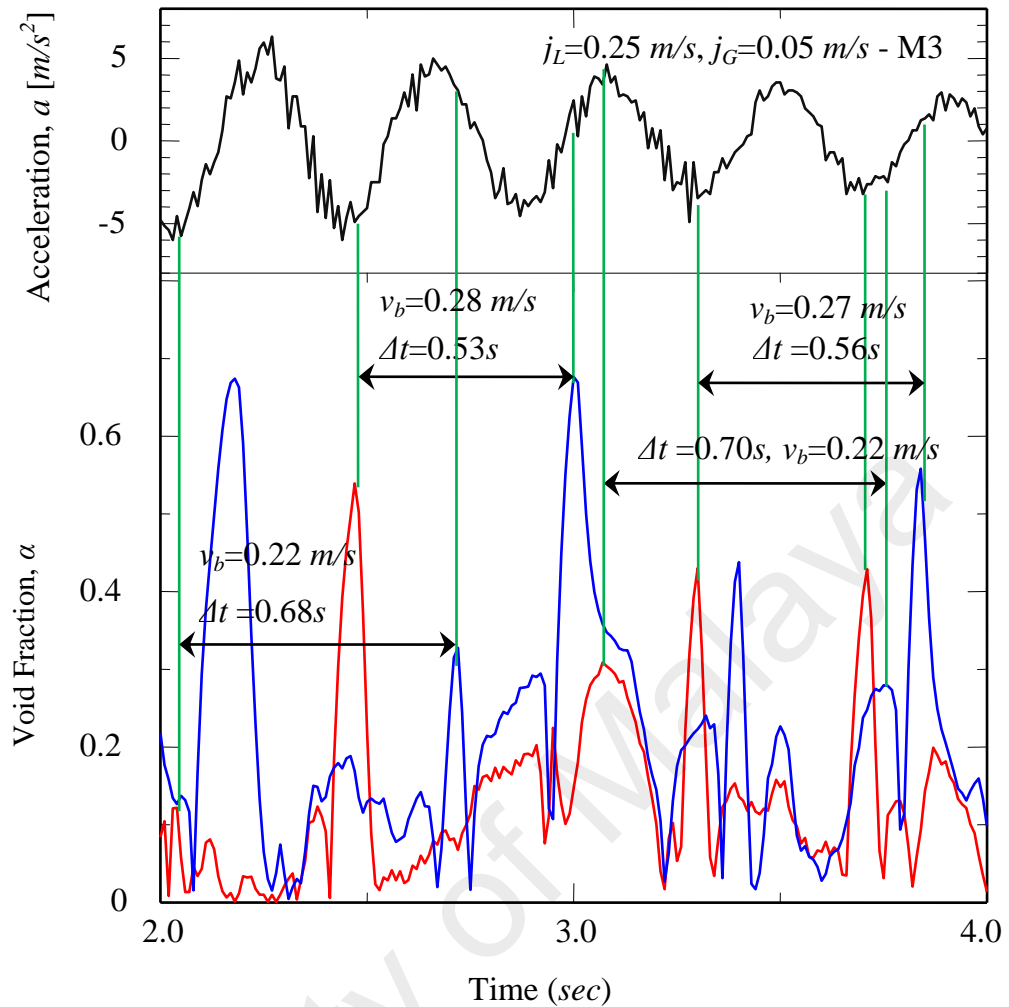


Figure 7.78 : Evaluation of bubble velocity using the void peaks on the effects of gas superficial velocities under vibration with mode M3 with flow condition at $j_L=0.25\text{m/s}$, $j_G=0.05\text{ m/s}$.

Figure 7.78 shows that with low liquid superficial velocity at 0.25 m/s , the bubble velocities were much slower than the steady state condition, where they differ about 50%, with the later having a liquid superficial velocity at 0.50 m/s . Comparison with the same case of vibration in figure 7.76, and with $j_L=0.50\text{ m/s}$, obviously shows that this condition have much lower velocities. This result gives an idea that in the bubble velocities are strongly dependent on the liquid superficial velocities in the case of lower gas superficial velocities and it is regardless of the vibration effects when examined through comparison with the steady state condition.

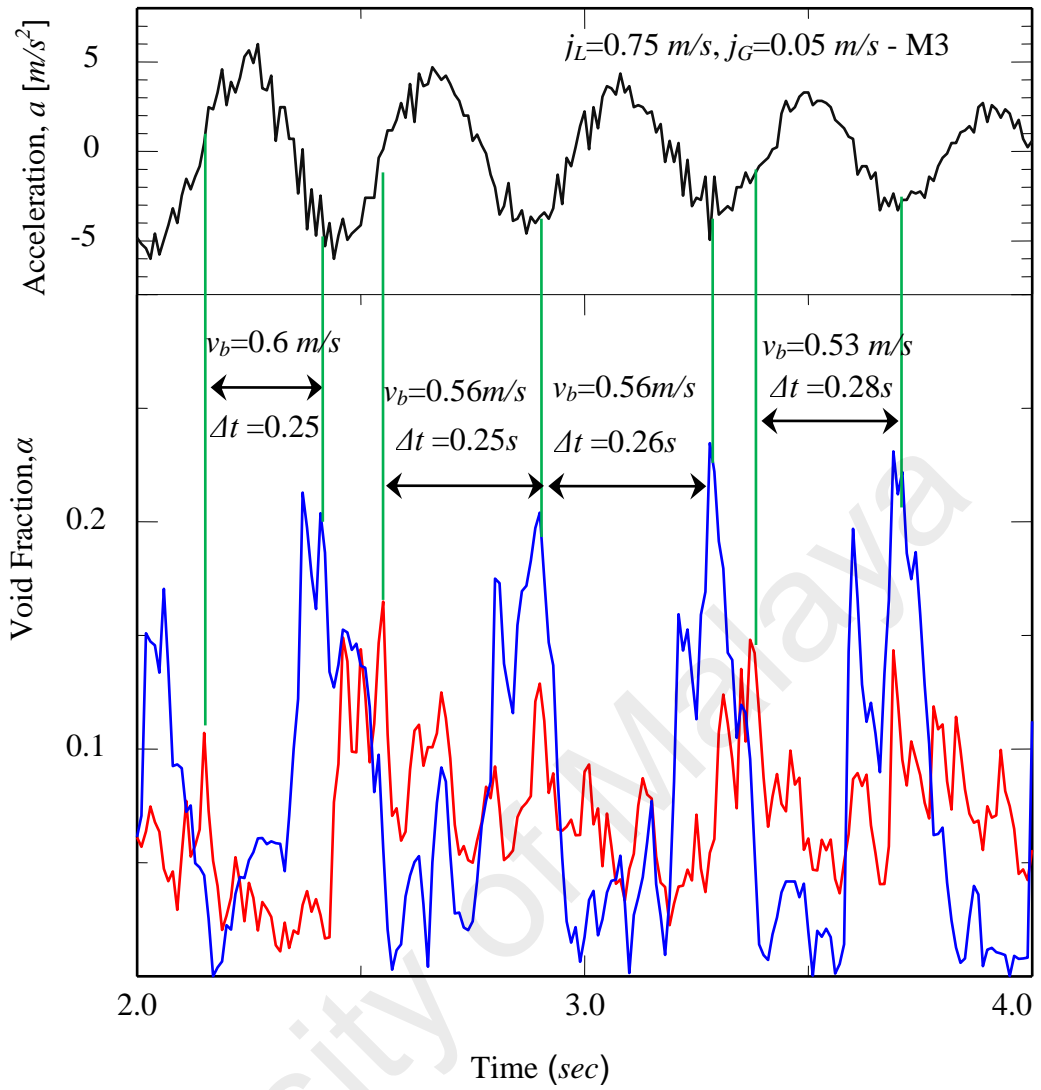


Figure 7.79 : Evaluation of bubble velocity using the void peaks on the effects of gas superficial velocities under vibration with mode(M3) with flow condition at $j_L=0.75m/s, j_G=0.05 m/s$

An increased of liquid superficial velocities to $0.75m/s$ is shown in figure 7.78, confirmed that increases in liquid superficial velocities increased the bubble velocities in liquid superficial velocity dominant regime. In this case, the bubble velocities are about 30% higher than the velocities evaluated during the steady state condition and compared with the different scales of vibration as in the previous figures, they still show much higher value. Observation in figures 7.78 and 7.79 also confirmed that, the value

of void fraction does not actually affect the velocity of bubbles in the case of vibration, since they were drag away by the motion of liquid flow due to its dominant effects.

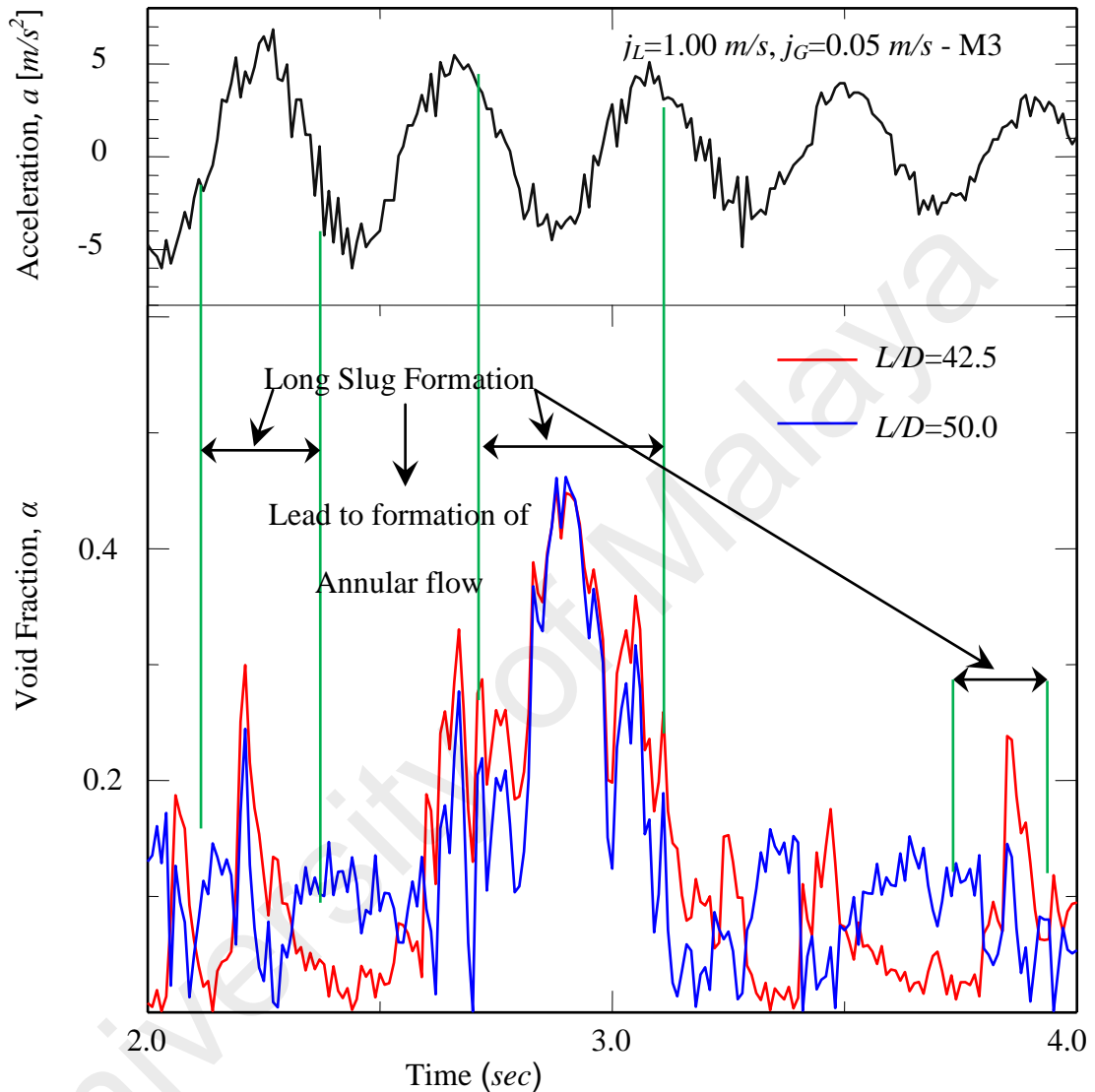


Figure 7.80 : Evaluation of bubble velocity using the void peaks on the effects of gas superficial velocities under vibration with mode(M3) with flow condition at $j_L=1.0\text{m/s}$, $j_G=0.05\text{ m/s}$

Figure 7.80 shows the fluctuation of void fraction in the condition of much higher liquid superficial velocity at 1.0 m/s . It is very difficult to select any peak to evaluate the bubble velocity since both of the curves are overlapping. It can be predicted that with this flow condition, and associated with the effect of vibration the flow totally

change into annular or froth flow. In the ideal condition, the annular flow will strongly follow the velocity of the gas superficial velocity and most of the regions are dominated by the type of flow pattern. However, in this condition not all the region are in the form of annular flow, and there still bubble flow with low void fraction, which the effect from the gas superficial velocity found to be less dominant.

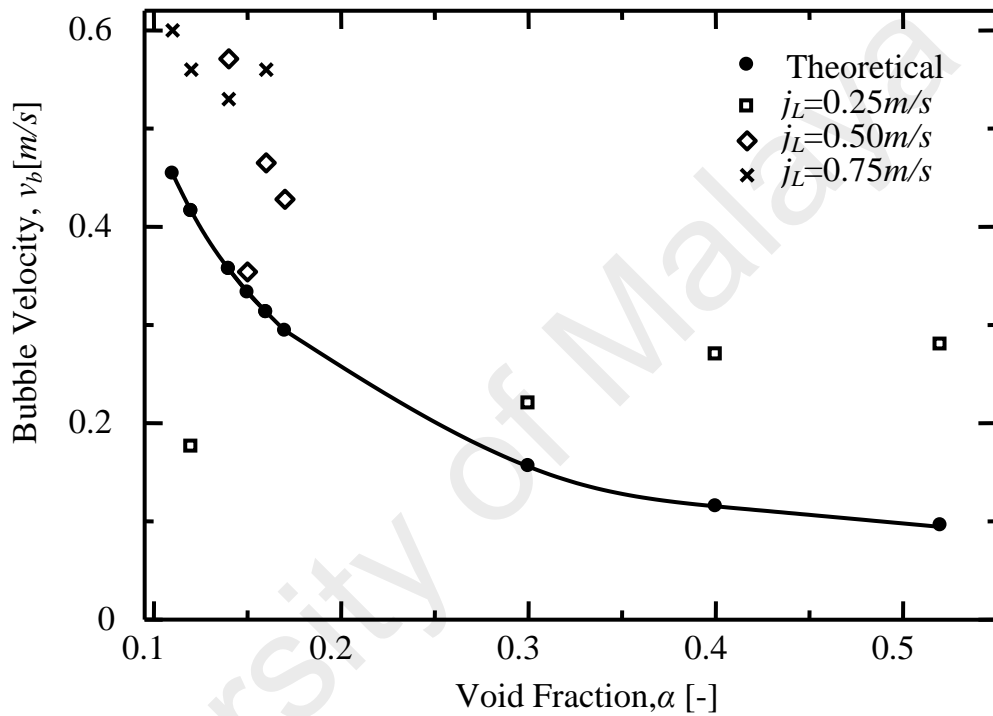


Figure 7.81 : Evaluation of bubble velocity with comparison to theoretical calculation under flow condition of $j_G=0.05$ m/s and various j_L with vibration modes M3

Figure 7.81 display the summary of this effects where the bubble velocities were measured under the fix gas superficial velocities and different liquid superficial velocities with vibration mode M3 and compared with theoretical calculation. Here, the void fraction contributed by higher liquid velocities were very much lower compared to the lower one, and therefore contribute to much higher bubble velocities. Therefore, as discussed earlier, in the liquid superficial velocity dominant region, the bubble velocity will be much less dependent on the gas superficial velocities.

With this very obvious contradictions as in this case, it can be concluded that vibration play very important role in changing the flow patterns. This is particularly in the region where the gas superficial velocity is dominant where vibration eliminates its effects. In contrary, in the case where liquid superficial velocity is in-charge, vibration with the current scales does not really contribute to any significant change on the flow patterns and other parameters.

Since measurement in two-phase flow is very important, there are also many other methods that can be applied to measure bubble velocities such as, visual techniques (Kubie, 2000) and Particle Image Velocimetry (Sousa et al., 2006). However, since the current work require the measurement of void fraction and the measurement of the parameters has been carried out, the void data has been optimized to evaluate the bubble velocity. This method however is very tedious and requires thorough analysis that limited the applications particularly in setting the range of flow condition. Since it can predict the position of the bubble using the void curve, it is still a good way of solving one of the problems in this study. With the current result, roughly it can be concluded that using the current method, the bubble velocity can be evaluated down to slip ratio of 0.05.

From this analysis, it was found that the vibration effect play very dominant role in accelerating the bubble motion even though with very low gas superficial velocities. The interaction among bubbles in the gas-liquid two-phase flow will totally change when they travel along the vertical upward flow channel under the influence of vibration. Therefore, the measurement of this parameter will provide an important data for prediction of flow patterns and their transitions in order to carry out any works on the design and safety analysis, particularly the one that involve the heat transfer and phase changes flow as have been discussed throughout this work.

8.1 Conclusion

Outline of the Summary

There are five different categories of works that have been conducted for the current study. They were concluded shortly at the end of each chapter. This chapter will summarize further details on those works with some recommendations for other task that are not conducted due to time constrain and the limitations of the current facilities.

8.1.1 Chapter 1 : Introduction

The formal presentation and brief explanation on the chosen topic has been discussed in chapter 1 where the complication of two-phase flow has been addressed. This complication were then being brought together with the hazardous possibility that will come when the external forces such as vibrations with a scale of heavy disaster shakes that hit the processing or power plant.

With these catastrophic consequences which have been discussed from chapter 1, the current study tried to bring more details analyses on the vibration effects on the two-phase flow, particularly in the event where this type of flow is employed in very heavy applications as discussed above. The fact to this application is that most of the flow systems are of high-temperature condition, including flow and pool boiling, whereby the two-phase flow is very significant that as a result multiplying the hazardous level of operations, controls and safety procedures. However, in the current study, due to the limitation of the current facilities, the high temperature flow condition could not be conducted. As a substitute to this condition, two-phase flow with wide range of flow conditions that met some of the characteristics of high energy and high temperature were applied. They were analyzed in many angles in order to replicate the real situation and to be as close as the problem that can be found in the real plants.

Since the current topic is a new subject in the two-phase flow, the approach on analyses were based on very limited source of literatures where most of them do not discuss about a direct vibration impact on the two-phase flow. There were several literatures that discuss about the relation between the vibration and the two-phase flow but they were limited to the flow induced vibrations in the flow channel which do not at all reflect the real situation of a direct impact. However, they still provide some good information for the current studies in term of flow pattern transition and as one of the additional forces that exist in the two-phase flow channel.

8.1.2 Chapter 2 and 5 : Literature Review

Chapter 2 and 5 introduced all the literatures that have been reviewed for the current work where they were discussed topic by topic in the two-phase flow and a heavy class of disaster shakes that applied for the analyses throughout this work. The subject of two-phase flow was discussed in more details with elaboration on its fundamentals including the definition and structure of flow that will be applied in the work which is the combination of gas-liquid and particularly with focus on working fluids of air and water. The applications, problems and accidents were discussed with some recommended solutions that have been practised so far, in the history of two-phase flow were introduced.

Two-phase flow in two-dimensional column is one of the important applications was discussed where the studies on this subject were basically concentrated on the bubble rising and their characteristics. The relevant of this subject is particularly very important in the analysis of pool boiling where it replicates the bubbles nucleation from the heating surface and rise up to upper level of the container. In this case, the discussions were extended with more details on single and swarm bubbles on the possibility of application for mixing and processing technologies in many industries.

Two-phase flow in pipes was later on introduced as the main subject to be discussed in this work with discussion on various arrangement of pipe flow in applications. For this purpose, the analyses that proposed to be discussed were flow patterns, mapping of flow patterns, measurement of void fraction and instantaneous bubble velocity in the pipe due to vibration, with comparison to steady state condition. This section also discussed about various types of flow patterns in two-phase flow and the methods of identification of those patterns. It was then continued with the process of mapping these patterns in wide range of flow conditions with some introduction of some examples of the maps that normally used for analyses such as Fair (1960), Hewitt and Roberts (1969), Taitel and Duckler (1980) and development of flow patterns in a vertical flow boiling by Collier (1994).

Definition and description of void fraction were also being conducted in this chapter. It was detailed with explanation on the models of void fraction in gas-liquid two-phase flow and the governing equations that determined the void fraction. In order to conduct experimentations for this study, the techniques of void fraction measurement were explained and they were discussed in a very good manner with comparisons of advantages and shortcoming of all the methods.

The two-phase flow boiling which is always the fundamental and important subject was touched briefly here with examples of works by various researchers and some issues such as critical heat flux (CHF), boiling characteristics, governing parameters and so on were highlighted as well in order to relate the phenomena with the current work.

Another important parameter that was put into account was the instantaneous bubble velocity. This subject was discussed in focus with the range of velocities, effect to flow patterns and their measurement techniques as well. Discussion on this subject was extended to correlations that can be applied to predict

the bubble velocity also being introduced here, with comparison on bubble sizes and their velocities.

The next subject was really very important for the current study which is the relation between the two-phase flow and the vibration. As mentioned earlier, most of the literatures do not discuss on the direct vibration impact on the two-phase flow but more on the flow induced vibration and natural frequencies. They were introduced in this section as references of works conducted as to date that relate vibration and the two-phase flow. However, there were some works by Krishna and his associates (Krishna et al., Ellenberger et al., and Vandu et al., 2002-2007) that applied direct vibration impact on the two-phase flow but they only concentrated on the two-dimensional column that discussed on the elevation of fluid surface and characteristics of rising bubbles.

Therefore, the real impacts were analyzed by literatures that concentrated on the seismic vibration which composed from theoretical, simulation and experimental studies. This is very important in order to gain information about the situation during a heavy disaster shakes such as the earthquake where it has lead to investigate the patterns of vibration spectra during those events which as a result provide the basic information for the design of the vibration platform. In this case, they were a lot of studies that uses a huge scale shaker that reproduced the recorded spectrum of earthquake and test the structures on it. These experimentations were particularly for the design and analyses of building and facilities that do not involve with flow in pipes. Therefore it was like no chance to observe the phenomena of two-phase flow during the occurrence of earthquake and that is the reason why there is no literature that discussed the issues that have been highlighted here.

Therefore, several attempts have carried out in this study to provide such solution or at least as subject of knowledge for awareness for the two-phase flow

researchers. The following conclusion made the above unknown phenomena to become a good subject to be further experimented, studied and analyzed. Since this work concentrated only on experimentation, it may contribute a very important database for analyses using computer simulation in the future, and perhaps with more complicated arrangement of pipe flow.

8.1.3 Chapter 3 : Development of Vibration Platform

In order to reproduce a class of heavy disaster shakes such as the earthquake for this study, a special vibration platform was constructed. From the information provided by the literature review as has been discussed previously, the data for range of spectrum during the mentioned vibration were obtained. It was judged that the ground acceleration for that particular shakes would be fair in the range of $-10 \sim 10 \text{ m/s}^2$ or $0 \sim 1.0 \text{ G}$ ($\pm 10\text{gal}$) and the frequencies in the range of $0 \sim 26 \text{ Hz}$.

The design of the vibration platform requires analyses on the vibration that will be reproduced. For this purpose, some basic analyses on the damped free harmonic vibration have been conducted and some results for theoretical studies were produced. Due to financial constrain of the current work, a sophisticated shaker as applied in many experimentations for structural studies was impossible. However, based on the information from literature study and the basic analyses conducted, vibration with the range that has been discussed, in whatever spectral formation would be a comfortable environment for experimental works.

Therefore, the current shaker was designed to meet this range of acceleration but with a slight wider range which is with acceleration of $\pm 12 \text{ m/s}^2$ and frequency was fixed at 2.5 Hz . This shaker was composed from three tiers as shown in figure 3.2, and uses four springs with constant of 0.1658kgf/mm each to support the piston rods that as a result will activate the vibration to whole part of the test section. It uses the concept

of pull and release and by this method; the spectral pattern is harmonic vibration, where it damped slowly due to the damping ratio of the spring.

The ranges of ground accelerations were divided into four categories or scales based on the released amplitude, and they were named in the form of modes. Mode I of the vibration is based on the 10mm amplitude which gives a fluctuation of vertical acceleration in the range of $\pm 3 \text{ m/s}^2$. Similarly, Mode II is set as a bigger shakes based on 20mm amplitude that produces acceleration at $\pm 6 \text{ m/s}^2$ as well as Mode III that based on 30mm amplitude with acceleration at $\pm 10 \text{ m/s}^2$. The largest shakes obtained in this experiment is Mode IV at amplitude 40mm which is the highest limit allowed by the current spring, produced the ground acceleration at $\pm 12 \text{ m/s}^2$.

8.1.4 Chapter 4 : Bubble behaviour in a 2-D column

The first experiment to analyze the effect of vibration onto the two-phase flow was by the investigation on the bubble rising in a two-dimensional column. A two-dimensional column made from transparent board and filled with water was placed on the vibration platform. Trajectories of the single bubbles in this 2-dimensional column were studied in the condition of with and without vibration with comparable parameters such as vibration modes and the bubble sizes. The results show that they are strongly influenced by these two factors. Increases on vertical acceleration that gives bigger shakes, disturbed the trajectories of the rising bubbles and promoted bigger diversion, far from the meandering line to compare as how they travel without the vibration.

Formations of bubble at the nozzle are also observed with the shapes oscillations seem to be affected by the scales of the ground acceleration. Decreases on bubble sizes that give big excursion amplitudes during the rising without the vibration make this amplitude bigger at the beginning during the vibration and soon divert them as well.

Here all the bubbles did not exhibit the traditional motion as sinuous curve but the motions were in disordered parabolic curves.

On the other hand, the rising velocities of the bubbles were also affected by the vibration, which differ according to the bubble sizes and the vibration modes. In this case, bigger size bubbles were seen to be less affected by the vibration. When the scale of vibration increased or in other word, with higher ground acceleration, the rising speeds of the bubbles decreased and the initial velocity while receiving the external forces was quicker for smaller bubbles.

Interaction of two single bubbles with different diameter that released from close gap was observed. They shown with very interesting phenomenon where the smaller bubble was attracted to the bigger one, and they clustered and coalesced. However, due to external force from vibration this coalescence was not strong and they soon separated again, with smaller bubble overtook the bigger bubble and continued to move upward. This incident confirmed that the smaller bubble will move faster compared to bigger bubble under the influence of vibration as the above statement.

Part II : Two-phase flow in vertical pipe

8.1.5 Chapter 5 : Literature Review - As discussed above.

8.1.6 Chapter 6 : Methodology

A scale down two-phase flow experimental rig was developed in order to conduct experimentations for the main objective of this study which is to investigate the vibration effects on the flow structures and dynamics of two-phase flow and it was design to be operated for wide range of flow conditions. This experimental rig was equipped with high end of measurement technologies and reliable sensors developed

based on previously successful results by other scholars. It consists of a 1.2-m length of transparent pipe with inner diameter of 20-mm and an implanted void sensor on the inner wall. The construction of the current facilities is shown in figure 5.1 where in this flow loop, the air was injected into the system from the compressed tank or compressor. It flows through the gas line which was covered with porous cap with very fine holes in order to produce very fine small bubbles into the test section. At the mixing section, the gas and liquid mix together and the gas bubbles move upward co-currently with the liquid flow. The test section part was placed on the vibration platform in order to examine the effects of vibration onto the two-phase flow. This rig was equipped with photographic facility and sensors where all the data recorded via a very reliable data acquisition.

For measurement of various parameters in this gas-liquid two-phase flow rig, a systematic sensor has been developed based on the Constant Electric Current Method (CECM). The performance of this sensor has been validated by the calibration conducted both for the static and dynamics methods. The static calibration shows that the sensor has a good accuracy with 3% of overall error while the dynamic calibration gives a diversion of accuracy around 5%. The reliability of this sensor has been tested to measure the volumetric gas rate in the two-phase flow (void fraction), liquid film thickness on the wall of flow channel and instantaneous bubble velocity in wide range of flow conditions. The results shows that all the measured parameters agreed well with previously obtained data from various scholars. The current sensor also provides very good data for the predictions of flow patterns, flow transition and can be applied to conduct the flow mapping. Hence, this sensor is highly reliable in measuring the two-phase flow parameters in wide range of flow condition.

8.1.7 Chapter 7 : Results and Discussions

Flow Patterns

The first investigation performed using this rig was the flow patterns during the vibration and they were compared with steady state condition. For a combination of relatively low gas and liquid superficial velocities, for example ($j_G=0.025$ m/s, $j_L=0.25$ m/s) the bubbly flow that normally formed during the steady state completely developed into slug flow even at the lowest mode of vibration (M1). As the ground accelerations increase, the longer slugs were formed with bubbly flow before and after the slugs. With the changes of motions, the bubbles seems to experience up and down movement and in between they were stagnant due to transition from the positive to negative acceleration which reflects the downward and upwards travel. These kinds of motions contribute to more bubble congregations and coalescences and therefore resulting in the formation of longer slug.

The slug seems to breakdown into smaller distorted bubbles due to downward movement which also drag the liquid holdup down. From this observation, it can be said that the vibration give a strong influence in the downward slip motion of the liquid hold up, and this case may slow down the bubble motion in the two-phase flow. When the gas superficial velocity is further increased, for instant above the 0.1 m/s, the flow patterns change immediately into slug flow even without vibration. At low ground acceleration, bigger slugs start to form and as the accelerations increases, they become more longer but unstable. The shapes of the slugs were distorted and more small bubbles exist on their heads and tails. This is also a result from the downward flow of liquid hold up that disturbs the smoothness of slug flow, break them down into smaller bubbles where these bubbles also move downward and surrounded the slug while travelling under the effects of higher ground accelerations. With higher vibration mode, there were also the formations of churn flows that coalesced to form annular flow.

Under the condition of higher liquid superficial velocity, in particular when it reach $j_L=0.75$ m/s, very stable bubble flow is formed in most of the condition for wide range of gas superficial velocities. At very low gas superficial velocities of, $j_G=0.025$ m/s and $j_G=0.050$ m/s, the flow pattern remain as bubble flow through out all the steady state and transient rough conditions even with higher degree of vibrations. The only observation that can be compelled here is the bigger sizes of bubbles were formed under this flow condition. They move upward steadily but sometime demonstrated very close gap of congregations and dispersed away from other group due to vertical motion.

Flow pattern start to change with vibration higher mode of vibration (M3 and M4) where slugs were formed but they were not in proper shape. This situation might due to imbalance interfacial forces between the vertical motion and the gas velocity in the flow channel that somehow disturbed the formation of steady slug even though the effects of downward liquid holdup considered being small.

A simple conclusion that can be addressed here is again about the vertical motion that promotes a disordered bubble rising; in term of velocity and interfacial forces. Hence, in further analysis, the relation of slip ratio and ground acceleration sizes can be remarked as having some degree of effect.

For higher liquid superficial velocities $j_L=2.0$ m/s and above, there is tendency where the ground accelerations from vertical vibration do not contribute strong impact on the flow patterns with low gas superficial velocities such as tested in the current work which is in the range of 0.025 ~ 0.25 m/s. However, with high vibration mode, there were slugs formation within the bubbly flow but were easily distorted to form smaller bubbles but there do not show any transition into the churn flow.

The structures of flow during the event of vibration can be observed based on their development in time series as the vibration damped harmonically during the experiments. For instant with slip ratio at $S=0.1$, and with a vibration mode M3, the

flow started with steady bubbly flow in the beginning of the experiment and bubble congregations in very close gap when the vibration was applied. During the upward movement the liquid holdup tends to be pulled or slowing down as the vertical vibration experiencing a negative acceleration. It therefore dragging together the bubbles and as a result a high percentage of liquid occupied in this position. The effects of downward liquid flow resulted in the huge congregations of bubbles and lead to easy coalescences and as a result developed the slug flow with some trailing bubbles on the tails.

Since the coalescences happened very rapid and easy, more slugs were produced but again with the effects of downward liquid flow due to vertical motion, these slug were seen to be very unstable, distorted and breaking up forming smaller bubbles in the flow channel. This discomfort situation does not extend for long until the motion change its direction along the sinuous curve of vibration to move downward. During the downward motion, the system is then experiencing a positive acceleration and therefore accelerating the liquid flow as well.

With the same impact of vibration mode and higher slip ratio, rapid coalescences occurred and forming slugs with trailing of small bubbles at the tail and the slug look like an uncompleted structure. This phenomenon is due to the downward liquid holdup that disturbs it and tearing down the surrounded liquid that hold the slug proportion, and throughout this flow condition, the slug structure never been established in a proper shape and furthermore, these long slugs easily broke up. The effect of vertical motion also sometime forced these slugs to coalesce with other slugs forming super long slug which having a length of about 300-*mm* with very thin liquid film thickness. With this length, they are sometime behaving as or misinterpreted like an annular flow and again with continuous vertical motion effects they break up again forming a very unstable flow regime as a churn flow.

Therefore, the effect of vibration heavily changed the flow patterns into varieties of flow pattern with the same gas and liquid superficial velocities. These unstable flow patterns create very dangerous conditions for two-phase flow since they cannot be predicted under a particular condition. In conclusion, very careful treatment must be taken into account in the event of heavy disaster shakes that hit any two-phase flow piping systems during their operation.

Flow Patterns Mapping

The flow patterns maps are presented based on the results obtained from photographic data used to examine the flow patterns. These data were analyzed for various set of flow conditions which are the combination of gas and liquid superficial velocities (j_G and j_L). They are expressed to show the vibration effects on the total map with comparison to the steady state condition. As a calibration or references for the current work, flow patterns map developed by other scholars were compared with the current result and it agrees well with flow patterns map developed both by Furukawa (2001) and Hughmark (1965), and in the range of map developed by Taitel and Duckler (1980).

Detail evaluation was performed firstly for the steady state condition (mode M0) as comparison for others under the influence of vibration. It shows that in this case, the boundary between bubbly and slug is quite clear, with composition of only a firm bubbly and slug flow. Here, the slug flow increases as j_G increases particularly when j_L is small, and this result indicates that the formation of slug is very much easier at high j_G and low j_L .

Under the influence of ground accelerations in the range of $\pm 3m/s^2$, the same behavior presented under the flow condition with combination of very low j_G and j_L that formed only bubbly flow along the flow channel about 50%. The same event also

occurred for early transitional from bubbly to slug flow and the formation of slugs also become more intense which resulted in formation of another 50% of population.

With higher vibration mode, the flow patterns map is completely transformed into different composition where there were only three main regime can be mapped, which are the bubbly to slug, short slugs and the slug flow. In this case, the bubbly flow was mostly in the form of spherical caps at bigger sizes and there were also mushroom type bubbles dominated this flow regime and they were both developed to become short slugs and soon becoming more stable and flow in very high volume in the flow channel. The extra force from vibration alleviates more congregations and making it easier for these short slugs to coalesce to form solid slugs in the flow channel. The flow pattern progress with time and with more forces from vibration, some of the slug break up into short slugs and again coalesce to form solid slugs with the increase velocity of both phases.

Therefore, as a short conclusion, it can be said that vibration with mode M2 or in other words ground acceleration with range of $\pm 6 \text{ m/s}^2$, can contribute to a totally different flow pattern when compared to steady state condition. This is a very serious alteration to the normal flow patterns and therefore attention on this subject must be paid in order to predict any hazardous possibility in an event of any two-phase flow facilities that undergo the same situation.

With mode M3 or with ground acceleration with scale of $\pm 9 \text{ m/s}^2$ a more distinguish composition of flow regime compared to the previous two modes of vibration was presented. Here, there are three different regimes which are the bubbly to slug flow, slugs, and longer slugs the one that looked like churn and annular flow. The same phenomena repeated in the process of solid slugs formations where the short slugs with higher mass and assisted by the vibration, coalesce well with their counterparts, easily form and break up. In the low gas superficial velocities, there are huge volume of

slugs but they are distorted and break up, forming very distinctive shape, looked like the churn flow. These slugs however, coalesce back with each other and forming longer slugs. This incident happened when the vertical movements due to vibration, speed up the motion of these slugs and they coalesce with each other, and during the negative acceleration, slowed down to collide and break them up into small pieces with the mentioned shapes.

Domination of slugs is very obvious during this mode of vibration, where as can be observed from the figure, the slugs composed around 70 ~ 80% of the whole population, which reveal another interesting development yet very dangerous assumption in the event of heavy disaster shakes.

At mode M4, or with ground acceleration at $\pm 12 \text{ m/s}^2$, it does not require much effort for the small and short slugs to form solid shape slugs as they were developed shortly after the small volume of short slugs domination in the flow channel, even at low gas superficial velocity in the high velocity of liquid phase. The volume of this slug regime only occupy 30 ~ 40% of entire population.

However, the most significant changes here are the development of slug flow in the upper region of gas superficial velocities as the slugs broke up and forming the churn flow shape and with the higher velocity of both phases, very much longer slugs were formed and the flow pattern during this time looks like the annular flow.

However, the classification of the annular flow still cannot be carried out for this case since these slugs were in their shape, and sometime because of their sizes collide with the wall of the flow, and break up, becoming as the same condition for lower region of gas superficial velocities. These breaks up were then refilled by another long slugs and this condition continuously repeated forming a very unstable flow pattern and making the most chaotic regime which can be considered in a very critical and

hazardous condition particularly if the system involve the heat transfer such as boiling and condensation.

Flow mapping for continuous vibration with 20-mm amplitude or under the ground acceleration of $\pm 6 \text{ m/s}^2$ is similar to the maps for vibration with modes M3 and M4, where the composition of flow regime under this vibration effects consists of bubbly to slug flow, short slugs, stable slugs and longer slugs. In this case, the continuous vibration contributes to the effects between mode M3 and M4, where the volume of slugs is very much the same as the two cases.

The combination of higher velocity in both phases with continuous vibration leads to more collision among bubbles and the wall of the flow channel, making the break up more frequent and those big bubbles dispersed into smaller bubbles with different shapes and sizes. Longer slugs of which more stable in form of shapes and structure were broke up into shorter shapes. Some of these shorter slugs with huge diameter were easily move toward the wall of flow channel coalesce with smaller bubble that crowding on the wall forming slightly bigger slugs and move back to the core of the flow, collided with the incoming slugs from the bottom and move upward together in a longer shape.

Discrete bubble distribution

Under the influence of vibration, the bubbles were very easy to be swung to any side of the flow channel and they were also being pulled up and down very frequently due to the vertical motion under the nature of the degree of freedom of this vibration. These bubbles will therefore can be seen anywhere in the flow channel, and they were particularly populated in very high density after the breakup of bigger bubbles and slugs. In the free space, they tend to attract to bigger bubbles and slugs due to their small sizes and lower mass. This makes the trailing bubbles behind big bubbles and

slugs occur everywhere in the flow channel, which as a result very difficult to identify a specific flow pattern at a particular flow condition.

Void Fraction

Using the same experimental facility and test section, the measurement of void fraction has been carried out.

The average void fraction for all of the flow condition shows that the increases of vibration modes contribute to higher rate of void fraction, with the lowest liquid superficial velocity, $j_L=0.25 \text{ m/s}$ shown the increments for about 25% compared to the steady state condition and the developments of this increments are nearly linear. With this development, it can be predicted that the further increase of the slip ratio also will show the same trend of result. In this case, the continuous vibration contributed the highest fluctuation among all of the vibration modes.

The average void fraction for a higher liquid superficial velocity at 0.5 m/s shows a little different phenomenon where it not as linear as the previous case with the highest void fraction at around 0.3, 5% lower than the previous flow condition. Therefore, the effects of vibrations also demonstrate a different trend where during this range vibrations seem does not contribute much to the increment of average void fraction. The continuous vibration also shows the void fraction at around the same value as the other modes of vibrations.

With liquid superficial velocity, $j_L=0.75 \text{ m/s}$, the trend of void fraction increment is as about the same as represented in the case of $j_L=0.5 \text{ m/s}$ where there are linearly increase and settled at some range of slip ratio around $S = 0.13 \sim 0.2$ ($j_L=0.1 \sim 0.15 \text{ m/s}$) and then linearly increased again to achieve the maximum average void fraction value of 0.275. The value is a little lower (6% decrement) and it is due to the effects of higher liquid superficial velocity with shows that higher mass flow rate of liquid phase start to

dominate the flow channel. The same effect of higher modes of vibration contribute to higher rate of void fraction but from the development trend it can be predicted that with further increase of gas superficial velocities, the void will surely increase but the effect of vibration seem to be weaker.

The average void fractions for higher liquid superficial velocity $j_L=1.0$ m/s had the same trend of increments with shows that the effects of vibration still play an important role. The continuous vibration also shows about the same value of void fraction in between mode M3 and M4, with over all of the percentage of void fraction increment due to vibration as recorded at about 25%.

The average void fraction for superficial velocity, $j_L=2.0$ m/s fluctuate with trend of almost in straight line. The increment of void fraction in this case is about 37%. This phenomenon is very hard to understand but it might probably due vertical motion of the flow channel associated with high liquid superficial velocity that disturbed the bubble motion, where the agitated bubble motion will therefore create more congregation of bubbles, making close crowding and this will occur regardless of the degree of vibration.

The final case study was conducted for flow condition with liquid superficial velocity of 2.5 m/s with the fluctuations of average void fraction value are very obvious as they seem cannot be settled at any fixed point. In this flow condition, as the flow progressed, the effect of vibration is lowering down leaving the value of void fraction during the steady state condition to be the highest among all. The only conclusion that can be taken is on the chaotic behavior during turbulent flow in the channel where it eliminated all the vibration effect on the two-phase flow as the flow patterns during this flow condition are almost unchanged regardless of the increasing gas superficial velocities. Therefore, as short judgment it can be said that the effect of current slip ratio

with respect to vibration onto the average void fraction stop when the superficial velocity reaches 2.5 m/s.

The effect of axial position were evaluated for the position of $L/D = 50$ and $L/D = 35$, where L is the length of the flow channel and D is the channel diameter. This effect was discussed in detail with comparison on the fluctuations of void fraction at local averages and peaks.

The Effects of Axial Position (average void fraction)

The analysis started with liquid superficial velocity, $j_L=0.25$ m/s where most of the void fraction for the position of $L/D = 50$ are in linear increment and for the position of $L/D = 35$, there are a slight polynomial curve of increment. Difference during the steady state (M0), is 10.8%. When vibrations were applied the difference becoming higher as during modes M1 and M2 show nearly the same degree of differences at 14.6 ~ 14.7 % modes M3 and M4 the differences of void fraction fluctuate to about 15.3%. When the whole test section receives continuous vibration with mode M2, the differences of average void fraction for both locations increase to about 20%.

For liquid superficial velocity, $j_L=0.50$ m/s the same trend of void fraction differences was demonstrated for the entire vibration modes showing the increase of difference percentage with higher order of vibration modes with high spread of value for both of the measured positions but showing steady state condition with the minimum disagreement. However, the continuous vibration did not demonstrate much higher disagreement where it lies between the M2 and M3. Again, the result reveals that a longer time for vibration will contribute to more significant disagreement in the value of void fraction between locations due to formation of different flow patterns. The highest average void fraction obtained under this flow condition is $\alpha_{avg(H)}= 0.375$, with vibration mode M4 at location $L/D = 50$, much lower value compared to $j_L=0.25$ m/s.

For liquid superficial velocity, $j_L=0.75$ m/s, the difference of average void fraction for steady state shows around 16.4% and vibrations at mode M1 and M2 shows differences of about 15.2 ~ 15.5% while the higher order vibration at modes M3 and M4 shows differences respectively at 14.2 and 13.5%. On the other hand, the continuous vibration shows difference of 25.5% for both of the positions analyzed.

For liquid superficial velocity to $j_L=1.0$ m/s, the significant spread is smaller in the case with vibration but it is larger during the steady state at 20.4%. The modes M1 and M2 differ in very acceptable range at 1%. In mode M3 and M4, the average void fraction value reach the maximum value and decreased as the gas superficial velocities increases. In all of the vibration modes, the void fraction value transverse between these two position and the two highest values obtained at $\alpha_{avg(H)}=0.3$ and 0.35 under modes M3 and M4 respectively, both at the position, $L/D = 35$.

This phenomenon might be due to higher liquid superficial velocity that does not allow a well manner flow patterns to be formed. It alternately changes from one pattern to another and therefore varied the value of void fraction along the flow channel.

The result for a higher rate of liquid superficial velocity, $j_L=2.0$ m/s shows odd situation compared to lower liquid superficial velocities performed so far where it has a very high differences of void fraction value in the entire cases. During the steady state condition, the spread is at 44% and even it gradually decreasing, it still has a difference of 27.4 % during the vibration with mode M4 and becoming 23.2% as during the continuous vibration mode (C).

The final result for this examination is for liquid superficial velocity, $j_L=2.5$ m/s, shows the spread of void fraction value is very slim in all of the condition and they are not in the uniform pattern, but somehow show the ascending and descending changes. During the steady state condition, the difference is about 7.2% and the decrement of this spread occurred during the vibration with mode M1 and M2 at 6.6 and 5.0 respectively.

Higher order of vibration mode at M3 and M4 show the increment of differences from 7.4 to 9.0%. On the other hand, the continuous vibration shows a total spread of 11%, the highest among all.

The Effects of Axial Position (maximum void fraction)

With flow condition at $j_L=0.25$ m/s the void fraction during the steady state increase from 0.1 to 0.7 with difference between both locations at 5.6%. During vibration the difference increased to 6.4% for mode M1, mode M2 at 16.2%, mode M3 at 15.3% and mode M4 at 11.5% about the same range of gap when the continuous vibration (C) took place.

The highest or maximum void fraction (α_{max}) is about 0.8, very much higher than the overall average void fraction in the flow channel (α_{avg}) which recorded at 0.35, and differs about 30% compared to local average void fraction ($\alpha_{avg(l)}$) which recorded at 0.6.

For $j_L=0.50$ m/s, the trend of increment is about the same just in terms of differences of percentage, where in this case, the entire vibration modes exhibit about 40% larger in gaps for maximum void fraction between the two locations, making the spread between 12.2 – 22%.

For this case, the steady state condition shows 12.2 % of spread and mode M1 shows 13%, mode M2 at 16.5%, mode M3 at 18% and mode M4 at 18.5%. On the other hand, this flow condition recorded the highest spread during the continuous vibration (C), at 22%. This trend however differs from the spread increment for the local average void fraction in the previous section.

The transverse phenomenon were seen under flow condition with $j_L=1.0$ m/s, as also for local average void fraction analysis with difference of values between these two positions also considerably high around 23 ~ 30 % a little lower than the result for

average void fraction. This shows that the flow starts to establish a fix pattern in the flow channel, as a moderate liquid superficial velocity at $j_L=1.0$ m/s reducing the formation of slugs with highest maximum void fraction at 0.6 about 40% differ from the average of total void fraction at 0.35. In term of differences from steady state condition, this case recorded 8.3% disagreement.

With flow condition at $j_L=2.0$ m/s the increment of void fraction due to increasing gas superficial velocities is very much similar with the previous case. For steady state condition, spread of void fraction values is about 18.3%. When the order of vibration getting higher, the spread getting slimmer and move down between 12.5 ~ 7.2 %, making the continuous vibration (C) contributing to the lowest gap and the same comparison between the $\alpha_{max(H)}$ and $\alpha_{avg(H)}$ shows the difference about 44%.

From this result, it can be addressed that there is a remarkable change on differences or spread of value among j_L types of void fractions. The effects of vibration on the spread of void fraction in two-phase flow is therefore very important to be analyzed in order to receive a clear picture of variation of void fraction under a certain flow condition and so far they are mostly determined by the size of accelerations in the vibration.

Considering the effect of vibration, with simply summarizing the entire modes, the above two results for a considerably at high liquid superficial velocity reveal that as this velocity increases, the maximum void fraction becoming lower. This result also shows that with higher liquid superficial velocity, there will be difficult for the bubble to coalesce to form another flow pattern and therefore, the effect of vibrations also will be weaker.

Drift Flux Model - Void Fraction, Slip Ratio and Vibration Relation

Using the overall obtained data, the wide range of void fraction has been evaluated using the Drift Flux Model where the result for all the three values of void fractions were plotted against slip ratios with the effects of vibration modes conducted in this study.

For the average void fraction, during the low slip ratio, the differences of average void fraction between modes of vibration are not so obvious, but as the slip ratio increases, the value of α_{avg} also increases. With extra forces from the vibration, the increment of void fraction become more obvious and this result indicates that, the average void fraction follows the simple rule as discussed above, which is increasing with the increase of slip ratios. At the same time the average void fraction will also increase as the mode of vibration move into higher order.

For the average of local void fraction spread of void fraction values is almost constant where the modes of vibration show strong effect on the value of void fraction. In other words, as the ground accelerations becoming higher, the average void fraction in a flow channel will also increase.

However at low slip ratio, the spread of maximum void fraction is very big, where the lower void fraction values were particularly contributed by the steady state condition and followed by low order vibration modes. As the slip ratio becomes higher the void fraction value also increases, following the law of nature but the effects of vibration in spreading the value of void fraction becoming weaker.

Therefore, it can be concluded that during the low slip ratio region, vibration plays a very important role to spread the void fraction value for local void fraction, the $\alpha_{avg(l)}$ and $\alpha_{max(l)}$ but contribute quiet small effect on the overall average void fraction, α_{avg} in the entire channel. As the slip ratio increases, the void fraction also increases and the spread are almost constant for all the cases, particularly for entire average and local

average void fraction suggesting that the vibration plays very important role in void fraction fluctuation. However, even though the value of maximum void fraction keep increasing, the spread of void fraction value between modes of vibration becoming slimmer; suggesting that in the high slip ratio region, the flow have almost established a fixed pattern, that contribute to almost fix number of maximum value of void fraction.

Therefore, analyses on both of maximum and average void faction is very important in order to have a clear picture of the whole phenomena happened when a particular flow channel receives extra forces such as vibration, as studied in this work.

Instantaneous Bubble Velocity

Bubble velocity is a parameter that will contribute to the transition in flow patterns. The effects of vibration were examined for some selected cases of flow condition to study the sizes of vibration that change the scale this velocity. With the influence from the ground acceleration they were delayed and accelerated as well depending on the direction of the motion. However, on average, they have shown a little increase of velocity compared to the steady state condition and with higher void fraction. This is somehow contradict with theoretical, where the bubble velocity will inverse proportionate with void fraction. This is because when the bubbles travel they experienced an accelerated vibration and then underwent the decelerated vibration before reaching the next position. At the same time, the void fractions also having lower minimum value as the valley of the void fluctuation curve went deep down and nearly reached zero. This indicates that there are times when the voids are super high and extremely low, which actually suggests that there are variations of proportion of gas bubbles along the flow channel during the vibration. Therefore, when the bubbles start the travel with higher mass or with having higher void fraction, and moving under the negative acceleration, the velocities are somehow decreased but not as low as during the

steady state condition. This might be due to their delayed motions as they underwent the negative acceleration, where they tend to breakup and forming smaller bubbles and therefore contribute to lower void fraction. They also do not exhibit the same behavior during steady state with more or less having constant void fraction.

In addition, with more forces from the positive acceleration that surpassed this shortcoming, the overall velocities are found to be much higher if compared to the steady state condition and particularly with higher ground accelerations that contribute more forces onto the liquid holdup which indirectly contribute to more momentum on the bubble motions. The higher mode of vibration displayed higher bubble velocities and they depart far away from the theoretical value while the lower modes of vibration seem to follow the rule by theoretical calculation but have a slight range of differences particularly in the higher value of void fraction. This result indicates that, the normal rule of void fraction-bubble velocity relation can no longer be applied when the bubbles travel under the influence of vibrations. On the other hand, in the liquid superficial velocity dominant region, the bubble velocity will be much less dependent on the gas superficial velocities where vibration play very important role in changing the flow patterns. In contrary, in the case where liquid superficial velocity is in-charge, vibration with the current scales does not really contribute to any significant change.

8.1.8 General Conclusions

The results presented in this work suggest that a vertical two-phase flow channel is in a very severe condition when receive an external force such as vibration particularly in a scale of heavy disaster shakes. Vibration change the flow patterns, flow maps, void fraction and bubble velocities up to a certain level that will contribute to a very serious damage in plants that operating under the condition of two-phase flow.

8.2 Recommendations

This work has investigated the effects of vibration on the flow structures and dynamics of gas liquid two-phase flow under various flow conditions. They were varied from stagnant liquid in a two-dimensional column to the high velocities of both phases in a vertical flow channel. However, there are a lot of conditions that need to be improved in order to obtain more satisfactory result if possible to be conducted in the future. The following recommendations provide some improvement base on the idea of this work:

(i) Development of sophisticated vibration platform

Even though the current vibration platform has performed well in term of reproducing the spectrum of vertical acceleration with a scale of heavy disaster shakes, it is only worked based on the manual operation. It is desirable to have a fully automatic shaker that can reproduce any recorded vibration data in order to reconstruct the same phenomena as happened in the past. It is also very important if the shaker has an ability to move in three dimensional where more variation of vibration data can be tested and therefore wider investigations on the effects onto the two-phase flow can be carried out.

(ii) Construction of a better container for two-dimensional column

The current two-dimensional column has been constructed in quite a small dimension as mentioned in chapter 3 due to limitation of the experimental facility. A bigger column would offer more interesting bubble rising phenomena and the observation also could be improved.

(iii) Three dimensional observation

As continuation to the above, observation using bigger and higher column would offer wider range of investigation such as three dimensional

photographic recording and perhaps bubble rising motion such as helical and spherical can be recorded at the same time.

(iv) Construction of a longer channel for vertical upward flow

Again as the current vibration platform is quite small, there was a limitation on the installation of vertical upward flow channel where in the current work, only permitted a 1.2-*m* apparatus. With longer channel, more sensors can be installed and therefore, wider range of data might be able to be obtained as bubble rising might change at the higher part of the flow channel.

(v) Investigation on the horizontal and inclined flow channel

The current work successfully investigated the effects of vibration onto a vertical arrangement of two-phase flow. However, it is desirable to conduct further investigations on the horizontal and incline flow channel as they are also very important in practical application in industries.

(vi) Investigation on vibration effects on the pool boiling heat transfer

Investigation based on the two-dimensional column offered very good data base. However, in more wide range of application it can be extended to the investigation on the effects of vibration onto the bubble nucleation in the pool boiling where different observation can be obtained as well.

(vii) Investigation on the flow boiling heat transfer

The same reason as in the recommendation (vi), investigation using a flow boiling channel would also offer very interesting observation and data collection as well. This is due to the real application in the power plant that involve high temperature and high pressure fluid would produce different phenomena in term of phase changes resulted from boiling and

condensation, which therefore required more safety procedures during experimentations. Hence, a more challenging works is expected as well.

(viii) Improvement of visualization method

The current method of visualization is quite poor as can be seen in flow patterns photos in section 7.2. It is very desirable to have a better quality of high speed video camera and most importantly more patient should be paid on the lighting system for this work.

Beside the above recommendation, it is very important to construct a very steady piping system for any type of two-phase flow investigation. This is due to very delicate experiments that can easily damage even by a very small mistake. The application of CECM sensor is very helpful and performed very well throughout the experimentation, but the installation of this sensor was very tedious and can easily cause the leakage. Since it is dealing with air and water that flow together in the same channel and associated with external force from vibration, a small leakage can ruin the whole work. Therefore, most importantly for any researcher that would like venture into the same experimentation as in this work it is recommended to poses a very high level of patient.

Overall, this work has presented some interesting new results in the area of two-phase flow. It is hoped that the current result would be a good database for future works since there are still very few works similar so far even though many sectors requires this kind of database such as power and processing plant as discussed throughout this thesis. Therefore, more progresses in this area are desired in order to enrich the knowledge to overcome some serious problem due to the effects of vibration in the application of gas-liquid two-phase flow. It is very important to take this issue seriously for the safety design and analyses of various equipment, machineries and also for benefit of future generation.

- Acuña, C. A. and Finch, J.A., 2010. Tracking velocity of multiple bubbles in a swarm, *International Journal of Mineral Processing*, Volume 94, Issues 3–4, pp. 147 ~ 158
- Aloui, F., Doublicz, L., Legrand, J. and Souhar, M., 1999. Bubbly flow in an axisymmetric sudden expansion: Pressure drop, void fraction, wall shear stress, bubble velocities and sizes, *Experimental Thermal and Fluid Science*, Volume 19, pp. 118 ~ 130
- ArifS. J., Imdadullah, M. and Asghar, M. S. J., 2012. Accurate Measurement of Velocity and Acceleration of Seismic Vibrations near Nuclear Power Plants, *Physics Procedia*, Volume 37, pp. 43 ~ 50
- Baker, D., 1954. Simultaneous Flow of Oil and Gas, *Journal of Oil and Gas*, Volume 53, pp. 183 ~ 195
- Bakrea, S. V., Jangida, R. S. and Reddy G. R., 2006. Optimum X-plate dampers for seismic response control of piping systems, *International Journal of Pressure Vessels and Piping*, Volume 83, pp. 672 ~ 685
- Barcozy, C.J., 1966. A systematic correlation for two-phase pressure drop, *Chemical Engineering Program Symposium*, Series 62, pp. 232 ~ 249
- Barnea, D., Shoham, O. and Taitel, Y., 1980. Flow pattern characterization in two phase flow by electrical conductance probe, *International Journal of Multiphase Flow*, Volume 6, Issue 5, pp. 387-397
- Barnea, D. and Taitel, Y., 1985. Stability of annular flow, *International Communication of Heat and Mass Transfer*, Volume 12, pp. 611 ~ 620
- Bartel, M. D., Ishii, M., Masukawa, T., Mi, Y. and Situ, R., 2001. Interfacial area measurements in subcooled flow boiling, *Nuclear Engineering and Design*, Volume 210, pp. 135 ~ 155

- Bazzurro, P., Cornell, C. A., Diamantidis, D. and Manfredin, G. M., 1996. Seismic damage hazard analysis for requalification of nuclear power plant structures: methodology and application, *Nuclear Engineering and Design*, Volume 160, pp. 321 ~ 332
- Bergant, A., Simpson, A. R., and Tijsseling, A. S., 2006. Water hammer with column separation : A historical overview, *Journal of Fluid and Structures*, Volume 22, pp. 135 ~ 171
- Beilor, E., Brettschuh, W., Krutzik, N. J. and Tropp, R., 2001. Dynamic Characteristics and structural response of the SWR 1000 under earthquake loading conditions, *Nuclear Engineering and Design*, Volume 207, pp. 77 ~ 93
- Bergles, A. E., Collier, J.G., Delhaye, J. M., Hewitt, G. F. and Mayinger, F., 1981. Two-phase flow and heat transfer in the power and process industries, (Textbook), *McGraw-Hill Publication*.
- Bestion, D., 1990. The physical closure laws in the CATHARE code. *Nuclear Engineering and Design*, Volume 124, pp. 229 ~ 245.
- Bhargava, K., Ghosh, A. K., Agrawal, M. K., Patnaik, R., Ramanujam S., and Kushwaha H. S., 2002. Evaluation of seismic fragility of structures—a case study, *Nuclear Engineering and Design*, Volume 212, pp. 253 ~ 272
- Bretherton, F. P., 1961. The motion of long bubbles in tubes, *Journal of Fluid Mechanics*, Volume 10, pp. 166–188.
- Boccardi, G., Bubbico, R., Celata, G. P. and Di Tosto, F., 2008. Geometry influence on safety valves sizing in two-phase flow, *Journal of Loss Prevention in the Process Industries*, Volume 21, Issue 1, pp. 66 ~ 73
- Bommer, J. J., Papaspiliou, M. and Price, W., Earthquake response spectra for seismic design of nuclear power plants in the UK, *Nuclear Engineering and Design*, Volume 241, pp. 968 ~ 977

- Bonekamp, S. and Bier, K., 1997. Influence of ultrasound on poolboiling heat transfer to mixtures of the refrigerants R23 and R134A, *International Journal of Refrigeration*, Volume 20, pp. 606 ~ 615.
- Butterworth, D., 1975. A comparison of some void fraction relationship for the co-current gas-liquid flow, *International Journal of Multi-phase Flow*, Volume 1, pp. 845 ~ 850
- Celata, G. P., Cumo, M., Mariani, A., Simonchini, M. and Cumo, G., 1994. Rationalization of existing mechanistic models for the prediction of water subcooled flow boiling critical heat flux, *International Journal of Heat and Mass Transfer*, Volume 37, suppl. 1, pp. 347 ~ 360
- Celata, G.P., Cumo, M., and Mariani, A., 1997. Experimental evaluation of the onset of subcooled flow boiling at high liquid velocity and subcooling, *International Journal Heat and Mass Transfer*, Volume 40, pp. 2879 ~ 2885.
- Celata, G. P., D'Annibale, F., Di Marco, P., Memoli, G., and Tomiyama, A., 2002. Measurements of rising velocity of a small bubble in a stagnant fluid in one- and two-component systems, *Experimental Thermal and Fluid Science*, Volume 31, Issue 6, pp. 609 ~ 623
- Cha, J. E., Ahn, Y. C., and Kim, M. H., 2002. Flow measurement with an electromagnetic flow meter in two-phase bubbly and slug flow regimes, *Flow Measurement and Instrumentation*, Volume 12, pp. 329 ~ 339
- Cheng, W., Murai, Y., Sasaki, T. and Yamamoto, F., 2005. Bubble velocity measurement with a recursive cross correlation PIV technique, *Flow Measurement and Instrumentation*, Volume 16, pp. 35 ~ 46
- Cheng, H., Hills, J. H., and Azzopardi, B. J., 2002. Effects of initial bubble size on flow pattern transition in a 28.9 mm diameter column, *International Journal of Multiphase Flow*, Volume 28, Issue 6, pp. 1047 ~ 1062

- Chexal, B. and Lellouche, G., 1991. *Void Fraction Correlation for Generalized Applications*, Nuclear Safety Analysis Centre of the Electric Power Research Institute, Report NSAC/139 pp. 131 ~ 138
- Cho, S. G., Kim, D., and Chaudhary, S., 2011. A simplified model for nonlinear seismic response analysis of equipment cabinets in nuclear power plants, *Nuclear Engineering and Design*, Volume 241, pp. 2750 ~ 2757
- Clark, N. N., Van Egmond, J. W., and Nebiolo, E. P., 1990. The drift-flux model applied to bubble columns and low velocity flows, *International Journal of Multiphase Flow*, Volume 16, Issue 2, pp. 261 ~ 279
- Chun, M. H. and Ryu, Y. H., 2000. Thermal analysis of a simulated CANDU 37-element spent fuel bundle with air backfill, *Nuclear Engineering and Design*, Volume 199, Issues 1–2, 11 pp. 85 ~ 99
- Coddington, P. and Macian, R., 2002. A study of the performance of void fraction correlations used in the context of drift-flux two-phase flow models, *Nuclear Engineering and Design*, Volume 215, pp. 199 ~ 216
- Collier, J. G., 1981. *Convective Boiling and Condensation*, Oxford University Press
- Costigan, G. and Whalley, P. B., 1997. Slug flow regime identification from dynamic void fraction measurements in vertical air-water flows, *International Journal of Multiphase Flow*, Volume 23, Issue 2, pp. 263 ~ 282
- Dalkilic, A. C. and Wongwises, S., 2010. An investigation of a model of the flow pattern transition mechanism in relation to the identification of annular flow of R134a in a vertical tube using various void fraction models and flow regime maps, *Experimental Thermal and Fluid Science*, Volume 34 (2010) 692–705
- Davidson J. K., and D. Harisson, D., 1963. *Fluidized Particles*, (Textbook) Cambridge University Press, London

- Dillon, M., Ghiaasiaan, S. M., Abdel-Khalik, S. I., Jeter, S. M. and Sadowski, D. L., 2005. Two-phase pressure drop in a horizontal thin annulus: Effects of channel vibration and wall gas injection, *Experimental Thermal and Fluid Science*, Volume 30, pp. 67 ~ 78
- Dimovaa, S. L., and Elenas, A., 2002. Seismic intensity parameters for fragility analysis of structures with energy dissipating devices, *Structural Safety*, Volume 24, pp. 1 ~ 28
- Ebisawa, K., Ando, K., and Shibata, K., 2000. Progress of a research program on seismic base isolation of nuclear components, *Nuclear Engineering and Design*, Volume 198, pp. 61 ~ 74
- Ellenberger, J. and Krishna, R., 2002. Improving mass transfer in gas-liquid dispersions by vibration excitement, *Chemical Engineering Science*, Volume 57, pp. 4809 ~ 4815
- Ellenberger, J. and Krishna, R., 2003. Shaken, not stirred bubble column reactors: Enhancement of mass transfer by vibration excitement, *Chemical Engineering Science*, Volume 58, pp. 705 ~ 710
- Ellenberger, J., van Baten, J. M. and Krishna, R., 2003. Intensification of bubble columns by vibration excitement, *Catalysis Today* 79-80, pp. 181 ~ 188
- Ellenberger, J. and Krishna, R., 2007a. Levitation of air bubbles and slugs in liquids under low-frequency vibration excitement, *Chemical Engineering Science*, Volume 62, pp. 7548 ~ 7553
- Ellenberger, J. and Krishna, R., 2007b. Levitation of air bubbles in liquid under low frequency vibration excitement, *Chemical Engineering Science*, Volume 62, pp. 5669 ~ 5673
- Fair, J. R., 1960. What you need to know to design thermosyphon re-boilers, *Petroleum Refiner*, Volume 39 (2), 105

- Farrar, C. R., Duffey, T. A. and Reniek, D. H., 1995. Simplified method for evaluating the seismic buckling capacity of unstiffened steel containment structures, *Nuclear Engineering and Design*, Volume 158, pp. 31 ~ 45
- Fan, J.M., Cui, Z., 2005. Effect of acoustic standing wave in a bubble column, *Industrial & Engineering Chemistry Research*, Volume 44, pp. 7010 ~ 7018
- Fand, R. M., 1965., The influence of acoustic vibrations on heat transfer by natural convection from a horizontal cylinder to water, *Journal of Heat Transfer*, Volume 87 pp. 309 ~ 310.
- Fossa, M., 1998. Design and performance of a conductance probe for measuring the liquid fraction in two-phase gas-liquid flows, *Flow Measurement and Instrumentation*, Volume 9, pp. 103 ~ 109
- Fujiwara, A., Minato, D., and Hishida, K. 2004. Effect of bubble diameter on modification of turbulence in an upward pipe flow, *International Journal of Heat and Fluid Flow*, Volume 25, Turbulence and Shear Flow Phenomena (TSFP-3), Issue 3, pp. 481 ~ 488
- Fukano, T., 1998. Measurement of time varying thickness of liquid film flowing with high speed gas flow by a constant electric current method (CECM), *Nuclear Engineering and Design*, Volume 184, Issues 2–3, pp. 363 ~ 377
- Fukuyama, M., Nakagawa, M., Yashiro, T., Toyoda Y. and Akiyama, H., 2001. Seismic design method of clamped-free thin cylindrical shells immersed in fluid, *Nuclear Engineering and Design*, Volume 207, pp. 147 ~ 162
- Furukawa, T. and Fukano, T., 2001. Effects of liquid viscosity on flow pattern in vertical upward gas-liquid two-phase flow, *International Journal of Multiphase flow*, Volume 27, pp. 1109 ~ 1126
- Gardner, G. C., 1980, Fractional vapor content of a liquid pool through which vapor is bubbled, *International Journal of Multi-phase Flow*, Volume 6, pp. 339 ~ 410

- Gnotke, O., Benk, H., Loth, R., 2003. Experimental study on the number density distribution function in turbulent bubbly flows with coalescence and break-up, *Experimental Thermal and Fluid Science*, Volume 27, Issue 7, pp. 803 ~ 816
- Gorman D. G., Liu, M., and Horacek, J., 1998. The effect of annular two-phase flow upon the natural frequencies of a pipe, *Engineering Structures*, Volume 20, No. 8, pp. 726 ~ 731
- Gray, P. 2002, The Human Consequences of the Chernobyl Nuclear Accident A Strategy for Recovery, A Report Commissioned by UNDP and UNICEF with the support of UN-OCHA and WHO.
- Gregory G. A., Nickolson, M. K., and Aziz, K., 1978. Correlation of the liquid volume fraction in the slug for horizontal gas-liquid slug flow, *International Journal of Multiphase Flow*, Volume 4, pp. 33 ~ 39
- Groothuis H., and Hendal, W. P., 1959. Heat transfer in two-phase flow, *Chemical Engineering Science*, Volume 11, pp. 212 ~ 220
- Guet, S., Ooms, G. and Oliemans, R. V. A., 2002. Influence of bubble size on the transition from low-Re bubbly flow to slug flow in a vertical pipe, *Experimental Thermal and Fluid Science*, Volume 26, Issues 6–7, pp. 635 ~ 641
- Hadjian, A. H., 1993. The Spitak, Armenia earthquake of 7 December 1988 - why so much destruction, *Soil Dynamics and Earthquake Engineering*, Volume 12, pp. 1 ~ 24
- Harvel, G. D., Hori, K., Kawanishi, K. and Chang, J. S., 1999. Cross-sectional void fraction distribution measurements in a vertical annulus two-phase flow by high speed X-ray computed tomography and real-time neutron radiography techniques, *Flow Measurement and Instrumentation*, Volume 10, Issue 4, pp. 259 ~ 266

- Hassan, A. R., Kabir, C. S., and Srinivasan, S., 1994. Countercurrent bubble and slug flow in vertical system, *Chemical Engineering Science*, Vol.49, No. 16, pp.2567~2514
- Hayashi, K., Kurimoto, R. and Tomiyama, A., 2011. Terminal velocity of a Taylor drop in a vertical pipe, *International Journal of Multiphase Flow*, Vol. 37, Issue 3, pp. 241~251
- Hayashi, K. and Tomiyama, A., 2012. Effects of surfactant on terminal velocity of a Taylor bubble in a vertical pipe, *International Journal of Multiphase Flow*, Volume 39, pp. 78~87
- Heindel, T. J., Gray, J. N. and Jensen, T. C., 2008. An X-ray system for visualizing fluid flows, *Flow Measurement and Instrument*, Volume 10, pp. 67 ~ 78
- Hervieu, E. and Seleghim, Jr., P., 1998. An objective indicator for two-phase flow pattern transition, *Nuclear Engineering and Design*, Volume 184, pp. 421 ~ 435
- Hewitt, G. F. and Robertson, D. N., 1969. "Studies of Two-Phase Flow Patterns by Simultaneous X-ray and Flash Photography," *Report for AERE-M2159*, UKAEA, Harwell
- Hewitt, G. F. and Whalley, P. B., 1980. Advanced optical instrumentation methods, *International Journal of Multiphase Flow*, Volume 6, Issues 1–2, pp. 139~15
- Hewitt, G. F., 1996. In search of two-phase flow, *Transaction of ASME Journal of Heat Transfer*, 118/3, pp. 518 ~ 527
- Hibiki, T. and Ishii, M., 1998. Effect of flow-induced vibration on local flow parameters of two-phase flow, *Nuclear Engineering and Design*, Volume 185, pp. 113 ~ 125
- Hibiki T., Ishii M., and Xiao, Z., 2001. Axial interfacial area transport of vertical bubbly flows, *International Journal of Heat and Mass Transfer* 44, pp. 1869 ~ 1888

- Hibiki, T. and Ishii, M., 2003a. One-dimensional drift–flux model for two-phase flow in a large diameter pipe, *International Journal of Heat and Mass Transfer*, Volume 46, Issue 10, pp. 1773 ~ 1790
- Hibiki, T., Situ, R., Mi Y., and Ishii, M., 2003b. Local flow measurements of vertical upward bubbly flow in an annulus, *International Journal of Heat and Mass Transfer*, Volume 46, pp. 1479~1496
- Hirao, Y., Kawanishi, K., Tsuge, A., Kohriyama, T., 1986. Experimental study on drift–flux correlation formulas for two-phase flow in large diameter tubes, in: *Proceedings of 2nd International Topical Meeting on Nuclear Power Plant Thermal Hydraulics and Operations*, Tokyo, Japan, pp. 188 ~ 194
- Hirt, C. W., and Nichols, B. D., 1981. Volume of Fluid (VOF) method for the dynamics of free boundaries, *Journal of Computational Physics*, Volume 39, Issue 1, pp. 201~ 225
- Huda, K., 1998, *Doctor of Engineering Thesis*, Kyoto University, Japan.
- Hug, R. H. and Loth, J. L., 1992. Analytical void fraction prediction method, *Journal of Thermophysics* 6, pp. 139 ~ 144
- Hughmark, G.A., 1962. Holdup in gas liquid two-phase flow, *Chemical Engineering Science*, Volume 20, 1007 ~ 1010
- Iida, Y. and Tsutsui, K., 1992. Effects of ultrasonic waves on natural convection, nucleate boiling and film boiling heat transfer from a wire to a saturated liquid, *Experimental Thermal Fluid Science*, Volume 5 (1992) 108–115.
- IRSN (Institut de Radioprotection et de Surete Nucleaire), 2013. News Magazine
- Ishii, M., 1977. One-dimensional drift–flux model and constitutive equations for relative motion between phases in various two-phase flow regimes, *Argonne National Laboratory Reports*, USA, pp. 77 ~ 47

- Ishii, M., N. Zuber, N., 1979. Drag Coefficient and Relative Velocity in Bubbly, Droplet or Particulate Flows, *American Institute of Chemical Engineers Journal*, Volume 25, No. 2, pp. 843 ~ 850
- Ismail, I., Gamio, J. C., Bukhari, S. F. A., Yang, W. Q., 2005. Tomography for multi-phase flow measurement in the oil industry, *Flow Measurement and Instrumentation*, Volume 16, Issues 2–3, pp. 145 ~ 155
- Jain, S. K., 2005. Quick Report on the Study of the 2004 Sumatra Earthquake and Tsunami Effects
- Jameson, G. J. and Davidson, J. F., 1966. The motion of a bubble in a vertically oscillating liquid: theory for an inviscid liquid, and experimental results, *Chemical Engineering Science*, Volume 21, pp. 29 ~ 34.
- Jones Jr., O. C. and Zuber, N., 1975. The interrelation between void fraction fluctuations and flow patterns in two-phase flow, *International Journal of Multiphase Flow*, Volume 2, Issue 3, pp. 273 ~ 306
- Kamei, T. and Serizawa, A., 1998. Measurement of 2-dimensional local instantaneous liquid film thickness around simulated nuclear fuel rod by ultrasonic transmission technique, *Nuclear Engineering and Design*, Volume 184, Issues 2–3, pp. 349-362
- Kataoka, I. and Ishii, M., 1987. Drift-flux model for large diameter pipe and new correlation for pool void fraction, *International Journal of Heat and Mass Transfer*, Volume 30, pp. 1927 ~ 1939
- Kataoka, I., Ishii, M., and Serizawa, A., 1994. Sensitivity analysis of bubble size and probe geometry on the measurements of interfacial area concentration in gas-liquid two-phase flow, *Nuclear Engineering and Design*, Volume 146, Issues 1–3, pp. 53 ~ 70

- Kataoka, I., Serizawa, A., 1997. Analyses of turbulent structure of gas-liquid two-phase flow under forced convective subcooled boiling, *Proceedings 2nd Japanese-German Symposium on Multiphase Flow*, Tokyo, Japan, paper no. 1-1-5, pp. 43 ~ 54
- Kattan, N., Thome, J. R. and Favrat D., 1998. Flow boiling in horizontal tube, part 1 : development of adiabatic two-phase flow pattern maps, *Journal of Heat and Mass Transfer*, Volume120, pp. 140 ~ 147
- Katto, Y. 1992. A prediction model of subcooled water flow boiling CHF for pressure in the range of 0.1 ~ 20 Mpa. *International Journal of Heat and Mass Transfer*, Volume 35, No. 5, pp. 1115 ~ 1123
- Kawanishi, K., Hirao, Y., Tsuge, A., 1990. An experimental study on drift-flux parameters for two-phase flow in vertical round tubes, *Nuclear Engineering and Design*, Volume120, pp. 447 ~ 458
- Kawara, Z., Kataoka, I., Serizawa A., Ko, Y. J., and Takahashi, O., 1999. *Proceedings of International Heat Transfer Conference*, Volume 2, August 23-28, Kyongju, Korea
- Kemeny, J. G., 1979. Reports Of The President's Commission on The Accidents at Three Miles Island
- Keska, J. K. and Williams, B. E., 1999. Experimental comparison of flow pattern detection techniques for air-water mixture flow, *Experimental Thermal and Fluid Science*. Volume19, pp. 1 ~ 12
- Khushnood, S., Khan, Z. F., Malik, M. A., Koreshi, Z. U., Khan, M. A, 2004. A review of heat exchanger tube bundle vibrations in two-phase cross-flow, *Nuclear Engineering and Design*, Volume230, pp. 233 ~ 251.

- Kim, H. Y., Kim, Y. G., Kang, B. H., 2004. Enhancement of natural convection and pool boiling heat transfer via ultrasonic vibration, *International Journal of Heat and Mass Transfer*, Volume 47, pp. 2831 ~ 2840
- Kim, S., Sun, X., Ishii, M., Beus, S. G. and Lincoln, F., 2003. Interfacial area transport and evaluation of source and sink terms for confined air–water bubbly flow, *Nuclear Engineering and Design*, Volume 219, Issue 1, pp. 61 ~ 75
- Kim, M. K., Choi, I. K. and Seo, J. M., 2012. A shaking table test for an evaluation of seismic behavior of 480 V MCC, *Nuclear Engineering and Design*, Volume 243, pp. 341 ~ 355
- Koo, K. Y., Cho, S. G., Cui, J., Kim, D., 2010. *Nuclear Engineering and Design*, Volume 240, pp. 2500 ~ 2511
- Krishna, R., Wilkinson, P. M., van Dierendonck, L. L., 1991. A model for gas holdup in bubble columns incorporating the influence of gas density on flow regime transition, *Chemical Engineering Science* Volume 46, No. 10, pp. 2491 ~ 2496
- Krishna, R., Ellenberger, J., 2002. Improving gas–liquid contacting in bubble columns by vibration excitation, *International Journal of Multiphase Flow* 28, pp. 1223 ~ 1234
- Krishna, R., and van Baten, J. M., 1999. Rise characteristics of gas bubbles in a 2D rectangular column: VOF simulations vs experiments, *International Communication of Heat and Mass Transfer*, Volume 26, No. 7, pp. 965 ~ 974
- Kureta, M., 1997. A study on forced convective boiling in a small pipe under atmospheric pressure, *Doctor of Engineering Thesis*, Kyoto University, Japan (in Japanese)
- Larson, R. G., Scriven L. E. and H. T. Davis, H. T., 1980. Percolation Theory of Two-phase flow in Porous Media, *Chemical Engineering Science*, Volume 36, pp. 57 ~

- Lenzinger, M. and Schweizer B., 2010, Two-phase flow equations with outflow boundary conditions in the hydrophobic–hydrophilic case, *Nonlinear Analysis: Theory, Methods & Applications*, Volume 73, Issue 4, pp. 840 ~ 853
- Lewis, S., Fu, W. L., and Kojasoy, G., 2002. Internal flow structure description of slug flow-pattern in a horizontal pipe, *International Journal of Heat and Mass Transfer*, Volume 45, pp. 3897 ~ 3910
- Li, K. W. and Parker, J. D., 1967. Acoustical effects on free convective heat transfer from a horizontal wire, *Journal of Heat Transfer*, Volume 89, pp. 277 ~ 278.
- Lin, T. K. and Yu, M. H., 2005. An experimental study on the cross-flow vibration of a flexible cylinder in cylinder arrays, *Experimental Thermal and Fluid Science*, Volume 29, pp. 523 ~ 536
- Lo Frano, R. and Forasassi, G., 2009. Conceptual evaluation of fluid structure interaction effects coupled to a seismic event in an innovative liquid metal nuclear reactor, *Nuclear Engineering and Design*, Volume 239, pp. 2333 ~ 2342
- Lucas, D., Beyer, M., Szalinski, L. and Schütz, P., 2010. A new database on the evolution of air–water flows along a large vertical pipe, *International Journal of Thermal Sciences*, Volume 49, Issue 4, pp. 664 ~ 674
- Lucas, G., Zhao, X. and Pradhan, S., 2011. Optimization of four-sensor probes for measuring bubble velocity components in bubbly air–water and oil–water flows *Flow Measurement and Instrumentation*, Volume 22, Issue 1, pp. 50 ~ 63
- Ma, Y. P., Chung, N. M., Pei, B. S. and Lin, W. K., 1991. Two simplified method to determine void fractions for two-phase flow, *Nuclear Technology*, Volume 94, pp. 124 ~ 133.
- Matsumoto, T., Hosokawa, S. and Akio Tomiyama, A., 2012. Measurement of Bubble Velocity using Spatial Filter Velocimetry, *Proceedings of 16th International*

Symposium on Applications of Laser Techniques to Fluid Mechanics, 09-12 July,
Lisbon, Portugal

- Mi, Y., Ishii, M., and Tsoukalas, L. H., 2001. Investigation of vertical slug flow with advanced two-phase flow instrumentation, *Nuclear Engineering and Design*, Volume 204 pp. 69 ~ 85
- Mishima, K. and Ishii, M., 1984. Flow regime transition criteria for upward two-phase flow in vertical tubes, *International Journal of Heat and Mass Transfer*, Volume 27, Issue 5, pp.723 ~ 737
- Mishima, K. and Hibiki, T., 1996. Quantitative limits of thermal and fluid phenomena measurements using the neutron attenuation characteristics of materials *Experimental Thermal and Fluid Science*, Volume 12, Issue 4, pp. 461 ~ 472
- Mukherjee, H., and Brill, J. P., 1983. Liquid holdup correlation for inclined two-phase flow, *Journal of Petroleum Technology*, Volume 4, pp. 1003 ~ 1008
- Nakamura, N., Akita, S., Suzuki, T., Koba, M., Nakamura, S., Nakano, T., 2010, Study of ultimate seismic response and fragility evaluation of nuclear power building using nonlinear three-dimensional finite element model, *Nuclear Engineering and Design*, Volume 240, pp. 166 ~ 180
- Nicklin, D. J., Wilkes, J. O., Davidson, J. F., 1972. Two-phase flow in vertical tubes, *Transaction of Institute of Chemical Engineers*, Volume 40, pp. 61 ~ 68
- Okawa, T., Kataoka, I., and Mori M., 2002. Numerical simulation of lateral phase distribution in turbulent upward bubbly two-phase flows, *Nuclear Engineering and Design*, Volume 213, pp. 183 ~ 197
- Ohnuki, A., and Akimoto, H., 2000. Experimental study on transition of flow pattern and phase distribution in upward air-water two-phase flow along a large vertical pipe, *International Journal of Multiphase Flow*, Volume 26, pp. 367 ~ 386

- Panidis, T., and Papailiou, D. D., 2000. The structure of two-phase grid turbulence in a rectangular channel: an experimental study, *International Journal of Multiphase Flow*, Volume 26, pp. 1369 ~ 1400
- Park, D., Sagong, M., Kwak, D-Y., and Jeong, C-G., 2009. Simulation of tunnel response under spatially varying ground motion, *Soil Dynamics and Earthquake Engineering*, Volume 29, pp. 1417–1424
- Park, S-K., Park, H. W., Shin S. and Lee H. S., 2008. Detection of abrupt structural damage induced by an earthquake using a moving time window technique, *Computers & Structures*, Volume 86, pp. 1253–1265
- Petrangeli, G., 2010. Large airplane crash on a nuclear plant: Design study against excessive shaking of components, *Nuclear Engineering and Design*, Volume 240, pp. 4037 ~ 4042
- Petritsch, G., and Mewes, D., 1999. Experimental investigations of the flow patterns in the hot leg of a pressurized water reactor, *Nuclear Engineering and Design*, Volume 188, pp. 75 ~ 84
- Qi, F. S., Yeoh, G. H., Cheung, S. C. P., Tu, J. Y., Krepper, E., and Lucas, D., 2012. Classification of bubbles in vertical gas–liquid flow: Part 1 – An analysis of experimental data, *International Journal of Multiphase Flow*, Volume 39, pp. 121 ~ 134
- Rahmani, A., Bouchami, T., Bélaïd, A, Bousbia-Salah, A. and Boulheouchat, M. A., 2009. Assessment of boiler tubes overheating mechanisms during a postulated loss of feedwater accident, *Applied Thermal Engineering*, Volume 29, Issues 2–3, pp. 501~508
- Revankar, S. T., and Ishii, M., 1992. Local Interfacial area measurement in bubble flow, *International Journal of Heat and Mass Transfer*, Volume 35, pp. 913 ~ 925

- Revellin, R., Agostini, B., Ursenbacher, T., and Thome, J. R., 2008. Experimental investigation of velocity and length of elongated bubbles for flow of R-134a in a 0.5 mm micro-channel, *Experimental Thermal and Fluid Science*, Volume 32, Issue 3, pp. 870 ~ 881
- Rivière, N., A. and Cartellier, A., 1999a. Wall shear stress and void fraction in Poiseuille bubbly flows: Part I: simple analytic predictions, *European Journal of Mechanical Engineering*, Volume 18, pp. 823 ~ 846
- Rivière, N., A. Cartellier, A., Timkin, L., and Kashinsky, O., 1999b. Wall shear stress and void fraction in Poiseuille bubbly flows: Part II: experiments and validity of analytical predictions, *European Journal of Mechanical Engineering*, Volume 18, pp. 847 ~ 867
- Ruckenstein, E., and Muntean, O., 1970. Mass transfer between a bubble and an oscillating liquid, *Chemical Engineering Science*, Volume 25, pp. 1159 ~ 1166
- Rzasa, M. R., 2009. The measuring method for tests of horizontal two-phase gas-liquid flows, using optical and capacitance tomography, *Nuclear Engineering and Design*, Volume 239, Issue 4, pp. 699 ~ 707
- Sasakawa, T., Serizawa, A., and Kawara, Z., 2005. Fluid-elastic vibration in two-phase cross flow, *Experimental Thermal and Fluid Science*, Volume 29, Issue 3, pp. 403 ~ 413
- Saha, P. and Zuber, N., 1974, Point of net vapor generation and vapor void fraction in subcooled boiling, *Proceedings of 5th International Journal Heat Transfer Conference*, Tokyo, Japan, Volume 4, pp. 175 ~ 179
- Scott, S. L., 1969. Void Fraction in horizontal co-current gas-liquid flow, *Canada Journal of Chemical Engineering*, Volume 40, pp. 224 ~ 230

- Sekoguchi, K. and Takeishi, M., 1989. Interfacial structures in upward huge wave flow and annular flow regimes, *International Journal of Multiphase Flow*, Volume 15, Issue 3, pp. 295-305
- Serizawa, A., 1974, Fluid Dynamic Characteristics in Gas-Liquid Two-Phase Flow, *Doctor of Engineering Thesis*, Kyoto University
- Serizawa, A., 1983. Theoretical prediction of maximum heat flux in power transient, *International Journal of Heat and Mass Transfer*, Volume 26-II, pp. 921 ~ 932
- Shawkat, M. E., Ching, C. Y. and Shoukri, M., 2008. Bubble and liquid turbulence characteristics of bubbly flow in a large diameter vertical pipe, *International Journal of Multiphase Flow*, Volume 34, Issue 8, pp. 767 ~ 785
- Shibata, H., 1998. Design basis earthquakes for critical industrial facilities and their characteristics, and the Southern Hyogo prefecture earthquake, 17 January 1995, *Reliability Engineering and System Safety*, Volume 62, pp. 157 ~ 169
- Shen, X., Mishima, K. and Nakamura, H., 2005. Two-phase phase distribution in a vertical large diameter pipe, *International Journal of Heat and Mass Transfer*, Volume 48, Issue 1, pp. 211-225
- Singh, R. K., Sinha, S. K., Rama Rao, A., 2010. Study of incident water hammer in an engineering loop under two-phase flow experiment, *Nuclear Engineering and Design*, Volume 240, Issue 8, August 2010, pp. 1967 ~ 1974
- Smith, J. W., 1998. Vibration of Structures, (Text) *Chapman and Hall* : 150 ~ 201
- Song, C-H., Chung, M. K. and No, H. C., 1998, Measurements of void fraction by an improved multi-channel conductance void meter, *Nuclear Engineering and Design*, Volume 184, pp. 269 ~ 285
- Sousa, R. G., Pinto, A. M. F. R., Campos, J. B. L. M. , 2006. Effect of gas expansion on the velocity of a Taylor bubble: PIV measurements, *International Journal of Multiphase Flow*, Volume 32, pp. 1182 ~ 1190

- Sterman, L.S., 1950. The generalization of experimental data concerning the bubbling of vapor through the liquid, *Technical Physics USSR* 1, pp. 1479 ~ 1485
- Sun, B., Wang, R., Zhao, X., Yan, D., 2002. The mechanism for the formation of slug flow in vertical gas-liquid two-phase flow, *Solid-State Electronics*, Volume 46, pp. 2323 ~ 2329
- Suzuki, K., Hagiwara, Y., Sato, T., 1983. Heat transfer and flow characteristics of two-phase two-component annular flow, *International Journal of Heat and Mass Transfer*, Vol. 26-I, pp. 597 ~ 604
- Suzuki, Y., Nakagawa, N., Aritomi, M., Murakawa, H., Kikura, H., and Mori, M., 2002. Microstructure of the flow field around a bubble in counter-current bubbly flow, *Experimental Thermal and Fluid Science*, Volume 26, pp. 221 ~ 227
- Taitel, Y. and Dukler, A. E., 1976. A model for predicting flow regime transitions in horizontal and near horizontal gas-liquid flow, *American Institute for Chemical Engineers Journal*, Volume 22, pp. 47 ~ 55
- Talaia, M. A. R., Terminal Velocity of a Bubble Rise in a Liquid Column, *Engineering and Technology* (2007) Volume: 22, Issue: 5, Publisher: World Academy of Science, Engineering and Technology, pp. 264 ~ 268
- Talavera, P. G., 1994. Hydraulic Hammer Theory and Application, PVP-Vol 278, ASME.
- Takenaka, N., Asano, H., Fujii, T. and Matsubayashi, M., 1998. Three-dimensional visualization of void fraction distribution in steady two-phase flow by thermal neutron radiography, *Nuclear Engineering and Design*, Volume 184, Issues 2-3, pp. 203 ~ 212
- Tan, C., Dong, F. and Wu, M., 2007. Identification of gas/liquid two-phase flow regime through ERT-based measurement and feature extraction, *Flow Measurement and Instrumentation*, Volume 18, Issues 5-6, pp. 255-261

- Taylor, N. H., Hewitt, G. F. and Lacey, P. M. C., 1970. The motion and frequency of large disturbance waves in annular two-phase flow of air-water mixtures, *Chemical Engineering Science*, Volume 18, pp. 537 ~ 552
- Theofanous, T. G., Dinh, T. N., Tu, J. P., Dinh, A. T., 2002. The boiling crisis phenomenon Part II: dryout dynamics and burnout, *Experimental Thermal and Fluid Science*, Volume 26, pp. 793 ~ 810
- TNB (Tenaga Nasional Berhad), 2006. Technical Report on Water Hammer Problems in Janamanjung Power Plant
- Tomiyama, A., Celata, G. P., Hosokawa, S. and Yoshida, S., 2001. *Proceedings of 39th European Two-phase Flow Meeting*, F-2, Portugal, pp. 1~ 8
- Uesawa, S., Kaneko, A., and Abe, Y., 2012. Measurement of void fraction in dispersed bubbly flow containing micro-bubbles with the constant electric current method, *Flow Measurement and Instrumentation*, Volume 24, pp. 50 ~ 62
- Utaka, Y., Okuda, S. and Tasaki, Y., 2007. Structure of micro-layer and characteristics of boiling heat transfer in narrow gap mini-channel system, *Transaction of Japan Society of Mechanical Engineers - Series B* 73, 2007, pp. 1929–1935
- Vallejo, L.M., and Reiriz, J.Z., 2011, A Theoretical and Experimental Studies on Horizontal two-phase Flow with a Spool Piece, *Master of Engineering Thesis*, Politecnico de Torino, Spain
- vanHout, R., Barnea, D. and Shemer, L., 2002. Translational velocities of elongated bubbles in continuous slug flow, *International Journal of Multiphase Flow*, Volume 28, Issue 8, pp. 1333 ~ 1350
- Vandu, C. O., Ellenberger, J. and Krishna, R., 2004. Hydrodynamics and mass transfer in an up-flow monolith loop reactor: influence of vibration excitement, *Chemical Engineering Science*, Volume 59, pp. 4999 ~ 5008

- Vassallo, P. F. and Kumar, R., 1999. Liquid and gas velocity measurements using LDV in air-water duct flow, *Experimental Thermal and Fluid Science*, Volume 19, pp. 85 ~ 92
- Wallis, G., 1969. One-dimensional two-phase flow, *McGraw Hill Publication (Text)*; 1st Edition, 5th Printing edition (August 1979)
- Weisman, J. and Pei, B. S., 1983. Critical heat flux for low flow boiling in vertical uniformly heated thin rectangular channels, *International Journal of Heat and Mass Transfer*, Volume 26, No. 2, , pp.325 ~ 335
- Woldesemayat, M. A. and Gahjar, A. J., Comparison of void fraction correlations for horizontal and upward inclined pipes, *International Journal of Multiphase Flow*, Volume 33, Issue 3, pp.347 ~ 370
- Wu, Q., Welter, K., McCreary, D., and Reyes, J. N., 2001. Theoretical studies on the design criteria of double-sensor probe for the measurement of bubble velocity, *Flow Measurement and Instrumentation*, Volume 12, Issue 1, pp. 43 ~ 51
- Yang, C. Y., and Shieh, C. C., 2001. Flow Patterns of air-water and two-phase R-134a in small circular tube, *International Journal of Multiphase Flow*, Volume 27, pp. 1163 ~ 1177
- Yang, H. C., Kim, D. K. and Kim, M. H., 2003. Void fraction measurement using impedance method, *Flow Measurement and Instrumentation*, Volume 14, Issues 4-5, pp. 151 ~ 160
- Yoneda, K., Akira Yasuo, A. and Okawa, T., 2002. Bubble characteristics of steam-water two-phase flow in a large-diameter pipe, *Experimental Thermal and Fluid Science*, Volume 26, 669-676
- You, J. S. and Wu, W. F., 2002. Probabilistic failure analysis of nuclear piping with empirical study of Taiwan's BWR plants, *International Journal of Pressure Vessels and Piping*, Volume 79, pp. 483 ~ 492

- Zainon, M. Z., 1997. An analysis of critical heat flux in forced convective boiling, *Master of Engineering Thesis*, Kyoto University, Japan
- Zainon, M. Z., Ko, Y. J. and Serizawa A., 2001. SDOF Vibration Effects on a Rising Bubble, *Annual Report of Quantum Science and Engineering Center, Kyoto University*, Japan, Volume 4, pp. 57 ~ 59
- Zainon, M. Z. and Serizawa, A., 2002a. Behavior of a rising bubble during a class of heavy disaster shakes, *Proceedings of Japan Society of Multiphase Flow Annual Meeting*, July 29 -31, Nagoya, Japan, pp. 229 ~ 232
- Zainon, M. Z. and Serizawa A., 2002b. Photographic Study on Swarms Bubble Behavior in a Vibrated Container , *Annual Report of Quantum Science and Engineering Center, Kyoto University*, Japan, Volume 3, pp. 52 ~ 55
- Zhang, J., and Fan, L. S., 2003. On the rise velocity of an interactive bubble in liquids, *Chemical Engineering Journal*, Volume 92, pp. 169 ~ 176
- Zhao, J. F. and Hu, W. R., 2000. Slug to annular flow transition of microgravity two-phase flow, *International Journal of Multiphase Flow*, 26, pp. 1295 ~ 1304
- Zhengming, Z., Shuyan, H. and Ming, X., 2007. Seismic analysis of liquid storage container in nuclear reactors, *Nuclear Engineering and Design*, Volume 237, pp. 1325 ~ 1331
- Zuber, N. and Finlay, J. A., 1965. Average volumetric concentration in two-phase flow system, *ASME Journal of Heat Transfer*, Volume 87, pp. 435 ~ 468
- Zubir, M. A. and Zainon, M. Z., 2011. Two-phase flow behavior and patterns in pipes, *Journal of Applied Science*, Volume 11, pp. 1491 ~ 1500
- Zurcher, O., Favrat, D. and Thome, J. R., 2002. Development of adiabatic two-phase flow patterns map for horizontal flow boiling, *International Journal of Heat and Mass Transfer*, Volume 45, pp. 291 ~ 301

Internet Sources

BBC News, 27 February 2012, Tilbury power station blazes

<http://www.bbc.co.uk/news/uk-england-esssex-17177035>

European Nuclear Society News Bulletin 2013, *<http://www.euronuclear.org>*

Guardian, The., 2011. Greek debt crisis and power plant explosion leave Cyprus on 'verge of economic collapse', Friday 29 July 2011, Reported by Smith, H.,

<http://www.guardian.co.uk/business/2011/jul/29/european-debt-crisis-cyprus>

Guardian, The., 2012. More than 1,000 new coal plants planned worldwide, figures show, The Guardian, Tuesday 20 November 2012, Reported by Carrington, D

<http://www.guardian.co.uk/environment/2012/nov/20/coal-plants-world-resources-institute>

IEA (International Energy Agency) Reports 2011. *<http://www.iea.org>*

Reuters, 2011, Analysis: Study warns of leak risks of Canada-U.S. oil pipe, reported by Timothy Gardner, Monday, July 11, 2011,

<http://www.reuters.com/article/2011/07/11/us-usa-pipeline-analysis-idUSTRE76A67R20110711>

WNA (World Nuclear Association), 2012.

<http://www.world-nuclear.org/info/Safety-and-Security/Safety-of-Plants/Chernobyl-Accident/#.UbW3d9jsONU>

WNA (World Nuclear Association), 2013.

<http://www.world-nuclear.org/info/Safety-and-Security/Safety-of-Plants/Nuclear-Power-Plants-and-Earthquakes/#.UbWYFtjsPBJ>